Modelling Solidification of Binary Alloys



Ferran Brosa Planella

Mansfield College

University of Oxford

A thesis submitted for the degree of

Doctor of Philosophy

Trinity Term 2018

Als meus pares i al meu germà

Acknowledgements

First and foremost, I want to thank my supervisors Robert Van Gorder and Colin Please, without whom none of this work would have been possible. To Robert, for being always there (literally) and ready to discuss mathematics or to give clear-sighted counsel. Here's to you! And to Colin, for always having an enlightening idea to discuss with "a young Catalan".

I would like also to thank my industrial supervisors at Elkem, Kjetil Hildal and Aasgeir Valderhaug, for their supervision. Special thanks also to Antoine Autruffe, Rolf Birkeland, and Bente Kroka, for the useful discussions. Finally, I am grateful to Elkem ASA for the financial support and the opportunity to work on-site during parts of this project.

I would like to express my deepest appreciation to all the exceptional people that have shared with me these past four years in Oxford. First, to Nabil, for being the best of the buddies in this long adventure. To Andrew, for having always wise words, either math-wise or life-wise. To Attila, for being always ready to prove me wrong. To Ben, Helen, James, Maxi, Niall, Ozzy, Rachel and Roxana for always being up for a table football match, a board game or a pint after work. Also, to my family and friends from back home who, despite the distance, have always been there for me.

Finalment, voldria donar les gràcies als meus pares i al meu germà per ser-hi sempre. El vostre suport incondicional i el vostre exemple han sigut imprescindibles per arribar fins aquí. Moltíssimes gràcies!

Abstract

Solidification processes are crucial for many industrial applications, and understanding these processes is important if one wants to improve various material production techniques. The dynamics of some solidification processes can be modelled using Stefan problems, a type of free boundary problem. The aim of this dissertation is to study different aspects of the extended Stefan problem for the solidification of binary alloys with a special interest in the manufacturing of metallurgical grade silicon.

First, we derive the extended Stefan problem in an arbitrary n-dimensional domain from basic physical principles, and from this we derive more specific models for different geometries of interest. Then, we perform a linear stability analysis for the exact self-similar solutions that can be found in the semi-infinite and infinite one-dimensional planar geometries. Introducing self-similar perturbations, we find that the solutions to both problems are unstable regardless of the parameter choice, and that the instability that arises is driven by the moving boundary.

Having understood the relevant dynamics in unbounded domains, we next direct our attention to the extended Stefan problem in finite domains, which are of greater relevance to realistic applications. We first consider a one-dimensional finite planar geometry. In order to obtain analytical solutions we use the method of matched asymptotic analysis in the large Lewis number limit. The analysis requires us to consider ten different layers, spread over four different time regimes. We find good agreement with numerical simulations calculated using a fixed boundary method, and with experimental data from the cast of metallurgical grade silicon performed by our industrial sponsor, Elkem.

Finally, we study the three-dimensional spherically symmetric geometry, in order to model the inward solidification of a binary alloy taking the form of a sphere. To determine the asymptotic solutions, we consider the large Lewis number limit and the small Stefan number limit. We distinguish several layers, and we notice qualitative differences between the spherical and planar geometries. To validate the asymptotic results, we compare them with numerical simulations, finding good agreement.

Contents

1 Introduction **1**

1.1 Background 1
1.2 Description of the industrial problem 3
1.3 Literature review 6
1.4 Scope of the thesis 12
1.5 Statement of originality 14
1.6 Acknowledgement of funding 14

2 Model for the solidification of a binary alloy **15**

2.1 Introduction 15
2.1.1 Outline of the chapter 17
2.2 General two-phase solidification model 17
2.2.1 Heat and mass conservation in Ω_j 18
2.2.2 Heat and mass conservation across the interface 20
2.2.3 Constitutional supercooling 23
2.2.4 Initial and boundary conditions 25
2.2.5 Dimensional general model 26
2.2.6 Dimensionless general model 27
2.3 1D Cartesian model 28
2.3.1 Dimensionless model 29
2.3.1.1 Finite domain 31
2.3.1.2 Semi-infinite domain 31
2.3.1.3 Infinite domain 32
2.3.2 Similarity solutions 32
2.3.2.1 Semi-infinite domain 33
2.3.2.2 Infinite domain 34
2.4 n-dimensional radially symmetric model 36
2.4.1 Dimensionless model 36

2.5 Parameter values relevant to the solidification of silicon 37
2.6 Discussion 39

3 Stability analysis of the self-similar solutions 41
3.1 Introduction 41
3.1.1 Outline of the chapter 43
3.2 The linear stability problem 43
3.3 Stability analysis of the semi-infinite domain problem 47
3.3.1 No instability for $\beta \geq 0$ 49
3.3.2 Instability for $-\frac{1}{2} \leq \beta < 0$ 50
3.4 Stability analysis of the infinite domain problem 54
3.4.1 Instability for $-\frac{1}{2} \leq \beta < 0$ 56
3.5 Discussion 63

4 Asymptotic analysis of the inward solidification of a planar slab 66
4.1 Introduction 66
4.1.1 Outline of the chapter 68
4.2 Model for the solidification of a planar slab 68
4.3 Asymptotic solutions in regime i 73
4.3.1 Layer A 73
4.3.2 Layer B 75
4.3.3 Layer C 78
4.3.4 Matching of the solutions 80
4.4 Asymptotic solutions in regime ii 83
4.4.1 Layer D 83
4.4.2 Layer E 84
4.4.3 Matching of the solutions 87
4.5 Asymptotic solutions in regime iii 88
4.5.1 Layer F 89
4.5.2 Layer G 89
4.5.3 Layer H 95
4.5.4 Matching of the solutions 98
4.6 Asymptotic solutions in regime iv 99
4.6.1 Layer I 100
4.6.2 Layer J 100
4.6.3 Matching of the solutions 102
4.7 Summary of the asymptotic solutions 103

4.8 Comparison with numerical simulations and experimental data 107
4.8.1 Numerical scheme 107
4.8.2 Comparison with numerical results 109
4.8.3 Comparison with experimental results 110
4.9 Discussion 114

5 Asymptotic analysis of the inward solidification of a sphere 116
5.1 Introduction 116
5.1.1 Outline of the chapter 117
5.2 Model for the solidification of a sphere 118
5.3 Asymptotic solutions in regime i 120
5.3.1 Layer A 122
5.3.2 Layer B 123
5.3.3 Layer C 126
5.3.4 Matching of the solutions 127
5.4 Small St analysis of regime i 129
5.4.1 Subregime i(1) 130
5.4.1.1 Layer a 132
5.4.1.2 Layer b 132
5.4.2 Subregime i(2) (layer c) 134
5.4.3 Subregime i(3) 137
5.4.3.1 Layer d 137
5.4.3.2 Layer e 137
5.4.4 Discussion of the solutions 139
5.5 Asymptotic solutions in regime ii 139
5.5.1 Layer D 140
5.5.2 Layer E 140
5.5.3 Layer F 145
5.5.4 Matching of the solutions 146
5.6 Asymptotic solutions in regime iii 149
5.6.1 Layer G 149
5.6.2 Layer H 149
5.6.3 Matching of the solutions 154
5.7 Summary of the asymptotic solutions 155
5.8 Numerical simulations 157
5.8.1 Numerical scheme 158

5.8.2 Results 159
5.9 Discussion 161

6 Discussion **164**
6.1 Summary and discussion of the thesis 164
6.2 Guidelines for the industrial partner 167
6.3 Future work 169

Bibliography **170**

List of Figures

1.1 Drawing of the silicon production process, reproduced from [34]. The raw materials are fed into the furnace where the electrodes heat them at high temperatures to activate the relevant chemical reactions. Molten silicon from the furnace is then cast in moulds and solidifies. The fumes that come out of the furnace are filtered to obtain microsilica. 2

1.2 Drawing of the casting process in iron moulds, reproduced from [34]. The molten silicon is poured from the ladle into iron moulds and left to cool down and solidify in contact with the surrounding air. To protect the walls of the mould, a layer of silicon fines is deposited in the bottom of the mould. 4

1.3 Macroscopic picture of a metallurgical grade silicon sample, reproduced from personal communication with Elkem. Each different shade of grey is a silicon grain. Notice the different size and shape of the grains: mostly long and thin grains aligned vertically, with small and round grains near the centre. 4

1.4 Microscopic image of a metallurgical grade silicon sample, reproduced from personal communication with Elkem. The darker regions are the silicon grains (made of pure silicon) and the lighter region in between is the intermetallic phase. The labels show some of the different compounds that form the intermetallic phase, which are mainly composed of iron, aluminium, calcium, titanium, and silicon. 5

2.1 Sketch of the model geometry for a general domain defined as $\Omega = \Omega_s \cup \Omega_l \cup \{f_i = 0\} \cup \partial\Omega$, where Ω_s is the solid phase and Ω_l is the liquid phase. The boundary between both domains is assumed to be sharp and it is given by $f_i = 0$. The external boundary, where boundary conditions need to be specified, is given by $\partial\Omega$. 18

2.2 Sketch for the derivation of the conservation law across the interface. The blue surface $f_i = 0$ is the interface between the solid and liquid phase. The "box" $V(t)$ is the control volume in which we apply the conservation law and the surface $\mathcal{S}(t)$ is the resulting surface obtained when collapsing $V(t)$ onto the interface. Notice that even though this set-up is in three dimensions, it can be generalised to any dimension. 20

2.3 The top diagram is the full Al-Si equilibrium phase diagram, generated by Elkem using FactSage, a commercial thermodynamic database. As we focus on 99% pure silicon near the melting temperature, we consider only the region in the red box. Then, the phase diagram can be assumed to be linear and the slopes of the liquidus and solidus line are determined experimentally. In equilibrium, for temperatures above the liquidus line we have liquid silicon whereas for temperatures below the solidus line we have solid silicon. Between the liquidus and the solidus, solid and liquid phases can coexist. 24

2.4 Sketch of the three different one-dimensional geometries considered in this section. In each domain, we consider a solid phase and a liquid phase separated by a sharp interface at $z = S(t)$, and we need to impose boundary conditions and/or far field conditions, depending on the geometry. 30

2.5 Sketch of the n-dimensional solidification problem with radial symmetry (a). Due to this symmetry, the problem can be reduced to a one-dimensional model only in the radial component as shown in (b). 36

3.1 Perturbations for the semi-infinite domain problem for different representative values of β using the amplitudes given by $\mathbf{u}_{semi}(\beta)$ (numerical values shown in Table 3.1). The domain of the perturbations is $\eta \geq 0$, as we are in the semi-infinite domain problem defined by $z \geq 0$ and $t > 0$. The scaling is the same in all of the plots, so that they are directly comparable. The parameters of the system have been set to $\mathrm{St} = 0.77$, $\mathrm{Le} = 389$, $\rho = 0.95$, $c_p = 1$, $k = 0.34$, $\kappa = 0.36$, $m_s = 0.72$, $m_l = 360$, $D = 1.76 \cdot 10^{-2}$, $\alpha = 2 \cdot 10^{-3}$, $T_{l\infty} = 0$, and $c_{l\infty} = 1$. 53

3.2 Perturbations for the infinite domain problem for different representative values of β using the amplitudes given by $\mathbf{u}_{inf}(\beta)$ (numerical values shown in Table 3.2). The domain of the perturbations is $\eta \in (-\infty, +\infty)$, as we are in the infinite domain problem defined by $z \in (-\infty, +\infty)$ and $t > 0$. These perturbations introduce an instability because the amplitude of the perturbation of the interface C_S is non-zero (but it is not shown in the plots). Notice that, as was pointed out from the form of $\mathbf{u}_{inf}$, these perturbations are very similar to the ones in Figure 3.1. The scaling is the same in all of the plots, so that they are directly comparable. The parameters of the system have been set to St $= 0.77$, Le $= 389$, $\rho = 0.95$, $c_p = 1$, $k = 0.34$, $\kappa = 0.36$, $m_s = 0.72$, $m_l = 360$, $D = 1.76 \cdot 10^{-2}$, $\alpha = 2 \cdot 10^{-3}$, $T_{l\infty} = 0$, $c_{l\infty} = 1$, and $c_{s\infty} = 0$. 60

3.3 Perturbations for the infinite domain problem for different representative values of β using the amplitudes given by $\mathbf{v}_{inf}(\beta)$ (numerical values shown in Table 3.3). The domain of the perturbations is $\eta \in (-\infty, +\infty)$, as we are in the infinite domain problem defined by $z \in (-\infty, +\infty)$ and $t > 0$. These perturbations do not introduce an instability, even if $-\frac{1}{2} \leq \beta < 0$, because the amplitude of the perturbation to the interface C_S is identically zero. The scaling is the same in all of the plots, so that they are directly comparable. The parameters of the system have been set to St $= 0.77$, Le $= 389$, $\rho = 0.95$, $c_p = 1$, $k = 0.34$, $\kappa = 0.36$, $m_s = 0.72$, $m_l = 360$, $D = 1.76 \cdot 10^{-2}$, $\alpha = 2 \cdot 10^{-3}$, $T_{l\infty} = 0$, $c_{l\infty} = 1$, and $c_{s\infty} = 0$. 61

4.1 Diagram of the inward solidification problem of a finite slab. We assume that the problem is symmetric with respect to $z = 0$, so we consider the problem only in the region $0 \leq z \leq 1$ and impose symmetry conditions at the origin. 69

4.2 Sketch of the regimes and layers of the process. The sketch shows the evolution of the interface, $S(t)$, in time, so the area above (in white) is the solid phase and the area below (in blue) is the liquid phase. The four regimes identified with lower case Roman numerals are the behaviours at different times. In each regime, we consider various layers which are labelled with upper case letters. The scalings in each layer are shown in Table 4.1. 72

4.3 Sketch of the problem (4.59). The highlighted area is the domain in which we want to solve the problem (which extends to $\hat{\tau} \to -\infty$). We prescribe the initial condition $w \to e^{\hat{Z}+\hat{\tau}}$ as $\hat{\tau} \to -\infty$. 86
4.4 Numerical solutions to (4.78) for (a) the range $t \in [-100, 100]$ and (b) the range $t \in [-10, 10]$. 92
4.5 Comparison of the numerical solutions and the asymptotic behaviour in the limits (a) $t \to -\infty$ where the expected behaviour is $S \sim t$ given that for the initial conditions used in the simulations we have $C_4 = 0$ (notice that S is plotted against $-t$), and (b) $t \to +\infty$ where the expected behaviour is $S \sim \frac{\sqrt{\pi}}{2\sqrt{t}}$. 94
4.6 Comparison of the analytical and numerical solutions over time for the (a) interface position and (b) concentration of impurities on the liquid side of the interface. 111
4.7 (a) Sample of the cast used for the experimental data. The experiment corresponds to a 14mm silicon cast over a water cooled copper plate. The data is taken at a given central section of the cast, which has been polished and chemically treated in order to take the measurements. (b) Comparison of the asymptotic solution and experimental data for the concentration in the solid phase. Both the picture and the experimental data have been provided by Elkem. For the asymptotic solution, we used parameter values $c_0 = 0.01$, $\mu_r = 17$, $\mu_l = 10$, $\alpha = 0.03$, and $z_0 = 0.43$. 113

5.1 Sketch of the sphere solidification problem. As the problem is symmetric, we can just consider a one-dimensional problem with a symmetry condition at $r = 0$. 118
5.2 Sketch of the regimes and layers in the process. The sketch shows the evolution of the interface $S(t)$ in time, so the area above (in white) is the solid and the area below (in blue) is the liquid. The three regimes, identified with lower case Roman numerals, are the behaviours at different times. In each regime we consider various layers which are labelled with letters. The scalings in each layer are shown in Table 5.1. 121

5.3 Sketch of the layers in St in regime i. The new layers are shown on top of the layers in ϵ discussed in Figure 5.2, and they are identified with lower case letters. The subregimes within regime i are identified as subregimes i(1), i(2) and i(3). The scalings of these new layers are shown in Table 5.2. 131
5.4 Numerical solutions of problem (5.115), calculated using a fixed boundary method and a finite volume scheme. In (a) we show the position of interface against time. The interface quickly decays to the steady state value. In (b) we show the concentration profiles. For late time, we notice the flattening of the profile until it reaches the steady state. 153
5.5 Comparison of the analytical and numerical solution of (a) the interface position and (b) the concentration of impurities on the liquid side of the interface, plotted against time. 160

Chapter 1

Introduction

1.1 Background

Solidification processes are ubiquitous in nature: from formation of snowflakes in clouds to the solidification of lava flows. Regardless of the difference in temperatures, materials and length scales involved in these processes, the underlying phenomena are the same: when a liquid is cooled below a certain temperature, it goes through an exothermic process and solidifies to become a solid. These processes do not only occur in nature: humans have used solidification to create objects and buildings with metals, glass, and polymers. For all these reasons, solidification processes have drawn the attention of scientists from many different disciplines.

One motivation to better understand the solidification of binary alloys arises from production of silicon, proposed by the industrial partner Elkem ASA. Silicon plays an important role in many industrial processes: as an alloy for metals (especially steel, cast iron, and aluminium), as a raw material for the chemical industry (production of silicones and other derivatives), and as a raw material for the semiconductor industry (e.g. electronic devices and solar cells). Even though silicon is the second most abundant element on Earth (behind oxygen) it is seldom found in its pure form, and a series of processes are required to obtain pure silicon from raw materials.

The process of silicon production is shown in the diagram in Figure 1.1. The raw materials used in this process are silicon dioxide SiO_2 (in the form of quartz) and carbon C (in the form of coal, charcoal, and woodchips). These raw materials are fed from the top into the furnace, where the electrodes heat the mixture up to temperatures of over 2300K while the materials flow downwards. At these temperatures, a reduction process takes place between the quartz and the carbon. The products of the reactions are a liquid mixture of Si and other elements (such as iron, aluminium, calcium, and titanium), which is tapped into a ladle at the bottom of the furnace;

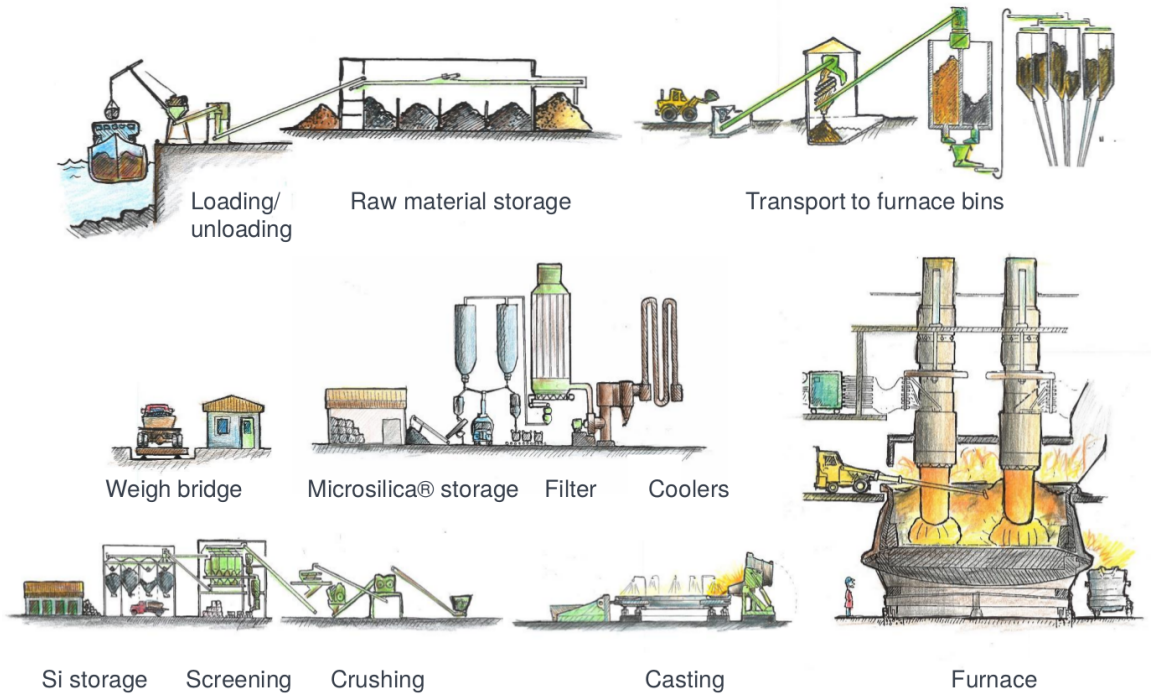


Figure 1.1: Drawing of the silicon production process, reproduced from [34]. The raw materials are fed into the furnace where the electrodes heat them at high temperatures to activate the relevant chemical reactions. Molten silicon from the furnace is then cast in moulds and solidifies. The fumes that come out of the furnace are filtered to obtain microsilica.

and hot gases (mainly SiO and CO) which escape through the top of the furnace. These gases are then oxidised with air to produce CO_2, SiO_2 and NO_x, which are used for energy recovery and microsilica production. The liquid metal in the ladle is then poured to separate it from the slag (a by-product made of metal oxides) and goes into various refining processes to reduce the amount of impurities in it. Once it is sufficiently pure, the molten silicon is cast into moulds and left to solidify. The resulting material is known as metallurgical grade silicon, with concentration of impurities about 1% in weight fraction. Then, the silicon cast is crushed and the chunks screened by size, so that they can be used for production of silicone and alloys. For electronic and solar applications, a much purer silicon is required, so further processes (such as directional solidification) are needed. More details on these processes can be found in [80].

1.2 Description of the industrial problem

In this thesis, we are primarily concerned with the solidification process, where the molten silicon tapped from the furnace is poured into large iron moulds and left to solidify, as shown in Figure 1.2. During this process, molten silicon at about 1700K is cooled so that it solidifies. Because the heat exchange of the process is not controlled, the liquid crystallises, creating a granular structure as shown in Figure 1.3. The size of these grains is primarily determined by how fast the silicon is cooled down, and grain size is one of the main factors that determines the mechanical properties of the final product.

Most of the impurities in the silicon are rejected from the solid phase into the liquid during solidification. At the end of the process, the bulk of the impurities are trapped between silicon grains, forming what is called an intermetallic phase. The main elements comprising this intermetallic phase are iron, aluminium, calcium, titanium, and silicon. The presence of these impurities is not a flaw of the product, as they act as useful catalysts for the reactions that take place when using silicon as an alloying element later on. These elements do not usually appear as pure materials, but rather form other compounds, such as $FeSi_2$ or $Al_6CaFe_4Si_8$, as we can see in Figure 1.4.

Despite all the different techniques used in solidification, there is still limited understanding of how the different ways of solidifying the liquid silicon affect the microstructure of the solid silicon and the distribution of impurities within it. It is well known that the behaviours of the solidification front and the impurities are

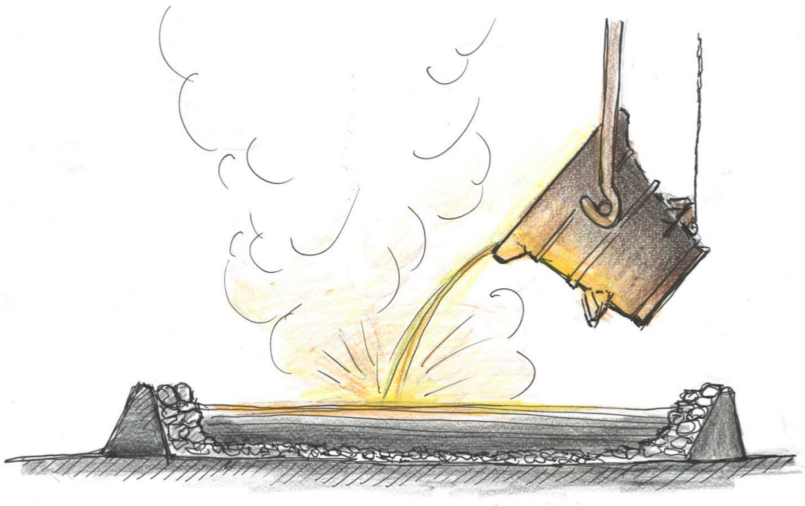


Figure 1.2: Drawing of the casting process in iron moulds, reproduced from [34]. The molten silicon is poured from the ladle into iron moulds and left to cool down and solidify in contact with the surrounding air. To protect the walls of the mould, a layer of silicon fines is deposited in the bottom of the mould.

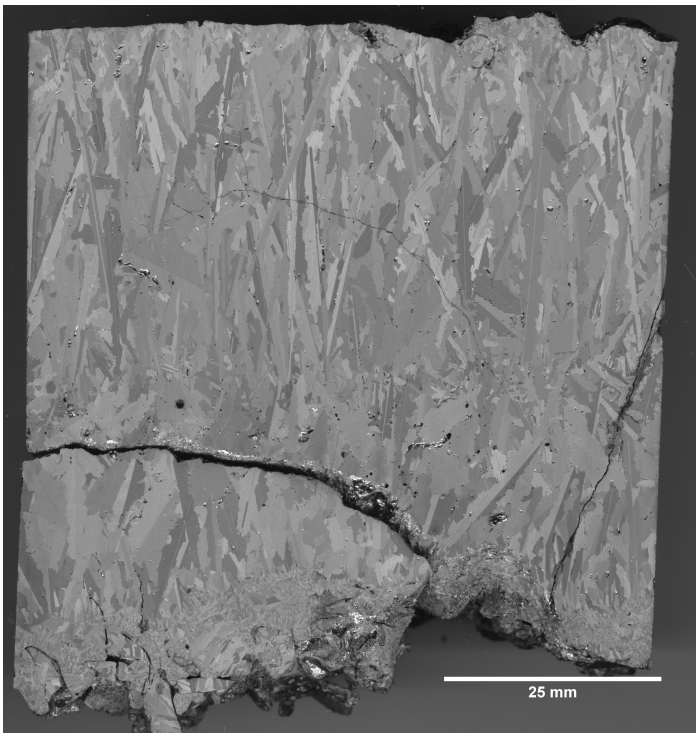


Figure 1.3: Macroscopic picture of a metallurgical grade silicon sample, reproduced from personal communication with Elkem. Each different shade of grey is a silicon grain. Notice the different size and shape of the grains: mostly long and thin grains aligned vertically, with small and round grains near the centre.

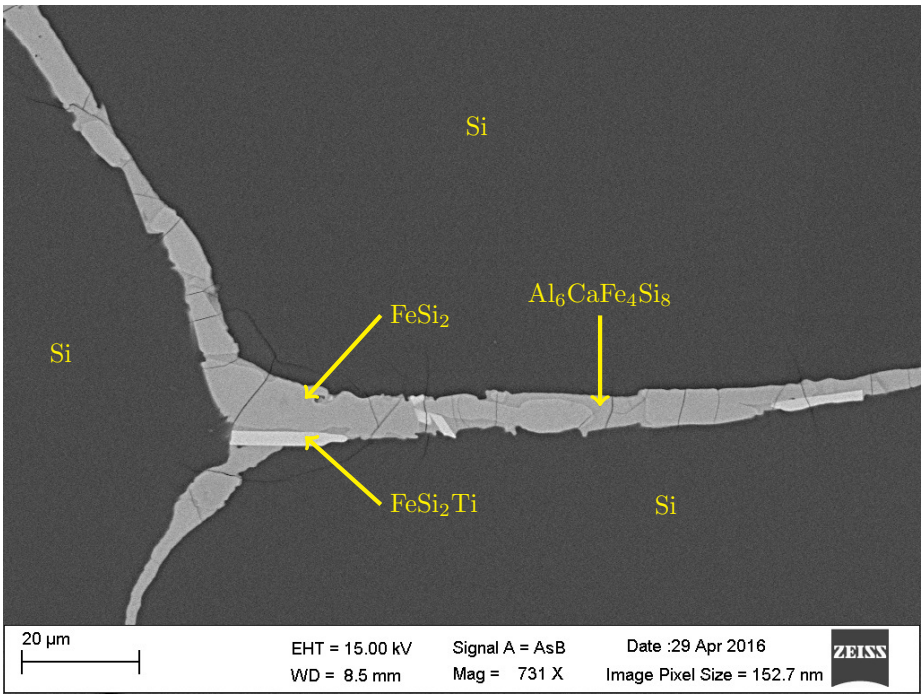


Figure 1.4: Microscopic image of a metallurgical grade silicon sample, reproduced from personal communication with Elkem. The darker regions are the silicon grains (made of pure silicon) and the lighter region in between is the intermetallic phase. The labels show some of the different compounds that form the intermetallic phase, which are mainly composed of iron, aluminium, calcium, titanium, and silicon.

strongly coupled due to constitutional supercooling, but there is a lack of quantitative knowledge. Elkem is interested in gaining a better understanding of the solidification process and how it affects the quality of the final product, so that casting methods can be improved and the final product better adapted to a customer's needs. One goal of this thesis is to develop mathematical models that help us to understand the dynamics of the solidification process and how the casting conditions affect the distribution of impurities. Insight from the models may then be used to improve the current methods of silicon production used by Elkem.

1.3 Literature review

The literature on solidification processes of metals is extensive, as it is a subject that has been studied for several decades. The detailed reviews given in [74] and [87] give a good understanding of how deeply this area has been studied from the engineering and material science point of view. The book [51] by Kurz and Fisher contains an extensive overview on solidification, highlighting different aspects of solidification processes, with a particular focus on the microstructure. This book gathers several mathematical models for nucleation, the stability of the freezing interface, and the different resulting microstructures. Each chapter includes the references to papers where the models are presented and described with more detail.

However, the literature on modelling solidification of silicon is more limited, especially on metallurgical grade silicon. Even though there are several papers discussing the Czochralski process (a casting process in which a single grain is slowly pulled out of a molten silicon pool), such as [31], they are not applicable for the processes we are studying because in the Czochralski process silicon is much purer and solidification happens much more slowly than in the processes we are interested in. Most of the literature for this type of silicon is from the engineering or chemistry point of view; see, for example, [5, 65, 80]. In [80], there is an extensive review of silicon production, focusing on silicon for alloying. It describes each step on the silicon production process, but focusing especially on the furnace processes and related chemical reactions. In particular, they provide a background on binary alloy solidification, the reactions that take place, and the grain growth. The book provides qualitative results on the effects of cooling rate over microstructure, but no quantitative models. The thesis [65], written by Møll at NTNU in collaboration with Elkem, investigates the effects of thermal history and composition on the macro- and micro-structure of silicon from an experimental point of view. The author provides a review of the theoretical background,

which is very useful to understand the basics of the casting process and solidification. The thesis studies the effects that thermal history has on microstructure. In the analysis, Møll compares both COMSOL simulations and experimental data provided by Elkem, which are shown to agree quite well. The thesis [5], written by Autruffe at NTNU, focuses on directional solidification of silicon. The thesis includes a detailed background on silicon casting and focuses on directional solidification, studying the metallic impurities macrosegregation during the solidification process.

From a mathematical point of view, the solidification process of a pure metal or a binary alloy can be described by Stefan problems, which were initially posed in the 19th century [55, 86]. In [79], Rubinstein presents several types of Stefan problems in multiple application fields, providing analytical solutions and analysing the behaviour of such systems. Elliott and Ockendon [23] provide the weak formulation for different free and moving boundary problems. One of the problems considered is the two-phase Stefan problem, for which they give the weak formulation. This weak formulation allows one to discuss the well-posedness of the problem and sets the ground for the enthalpy method. A more general background to the partial differential equations and free boundary problems involved in these kinds of models can be found in [68]. In [106], Worster presents a review of solidification process modelling, starting by defining the two-phase Stefan problem with latent heat and, progressively, incorporating other physical effects such as Gibbs-Thomson effect, constitutional supercooling, and convective heat transfer. Analytical solutions and stability results are provided for these models, although the solutions given neglect the concentration of impurities in the solid phase. [106] concludes with an overview of mushy layers, the effects of a forced external flow, and some examples of applications of the theory developed. Another review on solidification is given by Davis in [21]. The author presents the models for the solidification of pure substances and binary alloys, focusing on the instability behaviour of the process. Amongst other topics, it discusses anisotropy, eutectics and fluid flow as extensions to the basic models.

Mushy layer models are also used to describe solidification processes [38, 41, 42, 53, 105]. The mushy layer models include a smooth transition between solid and liquid phases through a mushy layer where both phases coexist. The problem is set up in each phase separately (solid, mushy and liquid), and then coupled together through interface conditions. Another type of model to describe solidification processes are phase-field models [100, 101, 102, 103]. These models assume that the interface that separates the solid phase from the liquid phase is diffuse instead of sharp, therefore a phase-field variable is introduced to describe the phase change. This new variable

is defined to be equal to zero in one phase, one in the other phase, and to transition smoothly from zero to one over a short length scale. By using this new variable the problem can be defined in the whole domain so we no longer have a free boundary problem. The definition of the phase-field variable depends on the physics of the problem we want to model and it is not unique. It can be shown [101] that, in the limit where the transition length scale goes to zero, the phase-field model reduces to the classical Stefan problem.

We can find analytical solutions for Stefan problems only for very particular situations. For planar geometries, both in semi-infinite and infinite domains, self-similar solutions exist and have been well studied in the literature [79]. For spherical regions solidifying outwards one can find closed-form solutions, as shown in [48]. Other configurations that admit self-similar solutions are ellipsoidal and hyperboloidal geometries [33, 39]. In particular, [39] presents as well solutions for the Stefan problem for binary alloys and for the problem accounting for the fluid flow induced by the change of density between the solid and liquid phases. A similar model is studied in [13] for the growth of spherical crystals in a supersaturated solution. The authors determine self-similar solutions to the problem and discuss their existence, uniqueness and linear stability.

But because Stefan problems only admit analytical solutions in very specific situations, there has been a tradition of asymptotic analysis of Stefan problems, usually in the latent heat dominated limit (the small Stefan number limit, according to the notation in this thesis). Most of the work has focused on the one-phase Stefan problem, in which only the thermal field in the solid is considered. The main motivation of this problem is to find solutions to the classical Stefan problem in the inward solidification of cylinders and spheres, as in these geometries exact solutions to the problem do not exist [71, 77, 84, 88]. Other geometries that have been considered are planar two-dimensional geometries such as corners [47] and the half-space [96]. Arbitrary two-dimensional [61] and three-dimensional [62] geometries have been studied as well near the end of the process finding that, regardless of the geometry of the problem, eventually the liquid region tends to an ellipse or an ellipsoid. Other articles focusing on the small-time behaviour of the solidification of a sphere are [20, 36, 37]. Two-phase Stefan problems in cylindrical and spherical geometries have received less attention [44, 50]. In particular, for spherical domains, the most comprehensive analysis is given by McCue et al. [63], where the authors generalise the analyses in [84] for the two-phase Stefan problem.

The extended Stefan problem for binary alloys has received even less attention in the literature. Ockendon and Tayler [69] present a model for the microstructure of a binary alloy, assuming that the velocity of the solidification front is constant and known. The analysis focuses on the growth of cellular dendrites and exploits the slender shape of such dendrites, with the authors finding an infinite family of solutions which depend on the radius of curvature at the dendrite tip, which the authors suggest to determine either experimentally or analytically from a stability analysis. Feltham and Garside [27] consider the solidification of binary alloys in planar, cylindrical, and spherical domains at early times, but they assume that supercooling effects are as small as needed so that the thermal problem decouples and becomes a classical Stefan problem. Other papers considering binary alloys, such as [107], consider a well mixed liquid, so that their models can be reduced to a Stefan problem with a supercooling condition that depends only on the position of the interface.

In the literature specifically for solidification of silicon there is the previous work done by Benham et al. in collaboration with Elkem, which is reflected in the technical report [6]. The main results of this report are summarised in the papers [7] and [8]. In [8], the authors consider a solidification model for pure substances and give both analytical solutions for a one-dimensional planar geometry and numerical solutions for a two-dimensional wedge geometry, the latter approach employing the enthalpy method. They use the proposed model to study the casting of silicon in a wedge, and their results are shown to agree with the experimental measurements provided by Elkem. In [7], the authors focus on the effect of the silicon fines that cover the walls of the mould during the casting process. They propose a model for silicon flowing and solidifying through a thin channel assuming a Darcy flow. Numerical solutions and simplified analytical solutions are given, and both approaches give similar results. However, none of this work considers the distribution of impurities. Solidification of silicon was also discussed in [12], the report of the 91st European Study Group with Industry on the challenge presented by Elkem and Teknova on thin casting of silicon. The report studies the model for solidification of silicon on a cooled conveyor moving at constant velocity, and steady state solutions are found. The model presented assumes the same physical effects as in [6] but additionally includes advection due to the motion of the conveyor. Even though the casting method is different to the one considered in this thesis, the heat transfer mechanisms accounted for are still applicable. The report provides analytical and numerical solutions, the latter obtained using the enthalpy method. Other aspects considered in the report are the heat transfer to the water in the cooling system, and the viscous spreading of molten silicon.

The solidification of binary alloys has been extensively studied from the numerical point of view, as well, with one goal being the understanding of microstructure formation, as can be seen in the reviews of Rappaz [75] and Jaafar et al. [43]. There are several different approaches to calculate numerical solutions to Stefan problems. Concerning numerical approaches, one can use the enthalpy method, introduced in [78], by formulating the problem in a weak form via the introduction of the enthalpy as a new variable. This allows one to solve the phase change problem without needing to track the moving boundary. More detail about the weak formulation can be found in [23]. The method was extended to two-dimensional problems by Crowley [18], and to account for binary alloys with constitutional supercooling by Crowley and Ockendon [19]. The efficiency of the enthalpy method was improved in Voller and Cross [95]. One of the drawbacks of the enthalpy method is that, due to the definition of enthalpy, supercooled liquid is not allowed in the problem, yet this is a crucial phenomenon in our problem of interest. In these cases, a mushy layer naturally appears in the problem so the mixture of solid and liquid in the mush satisfies thermodynamic equilibrium, as discussed in [23].

Other methods to solve Stefan problems in the presence of supercooled liquid are interface tracking methods, which calculate explicitly the position of the solidification front and impose interface conditions around it. These methods work well for one-dimensional problems, in which one can rescale the solid and liquid phases so they remain fixed in time, at the expense of introducing an advection term into the diffusion equations [32, 99]. However, interface tracking methods are hard to extend to higher dimensions and they are not capable of dealing with topological changes of the solid and liquid regions [82, 89].

More recently, due to modern advances in scientific computing, new methods have been developed that allow for both supercooled liquid and higher dimension problems with topological changes, such as the level set method. Level set methods introduce a level set variable which measures the signed distance to the interface (with the sign depending upon the phase) so that the interface position is given by the zero level set. Then, the Stefan problem can be written in terms of this level set variable so one does not have to explicitly track the interface position. At any time, the position of the interface can be found by taking the zero level set of the level set variable. However, the method is very computationally expensive. The approach was first introduced by Osher and Sethian [70], and since then the approach has been applied to a wide range of problems. Chen et al. [14] present a simple level set method to solve the Stefan problem for a pure material, accounting for kinetic supercooling and Gibbs-Thomson

effects. The method is extended to binary alloys by Theillard et al. [92] to account for constitutional supercooling.

Alternatively, one could opt to solve numerically a phase-field model. Similarly to the level set methods, phase-field models do not require to track the interface. In the phase-field model we have a phase-field variable which is zero at one phase and one at the other phase, transitioning smoothly over a very short interval, which accounts for the moving boundary without the need of tracking it. Wheeler et al. [103] presented the formulation and a numerical scheme for the solidification of a pure melt with kinetic undercooling and the Gibbs-Thomson effect. Some applications of the method where alloys with supercooling are considered are [45, 46]. The disadvantages of this method are that the definition of the phase-field variable depends on the physics included in the model, and that simulations require a small grid size in order to cope with the rapid transition of the phase-field variable from one phase to another. For further information on these methods, we refer the reader to the book [73].

An alternative approach is to use multi-scale models, which are more complex than Stefan problems as they include more physical phenomena. These models were introduced to modelling of solidification processes by Ni and Beckermann [67] and extended by Wang and Beckermann [97, 98]. The key idea of this method is to combine the macroscopic processes, including heat and mass transport, with the microscopic processes, such as nucleation or grain growth. The constitutive laws of these phenomena are coupled and solved numerically, to determine what is the microstructure of the model. An operator splitting scheme is considered by Založnik et al. [108, 109] to improve the stability of the algorithm. The idea is to decouple the global transport equations and the local grain growth equations to reduce the non-linearity of the problem.

Another type of numerical approach to solidification processes is to use stochastic models, such as the 2D cellular automaton (CA) model introduced in [76]. The idea is to divide the problem domain into cells and then define fixed transition rules for the state of the cell which depend on a given state of the cell and its neighbours, amongst other parameters, using probabilistic laws. At each time-step, the current state of the cell is calculated using the transition rules. The same idea is extended to 3D domains in [30], and integrated into a finite element scheme in [28, 29].

Another aspect of Stefan problems that has been extensively studied is their stability. The papers [66] and [104] present two approaches to the stability analysis of the interface. Both papers consider the stability analysis of solidification of a binary alloy as a two-phase Stefan problem with latent heat, constitutional supercooling,

and the Gibbs-Thomson effect, assuming that the freezing front moves at a known constant velocity. The latter assumption simplifies the model so that steady state solutions for the unperturbed base state can be found. The authors then introduce infinitesimal sinusoidal perturbations and find the criteria to decide when these perturbations grow or decay in time. They also assume that the perturbations grow or decay slowly enough so that the thermal and solute diffusion fields can be assumed quasi-steady. These approaches determine the stability of the system, but fail to give a good estimation of the grain size. The main difference between both analysis is that Mullins and Sekerka [66] consider a linear analysis while Wollkind and Segel [104] consider a weakly non-linear analysis, finding a subcritical instability that was not considered in [66]. Other authors have studied the stability of the solidification of a binary alloy as well [64, 83, 93], but in most of the cases they consider only a steady-state approximation. Langer [56] emphasises that one area of interest would be to perform a stability analysis around non-steady solutions.

Coriell et al. studied the multiplicity of solutions [16] and gave a stability analysis [15] for the one-dimensional non-steady two phase Stefan problem with constitutional supercooling in an infinite domain. In [15] they study the stability of the multiple similarity solutions, introducing self-similar perturbations. However, the analysis considers only a certain family of self-similar perturbations (parabolic cylinder functions) which are a particular case of the general solution. The work of Coriell et al. [15] has been extended to two spatial dimensions by Alexandrov [2, 3]. The approach is analogous to the one used in [15], but introduces a horizontal coordinate into the problem. Alexandrov [2] extends the model for a 2D infinite domain without making any assumption on the form of the perturbations in the horizontal direction. Alexandrov [3] considers the stability of the solidification problem in a semi-infinite domain with Dirichlet boundary conditions, assuming that the perturbations are linear in the horizontal direction. In both [2] and [3], there is a family of perturbations which has not been considered, like in [15]. We should also remark that a numerical approach for the non-steady 2D stability analysis is presented in [52].

1.4 Scope of the thesis

The goal of the thesis is to derive and study solutions of mathematical models which allow us to gain a better understanding of the solidification process for a binary alloy, with a special interest in the metallurgical grade silicon application. We expect that

the models will provide insight to our industrial partner, Elkem, that will lead to a better understanding and improvement of their casting process.

We begin by deriving a mathematical model for the solidification of a binary alloy in Chapter 2. The model is an extended Stefan problem which models a solid and a liquid phase separated by a sharp interface, and imposes conservation of heat and impurities in each phase, as well as across the interface. The thermal and solutal problems are coupled through a constitutional supercooling relation. We first present the general model for solidification of a binary alloy in an arbitrary geometry, derived from basic physical principles, and we non-dimensionalise it. We then reduce the dimensionless general model to specific cases that are used in the following chapters. These are the 1D Cartesian model and the 3D spherically symmetric model. For the Cartesian model in non-finite geometries, we provide exact self-similar solutions which are used in Chapter 3.

In Chapter 3, we perform a linear stability analysis for these exact self-similar solutions by introducing self-similar perturbations. The analysis generalises the existing literature by accounting for a more general type of self-similar perturbation than that considered in [15]. We determine the perturbations and we find that the solutions for both domains are unstable regardless of the parameter values. The instability mechanisms for both domains are shown to be similar, and they arise from the self-similar motion of the interface. We have published these results in [10].

In Chapter 4, we consider solidification in a planar finite domain, and therefore self-similar solutions are no longer obtained or expected. We perform an asymptotic analysis in the large Lewis number limit (i.e. the limit of slow impurity diffusion) to obtain asymptotic solutions. The analysis distinguishes a total of ten distinct layers, distributed over four different time regimes. Each layer is studied separately and then the solutions are matched between layers (via the method of matched asymptotics) to determine the leading order asymptotic solutions. The asymptotic solutions are then compared with numerical simulations of the full problem, with the two showing good agreement. The asymptotic solutions are next compared with experimental data from Elkem, and, again, the asymptotics show good agreement with this data. Our analysis of the problem via the method of matched asymptotics has been submitted for publication [9].

In Chapter 5, we consider the solidification of a sphere. Assuming that the problem has spherical symmetry, we reduce the problem to a quasi-one-dimensional model. Again, there are no exact solutions for this problem, so we use matched asymptotics, distinguishing several layers in the asymptotic limit of large Lewis number (i.e. the

limit of slow impurity diffusion) and small Stefan number (i.e. the limit where latent heat is dominant). We find that the behaviour is qualitatively different than the planar geometry problem in certain interesting ways, highlighting the role geometry may play in such solidification problems. These asymptotic solutions generalise those of McCue et al. [63] to a two-phase extended Stefan problem. Our asymptotic solutions are shown to be in good agreement with direct numerical simulations of the full problem.

Finally, in Chapter 6, we summarise the results and discuss the primary conclusions of the thesis, provide recommendations to the industrial partner, and suggest potential lines of research for future work.

1.5 Statement of originality

At the time of submission, one paper [10] has been published from this thesis, containing the work in Chapter 3; and a paper [9] has been submitted for publication, containing the work in Chapter 4. These papers were co-authored by F. Brosa Planella, C. P. Please, and R. A. Van Gorder (supervisors). Macro- and microscopic images of silicon samples and the experimental data in Chapter 4 were provided by Elkem; this is acknowledged in the figure captions. The models' analysis and numerical solutions were carried out by F. Brosa Planella under the supervision of C. P. Please and R. A. Van Gorder.

1.6 Acknowledgement of funding

This thesis is based on work supported by the EPSRC Centre for Doctoral Training in Industrially Focused Mathematical Modelling (EP/L015803/1) in collaboration with Elkem ASA. My thanks go to Elkem for financial support and the opportunity to work on-site during parts of this project.

Chapter 2

Model for the solidification of a binary alloy

2.1 Introduction

Solidification processes are very common both in nature and in industry, so they have been widely studied in the literature. For many applications, the materials considered are not pure liquids but homogeneous mixtures of different components. These are known as alloys and, in the particular case where they are made of two different components, they are known as binary alloys. During solidification, the dynamics of a binary alloy are quite different to the dynamics of a pure melt (i.e. a pure liquid) and thus an extended Stefan problem is required.

One way to model the solidification process of a pure liquid is with a classical Stefan problem, which is named after the mathematician Josef Stefan who, in 1890, posed what today is known as the two-phase Stefan problem [86]. However, he was not the first one to model the solidification of a liquid as Lamé and Clapeyron introduced what today is known as the one-phase Stefan problem in 1831 [55].

The classical Stefan problem is a free boundary problem that can be used to model, amongst other phenomena, the solidification of a pure material. The problem defines two regions (the solid and the liquid phase) where the temperature field in each regime is governed by conservation of heat. However, these two regions vary in time and are not known *a priori*. In order to properly specify the problem, additional information must be given at the interface between the two regions. The temperature at the interface is taken to be a known constant, giving the first interface condition. The second condition, the so-called Stefan condition, imposes conservation of heat flux across the moving interface (or solidification front), and allows one to determine the interface position. We refer the reader to [79] for a compilation of various extensions

of the Stefan problem and their analyses, and to [68] for a more general background on relevant partial differential equations and free boundary problems.

Analytical solutions to the classical Stefan problem can only be found in very specific situations, such as one-dimensional infinite and semi-infinite geometries. For these geometries self-similar solutions may exist, provided that the initial conditions and far field boundary conditions are consistent. Such solutions are well known, and were derived in [79]. However, for other geometries (such as a finite slab, a cylinder, or a sphere), solutions must be approximated either using asymptotic analysis or numerical simulations. Much work has been done on the one-phase Stefan problem (in which the temperature in the liquid is assumed to be constant and equal to the melting temperature, so only the evolution of the temperature in the solid phase is considered) in geometries such as cylinders or spheres, and a good example of the analysis of such solutions can be found in [84]. More generic geometries were considered in [61, 62], but only in the late-time regime. Asymptotic analysis for the two-phase Stefan problem is presented in [50], but the most complete analysis for the spherical geometry is given in [63]. There are several numerical approaches to solve the classical Stefan problem, but the most widely used in the literature is the enthalpy method, due to its simplicity (as it does not require one to track the moving boundary; see [95] for details).

The primary application motivating this thesis is the solidification of metallurgical grade silicon, which contains up to 1% of impurities (mainly iron, aluminium, calcium and titanium). These impurities have an impact on the quality of the final product, as an even distribution of these impurities is desirable, and they play a very important role in the solidification process itself. The main impact of these impurities is due to a phenomenon called constitutional supercooling, for which the concentration of impurities in the melt directly affects the melting point of the liquid. During the solidification process, the impurities are ejected from the solid phase into the liquid phase and therefore, near the interface, there is a build-up of impurities. This build-up causes a variation in the melting temperature which, in turn, affects the velocity of the solidification front. For modelling purposes, impurities can be considered to form a single phase, so the melt can be described as a binary alloy composed of silicon and impurities. Therefore, to model the solidification of silicon, we need to extend the Stefan problem to binary alloys, accounting for impurity transport which is coupled to the heat transport problem via constitutional supercooling (see [19, 79]). The interest in these types of problems increased in the mid 20th century, and since

then researchers have considered several aspects of the problem, such as its stability [15, 66, 104], analytical solutions [27, 69], and numerical simulations [19, 99].

2.1.1 Outline of the chapter

The goal of this chapter is to derive mathematical models for the solidification of a binary alloy which we shall later use in the chapters that follow. The general physical principles governing the system are conservation of heat and mass, and a constitutional supercooling condition which couples the heat and mass transfer problems.

We begin by deriving a general model for the solidification of a binary alloy in an arbitrary n-dimensional domain from first principles in Section 2.2. We pay special attention to the conditions imposed at the interface between the solid and the liquid phases. Once we have obtained the dimensional model, we non-dimensionalise it. In Section 2.3, we derive a one-dimensional planar model for three distinct geometries, consisting of finite, semi-infinite, and infinite regions. The first one is used in the asymptotic analysis of Chapter 4, and for the latter two we give the well-known similarity solutions, for which we perform a linear stability analysis in Chapter 3. In Section 2.4, we reduce the general model to an n-dimensional model with radial symmetry, which we shall later use in the asymptotic analysis of a solidifying three-dimensional sphere in Chapter 5. We conclude the chapter with a discussion of parameter values relevant to the solidification of silicon in Section 2.5, and summarise the chapter in Section 2.6.

2.2 General two-phase solidification model

Consider a domain $\Omega \subseteq \mathbb{R}^n$ which is split into two subdomains: a solid phase Ω_s and a liquid phase Ω_l. These two domains are separated by a sharp interface defined by the $n-1$ dimensional surface parametrised as $f_i = 0$, and they have an outer boundary $\partial\Omega$. Overall, we have $\Omega = \Omega_s \cup \Omega_l \cup \{f_i = 0\} \cup \partial\Omega$, and the intersection between any two of these sets is empty, except, perhaps, at $t = 0$. A two-dimensional sketch of this problem is shown in Figure 2.1. We remark that, even though the two domains Ω_l and Ω_s are sketched as connected domains, this is not a requirement. The size and shape of the domains Ω_s and Ω_l vary as the liquid solidifies and the interface between both is described by $f_i = 0$. There might be changes in the topology of both domains as the process evolves, for example the appearance of disconnected pockets of liquid phase.

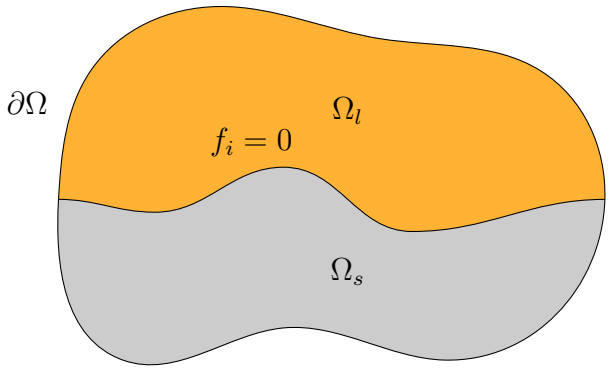


Figure 2.1: Sketch of the model geometry for a general domain defined as $\Omega = \Omega_s \cup \Omega_l \cup \{f_i = 0\} \cup \partial\Omega$, where Ω_s is the solid phase and Ω_l is the liquid phase. The boundary between both domains is assumed to be sharp and it is given by $f_i = 0$. The external boundary, where boundary conditions need to be specified, is given by $\partial\Omega$.

In each domain we will model the spatial and temporal variation of the temperature (T_s in the solid and T_l in the liquid) and the concentration of impurities (c_s and c_l, respectively) using conservation of heat and mass. We will take the Boussinesq approximation (see [38, 105]), hence we assume that the change in density affects the thermal diffusivity but it does not induce advection in the liquid. In fact, we will assume that the solid and liquid are stationary so heat and mass transport is driven only by diffusion. We will model as well the evolution in time of each domain or, equivalently, the evolution of the interface f_i. The physical mechanisms that allow us to determine how the interface moves are conservation of heat and mass through the interface, assuming that the latent heat of solidification of the material is not negligible. To complete the interface conditions, we need to impose continuity of temperature and the temperature-concentration thermodynamic equilibrium conditions due to constitutional supercooling.

In the following sections we derive the extended Stefan problem for the solidification of binary alloys from first principles and then proceed to non-dimensionalise it.

2.2.1 Heat and mass conservation in Ω_j

We want to derive the differential equations that describe the temperature and concentration of impurities in the liquid and solid phases. The physical principles that govern them are conservation of heat and mass respectively. The continuity equation

(see [40] for details) is given by

$$\frac{\mathrm{d}}{\mathrm{d}t}\iiint_{V(t)} P\mathrm{d}V = \iint_{\partial V(t)} \mathbf{q}\cdot\mathbf{n}\mathrm{d}A, \tag{2.1}$$

where $P(t,\mathbf{x})$ is called the density and $\mathbf{q}(t,\mathbf{x})$ is called the flux (both related to a certain conserved quantity), and $V(t)$ is an arbitrary volume. As this must hold for any volume $V(t)$, using divergence theorem we conclude that

$$\frac{\partial P}{\partial t} + \nabla\cdot\mathbf{q} = 0. \tag{2.2}$$

We apply the conservation law (2.2) in each of the domains Ω_s and Ω_l. For the energy conservation law, we take $P(t,\mathbf{x})$ to be the enthalpy of the material with the constitutive law

$$P(t,\mathbf{x}) = \rho c_p T + H_0, \tag{2.3}$$

where ρ is the density of the material, c_p is the heat capacity, $T(t,\mathbf{x})$ is the temperature field and H_0 is the enthalpy at $T = 0$. Since we are assuming that the material is stationary, the heat flux, $\mathbf{q}(t,\mathbf{x})$, can be modelled using Fourier's law

$$\mathbf{q} = -k\nabla T, \tag{2.4}$$

where k is the heat conductivity. Substituting (2.3)-(2.4) into (2.2), we find

$$\rho c_p \frac{\partial T}{\partial t} = \nabla\cdot(k\nabla T), \tag{2.5}$$

which is the heat equation. Further discussion on the derivation of this model can be found in Section 1.3 of [40].

We proceed similarly for the conservation of mass of the impurities. In our model we assume that all of the impurities are represented by a single impurity, even though they are different chemical elements with different physical properties. Assuming we have a dilute alloy, the density $P(t,\mathbf{x})$ is the concentration of the impurity, so we write

$$P(t,\mathbf{x}) = c, \tag{2.6}$$

where $c(t,\mathbf{x})$ is the volumetric concentration of impurity, measured in kg m^{-3}. The flux, $\mathbf{q}(t,\mathbf{x})$, relative to the stationary material, is given by Fick's law

$$\mathbf{q}(t,\mathbf{x}) = -D\nabla c, \tag{2.7}$$

where D is the mass diffusivity of the impurity. Substituting (2.6)-(2.7) into (2.2), we find

$$\frac{\partial c}{\partial t} = \nabla\cdot(D\nabla c), \tag{2.8}$$

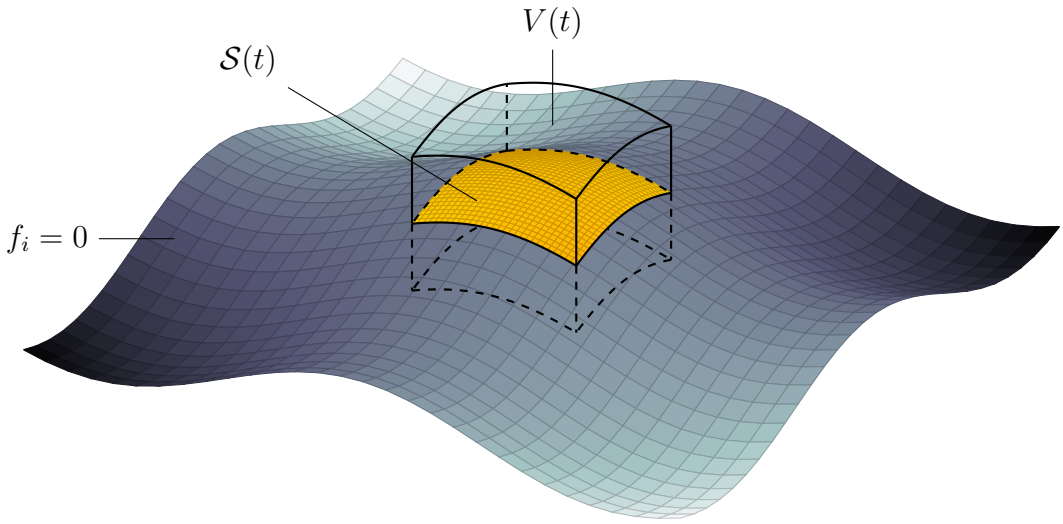


Figure 2.2: Sketch for the derivation of the conservation law across the interface. The blue surface $f_i = 0$ is the interface between the solid and liquid phase. The "box" $V(t)$ is the control volume in which we apply the conservation law and the surface $\mathcal{S}(t)$ is the resulting surface obtained when collapsing $V(t)$ onto the interface. Notice that even though this set-up is in three dimensions, it can be generalised to any dimension.

which is the diffusion equation.

We can now define (2.5) and (2.8) in both domains, using the values of the physical parameters corresponding to each phase.

2.2.2 Heat and mass conservation across the interface

As we mentioned before, heat and mass conservation are the physical principles governing the physical problem we study. These principles apply not only to each phase separately, but also hold across the solidification front. Therefore, we need to derive the conservation equations for heat and mass across the interface which give us two of the interface conditions. In particular, heat conservation across the interface is better known as the *Stefan condition*, as it was first introduced by Stefan in [86].

We start the derivation again from (2.1). We pick the volume $V(t)$ so it intersects the interface and moves along with it, as shown in Figure 2.2. Even though the sketch is for a three-dimensional problem, note that the approach works in any dimension, just by taking an n-dimensional box that intersects and moves along with the $n-1$-dimensional interface.

We apply the Reynolds Transport Theorem (see [58] for details) to the left hand

side of (2.1), obtaining

$$\iiint_{V(t)} \frac{\partial P}{\partial t} \mathrm{d}V + \iint_{\partial V(t)} u_n P \mathrm{d}A = \iint_{\partial V(t)} \mathbf{q} \cdot \mathbf{n} \mathrm{d}A, \tag{2.9}$$

where u_n is the normal velocity of $\partial V(t)$. Collapsing the box $V(t)$ onto the interface, we obtain the surface $\mathcal{S}(t)$, and hence we can write (2.9) as

$$\iint_{\mathcal{S}(t)^+ \cup \mathcal{S}(t)^-} u_n P \mathrm{d}A = \iint_{\mathcal{S}(t)^+ \cup \mathcal{S}(t)^-} \mathbf{q} \cdot \mathbf{n} \mathrm{d}A, \tag{2.10}$$

where superscripts $+$ and $-$ denote different sides of the interface. We can rewrite (2.10) into the form

$$\iint_{\mathcal{S}(t)} [u_n P]^+_- \, \mathrm{d}A = \iint_{\mathcal{S}(t)} [\mathbf{q} \cdot \mathbf{n}]^+_- \, \mathrm{d}A, \tag{2.11}$$

where $[x]^+_- = x^+ - x^-$ is the jump in the magnitude x across the interface. For the purpose of our model, it does not matter which side of the interface is defined as $+$ and which as $-$, as long as it is kept consistent. As this must be true for any arbitrary $\mathcal{S}(t)$, we have

$$u_n = \frac{[\mathbf{q} \cdot \mathbf{n}]^+_-}{[P]^+_-}, \tag{2.12}$$

which can be interpreted as an extended version of the Rankine-Hugoniot condition.

We now find the normal velocity of the interface u_n, and the normal vector $\mathbf{n}$, in terms of our parametrization of the interface $f_i = 0$. From [68, 85], we have that the normal velocity of the interface can be written as

$$u_n = -\frac{1}{\|\nabla f_i\|} \frac{\partial f_i}{\partial t}, \tag{2.13}$$

and the normal vector to the interface as

$$\mathbf{n} = \frac{1}{\|\nabla f_i\|} \nabla f_i. \tag{2.14}$$

Notice that the normal velocity and the normal vector both depend on the choice of the parameterisation of the interface. However, we can later check that the conservation law does not depend on the parametrisation, therefore we can choose any of the two normal unit vectors as long as we define the normal velocity accordingly.

Substituting these expressions into (2.12), and assuming $\|\nabla f_i\| \neq 0$, we obtain the conservation law across the interface:

$$\frac{\partial f_i}{\partial t} = -\frac{[\mathbf{q} \cdot \nabla f_i]^+_-}{[P]^+_-}. \tag{2.15}$$

We need to be careful in how we define the conserved quantities, as they now have to be defined consistently in both the solid and the liquid phases. For the conservation of heat, we need to define the enthalpy in a way that takes into account the latent heat of fusion. We can define the enthalpy as

$$P = \begin{cases} \rho_s c_{ps}(T - T_{m0}), & \text{in the solid,} \\ \rho_l c_{pl}(T - T_{m0}) + \rho_s L, & \text{in the liquid,} \end{cases} \tag{2.16}$$

where T_{m0} is the melting temperature of the pure material in a flat interface and L is the latent heat of fusion, which is assumed to be constant. The flux can be written as

$$\mathbf{q} = \begin{cases} -k_s \nabla T, & \text{in the solid,} \\ -k_l \nabla T, & \text{in the liquid.} \end{cases} \tag{2.17}$$

Then, substituting these expressions into (2.15), and rearranging algebraically, we find

$$\rho_s L \frac{\partial f_i}{\partial t} = -k_s \nabla T_s \cdot \nabla f_i + k_l \nabla T_l \cdot \nabla f_i, \tag{2.18}$$

where we have renamed the temperatures to T_s and T_l, to avoid confusion. This expression is a more general version of the Stefan condition given in [86]. Notice that the latent heat of fusion could depend on variables such as the temeperature. However, we expect the variations in the latent heat to be small and hence it is reasonable to assume it to be constant.

We can proceed similarly for the conservation of mass. Now, the density function is the volumetric concentration, so

$$P = c, \tag{2.19}$$

while the flux can be written as

$$\mathbf{q} = \begin{cases} -D_s \nabla c, & \text{in the solid,} \\ -D_l \nabla c, & \text{in the liquid.} \end{cases} \tag{2.20}$$

Then, the conservation equation reads

$$(c_l - c_s) \frac{\partial f_i}{\partial t} = -D_s \nabla c_s \cdot \nabla f_i + D_l \nabla c_l \cdot \nabla f_i, \tag{2.21}$$

where we have renamed concentrations in the same way as temperatures.

2.2.3 Constitutional supercooling

One of the main phenomena in the process we are interested in modelling is constitutional supercooling, which is when the melting temperature depends on the concentration of impurities in the melt. This effect couples the thermal and solutal problems.

In order to describe this relation, we take the modelling assumption of local thermodynamic equilibrium at the interface. The thermodynamic equilibrium relations in the temperature-concentration space are known as phase-diagrams. Each type of impurity has a different effect on the melting temperature, so there are phase diagrams for binary (two elements) and ternary (three elements) alloys. For most alloys, phase diagrams have been calculated experimentally and the data can be found in books (such as [49]) or generated by commercial software (such as FactSage). For more details on the phase diagrams we refer the reader to the handbook of the subject [11]. Because we have assumed thermodynamical equilibrium at the interface for both phases, we can use the phase diagram to obtain information on which proportion of impurities gets trapped in the solid phase.

Even though in the silicon melt there are at least four different types of impurities with a significant effect on the supercooling (iron, aluminium, calcium and titanium), for simplicity we consider a single impurity that groups all of them together. Therefore, we can use a binary phase diagram to model the constitutional supercooling. As we are interested in a mixture with a small amount of impurities (typically around 1% in mass), we are very close to one end of the phase diagram. Therefore, as shown in Figure 2.3, we can linearise the phase diagram, obtaining the interface conditions

$$c_s = -\alpha_s(T_s - T_{m0}), \tag{2.22a}$$

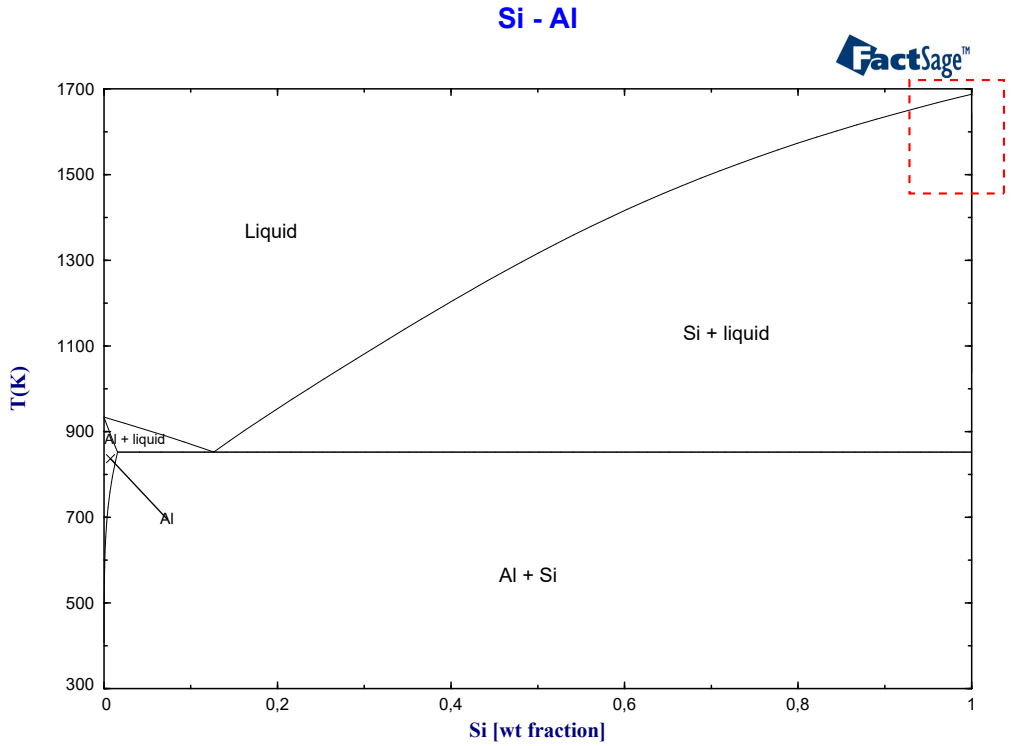
$$c_l = -\alpha_l(T_l - T_{m0}), \tag{2.22b}$$

where α_s and α_l are the slopes of the solidus and liquidus lines, respectively, and T_{m0} is the melting temperature of the pure material. Notice that the temperature cannot be discontinuous as, according to our model, this would imply an infinite heat flux; therefore, at the interface we have

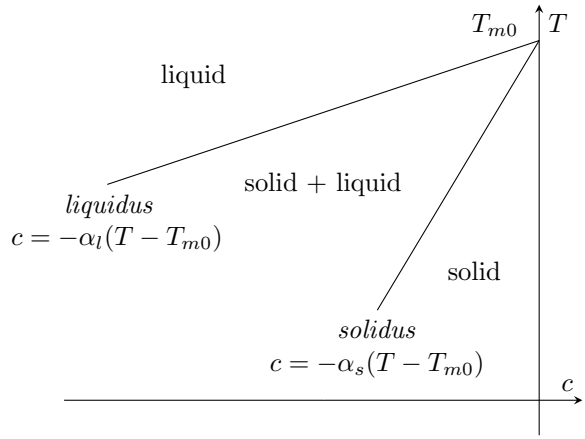
$$T_s = T_l, \tag{2.23}$$

so we can rewrite (2.22a) as

$$c_s = \alpha c_l. \tag{2.24}$$



(a) Binary phase diagram for Al-Si alloy.



(b) Linearised phase diagram.

Figure 2.3: The top diagram is the full Al-Si equilibrium phase diagram, generated by Elkem using FactSage, a commercial thermodynamic database. As we focus on 99% pure silicon near the melting temperature, we consider only the region in the red box. Then, the phase diagram can be assumed to be linear and the slopes of the liquidus and solidus line are determined experimentally. In equilibrium, for temperatures above the liquidus line we have liquid silicon whereas for temperatures below the solidus line we have solid silicon. Between the liquidus and the solidus, solid and liquid phases can coexist.

Here α is the segregation coefficient, which is defined as

$$\alpha = \frac{\alpha_s}{\alpha_l}. \tag{2.25}$$

The segregation coefficient describes the fraction of the impurities that get trapped in the solid phase. For convenience, we use (2.24) instead of (2.22a) for the rest of the thesis. Furthermore, we can use (2.24) to rewrite (2.21) as

$$(1-\alpha)c_l\frac{\partial f_i}{\partial t} = -D_s\nabla c_s \cdot \nabla f_i + D_l \nabla c_l \cdot \nabla f_i, \tag{2.26}$$

2.2.4 Initial and boundary conditions

In order to have a well-posed problem, we need to impose boundary conditions at $\partial\Omega$. The necessary boundary conditions depend on the specific problem we want to solve but in this section we discuss the underlying ideas of the different options.

For the temperature the most realistic approach is to prescribe a heat exchange condition. A natural way to prescribe this condition, as described in [8], is using Newton's law of cooling

$$k\frac{\partial T}{\partial n} = h(T - T_c), \tag{2.27}$$

where $\dfrac{\partial T}{\partial n}$ is the normal derivative to the boundary, k is the thermal conductivity, h is the heat exchange coefficient, and T_c is the cold temperature of the environment. This gives a Robin boundary condition which, even though it is quite realistic, adds an extra layer of complexity to the problem. However, as the heat exchange within the mould is very high, we can take the limit $h \to +\infty$ and reduce it to a Dirichlet boundary condition

$$T = T_c, \tag{2.28}$$

where T_c is a prescribed cold temperature. This condition has been found to work well for the casting of metallurgical grade silicon in [8].

As we have a closed system in terms of mass transfer, we impose a no-flux boundary condition to the concentration field, which can be written as

$$\frac{\partial c_j}{\partial n} = 0, \tag{2.29}$$

where, again, $\dfrac{\partial c_j}{\partial n}$ is the normal derivative and $j = s, l$.

Apart from the boundary conditions, we need to prescribe initial conditions for the concentration field, the temperature field, and the position of the interface. Again, this depends on the problem, but it is usual to start with a pool of liquid so that the initial position of the interface coincides with the boundary $\partial\Omega$. In this case, we would only need to provide initial conditions for T_l and c_l.

2.2.5 Dimensional general model

Considering all the mechanisms previously described, the general model for our problem is given by the following equations. In the solid phase, defined in Ω_s, the governing equations are conservation of mass for the impurities (2.30a) and conservation of heat (2.30b), so we write

$$\frac{\partial c_s}{\partial t} = \nabla \cdot (D_s \nabla c_s), \tag{2.30a}$$

$$\rho_s c_{ps} \frac{\partial T_s}{\partial t} = \nabla \cdot (k_s \nabla T_s), \tag{2.30b}$$

where c_s is the concentration of impurities, T_s is the temperature, D_s is the diffusivity of impurities, ρ_s is the density, c_{ps} is the specific heat and k_s is the thermal conductivity.

In the liquid phase, defined in Ω_l, the governing equations are, again, conservation of mass for the impurities (2.30c) and conservation of heat (2.30d), so we write

$$\frac{\partial c_l}{\partial t} = \nabla \cdot (D_l \nabla c_l), \tag{2.30c}$$

$$\rho_l c_{pl} \frac{\partial T_l}{\partial t} = \nabla \cdot (k_l \nabla T_l), \tag{2.30d}$$

where c_l is the concentration of impurities, T_l is the temperature, D_l is the diffusivity of impurities, ρ_l is the density, c_{pl} is the specific heat and k_l is the thermal conductivity.

The interface between both phases is at $f_i = 0$. The conditions at the interface are continuity of temperature (2.30e), a relation between constitutional supercooling and concentration of impurities given by the phase diagram, (2.30f) and (2.30g), and conservation of heat and mass through the interface, (2.30h) and (2.30i) respectively. These conditions can be written as

$$T_s = T_l, \tag{2.30e}$$

$$c_s = -\alpha_s (T_s - T_{m0}), \tag{2.30f}$$

$$c_l = -\alpha_l (T_l - T_{m0}), \tag{2.30g}$$

$$\rho_s L \frac{\partial f_i}{\partial t} = -k_s \nabla T_s \cdot \nabla f_i + k_l \nabla T_l \cdot \nabla f_i, \tag{2.30h}$$

$$(1-\alpha) c_l \frac{\partial f_i}{\partial t} = -D_s \nabla c_s \cdot \nabla f_i + D_l \nabla c_l \cdot \nabla f_i, \tag{2.30i}$$

where T_{m0} is the melting temperature for pure silicon, L is the latent heat of solidification, and α_s and α_l are the slopes of the liquidus and solidus curves, respectively.

The model is completed with the corresponding boundary conditions

$$\frac{\partial c_s}{\partial \hat{n}} = 0 \quad \text{and} \quad T_s = T_c \quad \text{at } \mathbf{x} \in \partial\Omega \quad \text{for} \quad t > 0, \tag{2.30j}$$

and initial conditions

$$c_l = \mathcal{C}_0, \quad T_l = \mathcal{T}_0, \quad \Omega_s = \emptyset, \quad \Omega_l = \Omega, \quad \text{and} \quad \{f_i = 0\} = \partial\Omega, \tag{2.30k}$$

at $t = 0$ for $\mathbf{x} \in \Omega$.

2.2.6 Dimensionless general model

We now proceed to non-dimensionalise the model (2.30). We choose the scalings

$$\begin{aligned} t &= \frac{R^2}{\kappa_l}\hat{t}, \quad \mathbf{x} = R\hat{\mathbf{x}}, \quad c = \Delta c\, \hat{c}, \quad T = \Delta T\, \hat{T} + T_{m0}, \\ \Omega_s &= R\hat{\Omega}_s, \quad \Omega_l = R\hat{\Omega}_l, \quad f_i = R\hat{f}_i, \quad \partial\Omega = R\partial\hat{\Omega}, \end{aligned} \tag{2.31}$$

where R is the scaling of the spatial coordinates, ΔT the scaling of temperature, T_{m0} the melting temperature for pure silicon, and Δc the scaling of concentration. We choose $\Delta T = T_{m0} - T_c$ and $\Delta c = \rho_l$. We assume that the material properties are homogeneous in each phase, so they can be pulled out of the divergence operators in (2.30).

We define the dimensionless parameters

$$\begin{aligned} \mathrm{St} &= \frac{\Delta T c_{pl}}{L}, \quad \rho = \frac{\rho_s}{\rho_l}, \quad k = \frac{k_s}{k_l}, \quad c_p = \frac{c_{ps}}{c_{pl}}, \quad \kappa = \frac{\kappa_s}{\kappa_l}, \\ \mathrm{Le} &= \frac{\kappa_l}{D_l}, \quad D = \frac{D_s}{D_l}, \quad \alpha = \frac{\alpha_s}{\alpha_l}, \quad m_s = \alpha_s \frac{\Delta T}{\Delta c}, \quad m_l = \alpha_l \frac{\Delta T}{\Delta c}, \end{aligned} \tag{2.32}$$

where κ_j is the thermal diffusivity of each phase which is defined as $\kappa_j = \frac{k_j}{\rho_j c_{pj}}$. The Stefan number, St, is defined as the ratio between the sensible heat and the latent heat. The Lewis number, Le, is the ratio between heat and mass diffusivities (both in the liquid phase) and its square root is the ratio between the length scales of the thermal and the solutal diffusion layers. The parameters m_l and m_s are the non-dimensionalised slopes of the liquidus and solidus lines, respectively. The other parameters ρ (density), c_p (specific heat), k (heat conductivity), κ (heat diffusivity), and D (mass diffusivity) are the ratios between the respective physical parameter in the solid and liquid phases. Notice that the segregation coefficient, α, is already dimensionless and can be defined as the ratio of the slopes of the liquidus and solidus lines (it does not matter if these are dimensional or dimensionless as they are scaled in the same way).

Defining the dimensionless nabla operator as $\hat{\nabla}$, the dimensional model (2.30) becomes the following. In the solid phase ($\hat{\mathbf{x}} \in \hat{\Omega}_s$), we have

$$\frac{\partial \hat{c}_s}{\partial \hat{t}} = \frac{D}{\mathrm{Le}} \hat{\nabla}^2 \hat{c}_s, \tag{2.33a}$$

$$\frac{\partial \hat{T}_s}{\partial \hat{t}} = \kappa \hat{\nabla}^2 \hat{T}_s, \tag{2.33b}$$

in the liquid phase ($\hat{\mathbf{x}} \in \hat{\Omega}_l$), we have

$$\frac{\partial \hat{c}_l}{\partial \hat{t}} = \frac{1}{\mathrm{Le}} \hat{\nabla}^2 \hat{c}_l, \tag{2.33c}$$

$$\frac{\partial \hat{T}_l}{\partial \hat{t}} = \hat{\nabla}^2 \hat{T}_l, \tag{2.33d}$$

and at the interface ($\hat{f}_i = 0$), we have

$$\hat{T}_s = \hat{T}_l, \tag{2.33e}$$

$$\hat{c}_s = -m_s \hat{T}_s = \alpha \hat{c}_l, \tag{2.33f}$$

$$\hat{c}_l = -m_l \hat{T}_l, \tag{2.33g}$$

$$\frac{\rho}{\mathrm{St}} \frac{\partial \hat{f}_i}{\partial \hat{t}} = -k \hat{\nabla} \hat{T}_s \cdot \hat{\nabla} \hat{f}_i + \hat{\nabla} \hat{T}_l \cdot \hat{\nabla} \hat{f}_i, \tag{2.33h}$$

$$(1-\alpha) \hat{c}_l \frac{\partial \hat{f}_i}{\partial \hat{t}} = -\frac{D}{\mathrm{Le}} \hat{\nabla} \hat{c}_s \cdot \hat{\nabla} \hat{f}_i + \frac{1}{\mathrm{Le}} \hat{\nabla} \hat{c}_l \cdot \hat{\nabla} \hat{f}_i. \tag{2.33i}$$

The boundary conditions are

$$\frac{\partial \hat{c}_s}{\partial \hat{n}} = 0 \quad \text{and} \quad \hat{T}_s = \frac{T_c - T_{m0}}{\Delta T} = -1, \tag{2.33j}$$

at $\hat{\mathbf{x}} \in \partial\hat{\Omega}$ for $\hat{t} > 0$, and the initial conditions are

$$\hat{c}_l = \frac{\mathcal{C}_0}{\Delta c} = c_0, \quad \hat{T}_l = \frac{\mathcal{T}_0 - T_{m0}}{\Delta T} = T_0, \quad \hat{\Omega}_s = \emptyset, \quad \hat{\Omega}_l = \hat{\Omega}, \quad \text{and} \quad \{\hat{f}_i = 0\} = \partial\hat{\Omega}, \tag{2.33k}$$

at $\hat{t} = 0$ for $\hat{\mathbf{x}} \in \hat{\Omega}$.

Going forward, we work only with dimensionless quantities. In order to simplify the notation, we drop the hats from the dimensionless variables.

2.3 1D Cartesian model

When casting silicon into moulds, the thickness of the liquid layer is much smaller than any other dimension (normally, one order of magnitude smaller). It is observed

that the effects in a direction transverse to the direction of the moving front are very small, therefore it is reasonable to assume a one-dimensional Cartesian model. In this section, we reduce the general model (2.33) presented in the previous section to the 1D Cartesian model. We formulate the model for three geometries: finite, semi-infinite and infinite domains. As we show later, the latter two geometries admit self-similar solutions.

The geometry of the finite domain is shown in Figure 2.4(a). We have assumed symmetry in the problem, so the initial data is symmetric and the boundary conditions are the same. Therefore we need only to study half of the domain. The wall of the mould, from where the material is cooled, is at $z = 1$ and the interface evolves from there toward the centre at $z = 0$. At the centre we prescribe symmetry conditions. Physically, this geometry represents a finite slab cooled from both ends at a fixed temperature.

The geometry of the semi-infinite domain is shown in Figure 2.4(b). The domain of the spatial coordinate z is assumed to be semi-infinite, with $z = 0$ denoting the wall of the mould and $z = S(t)$ denoting the position of the flat interface which moves away from the origin as times increases. Physically, it represents an initial semi-infinite column of molten silicon in contact with a cool mould wall.

The geometry of the infinite domain is shown in Figure 2.4(c). The domain of the spatial coordinate z is now assumed to be infinite, with the interface located at $z = S(t)$. Physically, it represents an initial semi-infinite column of molten silicon in contact with a semi-infinite column of solid silicon.

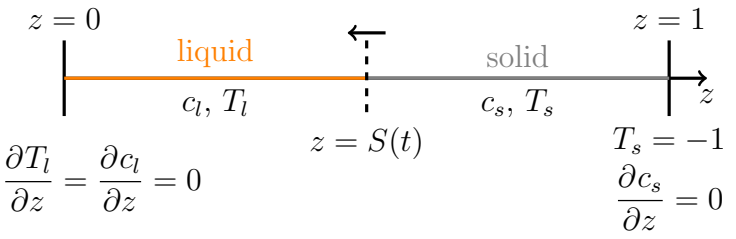
2.3.1 Dimensionless model

A one-dimensional model is found by simply assuming that c_s, c_l, T_s and T_l only depend on t and $z \in \mathbb{R}$ and that the interface position is given by $f_i = z - S(t)$. We take the scaling of the spatial coordinate, defined as R in (2.31), to be the size of the cast in the finite geometry. For the non-finite geometries, because the solutions will be self-similar, the length scale does not matter, so we are free to choose it.

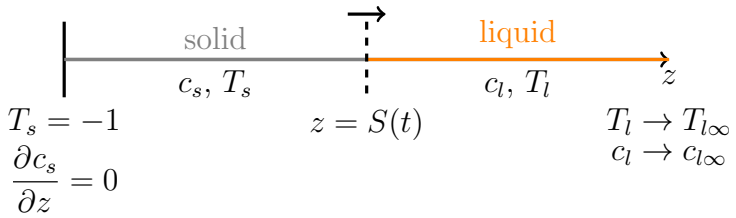
With these assumptions, the model (2.30) can be reduced to the following system (2.34). For the solid phase, which is now located in the region $z < S(t)$ ($z > S(t)$ for finite geometry), the equations read

$$\frac{\partial c_s}{\partial t} = \frac{D}{\mathrm{Le}} \frac{\partial^2 c_s}{\partial z^2}, \tag{2.34a}$$

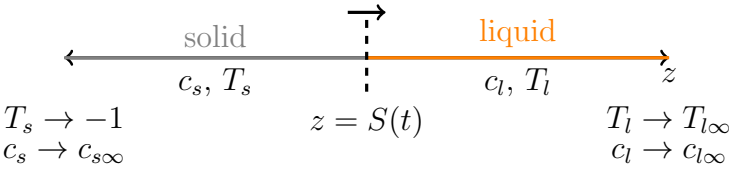
$$\frac{\partial T_s}{\partial t} = \kappa \frac{\partial^2 T_s}{\partial z^2}. \tag{2.34b}$$



(a) Finite domain



(b) Semi-infinite domain



(c) Infinite domain

Figure 2.4: Sketch of the three different one-dimensional geometries considered in this section. In each domain, we consider a solid phase and a liquid phase separated by a sharp interface at $z = S(t)$, and we need to impose boundary conditions and/or far field conditions, depending on the geometry.

Similarly, the liquid phase is now located in the region $z > S(t)$ ($z < S(t)$ for finite geometry) and the equations in this region of the domain are

$$\frac{\partial c_l}{\partial t} = \frac{1}{\mathrm{Le}} \frac{\partial^2 c_l}{\partial z^2}, \tag{2.34c}$$

$$\frac{\partial T_l}{\partial t} = \frac{\partial^2 T_l}{\partial z^2}. \tag{2.34d}$$

Now, the interface is given by $z = S(t)$, and the interface conditions reduce to

$$T_s = T_l, \tag{2.34e}$$

$$c_s = \alpha c_l, \tag{2.34f}$$

$$c_l = -m_l T_l, \tag{2.34g}$$

$$\frac{\rho}{\mathrm{St}} \frac{\mathrm{d}S}{\mathrm{d}t} = k \frac{\partial T_s}{\partial z} - \frac{\partial T_l}{\partial z}, \tag{2.34h}$$

$$(1-\alpha) c_l \frac{\mathrm{d}S}{\mathrm{d}t} = \frac{D}{\mathrm{Le}} \frac{\partial c_s}{\partial z} - \frac{1}{\mathrm{Le}} \frac{\partial c_l}{\partial z}. \tag{2.34i}$$

2.3.1.1 Finite domain

We discuss first the finite geometry. For simplicity, we consider the problem to be symmetric so we need only to study half of the domain upon imposing symmetry conditions, as shown in Figure 2.4a. Therefore, the domain considered is $0 \leq z \leq 1$, and we need to impose boundary conditions at $z = 1$ and symmetry conditions at $z = 0$. The boundary conditions are given by

$$\frac{\partial T_l}{\partial z} = 0 \quad \text{and} \quad \frac{\partial c_l}{\partial z} = 0, \quad \text{at } z = 0, \tag{2.35a}$$

$$T_s = -1 \quad \text{and} \quad \frac{\partial c_s}{\partial z} = 0, \quad \text{at } z = 1, \tag{2.35b}$$

while the initial conditions are

$$S = 1, \quad T_l = T_0, \quad \text{and} \quad c_l = c_0. \tag{2.36}$$

2.3.1.2 Semi-infinite domain

In the semi-infinite domain, as shown in Figure 2.4b, the domain is $z \geq 0$, therefore we require boundary conditions at $z = 0$. Because we are looking for self-similar solutions, we need to prescribe conditions at $z \to +\infty$, which should be consistent with the initial conditions. The boundary conditions are given by

$$T_s = -1 \quad \text{and} \quad \frac{\partial c_s}{\partial z} = 0, \quad \text{at } z = 0, \tag{2.37a}$$

$$T_l \to T_{l\infty} \quad \text{and} \quad c_l \to c_{l\infty}, \quad \text{as } z \to +\infty, \tag{2.37b}$$

while the initial conditions are

$$S = 0, \quad T_l = T_{l\infty}, \quad \text{and} \quad c_l = c_{l\infty}. \tag{2.38}$$

2.3.1.3 Infinite domain

In the semi-infinite domain, as shown in Figure 2.4c, the domain is $z \in \mathbb{R}$. Now we need to prescribe conditions at $z \to \pm\infty$, which should again be consistent with the initial conditions. The boundary conditions are given by

$$T_s \to -1 \quad \text{and} \quad c_s \to c_{s\infty}, \quad \text{as } z \to -\infty, \tag{2.39a}$$

$$T_l \to T_{l\infty} \quad \text{and} \quad c_l \to c_{l\infty}, \quad \text{as } z \to +\infty, \tag{2.39b}$$

while the initial conditions are

$$S = 0, \quad T_s = -1, \quad c_s = c_{s\infty}, \quad T_l = T_{l\infty}, \quad \text{and} \quad c_l = c_{l\infty}. \tag{2.40}$$

2.3.2 Similarity solutions

The 1D Cartesian problems in a semi-infinite and infinite domains admit self-similar solutions, as shown in [79]. In this section, for completeness, we derive the self-similar solutions for our form of the dimensionless problem.

The idea behind self-similar solutions is to introduce a new similarity variable $\eta \sim t^a z$ for a value of the constant a to be determined, and then seek solutions of the form $t^b f(\eta)$, where b is another constant to be determined. As our problem is governed by the heat equation, we find the similarity variable

$$\eta = \frac{z}{2\sqrt{t}}, \tag{2.41}$$

and solutions for concentration and temperature of the form $f(\eta)$. Therefore, in this time varying spatial coordinate, the solution is independent of time. Given a general diffusion equation with a given diffusivity $\mathcal{D}$,

$$\frac{\partial f}{\partial t} = \mathcal{D}\frac{\partial^2 f}{\partial z^2}, \tag{2.42}$$

using the definition of the similarity variable (2.41) and applying the chain rule, we find the following ODE for the self-similar solution

$$\mathcal{D}f''(\eta) + 2\eta f'(\eta) = 0. \tag{2.43}$$

The solution of (2.43) is given by

$$f(\eta) = C_1 \text{erf}\left(\frac{\eta}{\sqrt{\mathcal{D}}}\right) + C_2, \tag{2.44}$$

where C_1 and C_2 are integration constants and $\text{erf}(x)$ is the error function (see [1] for details). A more detailed discussion of the derivation of these self-similar solutions can be found in [68]. We find as well that, because the solution is assumed to only depend on η, the interface position must be at $\eta = \lambda$, or equivalently

$$S(t) = 2\lambda\sqrt{t}, \tag{2.45}$$

where λ is a constant yet to be determined. Using the boundary, initial, and interface conditions we can now determine the unknown constants C_1, C_2, and λ.

2.3.2.1 Semi-infinite domain

We first determine the self-similar solution on a semi-infinite domain. The boundary conditions (2.37), given in terms of η, read

$$T_s = -1, \qquad \text{and} \qquad \frac{\partial c_s}{\partial \eta} = 0, \qquad \text{at } \eta = 0, \tag{2.46a}$$

$$T_l \to T_{l\infty}, \qquad \text{and} \qquad c_l \to c_{l\infty}, \qquad \text{as } \eta \to +\infty. \tag{2.46b}$$

We remark that $\eta \to \infty$ corresponds to both $z \to \infty$ and $t \to 0$, so this is why we require the far field conditions and the initial conditions to be consistent for a similarity solution to exist. Under the conditions (2.46), and using (2.44)-(2.45), the solutions to (2.34) are

$$c_s(\eta) = \alpha c_i, \tag{2.47a}$$

$$c_l(\eta) = c_{l\infty} + (c_i - c_{l\infty})\frac{\text{erfc}(\sqrt{\text{Le}}\,\eta)}{\text{erfc}(\sqrt{\text{Le}}\,\lambda)}, \tag{2.47b}$$

$$T_s(\eta) = -1 + (T_i + 1)\frac{\text{erf}\left(\frac{\eta}{\sqrt{\kappa}}\right)}{\text{erf}\left(\frac{\lambda}{\sqrt{\kappa}}\right)}, \tag{2.47c}$$

$$T_l(\eta) = T_{l\infty} + (T_i - T_{l\infty})\frac{\text{erfc}\,(\eta)}{\text{erfc}\,(\lambda)}, \tag{2.47d}$$

where T_i and c_i are the values of temperature and concentration in the liquid side of the interface. T_i and c_i are constant but not yet determined.

Substituting these expressions into the interface equations (2.34h) and (2.34i), we obtain

$$F(\sqrt{\mathrm{Le}}\,\lambda) = \frac{c_i - 1}{c_i(1-\alpha)}, \tag{2.48a}$$

$$\frac{\rho}{\mathrm{St}} = \frac{k}{\kappa}\frac{T_i + 1}{G\left(\frac{\lambda}{\sqrt{\kappa}}\right)} + \frac{T_i - T_{l\infty}}{F(\lambda)}, \tag{2.48b}$$

where $F(\zeta)$ and $G(\zeta)$ are given by

$$F(\zeta) = \sqrt{\pi}\zeta \exp\left(\zeta^2\right) \mathrm{erfc}(\zeta), \tag{2.49a}$$

$$G(\zeta) = \sqrt{\pi}\zeta \exp\left(\zeta^2\right) \mathrm{erf}(\zeta). \tag{2.49b}$$

These two equations, jointly with (2.34g) (which gives $c_i = -m_l T_i$) result in a system of transcendental equations which allows us to calculate λ, T_i, and c_i. We find that

$$c_i = \frac{c_{l\infty}}{1 - (1-\alpha)F(\sqrt{\mathrm{Le}}\,\lambda)}, \tag{2.50a}$$

$$T_i = \frac{-k\mathrm{St}F(\lambda) + \kappa G\left(\frac{\lambda}{\sqrt{\kappa}}\right)\left(\rho F(\lambda) - \mathrm{St}T_{l\infty}\right)}{\mathrm{St}\left(kF(\lambda) - \kappa G\left(\frac{\lambda}{\sqrt{\kappa}}\right)\right)}, \tag{2.50b}$$

and

$$\frac{c_{l\infty}}{1 - (1-\alpha)F(\sqrt{\mathrm{Le}}\,\lambda)} = -m_l \frac{-k\mathrm{St}F(\lambda) + \kappa G\left(\frac{\lambda}{\sqrt{\kappa}}\right)\left(\rho F(\lambda) - \mathrm{St}T_{l\infty}\right)}{\mathrm{St}\left(kF(\lambda) - \kappa G\left(\frac{\lambda}{\sqrt{\kappa}}\right)\right)}. \tag{2.51}$$

Therefore, we have expressions c_i and T_i in terms of λ, and a transcendental equation (2.51) for λ which has to be solved numerically. It is not obvious if the value of λ is unique given a parameter configuration, but we can check its uniqueness numerically for our parameters of interest.

2.3.2.2 Infinite domain

Now we use the infinite domain boundary conditions (2.39), which written in terms of η read

$$T_s \to -1, \quad \text{and} \quad c_s \to c_{s\infty}, \quad \text{as } \eta \to -\infty, \tag{2.52a}$$

$$T_l \to T_{l\infty}, \quad \text{and} \quad c_l \to c_{l\infty}, \quad \text{as } \eta \to +\infty. \tag{2.52b}$$

Then the solutions to (2.34) with the boundary conditions (2.52) are

$$c_s(\eta) = c_{s\infty} + (\alpha c_i - c_{s\infty})\frac{\operatorname{erfc}(-\sqrt{\frac{\mathrm{Le}}{D}}\eta)}{\operatorname{erfc}(-\sqrt{\frac{\mathrm{Le}}{D}}\lambda)}, \tag{2.53a}$$

$$c_l(\eta) = c_{l\infty} + (c_i - c_{l\infty})\frac{\operatorname{erfc}(\sqrt{\mathrm{Le}}\,\eta)}{\operatorname{erfc}(\sqrt{\mathrm{Le}}\,\lambda)}, \tag{2.53b}$$

$$T_s(\eta) = -1 + (T_i + 1)\frac{\operatorname{erfc}\left(-\frac{\eta}{\sqrt{\kappa}}\right)}{\operatorname{erfc}\left(-\frac{\lambda}{\sqrt{\kappa}}\right)}, \tag{2.53c}$$

$$T_l(\eta) = T_{l\infty} + (T_i - T_{l\infty})\frac{\operatorname{erfc}(\eta)}{\operatorname{erfc}(\lambda)}. \tag{2.53d}$$

The interface conditions (2.34h) and (2.34i) now give

$$(1-\alpha)c_i = -\frac{\alpha c_i - c_{s\infty}}{F\left(-\sqrt{\frac{\mathrm{Le}}{D}}\lambda\right)} + \frac{c_i - c_{l\infty}}{F(\sqrt{\mathrm{Le}}\,\lambda)}, \tag{2.54a}$$

$$\frac{\rho}{\mathrm{St}} = -\frac{k}{\kappa}\frac{T_i + 1}{F\left(-\frac{\lambda}{\sqrt{\kappa}}\right)} + \frac{T_i - T_{l\infty}}{F(\lambda)}. \tag{2.54b}$$

In this case λ, T_i and c_i are given by

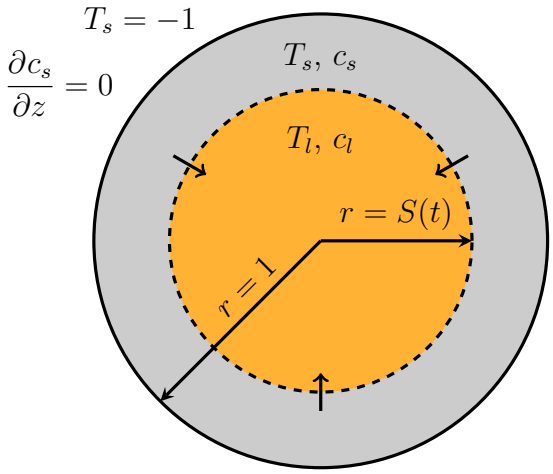
$$c_i = \frac{c_{l\infty}F\left(-\sqrt{\frac{\mathrm{Le}}{D}}\lambda\right) - c_{s\infty}F(\sqrt{\mathrm{Le}}\,\lambda)}{\left(1-(1-\alpha)F(\sqrt{\mathrm{Le}}\,\lambda)\right)F\left(-\sqrt{\frac{\mathrm{Le}}{D}}\lambda\right) - \alpha F(\sqrt{\mathrm{Le}}\,\lambda)}, \tag{2.55a}$$

$$T_i = -\frac{k\mathrm{St}F(\lambda) + \kappa F\left(-\frac{\lambda}{\sqrt{\kappa}}\right)(\rho F(\lambda) + \mathrm{St}T_{l\infty})}{\mathrm{St}\left(kF(\lambda) - \kappa F\left(-\frac{\lambda}{\sqrt{\kappa}}\right)\right)}, \tag{2.55b}$$

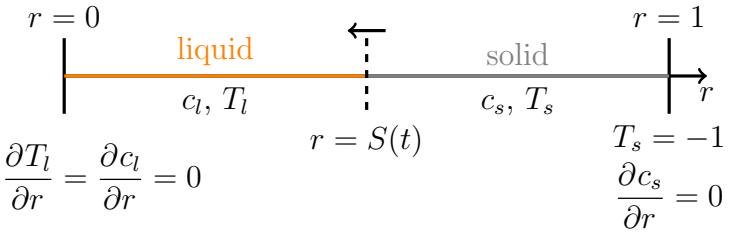
and

$$\frac{c_{l\infty}F\left(-\sqrt{\frac{\mathrm{Le}}{D}}\lambda\right) - c_{s\infty}F(\sqrt{\mathrm{Le}}\,\lambda)}{\left(1-(1-\alpha)F(\sqrt{\mathrm{Le}}\,\lambda)\right)F\left(-\sqrt{\frac{\mathrm{Le}}{D}}\lambda\right) - \alpha F(\sqrt{\mathrm{Le}}\,\lambda)} = m_l\frac{k\mathrm{St}F(\lambda) + \kappa F\left(-\frac{\lambda}{\sqrt{\kappa}}\right)(\rho F(\lambda) + \mathrm{St}T_{l\infty})}{\mathrm{St}\left(kF(\lambda) - \kappa F\left(-\frac{\lambda}{\sqrt{\kappa}}\right)\right)}. \tag{2.56}$$

Again, we need to solve (2.56) numerically for λ, and we cannot say anything about the uniqueness of the solution in general until we choose the parameter configuration. However, we can check numerically that for our parameter choice the solution is unique.



(a) The n-dimensional solidification problem with spherical symmetry.



(b) One-dimensional reduction.

Figure 2.5: Sketch of the n-dimensional solidification problem with radial symmetry (a). Due to this symmetry, the problem can be reduced to a one-dimensional model only in the radial component as shown in (b).

2.4 n-dimensional radially symmetric model

We are interested in the n-dimensional spherically symmetric model as well, which can be easily derived from the full model (2.33). Taking the length scale of the problem to be the radius of the particle, we can consider the n-dimensional spherical particle as a one-dimensional problem which depends only on the radial coordinate $r \in [0, 1]$. A sketch of the problem, and the one-dimensional reduction, is shown in Figure 2.5. When $n = 2$ we recover the radially symmetric cylinder problem, while when $n = 3$, we obtain the three-dimensional spherically symmetric problem.

2.4.1 Dimensionless model

We assume that the variables only depend on r and t, and thus the interface position is given by $f_i = r - S(t)$. Then, the model (2.33) reduces to the radially symmetric model (2.57). For the solid phase, which is given by $S(t) < r < 1$, the equations read

$$\frac{\partial c_s}{\partial t} = \frac{D}{\mathrm{Le}} \frac{1}{r^{n-1}} \frac{\partial}{\partial r} \left(r^{n-1} \frac{\partial c_s}{\partial r} \right), \tag{2.57a}$$

$$\frac{\partial T_s}{\partial t} = \kappa \frac{1}{r^{n-1}} \frac{\partial}{\partial r} \left(r^{n-1} \frac{\partial T_s}{\partial r} \right). \tag{2.57b}$$

The liquid phase is given by $0 < r < S(t)$, and the equations in this region of the domain are

$$\frac{\partial c_l}{\partial t} = \frac{1}{\mathrm{Le}} \frac{1}{r^{n-1}} \frac{\partial}{\partial r} \left(r^{n-1} \frac{\partial c_l}{\partial r} \right), \tag{2.57c}$$

$$\frac{\partial T_l}{\partial t} = \frac{1}{r^{n-1}} \frac{\partial}{\partial r} \left(r^{n-1} \frac{\partial T_l}{\partial r} \right). \tag{2.57d}$$

The interface is given by $r = S(t)$, and the interface conditions reduce to

$$T_s = T_l, \tag{2.57e}$$

$$c_s = \alpha c_l, \tag{2.57f}$$

$$c_l = -m_l T_l, \tag{2.57g}$$

$$\frac{\rho}{\mathrm{St}} \frac{\mathrm{d}S}{\mathrm{d}t} = k \frac{\partial T_s}{\partial r} - \frac{\partial T_l}{\partial r}, \tag{2.57h}$$

$$(1-\alpha) c_l \frac{\mathrm{d}S}{\mathrm{d}t} = \frac{D}{\mathrm{Le}} \frac{\partial c_s}{\partial r} - \frac{1}{\mathrm{Le}} \frac{\partial c_l}{\partial r}. \tag{2.57i}$$

The boundary conditions are given by

$$\frac{\partial T_l}{\partial r} = 0 \quad \text{and} \quad \frac{\partial c_l}{\partial r} = 0, \text{ at } r = 0, \tag{2.57j}$$

$$T_s = -1 \quad \text{and} \quad \frac{\partial c_s}{\partial r} = 0, \text{ at } r = 1, \tag{2.57k}$$

while the initial conditions read

$$S = 1, \quad T_l = T_0, \quad \text{and} \quad c_l = c_0. \tag{2.57l}$$

This model is used in Chapter 5 when we perform an asymptotic analysis of the solidification of a spherical droplet composed of a binary alloy, which corresponds to the $n = 3$ case.

2.5 Parameter values relevant to the solidification of silicon

In this section, we discuss the parameter values for the cast of metallurgical grade silicon. It is hard to measure the physical properties of silicon at high temperatures

Parameter	Typical value	Units	Source
ρ_s	2300	kg m^{-3}	[31]
ρ_l	2420	kg m^{-3}	[31]
c_{ps}	1000	J kg^{-1} K^{-1}	[31]
c_{pl}	1000	J kg^{-1} K^{-1}	[31]
k_s	22	W m^{-1} K^{-1}	[31]
k_l	64	W m^{-1} K^{-1}	[31]
κ_s	$9.57 \cdot 10^{-6}$	m^2 s^{-1}	*
κ_l	$2.64 \cdot 10^{-5}$	m^2 s^{-1}	*
D_s	$1.20 \cdot 10^{-9}$	m^2 s^{-1}	[90]
D_l	$6.79 \cdot 10^{-8}$	m^2 s^{-1}	[90]
L	$1.80 \cdot 10^{6}$	J kg^{-1}	[8]
α	$2 \cdot 10^{-3}$	-	[65]
α_s	$1.2 \cdot 10^{-2}$	kg m^{-3} K^{-1}	*
α_l	6	kg m^{-3} K^{-1}	†
T_{m0}	1683	K	[31]
T_c	298	K	-
$\mathcal{C}_0$	23	kg m^{-3}	†
$\mathcal{T}_0$	1713	K	†

Table 2.1: Typical parameter values for our problems. These values have been used to calculate the dimensionless numbers in Table 2.2. The symbol * means that the parameter value has been calculated from other parameters in the table. The symbol † means that the value was obtained from private communication with Elkem. The value for T_c is a modelling assumption.

and the data listed here comes from various sources. Most of the values are taken from [31], where many of the thermal properties are listed. The impurity diffusivities have been calculated from [90]. As the diffusivities are different for each element and in each phase, we have taken the maximum of the four diffusivities in each phase, as this gives us the smallest value of the Lewis number. Because in Chapters 4 and 5 we carry out an asymptotic analysis in the large Lewis number limit, we want to consider its smallest value as the "worst case scenario" to see if the analysis is valid. These diffusivities correspond to iron for the solid phase and aluminium for the liquid phase. In a similar way, because in the asymptotic analysis in Chapters 4 and 5 we assume small segregation coefficient α, we took the maximum value of the four elements according to the tabulated values in [65]. This value, jointly with the value for α_l given by Elkem in a private communication, has been used to calculate α_s. Finally, the latent heat of fusion has been taken from [8], and the environment temperature T_c is a modelling assumption which has been taken to be a typical value for the surrounding air, but which can be changed to describe different casting techniques. Notice that

Parameter	Typical value
St	0.77
Le	389
ρ	0.95
c_p	1
k	0.34
κ	0.36
m_s	0.72
m_l	360
D	$1.76 \cdot 10^{-2}$
α	$2 \cdot 10^{-3}$
c_0	10^{-2}
T_0	$2.17 \cdot 10^{-2}$

Table 2.2: Typical dimensionless parameter values for our problems. These values have been calculated from the expressions in (2.32) using the parameter values given in Table 2.1.

we have taken a very low value of T_c which corresponds to the "worst case scenario" for the small Stefan number analysis in Chapter 5. All of the relevant parameter values are listed in Table 2.1. We use these values to calculate the non-dimensional parameters of the system, which are given in Table 2.2.

We notice that the Stefan number is smaller than one and the Lewis number is very large, and both properties are exploited in Chapters 4 and 5 for the asymptotic analysis. We observe that ρ, c_p, k, and κ are all order one parameters. The small amount of expansion during solidification is reflected by the fact that ρ is only slightly less than unity. We observe that the supercooling coefficient for the liquid phase, m_l, is very large, while in the solid phase, m_s, is small. Both supercooling coefficients are related by the segregation coefficient, α, which is very small. Finally, the ratio between impurity diffusivities, D, is small since diffusivity is much smaller in the solid phase.

2.6 Discussion

In this section, we have presented the models for the various solidification problems to be analysed in the following chapters. We have started by deriving the problem for a general n-dimensional geometry from basic principles including the conservation of heat and mass in each phase and across the interface. In order to model the constitutional supercooling that couples the heat and mass transfer problems, we

have taken a linearised form of the phase diagram which is valid in the limit we are concerned with. The general model was closed with boundary and initial conditions. We then proceeded to non-dimensionalise the problem.

From the general dimensionless problem we then derived the models for the one-dimensional planar geometry and the n-dimensional radially symmetric geometry. For the first geometry, we considered three cases: the symmetric finite domain (which shall be considered further in the asymptotic analysis of Chapter 4) and the semi-infinite and infinite geometries for which we gave self-similar solutions (the stability of which will be studied in Chapter 3). We formulated the n-dimensional radially symmetric problem, which we shall consider more closely in the $n = 3$ case of solidifying sphere, in Chapter 5. We concluded with a discussion of the parameter values relevant for the particular case of casting of metallurgical grade silicon.

We start the analysis of these models in the next chapter, in which we study the linear stability of the self-similar solutions for the Cartesian one-dimensional model in semi-infinite and finite geometries. In Chapter 4 we calculate the asymptotic solutions to the planar finite geometry problem in the limit of large Lewis number. Finally, in Chapter 5, we determine asymptotic solutions to the three-dimensional spherically symmetric problem in the limit of large Lewis number and small Stefan number.

Chapter 3

Stability analysis of the self-similar solutions

3.1 Introduction

It is well known that when binary alloys solidify they can create a granular structure, where the solid is formed by large regions of a crystalline structure of the main phase, known as grains, and with small layers of impurities (or other phases) in between. For metallurgical grade silicon, grains of pure silicon with layers of impurities in between, composed mainly of iron, aluminium, calcium, titanium, and silicon are often observed in experiments. The grain structure and impurity layers for a silicon sample are shown in Figures 1.3 and 1.4. The size and distribution of these grains has a large impact on the quality of the final product. These structures appear when the solidification process is not controlled, so specific casting methods are often used in order to obtain single crystal grains of high purity silicon, like the Czochralski process [31] or directional solidification [5]. The formation of these grains can be seen as the breakdown of the planar solidification front, and this is one reason why there is an interest in studying the stability of the solutions to the Stefan problem we previously formulated for the solidification process.

There has been much work carried out on the directional solidification process, in the case where the velocity of the solidification front is constant and known. In such cases, by adopting a coordinate system relative to the front, the stability problem can be reduced to a stability analysis around a steady state, greatly simplifying the analysis. The stability analysis for the steady solidification binary alloy problem was first considered by Mullins and Sekerka [66], who considered the two-dimensional problem in an infinite domain under infinitesimal sinusoidal perturbations. By assuming that the velocity of the solidification front is both constant and known, they obtained a

steady state base solution, and found that the phenomenon which causes the instability in the problem is constitutional supercooling. This analysis was extended by Wollkind and Segel [104] to perturbations on a finite domain. The main difference between their analysis and that in [66] is that, for some parameter configurations, there is a subcritical instability and a non-trivial equilibrium point that was not predicted in [66]. This type of analysis has proven useful for modelling directional solidification, since in this case the velocity of the solidification front can be controlled in practical situations.

However, we are interested in casting methods where there is little control over the heat exchange, therefore the assumption of constant velocity for the solidification front is no longer reasonable. For non-finite geometries, for example, we expect a self-similar motion where the interface position scales with the square root of time, as shown in Section 2.3.2, and, as shown in [8], this is the behaviour we observe in the casting methods we are interested in. Therefore, to understand the stability of these solutions the analysis presented in [66] is no longer valid and we need to consider the variation in the velocity of the solidification front. This necessity was already highlighted in [56] and, therefore, it is this type of solidification which we shall focus our efforts on.

The stability analysis for non-steady solidification problems, in particular the problem of the self-similar motion of a solidification front, was first studied by Coriell et al. in [15], where exact one-dimensional self-similar solutions were obtained in an infinite domain and a stability analysis was performed. The stability analysis presented addresses a particular type of possible perturbation in terms of parabolic cylinder functions. However, as we show in this chapter, this is not the most general type of perturbation that can be considered for this type of problem, because it only considers one of the two families of perturbations that exist. Alexandrov extended the analysis to two-dimensional domains in [2, 3]. The analysis in both papers is based on the one-dimensional stability analysis described in [15] so, again, the perturbations considered are not the most general ones possible. In [2] there are no assumptions made on the conditions for the transverse coordinate, whereas in [3] the assumption that the perturbations are linear in the transverse direction is taken. The stability of the two-dimensional problem solutions in a semi-infinite domain has been considered as well in [54], using a frozen-time approach. This approach allows the authors to find the wavelength of the two-dimensional perturbations, but the result does not match the observed grain size well.

3.1.1 Outline of the chapter

In this chapter, we perform a comprehensive stability analysis for the one-dimensional binary alloy solidification problem due to self-similar motion of a planar solidification front. This analysis extends the results of [15] for a more general type of perturbation in both the infinite and semi-infinite domain problems. The results of this chapter have been published in [10].

The remainder of this chapter is structured as follows. In Section 3.2 we formulate the general linear stability problem, obtaining a more general form of perturbation than the one used in [2, 3, 15]. We apply this stability analysis to the semi-infinite domain problem (which has not been considered in the literature) in Section 3.3, and we find that the system admits only one type of perturbation, and show that solutions to this problem are unstable under this perturbation for any parameter regime. In Section 3.4 we perform the corresponding analysis for the infinite domain, and we find that the problem admits two families of perturbations: a stable one, and an unstable one. Therefore, we find that, again, the problem is unstable regardless of the parameter choice (thereby generalising results in [15]). We give a discussion of these results in Section 3.5.

3.2 The linear stability problem

As we are interested in the stability of the one-dimensional self-similar motion of a solidification front, we want to study the semi-infinite and infinite domain geometry models described in Section 2.3. These models have well-known self-similar solutions, which are the base states that we perturb in our linear stability analysis.

The model we want to study is described by (2.34). Notice that the dimensionless problem here is different from the one presented in [10] because in [10] we used the mass diffusion time scale rather than the thermal diffusion time scale used throughout this thesis. However, this change in the time scale has no relevance to the outcome of the stability analysis.

In order to perform a stability analysis for the solidification of a binary alloy, we

introduce the perturbed solutions

$$c_{s,pert} = c_{s0}(t,z) + \delta c_{s1}(t,z), \tag{3.1a}$$
$$c_{l,pert} = c_{l0}(t,z) + \delta c_{l1}(t,z), \tag{3.1b}$$
$$T_{s,pert} = T_{s0}(t,z) + \delta T_{s1}(t,z), \tag{3.1c}$$
$$T_{l,pert} = T_{l0}(t,z) + \delta T_{l1}(t,z), \tag{3.1d}$$
$$S_{pert} = S_0(t) + \delta S_1(t), \tag{3.1e}$$

where c_{s0}, c_{l0}, T_{s0}, T_{l0}, and S_0 are the base state self-similar solutions determined in Section 2.3.2. We assume that $0 < \delta \ll 1$ is a small parameter which measures the size of the perturbation. We will say that the system is unstable if any of the perturbations grows unboundedly in time. Notice that the interface position itself grows unboundedly in time, so we will consider the absolute size of S_1, not the relative size of S_1 to the base state S_0, for the stability criteria. Hence, an unstable solution is one for which the perturbation grows unboundedly away from the base state in time.

The $\mathcal{O}(1)$ problem reduces to (2.34), as expected. Meanwhile, $\mathcal{O}(\delta)$ perturbation equations are

$$\frac{\partial c_{s1}}{\partial t} = \frac{D}{\mathrm{Le}}\frac{\partial^2 c_{s1}}{\partial z^2}, \tag{3.2a}$$
$$\frac{\partial T_{s1}}{\partial t} = \kappa\frac{\partial^2 T_{s1}}{\partial z^2}, \tag{3.2b}$$
$$\frac{\partial c_{l1}}{\partial t} = \frac{1}{\mathrm{Le}}\frac{\partial^2 c_{l1}}{\partial z^2}, \tag{3.2c}$$
$$\frac{\partial T_{l1}}{\partial t} = \frac{\partial^2 T_{l1}}{\partial z^2}, \tag{3.2d}$$

while at the interface $z = S_0(t)$, the $\mathcal{O}(\delta)$ conditions are

$$S_1\frac{\partial T_{s0}}{\partial z} + T_{s1} = S_1\frac{\partial T_{l0}}{\partial z} + T_{l1}, \tag{3.2e}$$
$$S_1\frac{\partial c_{s0}}{\partial z} + c_{s1} = -m_s\left(S_1\frac{\partial T_{s0}}{\partial z} + T_{s1}\right), \tag{3.2f}$$
$$S_1\frac{\partial c_{l0}}{\partial z} + c_{l1} = -m_l\left(S_1\frac{\partial T_{l0}}{\partial z} + T_{l1}\right), \tag{3.2g}$$
$$\frac{\rho}{\mathrm{St}}\frac{\mathrm{d}S_1}{\mathrm{d}t} = k\left(S_1\frac{\partial^2 T_{s0}}{\partial z^2} + \frac{\partial T_{s1}}{\partial z}\right) - \left(S_1\frac{\partial^2 T_{l0}}{\partial z^2} + \frac{\partial T_{l1}}{\partial z}\right), \tag{3.2h}$$

$$(1-\alpha)\left[\left(S_1\frac{\partial c_{l0}}{\partial z} + c_{l1}\right)\frac{\mathrm{d}S_0}{\mathrm{d}t} + c_{l0}\frac{\mathrm{d}S_1}{\mathrm{d}t}\right] = \frac{D}{\mathrm{Le}}\left(S_1\frac{\partial^2 c_{s0}}{\partial z^2} + \frac{\partial c_{s1}}{\partial z}\right) - \frac{1}{\mathrm{Le}}\left(S_1\frac{\partial^2 c_{l0}}{\partial z^2} + \frac{\partial c_{l1}}{\partial z}\right). \tag{3.2i}$$

Notice that the linearisation of the interface condition reduces the initial free boundary problem to a moving boundary problem, as now the position of the interface $S_0(t)$ is known.

The first order perturbation terms are subject to boundary conditions which depend on the domain considered. For the semi-infinite domain problem, we have

$$T_{s1} = 0 \qquad \text{and} \qquad \frac{\partial c_{s1}}{\partial z} = 0 \qquad \text{at } z = 0, \tag{3.3a}$$

$$T_{l1} \to 0 \qquad \text{and} \qquad c_{l1} \to 0 \qquad \text{as } z \to +\infty. \tag{3.3b}$$

while for the infinite problem we have

$$T_{s1} \to 0 \qquad \text{and} \qquad c_{s1} \to 0 \qquad \text{as } z \to -\infty, \tag{3.4a}$$

$$T_{l1} \to 0 \qquad \text{and} \qquad c_{l1} \to 0 \qquad \text{as } z \to +\infty, \tag{3.4b}$$

We again make use of the similarity variable $\eta = \frac{z}{2\sqrt{t}}$, where the interface $z = S_0(t) = 2\lambda\sqrt{t}$ is at $\eta = \lambda$, but note that the solutions may still depend on time such as $c_{s1}(t, \eta)$. Changing variables from (t, z) to (t, η) in the governing PDEs (3.2a)-(3.2d), we obtain

$$\frac{\partial c_{s1}}{\partial t} = \frac{1}{4t}\frac{D}{\mathrm{Le}}\frac{\partial^2 c_{s1}}{\partial \eta^2} + \frac{\eta}{2t}\frac{\partial c_{s1}}{\partial \eta}, \tag{3.5a}$$

$$\frac{\partial T_{s1}}{\partial t} = \frac{\kappa}{4t}\frac{\partial^2 T_{s1}}{\partial \eta^2} + \frac{\eta}{2t}\frac{\partial T_{s1}}{\partial \eta}, \tag{3.5b}$$

$$\frac{\partial c_{l1}}{\partial t} = \frac{1}{4t}\frac{1}{\mathrm{Le}}\frac{\partial^2 c_{l1}}{\partial \eta^2} + \frac{\eta}{2t}\frac{\partial c_{l1}}{\partial \eta}, \tag{3.5c}$$

$$\frac{\partial T_{l1}}{\partial t} = \frac{1}{4t}\frac{\partial^2 T_{l1}}{\partial \eta^2} + \frac{\eta}{2t}\frac{\partial T_{l1}}{\partial \eta}. \tag{3.5d}$$

Seeking solutions to (3.5) by separation of variables, and using the interface conditions (3.2e)-(3.2i) to determine the exponents of the time powers, we conclude that these must take the form

$$c_{s1} = C_{c_s} t^{\beta} f_{c_s}(\eta), \tag{3.6a}$$

$$T_{s1} = C_{T_s} t^{\beta} f_{T_s}(\eta), \tag{3.6b}$$

$$c_{l1} = C_{c_l} t^{\beta} f_{c_l}(\eta), \tag{3.6c}$$

$$T_{l1} = C_{T_l} t^{\beta} f_{T_l}(\eta), \tag{3.6d}$$

$$S_1 = C_S t^{\beta + \frac{1}{2}}, \tag{3.6e}$$

where C_j are constants to be determined and f_j are the corresponding functions in η where $j \in \{c_s, T_s, c_l, T_l\}$ which we still have to find. We have chosen not to include C_j

into f_j as this will be convenient later in the analysis. Observe that the stability of the problem is dictated by the position of the interface, S_1, since this has the highest power of t and therefore it can be viewed as the least stable term. Hence, as the time exponent in the interface perturbation is $\beta + \frac{1}{2}$, we conclude that the system is unstable if $\beta > -\frac{1}{2}$, as for this case we can always find a perturbation to the system that grows unboudedly in time. Notice as well that, given that S_1 is the perturbation dictating the stability of the system and it only depends on t, the choice of the norm for the stability analysis does not matter as

$$\|S_0(t) - S_{pert}(t)\|_l = \|S_0(t) - S_0(t) - \delta S_1(t)\|_l = \|\delta S_1(t)\|_l = \delta |C_S||t|^{\beta+\frac{1}{2}}, \tag{3.7}$$

for any $l \in \mathbb{N}$. However, notice that if one wanted to show stability of the concentration or temperature fields, then one would have to show completeness of the basis of perturbations and in that case the choice of the norm would be relevant.

Using (3.6), the interface conditions (3.2e)-(3.2i) become

$$C_S \frac{T'_{s0}(\lambda)}{2} + C_{T_s} f_{T_s}(\lambda) = C_S \frac{T'_{l0}(\lambda)}{2} + C_{T_l} f_{T_l}(\lambda), \tag{3.8a}$$

$$C_S \frac{c'_{s0}(\lambda)}{2} + C_{c_s} f_{c_s}(\lambda) = -m_s \left(C_S \frac{T'_{s0}(\lambda)}{2} + C_{T_s} f_{T_s}(\lambda) \right), \tag{3.8b}$$

$$C_S \frac{c'_{l0}(\lambda)}{2} + C_{c_l} f_{c_l}(\lambda) = -m_l \left(C_S \frac{T'_{l0}(\lambda)}{2} + C_{T_l} f_{T_l}(\lambda) \right), \tag{3.8c}$$

$$C_S \left(\beta + \frac{1}{2} \right) \frac{\rho}{\mathrm{St}} = k \left(C_S \frac{T''_{s0}(\lambda)}{4} + C_{T_s} \frac{f'_{T_s}(\lambda)}{2} \right) - \left(C_S \frac{T''_{l0}(\lambda)}{4} + C_{T_l} \frac{f'_{T_l}(\lambda)}{2} \right), \tag{3.8d}$$

$$\begin{aligned} (1-\alpha) \left[\left(C_S \frac{c'_{l0}(\lambda)}{2} + C_{c_l} f_{c_l}(\lambda) \right) \lambda + C_S \left(\beta + \frac{1}{2} \right) c_i \right] \\ = \frac{D}{\mathrm{Le}} \left(C_S \frac{c''_{s0}(\lambda)}{4} + C_{c_s} \frac{f'_{c_s}(\lambda)}{2} \right) - \frac{1}{\mathrm{Le}} \left(C_S \frac{c''_{l0}(\lambda)}{4} + C_{c_l} \frac{f'_{c_l}(\lambda)}{2} \right), \end{aligned} \tag{3.8e}$$

where prime denotes differentiation with respect to the similarity variable, η. Observe that we have a homogeneous linear system of five equations for the five unknowns C_{c_s}, C_{c_l}, C_{T_s}, C_{T_l}, and C_S. Thus, if the system is of full rank, the only solution is the trivial solution. In order to have non-trivial solutions we need the determinant of the system to be zero. This condition determines the value (or values) of β where non-trivial solutions exist.

In order to find the functions $f_j(\eta)$ defined in (3.6), we need to solve the ODE obtained from using separation of variables in (3.5)

$$\frac{\mu_j}{4} f''_j(\eta) + \frac{\eta}{2} f'_j(\eta) - \beta f_j(\eta) = 0, \tag{3.9}$$

where μ_j are known constants which are different for each field j (for example, $\mu_{T_s} = \kappa$). Introducing the change of variable $\zeta_j = \frac{\eta}{\sqrt{\mu_j}}$, the solution is given by $f(\zeta_j) = C_j^{(P)} P_\beta(\zeta_j) + C_j^{(Q)} Q_\beta(\zeta_j)$, where we define

$$P_\beta(\zeta_j) = e^{-\zeta_j^2} \zeta_j M\left(\beta + 1, \frac{3}{2}, \zeta_j^2\right), \tag{3.10a}$$

$$Q_\beta(\zeta_j) = e^{-\zeta_j^2} \zeta_j U\left(\beta + 1, \frac{3}{2}, \zeta_j^2\right). \tag{3.10b}$$

Here $M(a, b, \zeta_j)$ and $U(a, b, \zeta_j)$ are Kummer's hypergeometric functions (see [1] for details). We restrict all the subsequent analysis to the case where β is real. We have not considered complex values of β in our analysis because some of the steps require the coefficients of the Kummer's hypergeometric functions to be real. Note that in the case where β is a negative integer, the two Kummer's functions are no longer linearly independent so we need to find a second linearly independent solution. However, this case is not relevant for our analysis, as from (3.6) we know that for these values of β all of the perturbations are stable, hence we do not consider it.

3.3 Stability analysis of the semi-infinite domain problem

In this section, we perform the stability analysis for the semi-infinite domain problem described in Section 2.3.2.1. As a reminder, in the semi-infinite domain (2.47a) gives $c_{s0} = \alpha c_i$ is constant, therefore $c'_{s0}(\eta) = c''_{s0}(\eta) = 0$, which significantly simplifies the problem.

Boundary conditions for the semi-infinite domain problem are given by (3.3) so, using (3.6), we can rewrite them as $f_{T_s}(0) = 0$, $f'_{c_s}(0) = 0$, and $f_j(\eta) \to 0$ as $\eta \to +\infty$, for the case of $j = T_l, c_l$. Yet, from [1], we know that in the limit $\eta \to 0^+$ we have

$$P_\beta(\eta) = \eta + \mathcal{O}\left(\eta^3\right), \tag{3.11a}$$

$$Q_\beta(\eta) = \frac{\sqrt{\pi}}{\Gamma(1+\beta)} + \mathcal{O}(\eta). \tag{3.11b}$$

Hence, for $f_{T_s}(0) = 0$, we have

$$f_{T_s}(0) = C_{T_s}^{(Q)} \sqrt{\pi} / \Gamma(1+\beta) = 0, \tag{3.12}$$

and because we know that β is not a negative integer, we require $C_{T_s}^{(Q)} = 0$. For $f'_{c_s}(0) = 0$, we therefore have

$$f'_{c_s}(0) = \sqrt{\frac{\mathrm{Le}}{D}} \left(C_{c_s}^{(P)} + C_{c_s}^{(Q)} U\left(\beta + 1, \frac{3}{2}, 0\right)\right) = 0, \tag{3.13}$$

from [1] we have that in the limit $\eta \to 0^+$

$$U\left(\beta+1, \frac{3}{2}, \eta^2\right) = \frac{\sqrt{\pi}}{\Gamma(1+\beta)}\frac{1}{\eta} + \mathcal{O}\left(1\right), \tag{3.14}$$

and because β is not a negative integer it blows up. Therefore, we need $C_{c_s}^{(Q)} = 0$, which implies $C_{c_s}^{(P)} = 0$. Then, the perturbation has the form $f_{c_s}(\eta) = 0$.

For the liquid phase, we need $f_j(\eta)$ with $j = T_l, c_l$ to decay as $\eta \to +\infty$. From [1], we know that

$$P_\beta\left(\eta\right) = \eta^{2\beta}\frac{\sqrt{\pi}}{2\Gamma(\beta+1)}\left(\sum_{n=0}^{N-1}\frac{(\frac{1}{2}-\beta)_n(-\beta)_n}{n!}\eta^{-2n} + \mathcal{O}\left(\eta^{-2N}\right)\right), \tag{3.15a}$$

$$Q_\beta\left(\eta\right) = e^{-\eta^2}\eta^{-2\beta-1}\left(\sum_{n=0}^{N-1}(-1)^n\frac{(\beta+1)_n(\beta+\frac{1}{2})_n}{n!}\eta^{-2n} + \mathcal{O}\left(\eta^{-2N}\right)\right), \tag{3.15b}$$

as $\eta \to +\infty$, where $(a)_n = \Gamma(a+n)/\Gamma(a)$ is Pochhammer's symbol. Notice that $Q_\beta(\eta)$ decays for any choice of β. In order for $P_\beta(\eta)$ to satisfy the boundary conditions, we need $\beta < 0$. Therefore, if we want $f_j(\eta)$ with $j = T_l, c_l$ to satisfy the boundary conditions at $\eta \to +\infty$, we require either $\beta < 0$ or $C_j^{(P)} = 0$. Then, we must separately study the cases $\beta \geq 0$ and $\beta < 0$.

Summarising, for the semi-infinite domain, we can conclude that the perturbations for $\beta \geq 0$ are of the form

$$c_{s1}(t,\eta) = 0, \tag{3.16a}$$

$$T_{s1}(t,\eta) = C_{T_s}t^\beta P_\beta\left(\frac{\eta}{\sqrt{\kappa}}\right), \tag{3.16b}$$

$$c_{l1}(t,\eta) = C_{c_l}t^\beta Q_\beta\left(\sqrt{\mathrm{Le}}\,\eta\right), \tag{3.16c}$$

$$T_{l1}(t,\eta) = C_{T_l}t^\beta Q_\beta\left(\eta\right), \tag{3.16d}$$

while for $\beta < 0$ we have that the perturbations take the form

$$c_{s1}(t,\eta) = 0, \tag{3.17a}$$

$$T_{s1}(t,\eta) = C_{T_s}t^\beta P_\beta\left(\frac{\eta}{\sqrt{\kappa}}\right), \tag{3.17b}$$

$$c_{l1}(t,\eta) = t^\beta\left(C_{c_l}^{(P)}P_\beta\left(\sqrt{\mathrm{Le}}\,\eta\right) + C_{c_l}^{(Q)}Q_\beta\left(\sqrt{\mathrm{Le}}\,\eta\right)\right), \tag{3.17c}$$

$$T_{l1}(t,\eta) = t^\beta\left(C_{T_l}^{(P)}P_\beta\left(\eta\right) + C_{T_l}^{(Q)}Q_\beta\left(\eta\right)\right), \tag{3.17d}$$

where the C_j's are constants.

3.3.1 No instability for $\beta \geq 0$

In the case where $\beta \geq 0$, we have (3.16), therefore we do not need to determine C_{c_s}, since $f_{c_s}(\eta) = 0$. The system (3.8) now reduces to an overdetermined system of five equations with four unknowns. In order to have non-trivial solutions, we require all 4×4 minors to be equal to zero. This will give five conditions, which can be shown to be equivalent to two algebraic conditions. Using the relations

$$\frac{T''_{s0}(\eta)}{T'_{s0}(\eta)} = -\frac{2\eta}{\kappa}, \quad \frac{T''_{l0}(\eta)}{T'_{l0}(\eta)} = -2\eta, \quad \text{and} \quad \frac{c''_{l0}(\eta)}{c'_{l0}(\eta)} = -2\eta\text{Le}, \tag{3.18}$$

and defining

$$\mathcal{M}_\beta(\lambda;\mu) = \lim_{\eta\to\lambda} \frac{\mathrm{d}}{\mathrm{d}\eta} \ln\left(P_\beta\left(\frac{\eta}{\sqrt{\mu}}\right)\right), \tag{3.19a}$$

$$\mathcal{U}_\beta(\lambda;\mu) = \lim_{\eta\to\lambda} \frac{\mathrm{d}}{\mathrm{d}\eta} \ln\left(Q_\beta\left(\frac{\eta}{\sqrt{\mu}}\right)\right), \tag{3.19b}$$

we can rewrite these two algebraic conditions as

$$k\left(\mathcal{M}_\beta(\lambda;\kappa) + \frac{2\lambda}{\kappa}\right) T'_{s0}(\lambda) - \left(\mathcal{U}_\beta(\lambda;1) + 2\lambda\right) T'_{l0}(\lambda) + 4\left(\beta + \frac{1}{2}\right)\frac{\rho}{\text{St}} = 0, \tag{3.20}$$

$$-\frac{1}{\text{Le}}(\mathcal{U}_\beta\left(\lambda;\text{Le}^{-1}\right) + 2\lambda\text{Le})c'_{l0}(\lambda) + 4\left(\beta + \frac{1}{2}\right)(1-\alpha)c_i = 0. \tag{3.21}$$

We want to show that there is no value of β that solves the system (3.20)-(3.21) for any choice of the model parameters. Using the definition of c_i in (2.50a), we know that $[c_i - c_{l\infty}]/F(\sqrt{\text{Le}}\,\lambda) = (1-\alpha)c_i$, hence we can rewrite (3.21) as

$$\left(1 - 2\lambda^2\text{Le}(\beta+1)\frac{U\left(\beta+2,\frac{5}{2},\text{Le}\,\lambda^2\right)}{U\left(\beta+1,\frac{3}{2},\text{Le}\,\lambda^2\right)}\right) + 2\left(\beta+\frac{1}{2}\right) = 0, \tag{3.22}$$

which can be rearranged into

$$2\left(\beta+1\right) - 2\lambda^2\text{Le}(\beta+1)\frac{U\left(\beta+2,\frac{5}{2},\text{Le}\,\lambda^2\right)}{U\left(\beta+1,\frac{3}{2},\text{Le}\,\lambda^2\right)} = 0. \tag{3.23}$$

We now have to show that if $\beta \geq 0$ there are no finite values of λ that satisfy (3.23), which can be reduced to

$$U\left(\beta+1,\frac{3}{2},\text{Le}\,\lambda^2\right) - \text{Le}\lambda^2 U\left(\beta+2,\frac{5}{2},\text{Le}\,\lambda^2\right) = 0, \tag{3.24}$$

and using identity 13.4.18 in [1], we find

$$U\left(\beta+1,\frac{3}{2},\text{Le}\,\lambda^2\right) - \text{Le}\,\lambda^2 U\left(\beta+2,\frac{5}{2},\text{Le}\,\lambda^2\right) = \left(\beta+\frac{1}{2}\right) U\left(\beta+2,\frac{3}{2},\text{Le}\,\lambda^2\right). \tag{3.25}$$

Hence, condition (3.21) is equivalent to

$$U\left(\beta+2,\frac{3}{2},\mathrm{Le}\,\lambda^2\right)=0. \tag{3.26}$$

However, as both a and b in $U(a,b,z)$ are positive, we can use the definition 13.2.6 in [1], which says

$$U(a,b,z)=\frac{e^z}{\Gamma(a)}\int_1^{+\infty}e^{-zt}(t-1)^{a-1}t^{b-a-1}\mathrm{d}t, \tag{3.27}$$

and as all the factors in (3.27) are positive for $t>1$, we conclude that there are no finite values of λ satisfying (3.22).

We can conclude that, for the semi-infinite domain and $\beta\geq 0$, there are no perturbations that satisfy the stability problem. Therefore, the temperature and concentration fields are always stable, so the instability in the problem will be driven by the position of the interface. This is reasonable, in light of the fact that the individual diffusion PDEs are stable, and motivates us to consider the situation where only the interface develops an instability, i.e. $-\frac{1}{2}\leq\beta<0$.

3.3.2 Instability for $-\frac{1}{2}\leq\beta<0$

For this case, the interface can lose stability even though the concentration and temperature fields are stable. From (3.6), this means that $-\frac{1}{2}\leq\beta<0$. For $\beta<0$ (and β not a negative integer), we have (3.17). Therefore, we have six unknowns and five equations to determine them. Normalising the perturbations with their value at the interface ($\eta=\lambda$) and after some manipulation, the system (3.8) can be written as $A_{semi}(\beta)\mathbf{C}_{semi}(\beta)=\mathbf{0}$, where

$$A_{semi}(\beta)=\begin{pmatrix}\mathbf{A}^1_{semi}(\beta) & \mathbf{A}^2_{semi}(\beta) & \mathbf{A}^3_{semi}(\beta) & \mathbf{A}^4_{semi}(\beta) & \mathbf{A}^5_{semi}(\beta) & \mathbf{A}^6_{semi}(\beta)\end{pmatrix}, \tag{3.28}$$

with

$$\mathbf{A}^1_{semi}(\beta) = \begin{pmatrix} 0 \\ 1 \\ 0 \\ \frac{k}{2}\mathcal{M}_\beta(\lambda;\kappa) \\ 0 \end{pmatrix}, \quad \mathbf{A}^4_{semi}(\beta) = \begin{pmatrix} 0 \\ 0 \\ 1 \\ 0 \\ -\frac{1}{2\mathrm{Le}}\mathcal{M}_\beta(\lambda;\mathrm{Le}^{-1}) \end{pmatrix},$$

$$\mathbf{A}^2_{semi}(\beta) = \begin{pmatrix} 1 \\ 0 \\ 0 \\ -\frac{1}{2}\mathcal{M}_\beta(\lambda;1) \\ 0 \end{pmatrix}, \quad \mathbf{A}^5_{semi}(\beta) = \begin{pmatrix} 0 \\ 0 \\ 1 \\ 0 \\ -\frac{1}{2\mathrm{Le}}\mathcal{U}_\beta(\lambda;\mathrm{Le}^{-1}) \end{pmatrix},$$

$$\mathbf{A}^3_{semi}(\beta) = \begin{pmatrix} 1 \\ 0 \\ 0 \\ -\frac{1}{2}\mathcal{U}_\beta(\lambda;1) \\ 0 \end{pmatrix}, \quad \mathbf{A}^6_{semi}(\beta) = \begin{pmatrix} \frac{1}{2}T'_{l0}(\lambda) \\ \frac{1}{2}T'_{s0}(\lambda) \\ \frac{1}{2}c'_{l0}(\lambda) \\ \frac{1}{4}\left[kT''_{s0}(\lambda) - T''_{l0}(\lambda)\right] - \left(\beta+\frac{1}{2}\right)\frac{\rho}{\mathrm{St}} \\ -\frac{1}{4}\frac{c''_{l0}(\lambda)}{\mathrm{Le}} - \left(\beta+\frac{1}{2}\right)(1-\alpha)c_i \end{pmatrix}, \tag{3.29}$$

and

$$\mathbf{C}_{semi}(\beta) = \left(C_{T_s}(\beta),\ C^{(P)}_{T_l}(\beta),\ C^{(Q)}_{T_l}(\beta),\ C^{(P)}_{c_l}(\beta),\ C^{(Q)}_{c_l}(\beta),\ C_S(\beta)\right)^T. \tag{3.30}$$

The components in $\mathbf{C}_{semi}(\beta)$ are the relative sizes of the perturbations.

If we take the 5×5 minor given by the first five columns of A_{semi}, we find that the determinant is

$$\det\left(A_{semi}(\beta)\right) = \frac{1}{4}\left(\mathcal{M}_\beta(\lambda;1) - \mathcal{U}_\beta(\lambda;1)\right)\left(\mathcal{M}_\beta(\lambda;\mathrm{Le}^{-1}) - \mathcal{U}_\beta(\lambda;\mathrm{Le}^{-1})\right). \tag{3.31}$$

We have to show that

$$\mathcal{M}_\beta(\lambda;\mu) - \mathcal{U}_\beta(\lambda;\mu) \neq 0, \tag{3.32}$$

for any $\lambda \neq 0$ and $\mu > 0$, so that matrix is always of full rank. From the rank-nullity theorem, we conclude that the kernel of the matrix has dimension one.

As μ only introduces a rescaling in λ, without loss of generality we can reduce (3.32) to the case

$$\mathcal{M}_\beta(\lambda;1) - \mathcal{U}_\beta(\lambda;1) \neq 0, \tag{3.33}$$

with $\lambda > 0$. Note that (3.33) can be expanded to obtain

$$2(\beta+1)\lambda\left[\frac{2}{3}\frac{M\left(\beta+2,\frac{5}{2},\lambda^2\right)}{M\left(\beta+1,\frac{3}{2},\lambda^2\right)} + \frac{U\left(\beta+2,\frac{5}{2},\lambda^2\right)}{U\left(\beta+1,\frac{3}{2},\lambda^2\right)}\right] \neq 0, \tag{3.34}$$

or, equivalently,

$$\frac{2}{3}M\left(\beta+2,\frac{5}{2},\lambda^2\right)U\left(\beta+1,\frac{3}{2},\lambda^2\right)+M\left(\beta+1,\frac{3}{2},\lambda^2\right)M\left(\beta+1,\frac{3}{2},\lambda^2\right)\neq 0. \tag{3.35}$$

Recall that we have already shown that if a and b are greater than zero, $U(a,b,z)$ is always positive for $z>0$. Similarly, we have that $M(a,b,z)$ for $a,b>0$ can be written as (see 13.2.1 in [1])

$$M(a,b,z)=\frac{\Gamma(b)}{\Gamma(a)\Gamma(b-a)}\int_0^1 e^{zt}t^{a-1}(1-t)^{b-a-1}\mathrm{d}t, \tag{3.36}$$

and as all the factors are greater than zero, we conclude that $M(a,b,z)$ is always greater than zero for $a,b>0$. Therefore, this proves (3.32).

The amplitudes $\mathbf{C}_{semi}(\beta)$ are given by linear combinations of the elements of the kernel of the matrix $A_{semi}(\beta)$. For the semi-infinite domain the kernel is generated by the vector

$$\mathbf{u}_{semi}(\beta)=\begin{pmatrix} -\frac{1}{2}T'_{s0}(\lambda) \\ -\dfrac{k\left(\mathcal{M}_\beta\left(\lambda;\kappa\right)+\frac{2\lambda}{\kappa}\right)T'_{s0}(\lambda)-\left(\mathcal{U}_\beta\left(\lambda;1\right)+2\lambda\right)T'_{l0}(\lambda)+4\left(\beta+\frac{1}{2}\right)\frac{\rho}{\mathrm{St}}}{2\left[\mathcal{M}_\beta\left(\lambda;1\right)-\mathcal{U}_\beta\left(\lambda;1\right)\right]} \\ \dfrac{k\left(\mathcal{M}_\beta\left(\lambda;\kappa\right)+\frac{2\lambda}{\kappa}\right)T'_{s0}(\lambda)-\left(\mathcal{M}_\beta\left(\lambda;1\right)+2\lambda\right)T'_{l0}(\lambda)+4\left(\beta+\frac{1}{2}\right)\frac{\rho}{\mathrm{St}}}{2\left[\mathcal{M}_\beta\left(\lambda;1\right)-\mathcal{U}_\beta\left(\lambda;1\right)\right]} \\ -\dfrac{-\left(\mathcal{U}_\beta\left(\lambda;\mathrm{Le}^{-1}\right)+2\lambda\mathrm{Le}\right)c'_{l0}(\lambda)+4\left(\beta+\frac{1}{2}\right)(1-\alpha)\mathrm{Le}c_i}{2\left[\mathcal{M}_\beta\left(\lambda;\mathrm{Le}^{-1}\right)-\mathcal{U}_\beta\left(\lambda;\mathrm{Le}^{-1}\right)\right]} \\ \dfrac{-\left(\mathcal{M}_\beta\left(\lambda;\mathrm{Le}^{-1}\right)+2\lambda\mathrm{Le}\right)c'_{l0}(\lambda)+4\left(\beta+\frac{1}{2}\right)(1-\alpha)\mathrm{Le}c_i}{2\left[\mathcal{M}_\beta\left(\lambda;\mathrm{Le}^{-1}\right)-\mathcal{U}_\beta\left(\lambda;\mathrm{Le}^{-1}\right)\right]} \\ 1 \end{pmatrix}. \tag{3.37}$$

Using (3.32), we know that the denominators of the elements of the kernel do not vanish for $\beta>-1$, $\lambda\neq 0$, and $\mu>0$, so the vector is well-defined.

Therefore, we can always find unstable perturbations of the system. The most unstable mode is the one given by $\beta\to 0$ (but note that the case of $\beta=0$ is out of the scope of our analysis, as the boundary conditions are not satisfied when $\beta=0$). Then, the perturbation of the interface can be written as

$$S(t)=2\lambda t^{\frac{1}{2}}+\delta t^{\frac{1}{2}-\epsilon} \tag{3.38}$$

for any $\epsilon>0$, so the growth rate of the most unstable perturbation tends to a multiple of the base state. When $\beta\to 0$, if $\lambda>0$ and $\mu>0$, we have

$$\mathcal{M}_\beta(\lambda;\mu)=\frac{2e^{-\frac{\lambda^2}{\mu}}}{\sqrt{\pi\mu}\,\mathrm{erf}\left(\frac{\lambda}{\sqrt{\mu}}\right)}\quad\text{and}\quad\mathcal{U}_\beta(\lambda;\mu)=-\frac{2e^{-\frac{\lambda^2}{\mu}}}{\sqrt{\pi\mu}\,\mathrm{erfc}\left(\frac{\lambda}{\sqrt{\mu}}\right)}, \tag{3.39}$$

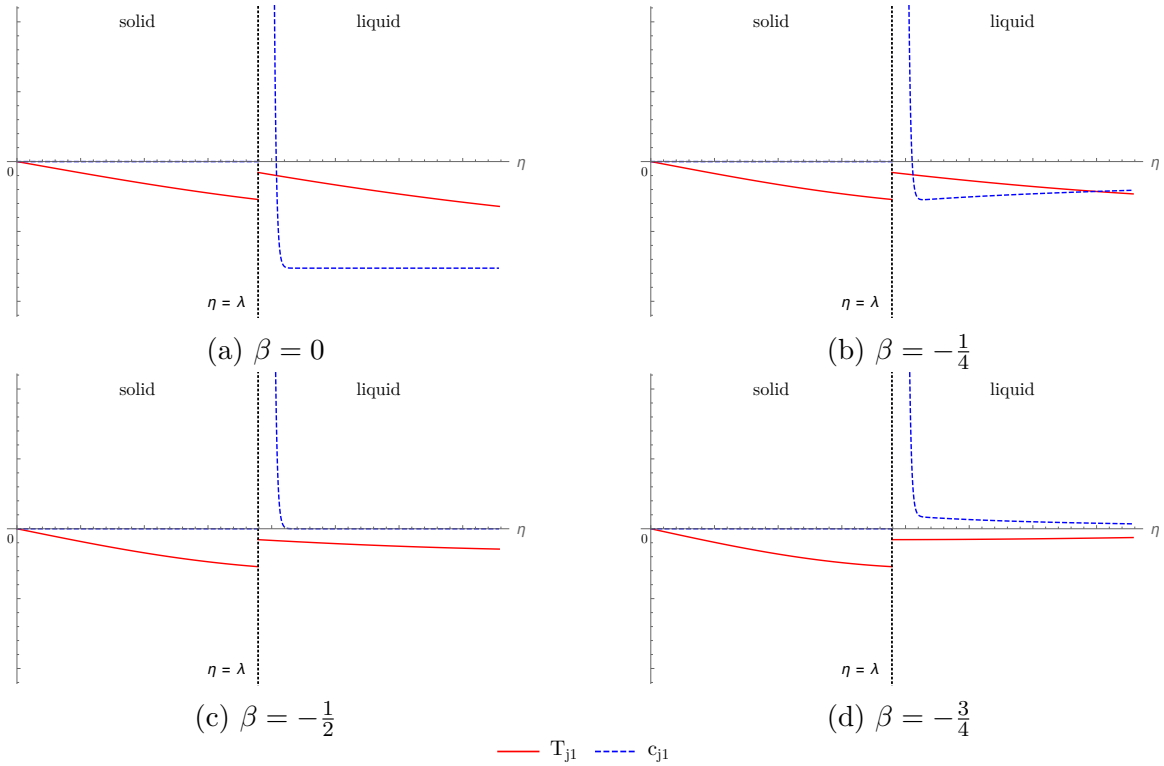


Figure 3.1: Perturbations for the semi-infinite domain problem for different representative values of β using the amplitudes given by $\mathbf{u}_{semi}(\beta)$ (numerical values shown in Table 3.1). The domain of the perturbations is $\eta \geq 0$, as we are in the semi-infinite domain problem defined by $z \geq 0$ and $t > 0$. The scaling is the same in all of the plots, so that they are directly comparable. The parameters of the system have been set to $\mathrm{St} = 0.77$, $\mathrm{Le} = 389$, $\rho = 0.95$, $c_p = 1$, $k = 0.34$, $\kappa = 0.36$, $m_s = 0.72$, $m_l = 360$, $D = 1.76 \cdot 10^{-2}$, $\alpha = 2 \cdot 10^{-3}$, $T_{l\infty} = 0$, and $c_{l\infty} = 1$.

so the vector which spans the kernel can be simplified. We observe that in this case $\mathcal{M}_\beta(\lambda;\mu)$ and $\mathcal{U}_\beta(\lambda;\mu)$ reduce to a multiple of the base state.

In Figure 3.1 we show the shape of the perturbations for the semi-infinite domain problem for different values of β, chosen to illustrate the different behaviours of the perturbation (stable, unstable and marginally stable). The parameter values are the ones commonly used to model solidification of metallurgical grade silicon in a mould (see Table 2.2). Note that the only constraint we have for β in order to have unstable perturbations is $-\frac{1}{2} < \beta < 0$, therefore we have a continuous spectrum of unstable perturbations. We observe that when $\beta = 0$ boundary conditions at infinity are not satisfied and the solution is equivalent to the base state, so it only modifies the amplitudes of the base state solutions, keeping their shape. The case $\beta = -\frac{1}{4}$ is in the unstable regime, as $-\frac{1}{2} < \beta < 0$. We observe that there is a spike in c_{l1} just ahead of the interface due to rejection of impurities during solidification.

β	0	$-\frac{1}{4}$	$-\frac{1}{2}$	$-\frac{3}{4}$
C_{T_s}	$-5.4281 \cdot 10^{-5}$	$-5.4286 \cdot 10^{-5}$	$-5.4290 \cdot 10^{-5}$	$-5.4291 \cdot 10^{-5}$
$C_{T_l}^{(P)}$	$-4.4407 \cdot 10^{-5}$	$-3.4641 \cdot 10^{-5}$	$-2.1741 \cdot 10^{-5}$	$5.7440 \cdot 10^{-7}$
$C_{T_l}^{(Q)}$	$2.8815 \cdot 10^{-5}$	$1.9048 \cdot 10^{-5}$	$6.1461 \cdot 10^{-6}$	$-1.6169 \cdot 10^{-5}$
$C_{c_l}^{(P)}$	$-1.5256 \cdot 10^{-4}$	$-5.8213 \cdot 10^{-5}$	0	$2.0105 \cdot 10^{-5}$
$C_{c_l}^{(Q)}$	1	1	1	1
C_S	$7.2876 \cdot 10^{-5}$	$7.2883 \cdot 10^{-5}$	$7.2887 \cdot 10^{-5}$	$7.2888 \cdot 10^{-5}$

Table 3.1: Amplitudes of the perturbations $\mathbf{u}_{semi}(\beta)$ for different representative values of β (recall that there is a continuous spectrum of perturbations). The values shown correspond to normalised vectors.

Even though it cannot be appreciated in the plot, the spike has a finite value at the interface so c_{l1} is bounded. However, away from this spike the perturbation has a negative contribution to the liquid concentration. The contribution of the temperature perturbations is negative in both phases. The case $\beta = -\frac{1}{2}$ corresponds to the marginally stable perturbation. Observe that in this case the temperature perturbations are still negative, while the perturbation in the liquid concentration still has a spike just ahead of the interface, which again quickly decays to zero. This can be shown analytically as the fourth component of $\mathbf{u}_{inf}$ is identically zero if $\beta = -\frac{1}{2}$ (the spike is due to the fifth component). Finally, the case $\beta = -\frac{3}{4}$ corresponds to a stable perturbation. In that case, we observe that the perturbation of the concentration in the liquid is positive.

The evolution of the perturbations for different values of β shown in the plots hints that the perturbation of the concentration in the liquid is the one dominating the stability of the problem. If we look at the amplitudes of the perturbations shown in Table 3.1, we observe that the largest amplitude is $C_{c_l}^{(Q)}$ for any choice of β, agreeing with the idea that the dominating perturbation is c_{l1}. Therefore, one could expect that c_{l1} will determine the behaviour of the system, with much less effect of the other perturbations on the system behaviour. Finally, notice that the small variations in the amplitudes C_{T_s} and C_S are due to the normalization, as from the form of $\mathbf{u}_{semi}(\beta)$ we observe that they do not depend on β.

3.4 Stability analysis of the infinite domain problem

Having considered a detailed stability analysis for the solidification front in the problem defined on a semi-infinite geometry, we now turn our attention to the correspond-

ing analysis for the infinite domain problem. We should remark that the infinite domain problem presented in this section is the same geometry as was considered in [15]. However, in their stability analysis, the perturbations introduced are of the particular form $e^{-\frac{\eta^2}{4}}\mathcal{D}_{-2\beta-1}(\eta)$, where $\mathcal{D}_\nu(\eta)$ is a parabolic cylinder function. This is a particular case of $Q_\beta(\eta)$, as, from 13.6.37 in [1], we know that

$$U\left(\frac{1}{2}(1-\nu),\frac{3}{2},\frac{z^2}{2}\right)=2^{\frac{1}{2}(1-\nu)}e^{\frac{z^2}{4}}\frac{\mathcal{D}_\nu(z)}{z}. \tag{3.40}$$

Therefore, the analysis here is different from that in [15] because it includes the contribution of $P_\beta(\eta)$, which we show to be necessary for understanding instabilities that may develop in the solidification boundary. In addition, [15] does not discuss the fact that, even though the velocity of the interface might decay in time, if this decay is not strong enough the interface may still develop instabilities, as we show in our analysis.

The boundary conditions are given by (3.4) and, translating these into the self-similar coordinate system, we have

$$f_j(\eta)\to 0 \quad \text{when} \quad \eta\to-\infty \quad \text{for } j=T_s,c_s, \tag{3.41a}$$
$$f_j(\eta)\to 0 \quad \text{when} \quad \eta\to+\infty \quad \text{for } j=T_l,c_l. \tag{3.41b}$$

Because the functions $P_\beta(\eta)$ and $Q_\beta(\eta)$ are odd, the behaviour in the limits $\eta\to+\infty$ and $\eta\to-\infty$ is the same except for a change in the sign which does not matter because our far field condition imposes that the value in the limit is zero. Hence, the analysis for f_{T_l} and f_{c_l} when $\eta\to-\infty$ is analogous to the analysis for f_{T_s} and f_{c_s} when $\eta\to+\infty$. Therefore, the analysis done in the previous section for the liquid perturbations can be applied here. Observe that $Q_\beta(\eta)$ is discontinuous at $\eta=0$, which is in the solid phase. Therefore, because we require the perturbations to be continuous, in the solid phase we need $C_j^{(Q)}=0$ for $j=T_s,c_s$. We conclude that the perturbations for $\beta\geq 0$ are

$$c_{s1}(t,\eta)=0, \tag{3.42a}$$
$$T_{s1}(t,\eta)=0, \tag{3.42b}$$
$$c_{l1}(t,\eta)=C_{c_l}t^\beta Q_\beta\left(\sqrt{\mathrm{Le}}\,\eta\right), \tag{3.42c}$$
$$T_{l1}(t,\eta)=C_{T_l}t^\beta Q_\beta\left(\eta\right), \tag{3.42d}$$

while if $\beta < 0$, we have

$$c_{s1}(t,\eta) = C_{c_s} t^{\beta} P_{\beta}\left(\sqrt{\frac{\mathrm{Le}}{D}}\eta\right), \tag{3.43a}$$

$$T_{s1}(t,\eta) = C_{T_s} t^{\beta} P_{\beta}\left(\frac{\eta}{\sqrt{\kappa}}\right), \tag{3.43b}$$

$$c_{l1}(t,\eta) = t^{\beta}(C_{c_l}^{(P)} P_{\beta}\left(\sqrt{\mathrm{Le}}\,\eta\right) + C_{c_l}^{(Q)} Q_{\beta}\left(\sqrt{\mathrm{Le}}\,\eta\right)), \tag{3.43c}$$

$$T_{l1}(t,\eta) = t^{\beta}\left(C_{T_l}^{(P)} P_{\beta}(\eta) + C_{T_l}^{(Q)} Q_{\beta}(\eta)\right), \tag{3.43d}$$

where C_j are undetermined constants.

As was the case for the semi-infinite domain, we can show that there are no non-trivial perturbations for $\beta \geq 0$. Therefore, we restrict our attention to the case of $-\frac{1}{2} \leq \beta < 0$.

3.4.1 Instability for $-\frac{1}{2} \leq \beta < 0$

For this case, the interface can become unstable even when the concentration and temperature fields are stable. We use the perturbations listed in (3.43), so we now have seven unknowns and five equations. The system (3.8) can be written as $A_{inf}(\beta)\mathbf{C}_{inf}(\beta) = \mathbf{0}$, where

$$A_{inf}(\beta) = \begin{pmatrix} \mathbf{A}_{inf}^1(\beta) & \mathbf{A}_{inf}^2(\beta) & \mathbf{A}_{inf}^3(\beta) & \mathbf{A}_{inf}^4(\beta) & \mathbf{A}_{inf}^5(\beta) & \mathbf{A}_{inf}^6(\beta) & \mathbf{A}_{inf}^7(\beta) \end{pmatrix}, \tag{3.44}$$

with

$$\mathbf{A}^1_{inf}(\beta) = \begin{pmatrix} 1 \\ m_s \\ 0 \\ \frac{k}{2}\mathcal{M}_\beta(\lambda;\kappa) \\ 0 \end{pmatrix}, \quad \mathbf{A}^4_{inf}(\beta) = \begin{pmatrix} 0 \\ 1 \\ 0 \\ 0 \\ \frac{D}{2\mathrm{Le}}\mathcal{M}_\beta(\lambda; D\mathrm{Le}^{-1}) \end{pmatrix},$$

$$\mathbf{A}^2_{inf}(\beta) = \begin{pmatrix} -1 \\ 0 \\ m_l \\ -\frac{1}{2}\mathcal{M}_\beta(\lambda;1) \\ 0 \end{pmatrix}, \quad \mathbf{A}^5_{inf}(\beta) = \begin{pmatrix} 0 \\ 0 \\ 1 \\ 0 \\ -\frac{1}{2\mathrm{Le}}\mathcal{M}_\beta(\lambda;\mathrm{Le}^{-1}) - (1-\alpha)\lambda \end{pmatrix},$$

$$\mathbf{A}^3_{inf}(\beta) = \begin{pmatrix} -1 \\ 0 \\ m_l \\ -\frac{1}{2}\mathcal{U}_\beta(\lambda;1) \\ 0 \end{pmatrix}, \quad \mathbf{A}^6_{inf}(\beta) = \begin{pmatrix} 0 \\ 0 \\ 1 \\ 0 \\ -\frac{1}{2\mathrm{Le}}\mathcal{U}_\beta(\lambda;\mathrm{Le}^{-1}) - (1-\alpha)\lambda \end{pmatrix}, \tag{3.45}$$

$$\mathbf{A}^7_{inf}(\beta) = \begin{pmatrix} \frac{1}{2}\left[T'_{s0}(\lambda) - T'_{l0}(\lambda)\right] \\ \frac{1}{2}\left[m_s T'_{s0}(\lambda) + c'_{s0}(\lambda)\right] \\ \frac{1}{2}\left[m_l T'_{l0}(\lambda) + c'_{l0}(\lambda)\right] \\ \frac{1}{4}\left[kT''_{s0}(\lambda) - T''_{l0}(\lambda)\right] - \left(\beta + \frac{1}{2}\right)\frac{\rho}{\mathrm{St}} \\ \frac{1}{4}\left[\frac{D}{\mathrm{Le}}c''_{s0}(\lambda) - \frac{1}{\mathrm{Le}}c''_{l0}(\lambda)\right] - (1-\alpha)\left[\left(\beta + \frac{1}{2}\right)c_i + \lambda\frac{c'_{l0}(\lambda)}{2}\right] \end{pmatrix},$$

and

$$\mathbf{C}_{inf}(\beta) = \left(C_{T_s}(\beta),\ C^{(P)}_{T_l}(\beta),\ C^{(Q)}_{T_l}(\beta),\ C_{c_s}(\beta),\ C^{(P)}_{c_l}(\beta),\ C^{(Q)}_{c_l}(\beta),\ C_S(\beta)\right)^T. \tag{3.46}$$

Taking the minor generated by columns 1, 2, 3, 5, and 6 of $A_{inf}(\beta)$, we can show, as in the semi-infinite domain problem, that if $\beta > -1$ the matrix is of full rank. Again, by the rank-nullity theorem, we conclude that the dimension of the kernel is equal to two. Thus, we can always find non-trivial values of C_{inf} by taking linear combinations of the elements of the kernel. The kernel for the infinite domain problem

is generated by the vectors

$$\mathbf{u}_{inf}(\beta) = \begin{pmatrix} -\frac{1}{2}T'_{s0}(\lambda) \\ -\dfrac{k\left(\mathcal{M}_\beta\left(\lambda;\kappa\right)+\frac{2\lambda}{\kappa}\right)T'_{s0}(\lambda)-\left(\mathcal{U}_\beta\left(\lambda;1\right)+2\lambda\right)T'_{l0}(\lambda)+4\left(\beta+\frac{1}{2}\right)\frac{\rho}{\mathrm{St}}}{2\left[\mathcal{M}_\beta\left(\lambda;1\right)-\mathcal{U}_\beta\left(\lambda;1\right)\right]} \\ \dfrac{k\left(\mathcal{M}_\beta\left(\lambda;\kappa\right)+\frac{2\lambda}{\kappa}\right)T'_{s0}(\lambda)-\left(\mathcal{M}_\beta\left(\lambda;1\right)+2\lambda\right)T'_{l0}(\lambda)+4\left(\beta+\frac{1}{2}\right)\frac{\rho}{\mathrm{St}}}{2\left[\mathcal{M}_\beta\left(\lambda;1\right)-\mathcal{U}_\beta\left(\lambda;1\right)\right]} \\ 0 \\ -\dfrac{-\left(\mathcal{U}_\beta\left(\lambda;\mathrm{Le}^{-1}\right)+2\lambda\mathrm{Le}\right)c'_{l0}(\lambda)+4\left(\beta+\frac{1}{2}\right)(1-\alpha)\mathrm{Le}c_i}{2\left[\mathcal{M}_\beta\left(\lambda;\mathrm{Le}^{-1}\right)-\mathcal{U}_\beta\left(\lambda;\mathrm{Le}^{-1}\right)\right]} \\ \dfrac{-\left(\mathcal{M}_\beta\left(\lambda;\mathrm{Le}^{-1}\right)+2\lambda\mathrm{Le}\right)c'_{l0}(\lambda)+4\left(\beta+\frac{1}{2}\right)(1-\alpha)\mathrm{Le}c_i}{2\left[\mathcal{M}_\beta\left(\lambda;\mathrm{Le}^{-1}\right)-\mathcal{U}_\beta\left(\lambda;\mathrm{Le}^{-1}\right)\right]} \\ 1 \end{pmatrix}$$
$$+\frac{c'_{s0}(\lambda)}{m_s}\begin{pmatrix} -\frac{1}{2} \\ -\dfrac{k\mathcal{M}_\beta(\lambda;\kappa)-\mathcal{U}_\beta(\lambda;1)}{2\left(\mathcal{M}_\beta(\lambda;1)-\mathcal{U}_\beta(\lambda;1)\right)} \\ \dfrac{k\mathcal{M}_\beta(\lambda;\kappa)-\mathcal{M}_\beta(\lambda;1)}{2\left(\mathcal{M}_\beta(\lambda;1)-\mathcal{U}_\beta(\lambda;1)\right)} \\ 0 \\ -\dfrac{m_l\left(\mathcal{U}_\beta(\lambda;\mathrm{Le}^{-1})+2\lambda\mathrm{Le}\right)}{2\left(\mathcal{M}_\beta(\lambda;\mathrm{Le}^{-1})-\mathcal{U}_\beta(\lambda;\mathrm{Le}^{-1})\right)} \\ \dfrac{m_l\left(\mathcal{M}_\beta(\lambda;\mathrm{Le}^{-1})+2\lambda\mathrm{Le}\right)}{2\left(\mathcal{M}_\beta(\lambda;\mathrm{Le}^{-1})-\mathcal{U}_\beta(\lambda;\mathrm{Le}^{-1})\right)} \\ 0 \end{pmatrix}, \tag{3.47}$$

and

$$\mathbf{v}_{inf}(\beta) = \begin{pmatrix} -\dfrac{1}{m_s} \\ -\dfrac{k\mathcal{M}_\beta(\lambda;\kappa)-\mathcal{U}_\beta(\lambda;1)}{m_s\left(\mathcal{M}_\beta(\lambda;1)-\mathcal{U}_\beta(\lambda;1)\right)} \\ \dfrac{k\mathcal{M}_\beta(\lambda;\kappa)-\mathcal{M}_\beta(\lambda;1)}{m_s\left(\mathcal{M}_\beta(\lambda;1)-\mathcal{U}_\beta(\lambda;1)\right)} \\ 1 \\ \dfrac{Dm_s\left(\mathcal{M}_\beta(\lambda;D\mathrm{Le}^{-1})+\frac{2\lambda\mathrm{Le}}{D}\right)-m_l\left(\mathcal{U}_\beta(\lambda;\mathrm{Le}^{-1})+2\lambda\mathrm{Le}\right)}{ms\left(\mathcal{M}_\beta(\lambda;\mathrm{Le}^{-1})-\mathcal{U}_\beta(\lambda;\mathrm{Le}^{-1})\right)} \\ -\dfrac{Dm_s\left(\mathcal{M}_\beta(\lambda;D\mathrm{Le}^{-1})+\frac{2\lambda\mathrm{Le}}{D}\right)-m_l\left(\mathcal{M}_\beta(\lambda;\mathrm{Le}^{-1})+2\lambda\mathrm{Le}\right)}{ms\left(\mathcal{M}_\beta(\lambda;\mathrm{Le}^{-1})-\mathcal{U}_\beta(\lambda;\mathrm{Le}^{-1})\right)} \\ 0 \end{pmatrix}. \tag{3.48}$$

This choice of the vectors that generate the kernel is quite convenient, as $\mathbf{v}_{inf}$ does not contribute to the perturbation of the interface (the last component, corresponding to C_S, is identically zero) and, because this is the only perturbation that will not

β	0	$-\frac{1}{4}$	$-\frac{1}{2}$	$-\frac{3}{4}$
C_{T_s}	$-5.6555 \cdot 10^{-4}$	$-5.6716 \cdot 10^{-4}$	$-5.6830 \cdot 10^{-4}$	$-5.6877 \cdot 10^{-4}$
$C_{T_l}^{(P)}$	$-3.1595 \cdot 10^{-4}$	$-2.5930 \cdot 10^{-4}$	$-1.9846 \cdot 10^{-4}$	$-1.3246 \cdot 10^{-4}$
$C_{T_l}^{(Q)}$	$2.8460 \cdot 10^{-4}$	$2.2786 \cdot 10^{-4}$	$1.6696 \cdot 10^{-4}$	$1.0093 \cdot 10^{-4}$
C_{c_s}	0	0	0	0
$C_{c_l}^{(P)}$	$-4.8270 \cdot 10^{-3}$	$-1.9986 \cdot 10^{-3}$	0	$8.4084 \cdot 10^{-4}$
$C_{c_l}^{(Q)}$	$9.9999 \cdot 10^{-1}$	$9.9999 \cdot 10^{-1}$	$9.9999 \cdot 10^{-1}$	$9.9999 \cdot 10^{-1}$
C_S	$8.6564 \cdot 10^{-4}$	$8.6811 \cdot 10^{-4}$	$8.6985 \cdot 10^{-4}$	$8.7058 \cdot 10^{-4}$

Table 3.2: Amplitudes of the perturbations $\mathbf{u}_{inf}(\beta)$ for different representative values of β (recall that there is a continuous spectrum of perturbations). The values shown correspond to normalised vectors.

β	0	$-\frac{1}{4}$	$-\frac{1}{2}$	$-\frac{3}{4}$
C_{T_s}	$-2.9225 \cdot 10^{-3}$	$-2.8579 \cdot 10^{-3}$	$-2.7837 \cdot 10^{-3}$	$-2.6967 \cdot 10^{-3}$
$C_{T_l}^{(P)}$	$-1.2971 \cdot 10^{-3}$	$-1.1674 \cdot 10^{-3}$	$-9.7904 \cdot 10^{-4}$	$-5.8641 \cdot 10^{-4}$
$C_{T_l}^{(Q)}$	$-1.6254 \cdot 10^{-3}$	$-1.6905 \cdot 10^{-3}$	$-1.8047 \cdot 10^{-3}$	$-2.1103 \cdot 10^{-3}$
C_{c_s}	$2.1042 \cdot 10^{-3}$	$2.0577 \cdot 10^{-3}$	$2.0043 \cdot 10^{-3}$	$1.9417 \cdot 10^{-3}$
$C_{c_l}^{(P)}$	$5.3536 \cdot 10^{-2}$	$2.9281 \cdot 10^{-2}$	$2.1452 \cdot 10^{-3}$	$-2.8754 \cdot 10^{-2}$
$C_{c_l}^{(Q)}$	$9.9856 \cdot 10^{-1}$	$9.9956 \cdot 10^{-1}$	$9.9999 \cdot 10^{-1}$	$9.9958 \cdot 10^{-1}$
C_S	0	0	0	0

Table 3.3: Amplitudes of the perturbations $\mathbf{v}_{inf}(\beta)$ for different representative values of β (recall that there is a continuous spectrum of perturbations). The values shown correspond to normalised vectors.

decay in time for $-\frac{1}{2} \leq \beta < 0$, we can conclude that the perturbations given by $\mathbf{v}_{inf}$ are stable for any $-\frac{1}{2} \leq \beta < 0$, so any instability must strictly be determined by the perturbations involving $\mathbf{u}_{inf}$. The other advantage of this choice is that in $\mathbf{u}_{inf}$ the amplitude of c_{s1} is zero, so the perturbations are similar to the ones in the semi-infinite domain. In fact, notice that if we take c_{s0} to be constant, as in the semi-infinite domain (by taking $c_{s\infty} = \alpha c_i$), the vector $\mathbf{u}_{inf}$ reduces to $\mathbf{u}_{semi}$.

Remember that, as we stated in the semi-infinite domain analysis, we have shown that the denominators of the elements of the kernel do not vanish for $\beta > -1$, hence in our range of interest, $-\frac{1}{2} \leq \beta < 0$, the kernel is well-defined. Similar to what we found for the semi-infinite domain problem, the most unstable perturbation is when $\beta \to 0$, so its growth rate tends to the $t^{\frac{1}{2}}$ of the base state. Hence, in this case, we can find simpler forms for the vectors spanning the kernel. Recall as well that the spectrum of the perturbations is continuous, so the unstable perturbations are given by any β in the range $-\frac{1}{2} < \beta < 0$.

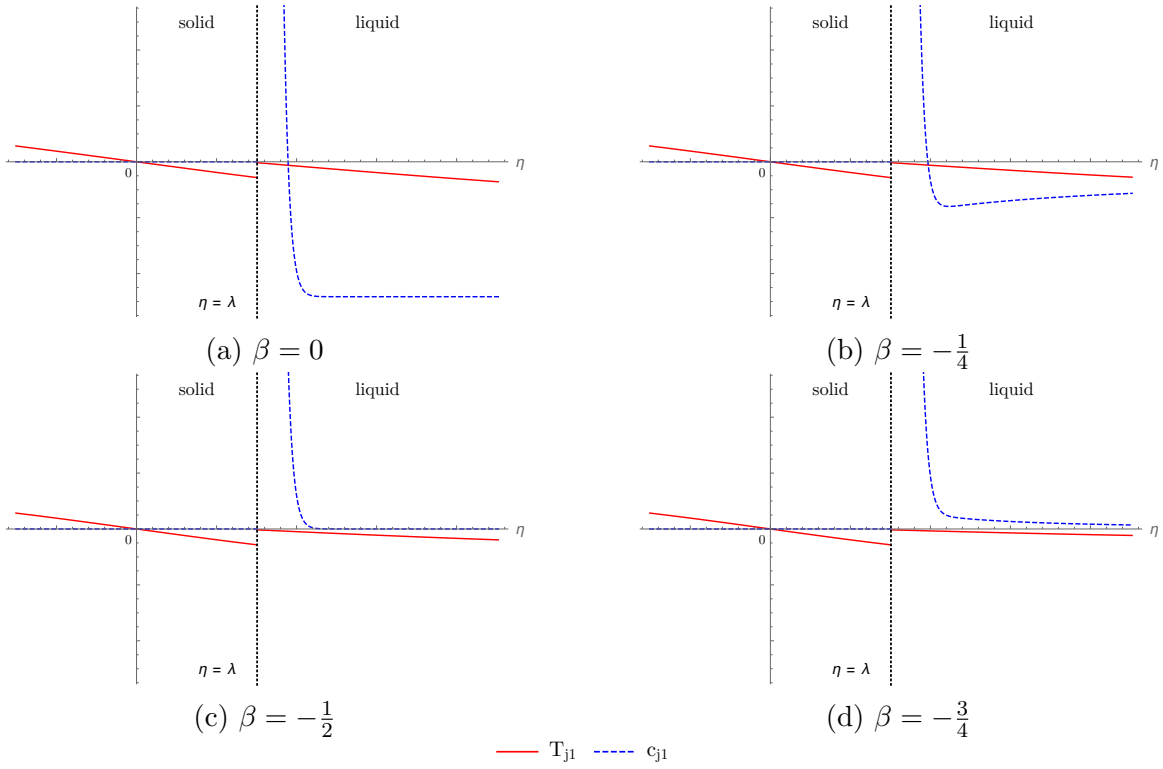


Figure 3.2: Perturbations for the infinite domain problem for different representative values of β using the amplitudes given by $\mathbf{u}_{inf}(\beta)$ (numerical values shown in Table 3.2). The domain of the perturbations is $\eta \in (-\infty, +\infty)$, as we are in the infinite domain problem defined by $z \in (-\infty, +\infty)$ and $t > 0$. These perturbations introduce an instability because the amplitude of the perturbation of the interface C_S is non-zero (but it is not shown in the plots). Notice that, as was pointed out from the form of $\mathbf{u}_{inf}$, these perturbations are very similar to the ones in Figure 3.1. The scaling is the same in all of the plots, so that they are directly comparable. The parameters of the system have been set to $\mathrm{St} = 0.77$, $\mathrm{Le} = 389$, $\rho = 0.95$, $c_p = 1$, $k = 0.34$, $\kappa = 0.36$, $m_s = 0.72$, $m_l = 360$, $D = 1.76 \cdot 10^{-2}$, $\alpha = 2 \cdot 10^{-3}$, $T_{l\infty} = 0$, $c_{l\infty} = 1$, and $c_{s\infty} = 0$.

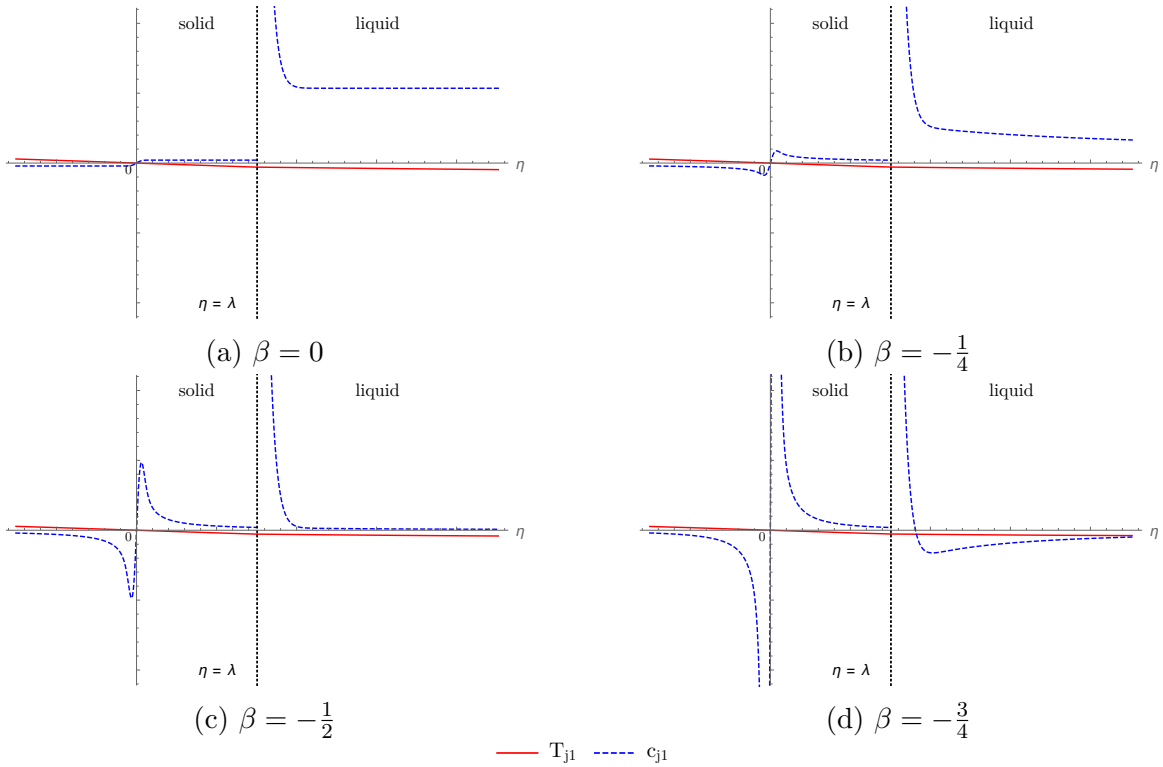


Figure 3.3: Perturbations for the infinite domain problem for different representative values of β using the amplitudes given by $\mathbf{v}_{inf}(\beta)$ (numerical values shown in Table 3.3). The domain of the perturbations is $\eta \in (-\infty, +\infty)$, as we are in the infinite domain problem defined by $z \in (-\infty, +\infty)$ and $t > 0$. These perturbations do not introduce an instability, even if $-\frac{1}{2} \leq \beta < 0$, because the amplitude of the perturbation to the interface C_S is identically zero. The scaling is the same in all of the plots, so that they are directly comparable. The parameters of the system have been set to St $= 0.77$, Le $= 389$, $\rho = 0.95$, $c_p = 1$, $k = 0.34$, $\kappa = 0.36$, $m_s = 0.72$, $m_l = 360$, $D = 1.76 \cdot 10^{-2}$, $\alpha = 2 \cdot 10^{-3}$, $T_{l\infty} = 0$, $c_{l\infty} = 1$, and $c_{s\infty} = 0$.

In Figure 3.2 we show the perturbations given by $\mathbf{u}_{inf}$ for the same parameter choice as in the semi-infinite domain problem. We observe that their behaviour is very similar to the perturbations for the semi-infinite domain. In this case, temperature perturbations are negative if $\eta > 0$, but T_{s1} is positive if $\eta < 0$. This was not captured in the semi-infinite domain, as we were restricted to $\eta \geq 0$. We still notice a finite spike of concentration just ahead of the interface and, again, the sign of the concentration of impurities in the liquid away from the interface is negative in the unstable regime and positive in the stable regime. The perturbation quickly decays to zero if $\beta = -\frac{1}{2}$, as we can show that the fifth component of $\mathbf{u}_{inf}$ is identically zero in this case.

In Figure 3.3, we show the perturbations given by $\mathbf{v}_{inf}$. In this case, the temperature perturbations are similar to the ones shown in the previous figures, but we notice qualitative changes in the concentration perturbations. The first change is that now we have a perturbation of the concentration in the solid. Bumps appear near the origin which become larger as β decreases, however, recall that these perturbations decay in time like t^{β} so that large bumps decay faster than do small bumps, in time. Given that these bumps appear near the origin, it suggests that they might be caused by the initial discontinuity of the base state in that point. The second difference is that, even though the finite spike ahead of the interface is still present, far from the interface c_{l1} behaves differently when we change β. Now, c_{l1} is positive near $\beta = 0$, and will become negative as we decrease β, but the sign change no longer happens at $\beta = -\frac{1}{2}$, as now the fifth component of $\mathbf{v}_{inf}$ does not vanish at $\beta = -\frac{1}{2}$.

The numerical values of the amplitudes used in the previous sketches are shown in Tables 3.2 and 3.3. For the amplitudes given by $\mathbf{u}_{inf}(\beta)$, we observe a similar behaviour as in the amplitudes for $\mathbf{u}_{semi}(\beta)$, shown in Table 3.1. For the amplitudes given by $\mathbf{v}_{inf}(\beta)$, we notice that, again, the main contribution is $C_{c_l}^{(Q)}$, even though these perturbations do not go unstable. We observe a very weak dependence of C_{T_s} and C_{c_s} on β, because this dependence is only introduced when normalising the vectors, as seen in the definition of $\mathbf{v}_{inf}(\beta)$

We remark that the analysis presented in this section is not only valid for solidification problems ($\lambda > 0$), but for melting problems as well ($\lambda < 0$). As the results for $\lambda < 0$ would be very similar, we do not show them here.

3.5 Discussion

In this chapter, we have considered the stability analysis for the self-similar motion of a planar solidification front for a binary alloy in two different geometries: the semi-infinite domain problem and the infinite domain problem. For both domains, we introduced perturbations in the concentration and temperature fields of the form $t^\beta f(\eta)$, where β is the parameter that determines the stability and η is the similarity variable. Then, we found that the perturbation of the position of the interface is proportional to $t^{\beta+\frac{1}{2}}$, hence the exact base solution is locally unstable if $\beta > -\frac{1}{2}$, because then at least one of the perturbations will grow unboudedly in time. Due to the nature of the perturbations, in each domain we needed to separate the analysis into the cases $\beta \geq 0$ and $-\frac{1}{2} \leq \beta < 0$. We found that in both domains, when $\beta \geq 0$, there are no non-trivial perturbations that satisfy the boundary conditions. Thus, we conclude that concentration and temperature fields are always stable, a result we expect since the individual diffusion equations should give stable solutions in the interior of each sub-domain. Therefore, the instability in the exact solution is due to the growth of the perturbation to the interface, alone.

Studying the case $-\frac{1}{2} \leq \beta < 0$, we found instability in the self-similar motion of the solidification front for any parameter regime. In our analysis, we have considered a more general type of perturbation than that considered in the analysis of [15], as we have kept *both* linearly independent first-order perturbation solutions. Keeping both solutions introduces a number of perturbations higher than the number of interface conditions available to determine them. Therefore, by the rank-nullity theorem, we can conclude that the kernel of the system will be of dimension one in the semi-infinite problem and dimension two in the infinite problem, and thus never empty. For $-\frac{1}{2} \leq \beta < 0$, the only perturbation that gives instability is the perturbation of the interface, but we have shown that one can always find a perturbation with a non-trivial perturbation of the interface. In conclusion, for both geometries, we can always find an unstable perturbation. We conclude that, regardless of the parameter choice, the system is unstable to perturbations and that there exist infinitely many unstable perturbations as the perturbation spectrum is continuous.

The main difference between the two geometries was in the fact that, in the semi-infinite domain problem, the kernel is of dimension one, while for the infinite domain problem, the kernel is of dimension two, so we find two linearly independent families of perturbations for the latter case. However, we can choose the elements of the kernel of the infinite domain problem so that for one of them we have $C_{c_s} = 0$,

and for the other we have $C_S = 0$. The advantage of this choice is that, for the vector for which $C_{c_s} = 0$, the perturbations are equivalent to the ones in the semi-infinite domain problem, while for the vector for which $C_S = 0$, the perturbations do not contribute to the instability of the problem. Hence, we find that even though the infinite domain geometry permits two types of perturbations, if we compare the unstable perturbation with the semi-infinite domain perturbations, we see that their behaviour is very similar. Therefore, the mechanism bringing about instability is the same for both geometries, and is related to the concentration of impurities in the liquid.

We recall that [66] found that the stability depended on the parameter choice of the system, with higher velocities and constitutional supercooling helping to destabilise the system. Our analysis shows that, for a self-similar moving solidification front, the interface is always unstable regardless of the parameter choice. Therefore, our results suggest that the cause of the instability may be intrinsic to the self-similar motion that appears when the cooling of the alloy is not controlled.

Regarding possible future work, one could try to extend these results to two-dimensional domains. We expect that such an analysis would give some insight into the grain size and would allow us to introduce two-dimensional physical effects as well, such as the Gibbs-Thomson effect. This may lead to a more realistic understanding of the loss of stability of the planar solidification front, and, perhaps, provide a relation between grain size and the mode of instability. However, it is not obvious how to extend the analysis presented in this chapter to a two-dimensional model, as the key point of the analysis was the fact that we could remove the dependence on time in the interface conditions and therefore we ended up with an algebraic linear system of equations. In two dimensions, there is the second space coordinate and it is not possible to remove the dependence on both the second space variable and the time variable, because each temperature and concentration field has a different diffusive length scale. Due to this technical complication, we have not proceeded further with two-dimensional perturbations.

The results presented here may be of use to the silicon industry, as they show that instability of the planar interface is likely to occur for any parameter regime if the velocity of the interface is not controlled and kept below a certain threshold. Therefore, these results provide a theoretical background to explain why special techniques, like the Czochralski process and directional solidification, are required to achieve a stable planar solidification front. Being able to understand these instabilities will possibly

allow for more efficient casting techniques, as well as more control over the quality of the silicon produced.

Notice that the geometries studied in this chapter are non-finite and thus the effects at the end of the solidification process, when the liquid region is small, have not been considered. In finite geometries, the self-similar solutions are no longer valid, so we need another approach to solve the Stefan problem. Hence, in the following chapter, we shall direct our attention to the solidification of binary alloys in finite one-dimensional domains.

Chapter 4

Asymptotic analysis of the inward solidification of a planar slab

4.1 Introduction

In Chapter 3 we studied the stability of the self-similar solutions of the planar solidification problem in semi-infinite and infinite domains. However, self-similar solutions are no longer valid when the domain considered is finite. Obviously, in the industrial problem that we are interested in, the layer of liquid is finite; therefore, considering a finite domain is a necessary step towards a better understanding of the solidification process. Because closed-form solutions cannot be found for this problem, in the past mathematicians have considered asymptotic approximations to study them.

Much attention has been devoted to finding asymptotic approximations for the inward solidification in various geometries where the liquid is initially at the melting temperature; such problems can at times be formulated as one-phase Stefan problems. A common asymptotic limit to consider is the large Stefan number limit, corresponding to the situation where latent heat dominates, with planar two-dimensional geometries, such as a halfspace [96] or a corner [47], cylindrical and spherical geometries [77, 84, 88], and arbitrary two-dimensional [61] and three-dimensional [62] geometries having been considered. Small-time behaviour [20, 36, 37] and end-time behaviour (near the end of the solidification process) [61, 62, 77, 84, 88] have been studied for the one-phase problem. In addition to asymptotic analysis, various numerical approaches for solving one-phase Stefan problems have been considered [4, 17, 18, 57, 60, 81, 91].

Despite their relevance to solidification problems, two-phase Stefan problems in finite domains have received less attention than their one-phase counterparts. Kucera and Hill [50] extended their previous small-time analysis to the two-phase problem, and compared their analytical solution with that found in [44]. They also employed

the enthalpy method [95], to solve the two-phase problem. The two-phase Stefan problem in spheres was considered in [63], which included a rigorous asymptotic analysis and numerical simulations via the enthalpy method.

The more complicated two-phase Stefan problem arising in the inward solidification of binary alloys has received even less attention. When constitutional supercooling is included in the model, the analysis becomes more difficult, as now the problem consists of heat and mass transport problems coupled by constitutional supercooling conditions. Feltham and Garside [27] study small time and large Stefan number behaviour from the extended two-phase problem for binary alloys, in the regime where supercooling is small enough to decouple the heat and mass problems. This reduces the problem to a classic two-phase Stefan problem for the temperature (which is solved first) and a diffusion problem for concentration in a shrinking domain that can be solved once the position of the interface is known. The analytical results give reasonable agreement with numerical simulations of the full problem, except that the analytical solution concentration in the liquid exhibits a non-physical discontinuity in the flux at the origin. The inward solidification of a spherical binary alloy has been considered in [107], but the authors considered the particular case where the liquid is well mixed and thus the concentration and temperature profiles are uniform in space in the liquid phase. Hence, their model is equivalent to a one-phase Stefan problem with a supercooling condition that depends on the position of the interface.

One physical application of the extended two-phase Stefan problem in finite domains is to the solidification of metallurgical grade silicon, which is composed of about 99% silicon, while the remaining fraction consists of impurities. The molten silicon is poured into iron moulds and left to solidify by heat exchange with the environment. As the thickness of the cast is small in comparison with the width, the solidification mainly involves two fronts, one starting at the bottom of the cast and one at the top of the cast, which move toward one another until they meet at the centre of the cast. During the solidification process, impurities are mostly rejected from the solid phase into the liquid, within which they diffuse. The role of the impurities is crucial, as they cause constitutional supercooling in the liquid and therefore have an impact on the motion of the solidification front. For silicon casting, a semi-infinite geometry can be useful to model the early stages of the process when the two solidification fronts are far from each other. However, such a formulation is no longer valid when the two fronts approach one another. Previous work showed good agreement between the classic two-phase Stefan problem and experimental data [8]. However, the distribution of impurities was neglected in the model of [8], and therefore the model

did not account for supercooling, which will modify the late-time dynamics when the solidification fronts approach.

4.1.1 Outline of the chapter

In the present chapter, we solve the extended Stefan problem with constitutional supercooling in a finite planar domain using matched asymptotics, exploiting the fact that the Lewis number is large. We assume also that the diffusivity of impurities in the solid, the segregation coefficient and the initial concentration and temperature are small; and that the supercooling coefficient is large, meaning that a large concentration of impurities is required to cause a significant change in the solidification temperature. All these assumptions are reasonable for our application of interest. While relatively simple, the one-dimensional planar geometry is still quite relevant to model a silicon cast. Our results extend the analysis of the solidification of a slab presented in [27] to include supercooling that couples the heat and mass problems, and we shall also consider all time-scales of the problem.

The outline of the chapter is as follows. In Section 4.2, we present the dimensionless model and introduce the asymptotic scalings to be employed in our analysis. In Sections 4.3 to 4.6, we perform an asymptotic analysis determining the leading order approximation to the solutions for the entire problem at various time-scales, and use these to assemble matched asymptotic solutions to the problem. In Section 4.7, we summarise our asymptotic results and discuss the asymptotic solutions calculated in previous sections. In Section 4.8, we compare the matched asymptotic solutions to numerical simulations of the full problem obtained with a finite volume method, and also to real experimental data obtained from silicon casting experiments. We discuss our results in Section 4.9.

4.2 Model for the solidification of a planar slab

As described in Chapter 2, the geometry of the planar solidification problem consists of a finite slab, initially a liquid with homogeneous temperature and concentration of impurities, which is cooled from both ends at a constant temperature. For simplicity, we assume the problem to be symmetric, therefore we need only consider half of the domain, provided we impose symmetry conditions at the origin. A diagram of the planar geometry is shown in Figure 4.1.

In order to perform the asymptotic analysis we consider the distinguished limit of large Lewis number (recall from Table 2.2 that for silicon we have Le = 389).

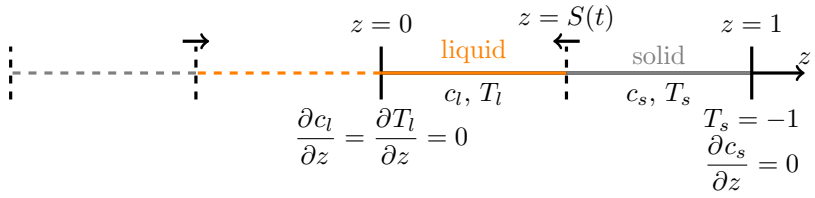


Figure 4.1: Diagram of the inward solidification problem of a finite slab. We assume that the problem is symmetric with respect to $z = 0$, so we consider the problem only in the region $0 \le z \le 1$ and impose symmetry conditions at the origin.

To simplify the notation, we define the small parameter $\epsilon = \mathrm{Le}^{-1}$, so that we may consider the limit $\epsilon \to 0$. We take further assumptions on the size of the parameters and scale them with ϵ. We assume small diffusivity of impurities in the liquid, even smaller diffusivity in the solid, small initial temperature and concentration, small constitutional supercooling, and almost complete rejection of impurities from the solid phase. From Table 2.2 (see page 39), the scaling for these dimensionless parameters is

$$D = \epsilon \hat{D}, \quad m_l = \frac{\hat{m}_l}{\epsilon}, \quad \alpha = \epsilon \hat{\alpha}, \quad c_0 = \epsilon \hat{c}_0, \quad \text{and} \quad T_0 = \epsilon \hat{T}_0, \tag{4.1}$$

where $\hat{D}$, $\hat{m}_l$, $\hat{\alpha}$, $\hat{c}_0$, and $\hat{T}_0$ are all order one. With these rescalings, the non-dimensional model (2.34) becomes the following. In the solid phase, $S(t) < z < 1$, we have

$$\frac{\partial c_s}{\partial t} = \epsilon^2 \hat{D} \frac{\partial^2 c_s}{\partial z^2}, \tag{4.2a}$$

$$\frac{\partial T_s}{\partial t} = \kappa \frac{\partial^2 T_s}{\partial z^2}. \tag{4.2b}$$

In the liquid phase, $0 < z < S(t)$, we have

$$\frac{\partial c_l}{\partial t} = \epsilon \frac{\partial^2 c_l}{\partial z^2}, \tag{4.2c}$$

$$\frac{\partial T_l}{\partial t} = \frac{\partial^2 T_l}{\partial z^2}. \tag{4.2d}$$

At the interface, $z = S(t)$, we have

$$T_s = T_l, \tag{4.2e}$$

$$c_s = \epsilon \hat{\alpha} c_l, \tag{4.2f}$$

$$\epsilon c_l = -\hat{m}_l T_l, \tag{4.2g}$$

$$\frac{\rho}{\mathrm{St}} \frac{\mathrm{d}S}{\mathrm{d}t} = k \frac{\partial T_s}{\partial z} - \frac{\partial T_l}{\partial z}, \tag{4.2h}$$

$$(1 - \epsilon \hat{\alpha}) c_l \frac{\mathrm{d}S}{\mathrm{d}t} = \epsilon^2 \hat{D} \frac{\partial c_s}{\partial z} - \epsilon \frac{\partial c_l}{\partial z}. \tag{4.2i}$$

We prescribe the boundary conditions

$$\frac{\partial c_l}{\partial z} = 0 \quad \text{and} \quad \frac{\partial T_l}{\partial z} = 0, \quad \text{at } z = 0, \tag{4.2j}$$

$$\frac{\partial c_s}{\partial z} = 0 \quad \text{and} \quad T_s = -1, \quad \text{at } z = 1, \tag{4.2k}$$

and the initial conditions

$$c_l = \epsilon \hat{c}_0, \quad T_l = \epsilon \hat{T}_0, \quad \text{and} \quad S = 1, \quad \text{at} \quad t = 0. \tag{4.2l}$$

As exact solutions are seemingly not possible for the problem (4.2), in the following sections we perform a matched asymptotic analysis to find asymptotic solutions of the problem. The asymptotic analysis of the problem in the limit $\epsilon \to 0$ reveals four distinct time regimes in the problem, and each regime is composed of different space layers. We identify ten layers overall, with a schematic diagram and list of relevant scalings shown in Figure 4.2 and Table 4.1, respectively. Notice that we use hats for the position of the interface and the temperature and concentration fields whenever they are rescaled. To minimise confusion, we give a reminder of the rescalings at the beginning of the analysis of each layer.

These scalings are primarily picked by the physics. At the beginning of the process, in what we call regime i, we expect to see diffusion of both heat and impurities, but, due to the disparity in diffusive length scales, we need to introduce an inner layer of size $\mathcal{O}(\epsilon)$ around the interface (named layer B) to capture the rejection and transport of impurities, while heat diffusion is observed in the outer layers (A and C). This regime holds until the interface is within a distance $\mathcal{O}(\epsilon)$ from the origin, as now the outer layer in the liquid vanishes and the inner layer around the interface needs to account for the symmetry conditions at the origin. This sets the scalings for S and z, and thus defines the two layers (D and E) in regime ii. The time scale arises from balancing the Stefan condition that appears in the inner layer E, as we need a time scale that allows us to observe the motion of the solidification front. We find that regime ii is valid until the inner layer E vanishes because the leading order interface position becomes zero. Therefore, we need to study a new regime, which we call regime iii. We expect this regime to be a transition between regimes ii and iv, which is discussed later. This transition is driven by the thermal problem in the solid, with the constitutional supercooling effect due to the build-up of impurities in the liquid phase. To capture this problem, we need to introduce the following layer structure: an outer layer F in the solid where both temperature and concentration fields remain constant, an intermediate layer G in the solid where we observe heat diffusion, and

		t	z	S	c_s	c_l	T_s	T_l
Regime i	A	t	z	S	$\epsilon\hat{c}_s$	-	T_s	-
	B	t	$S(t)+\epsilon Z$	S	$\epsilon\hat{c}_s$	c_l	$\epsilon\hat{T}_s$	$\epsilon\hat{T}_l$
	C	t	z	S	-	$\epsilon\hat{c}_l$	-	$\epsilon\hat{T}_l$
Regime ii	D	$t^*+\epsilon\tau$	z	$\epsilon\hat{S}$	$\epsilon\hat{c}_s$	-	T_s	-
	E	$t^*+\epsilon\tau$	ϵZ	$\epsilon\hat{S}$	$\epsilon\hat{c}_s$	c_l	$\epsilon\hat{T}_s$	$\epsilon\hat{T}_l$
Regime iii	F	$t^*+\epsilon\tau^*+\epsilon^{\frac{4}{3}}\theta$	z	$\epsilon^{\frac{4}{3}}\hat{S}$	$\epsilon\hat{c}_s$	-	T_s	-
	G	$t^*+\epsilon\tau^*+\epsilon^{\frac{4}{3}}\theta$	$\epsilon^{\frac{2}{3}}\xi$	$\epsilon^{\frac{4}{3}}\hat{S}$	$\epsilon\hat{c}_s$	-	$\epsilon^{\frac{2}{3}}\hat{T}_s$	-
	H	$t^*+\epsilon\tau^*+\epsilon^{\frac{4}{3}}\theta$	$\epsilon^{\frac{4}{3}}Z$	$\epsilon^{\frac{4}{3}}\hat{S}$	$\epsilon^{\frac{2}{3}}\hat{c}_s$	$\epsilon^{-\frac{1}{3}}\hat{c}_l$	$\epsilon^{\frac{2}{3}}\hat{T}_s$	$\epsilon^{\frac{2}{3}}\hat{T}_l$
Regime iv	I	t	z	$\epsilon^2\hat{S}$	$\epsilon\hat{c}_s$	-	T_s	-
	J	t	$\epsilon^2 Z$	$\epsilon^2\hat{S}$	c_s	$\epsilon^{-1}\hat{c}_l$	T_s	T_l

Table 4.1: Scalings for the variables in each layer of the problem. The variables τ and θ are the time variables in different regimes, while the variables ξ and Z are the space variables in the intermediate and inner layers of each regime, respectively. We use hats for temperature and concentration whenever they are rescaled.

an inner layer H that captures the motion of the interface and thus accounts for the interface conditions. A balance of the relevant terms gives the scalings reproduced in Table 4.1. Finally, we need to consider a last regime that holds up to $t \to +\infty$. This is regime iv, in which we observe the temperature in the solid to decay down to the minimum temperature of the system, which corresponds to the temperature at the boundary $z = 1$. This behaviour is observed in the outer layer I, but we need to account for the inner layer J to capture the moving boundary and the liquid region.

Notice that, according to the scalings in Table 4.1, we have concentrations in the liquid phase of $\mathcal{O}\left(\epsilon^{-\frac{1}{3}}\right)$ and $\mathcal{O}\left(\epsilon^{-1}\right)$ which are not physical. As we discuss later, regimes iii and iv are not physical because some of the modelling assumptions, such as the linear phase diagram, no longer hold. This is related to the fact that, according to the model, the solidification process never finishes and therefore we always end up with a thin layer of liquid, which obviously does not agree with experimental observations. However, from the mathematical point of view, regimes iii and iv are relevant to provide a full picture of (4.2) for $t \in [0, +\infty)$.

In what follows, we find asymptotic solutions in each region, and then match them to construct solutions valid over the whole problem domain.

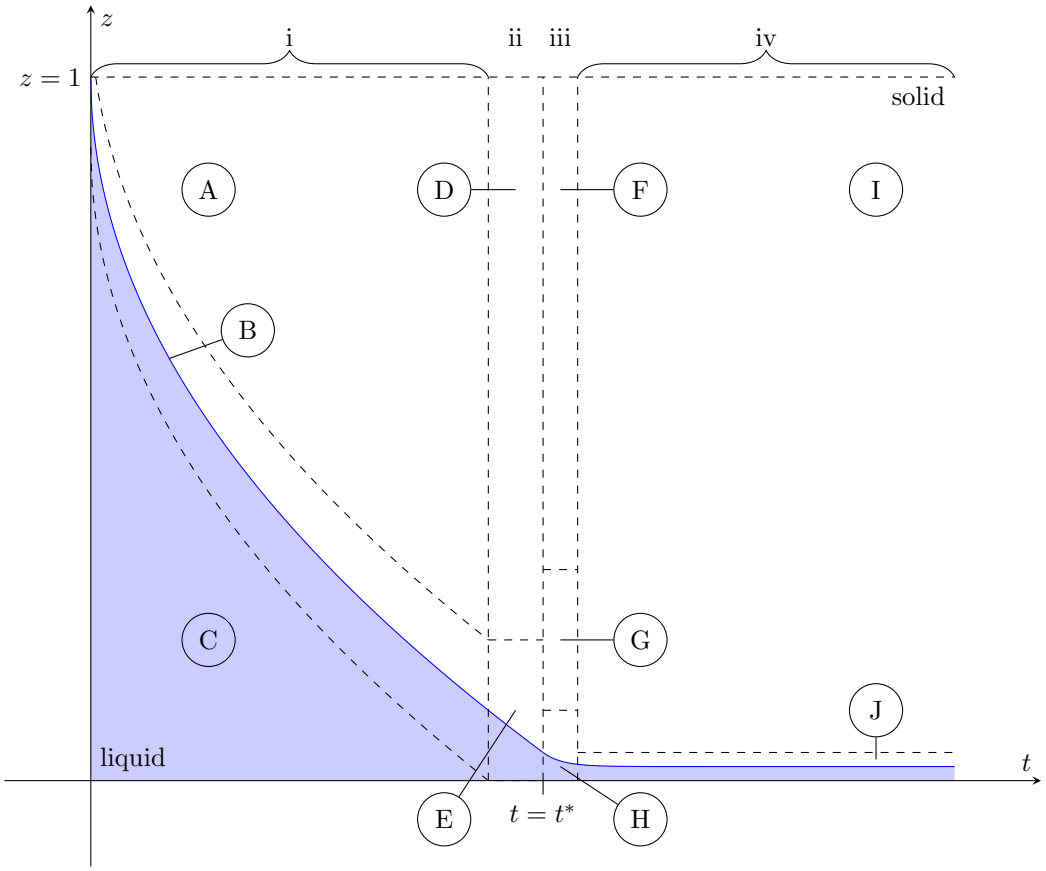


Figure 4.2: Sketch of the regimes and layers of the process. The sketch shows the evolution of the interface, $S(t)$, in time, so the area above (in white) is the solid phase and the area below (in blue) is the liquid phase. The four regimes identified with lower case Roman numerals are the behaviours at different times. In each regime, we consider various layers which are labelled with upper case letters. The scalings in each layer are shown in Table 4.1.

4.3 Asymptotic solutions in regime i

We start by considering the behaviour at the beginning of the solidification process, described by regime i in Figure 5.2. In this regime, the interface is far from the origin and we distinguish three space layers: the outer layer, A, in the solid, the inner layer, B, around the solidification front (which comprises both phases), and the outer layer, C, in the liquid. We start by solving the equations for each layer and then proceed to match the layers in order to fully determine the asymptotic solutions.

4.3.1 Layer A

The first layer we study in this regime is the outer layer in the solid phase: layer A. Rescaling the problem with the scalings in Table 4.1, which in this layer it is only $c_s = \epsilon \hat{c}_s$, we find that the problem is defined by

$$\frac{\partial \hat{c}_s}{\partial t} = \epsilon^2 \hat{D} \frac{\partial^2 \hat{c}_s}{\partial z^2}, \quad \frac{\partial T_s}{\partial t} = \kappa \frac{\partial^2 T_s}{\partial z^2} \quad \text{on} \quad S(t) < z < 1, \tag{4.3a}$$

$$\frac{\partial \hat{c}_s}{\partial z} = 0 \quad \text{and} \quad T_s = -1, \quad \text{at } z = 1, \tag{4.3b}$$

and as initially all the silicon is liquid ($S(0) = 1$), we need no additional initial conditions. The problem is completed with the corresponding matching conditions with layer B, which are discussed in Section 4.3.4. We expand $\hat{c}_s$, T_s, and S as

$$\hat{c}_s = \hat{c}_{s0} + \epsilon \hat{c}_{s1} + \mathcal{O}\left(\epsilon^2\right), \tag{4.4a}$$

$$T_s = T_{s0} + \epsilon T_{s1} + \mathcal{O}\left(\epsilon^2\right), \tag{4.4b}$$

$$S = S_0 + \epsilon S_1 + \mathcal{O}\left(\epsilon^2\right). \tag{4.4c}$$

At $\mathcal{O}(1)$, and using the matching conditions determined in Section 4.3.4, the problem for the concentration field is

$$\frac{\partial \hat{c}_{s0}}{\partial t} = 0, \qquad \text{in} \quad S_0(t) < z < 1, \tag{4.5a}$$

$$\hat{c}_{s0} = \hat{\alpha} c_i(t), \qquad \text{at} \quad z = S_0(t), \tag{4.5b}$$

where $c_i(t)$ is the concentration at the interface which is yet to be determined. The problem for the temperature field is

$$\frac{\partial T_{s0}}{\partial t} = \kappa \frac{\partial^2 T_{s0}}{\partial z^2}, \qquad \text{in} \quad S_0(t) < z < 1, \tag{4.6a}$$

$$T_{s0} = 0, \qquad \text{at} \quad z = S_0(t), \tag{4.6b}$$

$$\frac{\rho}{\mathrm{St}} S_0'(t) = k \frac{\partial T_{s0}}{\partial z}, \qquad \text{at} \quad z = S_0(t), \tag{4.6c}$$

$$T_{s0} = -1, \qquad \text{at} \quad z = 1, \tag{4.6d}$$

which is a classical one-phase Stefan problem. We find the the solutions

$$\hat{c}_{s0} = \hat{\alpha} c_i \left(S_0^{-1}(z) \right), \quad T_{s0} = -1 + \frac{\operatorname{erf}\left(\frac{1-z}{2\sqrt{\kappa t}} \right)}{\operatorname{erf}\left(\frac{\lambda}{\sqrt{\kappa}} \right)}, \quad \text{with} \quad S_0 = 1 - 2\lambda\sqrt{t}, \tag{4.7}$$

where λ is a constant to be determined, as shown in Section 4.3.4. At $\mathcal{O}(\epsilon)$, we consider only the temperature problem, as the concentration is not required for the purpose of our analysis. Using the $\mathcal{O}(1)$ solutions and the matching conditions from Section 4.3.4, we have the problem

$$\frac{\partial T_{s1}}{\partial t} = \kappa \frac{\partial^2 T_{s1}}{\partial z^2}, \qquad \text{in} \quad S_0(t) < z < 1, \tag{4.8a}$$

$$T_{s1} = -\frac{c_i}{\hat{m}_l} + \frac{\lambda}{k\sqrt{t}} \frac{\rho}{\mathrm{St}} S_1(t), \qquad \text{at} \quad z = S_0(t), \tag{4.8b}$$

$$T_{s1} = 0, \qquad \text{at} \quad z = 1, \tag{4.8c}$$

where the equation for $S_1(t)$ is given in Section 4.3.4 and the initial condition is not defined in this region.

We rescale the problem, introducing the variable $\eta = \frac{z - S_0(t)}{1 - S_0(t)}$, where $S_0(t) = 1 - 2\lambda\sqrt{t}$. This change of variable fixes the domain of the problem to $\eta \in [0, 1]$. The transformed problem reads

$$4\lambda^2 t \frac{\partial T_{s1}}{\partial t} = \kappa \frac{\partial^2 T_{s1}}{\partial \eta^2} - 2\lambda(1-\eta) \frac{\partial T_{s1}}{\partial \eta}, \qquad \text{in} \quad 0 < \eta < 1, \tag{4.9a}$$

$$T_{s1} = -\frac{c_i}{\hat{m}_l} + \frac{\lambda}{k\sqrt{t}} \frac{\rho}{\mathrm{St}} S_1(t), \qquad \text{at} \quad \eta = 0, \tag{4.9b}$$

$$T_{s1} = 0, \qquad \text{at} \quad \eta = 1. \tag{4.9c}$$

In order to solve the system (4.9), we shall assume $\lambda \ll 1$, and expand the solutions in powers of λ: $T_{s1} = T_{s1,0} + \lambda T_{s1,1} + \mathcal{O}(\lambda^2)$. As can be found from the transcendental equation (4.43), we have $\lambda \sim \sqrt{\mathrm{St}}$ so this limit of small λ is equivalent to the small Stefan number limit. Physically, it corresponds to the case where the interface moves slowly compared to heat diffusion and, as discussed in detail in Chapter 5, the limits $\epsilon \to 0$ and $\lambda \to 0$ can be taken independently as long as $\epsilon \ll \lambda^2 \ll 1$. The leading order problem is then

$$\frac{\partial^2 T_{s1,0}}{\partial \eta^2} = 0, \qquad \text{in} \quad 0 < \eta < 1, \tag{4.10a}$$

$$T_{s1,0} = -\frac{c_i}{\hat{m}_l}, \qquad \text{at} \quad \eta = 0, \tag{4.10b}$$

$$T_{s1,0} = 0, \qquad \text{at} \quad \eta = 1, \tag{4.10c}$$

and we find that

$$T_{s1,0} = -\frac{c_i}{\hat{m}_l}(1-\eta). \tag{4.11}$$

At $\mathcal{O}(\lambda)$, the problem is

$$\kappa\frac{\partial^2 T_{s1,1}}{\partial\eta^2} = 2(1-\eta)\frac{\partial T_{s1,0}}{\partial\eta}, \qquad \text{in} \quad 0<\eta<1, \tag{4.12a}$$

$$T_{s1,1} = \frac{1}{k\sqrt{t}}\frac{\rho}{\mathrm{St}}S_1(t), \qquad \text{at} \quad \eta = 0, \tag{4.12b}$$

$$T_{s1,1} = 0, \qquad \text{at} \quad \eta = 1, \tag{4.12c}$$

and we find

$$T_{s1,1} = (1-\eta)\left(-\frac{c_i}{\hat{m}_l}\frac{(2-\eta)\eta}{3\kappa} + \frac{\rho}{k\mathrm{St}}\frac{S_1(t)}{\sqrt{t}}\right). \tag{4.13}$$

We can proceed similarly to determine higher order terms in the solution.

4.3.2 Layer B

Layer B is the inner layer of size ϵ around the moving interface. Therefore, we define the inner variable

$$Z = \frac{z - S(t)}{\epsilon}, \tag{4.14}$$

and scaling the following variables as

$$c_s = \epsilon\hat{c}_s, \qquad T_s = \epsilon\hat{T}_s, \qquad \text{and} \qquad T_l = \epsilon\hat{T}_l, \tag{4.15}$$

we find that the problem in the solid phase, $Z > 0$, is

$$\epsilon\frac{\partial\hat{c}_s}{\partial t} = S'(t)\frac{\partial\hat{c}_s}{\partial Z} + \epsilon\hat{D}\frac{\partial^2\hat{c}_s}{\partial Z^2}, \tag{4.16a}$$

$$\epsilon^2\frac{\partial\hat{T}_s}{\partial t} = \epsilon S'(t)\frac{\partial\hat{T}_s}{\partial Z} + \kappa\frac{\partial^2\hat{T}_s}{\partial Z^2}, \tag{4.16b}$$

in the liquid phase $Z < 0$, the problem is

$$\epsilon\frac{\partial c_l}{\partial t} = S'(t)\frac{\partial c_l}{\partial Z} + \frac{\partial^2 c_l}{\partial Z^2}, \tag{4.16c}$$

$$\epsilon^2\frac{\partial\hat{T}_l}{\partial t} = \epsilon S'(t)\frac{\partial\hat{T}_l}{\partial Z} + \frac{\partial^2\hat{T}_l}{\partial Z^2}, \tag{4.16d}$$

and at the interface $Z = 0$, the problem is

$$\hat{T}_s = \hat{T}_l, \tag{4.16e}$$

$$\hat{c}_s = \hat{\alpha} c_l, \tag{4.16f}$$

$$c_l = -\hat{m}_l \hat{T}_l, \tag{4.16g}$$

$$\frac{\rho}{\mathrm{St}} \frac{\mathrm{d}S}{\mathrm{d}t} = k \frac{\partial \hat{T}_s}{\partial Z} - \frac{\partial \hat{T}_l}{\partial Z}, \tag{4.16h}$$

$$(1 - \epsilon \hat{\alpha}) c_l \frac{\mathrm{d}S}{\mathrm{d}t} = \epsilon^2 \hat{D} \frac{\partial \hat{c}_s}{\partial Z} - \frac{\partial c_l}{\partial Z}. \tag{4.16i}$$

The remaining conditions are given by the matching with the solutions in layers A and C. At $\mathcal{O}(1)$, (4.16) gives

$$S_0'(t) \frac{\partial \hat{c}_{s0}}{\partial Z} = 0, \tag{4.17a}$$

$$\frac{\partial^2 \hat{T}_{s0}}{\partial Z^2} = 0, \tag{4.17b}$$

in the solid phase ($Z > 0$),

$$S_0'(t) \frac{\partial c_{l0}}{\partial Z} + \frac{\partial^2 c_{l0}}{\partial Z^2} = 0, \tag{4.17c}$$

$$\frac{\partial^2 \hat{T}_{l0}}{\partial Z^2} = 0, \tag{4.17d}$$

in the liquid phase ($Z < 0$), and

$$\hat{T}_{s0} = \hat{T}_{l0}, \tag{4.17e}$$

$$\hat{c}_{s0} = \hat{\alpha} c_{l0}, \tag{4.17f}$$

$$c_{l0} = -\hat{m}_l \hat{T}_{l0}, \tag{4.17g}$$

$$\frac{\rho}{\mathrm{St}} \frac{\mathrm{d}S_0}{\mathrm{d}t} = k \frac{\partial \hat{T}_{s0}}{\partial Z} - \frac{\partial \hat{T}_{l0}}{\partial Z}, \tag{4.17h}$$

$$c_{l0} \frac{\mathrm{d}S_0}{\mathrm{d}t} + \frac{\partial c_{l0}}{\partial Z} = 0, \tag{4.17i}$$

at the interface ($Z = 0$). Solving the system (4.17) with the matching conditions derived in Section 4.3.4 we find

$$\hat{c}_{s0} = \hat{\alpha} c_i(t), \tag{4.18a}$$

$$c_{l0} = c_i(t) e^{-S_0'(t) Z}, \tag{4.18b}$$

$$\hat{T}_{s0} = A_1(t) Z - \frac{c_i(t)}{\hat{m}_l}, \tag{4.18c}$$

$$\hat{T}_{l0} = \left(k A_1(t) - \frac{\rho}{\mathrm{St}} S_0'(t) \right) Z - \frac{c_i(t)}{\hat{m}_l}, \tag{4.18d}$$

where $c_i(t)$ is the concentration of the interface and $A_1(t)$ an integration function, both to be determined by the matching conditions.

Meanwhile, at $\mathcal{O}(\epsilon)$, (4.16) gives

$$S_0'(t)\frac{\partial \hat{c}_{s1}}{\partial Z} = \frac{\partial \hat{c}_{s0}}{\partial t} - S_1'(t)\frac{\partial \hat{c}_{s0}}{\partial Z} - \hat{D}\frac{\partial^2 \hat{c}_{s0}}{\partial Z^2}, \tag{4.19a}$$

$$\kappa\frac{\partial^2 \hat{T}_{s1}}{\partial Z^2} = -S_0'(t)\frac{\partial \hat{T}_{s0}}{\partial Z}, \tag{4.19b}$$

in the solid phase ($Z > 0$),

$$S_0'(t)\frac{\partial c_{l1}}{\partial Z} + \frac{\partial^2 c_{l1}}{\partial Z^2} = \frac{\partial c_{l0}}{\partial t} - S_1'(t)\frac{\partial c_{l0}}{\partial Z}, \tag{4.19c}$$

$$\frac{\partial^2 \hat{T}_{l1}}{\partial Z^2} = -S_0'(t)\frac{\partial \hat{T}_{l0}}{\partial Z}, \tag{4.19d}$$

in the liquid phase ($Z < 0$), and

$$\hat{T}_{s1} = \hat{T}_{l1}, \tag{4.19e}$$

$$\hat{c}_{s1} = \hat{\alpha} c_{l1}, \tag{4.19f}$$

$$c_{l1} = -\hat{m}_l \hat{T}_{l1}, \tag{4.19g}$$

$$\frac{\rho}{\mathrm{St}}\frac{\mathrm{d}S_1}{\mathrm{d}t} = k\frac{\partial \hat{T}_{s1}}{\partial Z} - \frac{\partial \hat{T}_{l1}}{\partial Z}, \tag{4.19h}$$

$$c_{l1}\frac{\mathrm{d}S_0}{\mathrm{d}t} + \frac{\partial c_{l1}}{\partial Z} = c_{l0}\left(\hat{\alpha}\frac{\mathrm{d}S_0}{\mathrm{d}t} - \frac{\mathrm{d}S_1}{\mathrm{d}t}\right), \tag{4.19i}$$

at the interface ($Z = 0$). The solutions to (4.19) are

$$\hat{c}_{s1} = \frac{\hat{\alpha} c_i'(t)}{S_0'(t)} Z + \hat{\alpha}\mathcal{A}_2(t), \tag{4.20a}$$

$$c_{l1} = \mathcal{A}_1(t) + \mathcal{A}_3(t, Z)e^{-S_0'(t)Z}, \tag{4.20b}$$

$$\hat{T}_{s1} = -\frac{A_1(t)S_0'(t)}{2\kappa} Z^2 + A_3(t)Z - \frac{\mathcal{A}_2(t)}{\hat{m}_l}, \tag{4.20c}$$

$$\hat{T}_{l1} = -\frac{S_0'(t)}{2}\left(kA_1(t) - \frac{\rho}{\mathrm{St}}S_0'(t)\right)Z^2 + \left(kA_3(t) - \frac{\rho}{\mathrm{St}}S_1'(t)\right)Z - \frac{\mathcal{A}_2(t)}{\hat{m}_l}, \tag{4.20d}$$

with

$$\mathcal{A}_1(t) = \frac{c_i'(t)}{S_0'(t)^2} + c_i(t)\left(\hat{\alpha} - \frac{S_0''(t)}{S_0'(t)^3}\right), \tag{4.21a}$$

$$\mathcal{A}_2(t) = A_2(t) + c_i(t)\left(\hat{\alpha} - \frac{S_1'(t)}{S_0'(t)}\right), \tag{4.21b}$$

$$\begin{aligned}\mathcal{A}_3(t, Z) = &-\frac{c_i'(t)}{S_0'(t)^2}\left(1 + S_0'(t)Z\right) + A_2(t) \\ &- c_i(t)\left[\frac{S_1'(t)}{S_0'(t)}\left(1 + S_0'(t)Z\right) + \frac{S_0''(t)}{S_0'(t)^3}\left(1 + S_0'(t)Z + \frac{1}{2}S_0'(t)^2 Z^2\right)\right],\end{aligned} \tag{4.21c}$$

where $A_2(t)$, and $A_3(t)$ are determined from asymptotic matching with other regions.

4.3.3 Layer C

The last layer in regime i is layer C, the outer layer in the liquid ($0 < z < S(t)$). Rescaling the variables as

$$c_l = \epsilon \hat{c}_l \qquad \text{and} \qquad T_l = \epsilon \hat{T}_l, \tag{4.22}$$

we find that

$$\frac{\partial \hat{c}_l}{\partial t} = \epsilon \frac{\partial^2 \hat{c}_l}{\partial z^2}, \qquad \frac{\partial \hat{T}_l}{\partial t} = \frac{\partial^2 \hat{T}_l}{\partial z^2}, \qquad \text{in} \quad 0 < z < S(t), \tag{4.23a}$$

$$\frac{\partial \hat{c}_l}{\partial z} = 0, \qquad \frac{\partial \hat{T}_l}{\partial z} = 0, \qquad \text{at} \quad z = 0, \tag{4.23b}$$

$$\hat{c}_l = \hat{c}_0, \qquad \hat{T}_l = \hat{T}_0, \qquad \text{at} \quad t = 0, \tag{4.23c}$$

and we can complete the problem with the matching conditions with layer B, which are discussed in Section 4.3.4. At $\mathcal{O}(1)$, the problem for concentration is

$$\frac{\partial \hat{c}_{l0}}{\partial t} = 0, \qquad \text{in} \quad 0 < z < S(t), \tag{4.24a}$$

$$\hat{c}_{l0} = \hat{c}_0, \qquad \text{at} \quad t = 0, \tag{4.24b}$$

so $\hat{c}_{l0} = \hat{c}_0$. The problem for temperature is

$$\frac{\partial \hat{T}_{l0}}{\partial t} = \frac{\partial^2 \hat{T}_{l0}}{\partial z^2}, \qquad \text{in} \quad 0 < z < S(t), \tag{4.25a}$$

$$\frac{\partial \hat{T}_{l0}}{\partial z} = 0, \qquad \text{at} \quad z = 0, \tag{4.25b}$$

$$\hat{T}_{l0} = -\frac{c_i}{\hat{m}_l}, \qquad \text{at} \quad z = S_0(t), \tag{4.25c}$$

$$\hat{T}_{l0} = \hat{T}_0, \qquad \text{at} \quad t = 0, \tag{4.25d}$$

where the condition (4.25c) comes from the matching conditions with layer B. In order to determine $\hat{T}_{l0}$, we introduce the variable $\xi = \frac{z}{S_0(t)}$, which fixes the domain of the equation to $\xi \in [0, 1]$, and the rescaling for the temperature from $\hat{T}_{l0}$ to u where

$$\hat{T}_{l0} = \left(\hat{T}_0 + \frac{c_i}{\hat{m}_l} \right) u - \frac{c_i}{\hat{m}_l}, \tag{4.26}$$

in order to homogenise the boundary conditions. Then, the problem can be rewritten as

$$\frac{\partial u}{\partial t} = \frac{1}{(1 - 2\lambda\sqrt{t})^2} \frac{\partial^2 u}{\partial \xi^2} - \xi \frac{\lambda}{\sqrt{t}(1 - 2\lambda\sqrt{t})} \frac{\partial u}{\partial \xi}, \qquad \text{in} \quad 0 < \xi < 1, \tag{4.27a}$$

$$\frac{\partial u}{\partial \xi} = 0, \qquad \text{at} \quad \xi = 0, \tag{4.27b}$$

$$u = 0, \qquad \text{at} \quad \xi = 1, \tag{4.27c}$$

$$u = 1, \qquad \text{at} \quad t = 0. \tag{4.27d}$$

Again, no simple analytical solution is possible so, in order to solve the problem, we assume that $\lambda \ll 1$, and expand u in powers of λ. The problem, at $\mathcal{O}(1)$, is given by

$$\frac{\partial u_0}{\partial t} = \frac{\partial^2 u_0}{\partial \xi^2}, \qquad \text{in} \quad 0 < \xi < 1, \tag{4.28a}$$

$$\frac{\partial u_0}{\partial \xi} = 0, \qquad \text{at} \quad \xi = 0, \tag{4.28b}$$

$$u_0 = 0, \qquad \text{at} \quad \xi = 1, \tag{4.28c}$$

$$u_0 = 1, \qquad \text{at} \quad t = 0. \tag{4.28d}$$

We use separation of variables to solve (4.28), obtaining

$$u_0 = \frac{4}{\pi} \sum_{n=0}^{\infty} \frac{(-1)^n}{2n+1} e^{-\left(\frac{2n+1}{2}\pi\right)^2 t} \cos\left(\frac{2n+1}{2}\pi\xi\right). \tag{4.29}$$

Higher order problems have the structure

$$\frac{\partial u_j}{\partial t} - \frac{\partial^2 u_j}{\partial \xi^2} = f_j(t,\xi), \qquad \text{in} \quad 0 < \xi < 1, \tag{4.30a}$$

$$\frac{\partial u_j}{\partial \xi} = 0, \qquad \text{at} \quad \xi = 0, \tag{4.30b}$$

$$u_j = 0, \qquad \text{at} \quad \xi = 1, \tag{4.30c}$$

$$u_j = 0, \qquad \text{at} \quad t = 0, \tag{4.30d}$$

for $j > 1$. In all the cases, the function $f_j(t,\xi)$ is a known function that depends on the lower order solutions. We can find the solution to each problem using a Green's function $\mathcal{G}(t-\tau,\xi,\hat{\xi})$ which gives

$$u_j(t,\xi) = \int_0^t \int_0^1 f_j(\tau,\hat{\xi}) \mathcal{G}(t-\tau,\xi,\hat{\xi}) \mathrm{d}\hat{\xi}\mathrm{d}\tau, \tag{4.31}$$

where from [72] we know that the Green's function for this problem can be represented in the two forms

$$\begin{aligned} \mathcal{G}(t,\xi,\hat{\xi}) &= 2\sum_{n=0}^{\infty} \cos\left(\frac{2n+1}{2}\pi\xi\right) \cos\left(\frac{2n+1}{2}\pi\hat{\xi}\right) e^{-\left(\frac{2n+1}{2}\pi\right)^2 t} \\ &= \frac{1}{2\sqrt{\pi t}} \sum_{n=-\infty}^{n=+\infty} (-1)^n \left(e^{-\frac{(\xi-\hat{\xi}+2n)^2}{4t}} + e^{-\frac{(\xi+\hat{\xi}+2n)^2}{4t}}\right). \end{aligned} \tag{4.32}$$

Note that the first form converges rapidly for large t, while the second form converges rapidly for small t.

4.3.4 Matching of the solutions

In this section, we use Van Dyke's rule [94] to derive the matching conditions we have used to complete the problems in the previous sections. We start by matching c_l between the outer layer C and the inner layer B. We take two terms in the inner solution and two terms in the outer solution, and write them both in terms of the inner variable so that

$$(2\text{ti})(2\text{to}) = \epsilon\hat{c}_0, \tag{4.33a}$$

$$(2\text{to})(2\text{ti}) = \epsilon\mathcal{A}_1(t). \tag{4.33b}$$

Therefore, we have

$$\frac{c_i'(t)}{S_0'(t)^2} + c_i(t)\left(\hat{\alpha} - \frac{S_0''(t)}{S_0'(t)^3}\right) = \hat{c}_0, \tag{4.34}$$

and solving this ODE for $c_i(t)$ (using as initial condition that $c_i(t)$ must remain bounded) we determine that c_i is constant, and in particular is equal to

$$c_i = \frac{2\lambda^2\hat{c}_0}{2\lambda^2\hat{\alpha}+1}. \tag{4.35}$$

We then match c_s between the outer layer A and the inner layer B. We take two terms in the inner solution and two terms in the outer solution, and write them both in terms of the inner variable, so that

$$(2\text{ti})(2\text{to}) = \epsilon c_{s0}(S_0(t)), \tag{4.36a}$$

$$(2\text{to})(2\text{ti}) = \epsilon\hat{\alpha}c_i(t). \tag{4.36b}$$

Equating both expressions, we find $c_{s0}(z) = \hat{\alpha}c_i$.

We repeat the procedure for T_s and T_l. For simplicity of the calculations, we start expanding one term of the inner solution and one term of the outer solution in T_s to determine S_0. We find

$$(1\text{ti})(1\text{to}) = -1 + C_1\text{erf}\left(\frac{1-S_0(t)}{2\sqrt{\kappa t}}\right) = 0 = (1\text{to})(1\text{ti}), \tag{4.37}$$

where C_1 is a constant yet to be determined. Therefore, we require the interface position to be of the form $S_0(t) = 1 - 2\lambda\sqrt{t}$, determining thus the result in (4.7). We can use this expression to simplify the following expansions. We now take three terms in the outer solution (the term at $\mathcal{O}(\epsilon^2)$ is left as $T_{s2}(t,z)$, for simplicity) and

three terms in the inner solution, which give

$$(3\text{ti})(3\text{to}) = \left(-1 + C_1 \text{erf}\left(\frac{\lambda}{\sqrt{\kappa}}\right)\right) + \epsilon\left(T_{s1}|_{z=S_0(t)} - C_1 e^{-\frac{\lambda^2}{\kappa}} \frac{Z + S_1(t)}{\sqrt{\pi\kappa t}}\right) + \epsilon^2\left(-\frac{e^{-\frac{\lambda^2}{\kappa}}}{2\sqrt{\pi}t\kappa^{\frac{3}{2}}}\left(C_1\lambda\left(Z + S_1(t)\right)^2 + 2C_1\kappa\sqrt{t}S_2(t)\right) + \left(Z + S_1(t)\right)\left.\frac{\partial T_{s1}}{\partial z}\right|_{z=S_0(t)} + T_{s2}|_{z=S_0(t)}\right), \quad (4.38a)$$

$$(3\text{to})(3\text{ti}) = \epsilon\left(A_1(t)Z - \frac{c_i}{\hat{m}_l}\right) + \epsilon^2\left(-\frac{A_1(t)S_0'(t)}{2\kappa}Z^2 + A_3(t)Z - \frac{\mathcal{A}_2(t)}{\hat{m}_l}\right), \quad (4.38b)$$

and we determine that

$$C_1 = \frac{1}{\text{erf}\left(\frac{\lambda}{\sqrt{\kappa}}\right)}, \quad (4.39a)$$

$$T_{s1}|_{z=S_0(t)} = \frac{\lambda}{\kappa\sqrt{t}}\frac{S_1(t)}{G\left(\frac{\lambda}{\sqrt{\kappa}}\right)} - \frac{c_i}{\hat{m}_l}, \quad (4.39b)$$

$$A_1(t) = -\frac{\lambda}{\kappa\sqrt{t}}\frac{1}{G\left(\frac{\lambda}{\sqrt{\kappa}}\right)}, \quad (4.39c)$$

$$A_3(t) = \left.\frac{\partial T_{s1}}{\partial z}\right|_{z=S_0(t)} - \frac{\lambda^2}{\kappa^2 t}\frac{S_1(t)}{G\left(\frac{\lambda}{\sqrt{\kappa}}\right)}, \quad (4.39d)$$

where $G(x) = \sqrt{\pi}xe^{x^2}\text{erf}(x)$.

We proceed similarly for T_l. Taking three term inner and outer expansions, we find

$$(3\text{ti})(3\text{to}) = \epsilon\hat{T}_{l0}(t, S_0(t)) + \epsilon^2\left(\left(Z + S_1(t)\right)\left.\frac{\partial \hat{T}_{l0}}{\partial z}\right|_{z=S_0(t)} + \hat{T}_{l1}(t, S_0(t))\right), \quad (4.40a)$$

$$(3\text{to})(3\text{ti}) = \epsilon\left(\left(kA_1(t) - \frac{\rho}{\text{St}}S_0'(t)\right)Z - \frac{c_i}{\hat{m}_l}\right) + \epsilon^2\left(-\frac{S_0'(t)}{2}\left(kA_1(t) - \frac{\rho}{\text{St}}S_0'(t)\right)Z^2 + \left(kA_3(t) - \frac{\rho}{\text{St}}S_1'(t)\right)Z - \frac{\mathcal{A}_3(t)}{\hat{m}_l}\right), \quad (4.40b)$$

and we determine that

$$\hat{T}_{l0}(t, S_0(t)) = -\frac{c_i}{\hat{m}_l}, \quad (4.41a)$$

$$kA_1(t) - \frac{\rho}{\text{St}}S_0'(t) = 0, \quad (4.41b)$$

$$\left.\frac{\partial \hat{T}_{l0}}{\partial z}\right|_{z=S_0(t)} = kA_3(t) - \frac{\rho}{\mathrm{St}} S_1'(t). \tag{4.41c}$$

We can use (4.41) to determine λ, S_1, and the boundary conditions required to complete the $\hat{T}_{l0}$ problem (4.27). We start by finding λ using

$$\frac{\rho}{\mathrm{St}} S_0'(t) = kA_1(t), \tag{4.42}$$

and given that both $S_0(t)$ and $A_1(t)$ are known from (4.7) and (4.39c), we have

$$\sqrt{\pi}\frac{\lambda}{\sqrt{\kappa}} e^{\frac{\lambda^2}{\kappa}} \operatorname{erf}\left(\frac{\lambda}{\sqrt{\kappa}}\right) = c_p \mathrm{St}, \tag{4.43}$$

where c_p is the dimensionless heat capacity (see Table 2.2 in page 39). Solving this transcendental equation we find λ. The condition (4.41a) determines the remaining boundary condition needed for the problem for $\hat{T}_{l0}$ (4.27).

From condition (4.41c) and using (4.39d), we find

$$\frac{\rho}{\mathrm{St}}\left(S_1'(t) + \frac{\lambda^2}{\kappa t} S_1(t)\right) = k \left.\frac{\partial \hat{T}_{s1}}{\partial z}\right|_{z=S_0(t)} - \left.\frac{\partial \hat{T}_{l0}}{\partial z}\right|_{z=S_0(t)}, \tag{4.44}$$

and integrating this equation we can determine $S_1(t)$. However, as we have the temperature gradients in terms of series in λ in (4.11) and (4.29), we can write

$$\begin{aligned}\frac{\rho}{\mathrm{St}}\left(S_1'(t) + \frac{\lambda^2}{\kappa t} S_1(t)\right) = \frac{k}{2\lambda\sqrt{t}}\left(\frac{c_i}{\hat{m}_l} + \mathcal{O}(\lambda)\right) \\ + \frac{2}{1-2\lambda\sqrt{t}}\left(\hat{T}_0 + \frac{c_i}{\hat{m}_l}\right)\left(\sum_{n=0}^{\infty} e^{-\left(\frac{2n+1}{2}\pi\right)^2 t} + \mathcal{O}(\lambda)\right),\end{aligned} \tag{4.45}$$

therefore we see that the temperature gradient in the solid is of $\mathcal{O}(\lambda^{-1})$, and hence $S_1(t)$ will also be this order. Expanding $S_1(t)$ in powers of λ, $S_1 = \lambda^{-1} S_{1,-1} + S_{1,0} + \mathcal{O}(\lambda)$, we have that, at $\mathcal{O}(\lambda^{-1})$, (4.45) is

$$\frac{\rho}{\mathrm{St}} S_{1,-1}'(t) = \frac{k}{2\sqrt{t}} \frac{c_i}{\hat{m}_l}, \tag{4.46}$$

therefore

$$S_1(t) = \frac{k\mathrm{St}}{\rho} \frac{1}{2\lambda} \frac{c_i}{\hat{m}_l} \sqrt{t} + \mathcal{O}(1). \tag{4.47}$$

With this leading order approximation for $S_1(t)$ in powers of λ we conclude the analysis for regime i. This regime ranges for $t \in [0, t^*]$ where $t^* = \frac{1}{4\lambda^2}$ is the time when the leading order solution for the position of the interface becomes zero. In this regime, we have determined the solutions at leading order for all the variables and,

for some of them, such as T_s, T_l, and S, we have determined the next term in the asymptotic expansion in powers of ϵ. The motivation to calculate these corrections was to determine the position of the interface up to $\mathcal{O}(\epsilon)$ as it is needed for the matching with the solution in regime ii. In the next section we focus our attention on regime ii, which arises because the interface is so close to the origin that the outer layer in the liquid disappears and, therefore, the inner layer needs to capture the symmetry conditions at the origin. Physically, this new regime captures the interaction between the two approaching solidification fronts caused by the diffusion of impurities in the liquid.

4.4 Asymptotic solutions in regime ii

We now study regime ii, where the interface is within a distance $\mathcal{O}(\epsilon)$ from the origin and therefore the mass diffusion boundary layer reaches the symmetry line. In this case we distinguish two layers: the outer layer D and the inner layer E.

4.4.1 Layer D

We consider first the outer layer D, where the following variables are scaled as

$$t = t^* + \epsilon\tau, \qquad S = \epsilon\hat{S}, \qquad \text{and} \qquad c_s = \epsilon\hat{c}_s. \tag{4.48}$$

Then, the problem is defined on $0 < z < 1$ by

$$\frac{\partial \hat{c}_s}{\partial \tau} = \epsilon^3 \hat{D}\frac{\partial^2 \hat{c}_s}{\partial z^2}, \qquad \frac{\partial T_s}{\partial \tau} = \epsilon\kappa\frac{\partial^2 T_s}{\partial z^2}, \qquad \text{in} \quad 0 < z < 1, \tag{4.49a}$$

$$\frac{\partial \hat{c}_s}{\partial z} = 0, \qquad T_s = -1, \qquad \text{at} \quad z = 1, \tag{4.49b}$$

and the appropriate matching conditions with layers A and E.

At $\mathcal{O}(1)$, the problem is

$$\frac{\partial \hat{c}_{s0}}{\partial \tau} = 0 \quad \text{and} \quad \frac{\partial T_{s0}}{\partial \tau} = 0, \tag{4.50a}$$

therefore the leading order solutions do not depend on time τ, so we have to determine their values from matching with (4.7). As we show in Section 4.4.3, we find

$$\hat{c}_{s0} = \frac{2\lambda^2\hat{\alpha}}{2\lambda^2\hat{\alpha}+1}\hat{c}_0 \quad \text{and} \quad T_{s0} = -1 + \frac{\operatorname{erf}\left(\frac{\lambda}{\sqrt{\kappa}}(1-z)\right)}{\operatorname{erf}\left(\frac{\lambda}{\sqrt{\kappa}}\right)}. \tag{4.51}$$

4.4.2 Layer E

We determine the governing equations in the inner layer E using the scalings

$$t = t^* + \epsilon\tau, \quad z = \epsilon Z, \quad S = \epsilon\hat{S}, \quad c_s = \epsilon\hat{c}_s, \quad T_s = \epsilon\hat{T}_s, \quad \text{and} \quad T_l = \epsilon\hat{T}_l. \tag{4.52}$$

The problem becomes the following: in the solid phase ($Z > \hat{S}(\tau)$), we have

$$\frac{\partial \hat{c}_s}{\partial \tau} = \epsilon\hat{D}\frac{\partial^2 \hat{c}_s}{\partial Z^2}, \tag{4.53a}$$

$$\epsilon\frac{\partial \hat{T}_s}{\partial \tau} = \kappa\frac{\partial^2 \hat{T}_s}{\partial Z^2}, \tag{4.53b}$$

in the liquid phase ($0 < Z < \hat{S}(\tau)$), we have

$$\frac{\partial c_l}{\partial \tau} = \frac{\partial^2 c_l}{\partial Z^2}, \tag{4.53c}$$

$$\epsilon\frac{\partial \hat{T}_l}{\partial \tau} = \frac{\partial^2 \hat{T}_l}{\partial Z^2}, \tag{4.53d}$$

and at the interface ($Z = \hat{S}(\tau)$), we have

$$\hat{T}_s = \hat{T}_l, \tag{4.53e}$$

$$\hat{c}_s = \hat{\alpha}c_l, \tag{4.53f}$$

$$c_l = -\hat{m}_l\hat{T}_l, \tag{4.53g}$$

$$\frac{\rho}{\mathrm{St}}\frac{\mathrm{d}\hat{S}}{\mathrm{d}\tau} = k\frac{\partial \hat{T}_s}{\partial Z} - \frac{\partial \hat{T}_l}{\partial Z}, \tag{4.53h}$$

$$(1 - \epsilon\hat{\alpha})c_l\frac{\mathrm{d}\hat{S}}{\mathrm{d}\tau} = \epsilon^2\hat{D}\frac{\partial \hat{c}_s}{\partial Z} - \frac{\partial c_l}{\partial Z}, \tag{4.53i}$$

with the boundary conditions

$$\frac{\partial c_l}{\partial Z} = 0 \quad \text{and} \quad \frac{\partial \hat{T}_l}{\partial Z} = 0, \quad \text{at} \quad Z = 0. \tag{4.53j}$$

We need to impose matching conditions in space with layer D and in time with layer B.

At $\mathcal{O}(1)$, in the solid phase $Z > \hat{S}_0(\tau)$, we have

$$\frac{\partial \hat{c}_{s0}}{\partial \tau} = 0, \tag{4.54a}$$

$$\frac{\partial^2 \hat{T}_{s0}}{\partial Z^2} = 0, \tag{4.54b}$$

in the liquid phase $0 < Z < \hat{S}_0(\tau)$, we have

$$\frac{\partial c_{l0}}{\partial \tau} = \frac{\partial^2 c_{l0}}{\partial Z^2}, \tag{4.54c}$$

$$\frac{\partial^2 \hat{T}_{l0}}{\partial Z^2} = 0, \tag{4.54d}$$

and at the interface $Z = \hat{S}_0(\tau)$, we have

$$\hat{T}_{s0} = \hat{T}_{l0}, \tag{4.54e}$$

$$\hat{c}_{s0} = \hat{\alpha} c_{l0}, \tag{4.54f}$$

$$c_{l0} = -\hat{m}_l \hat{T}_{l0}, \tag{4.54g}$$

$$\frac{\rho}{\mathrm{St}} \frac{\mathrm{d}\hat{S}_0}{\mathrm{d}\tau} = k \frac{\partial \hat{T}_{s0}}{\partial Z} - \frac{\partial \hat{T}_{l0}}{\partial Z}, \tag{4.54h}$$

$$c_{l0} \frac{\mathrm{d}\hat{S}_0}{\mathrm{d}\tau} + \frac{\partial c_{l0}}{\partial Z} = 0, \tag{4.54i}$$

with boundary conditions

$$\frac{\partial c_{l0}}{\partial Z} = 0 \quad \text{and} \quad \frac{\partial \hat{T}_{l0}}{\partial Z} = 0, \quad \text{at } Z = 0. \tag{4.54j}$$

We find the solutions

$$\hat{c}_{s0} = \hat{\alpha} c_{l0} \left(\hat{S}_0^{-1}(Z), Z \right), \tag{4.55a}$$

$$\hat{T}_{s0} = \frac{\rho}{k\mathrm{St}} \frac{\mathrm{d}\hat{S}_0}{\mathrm{d}\tau} Z - \left(\frac{\rho}{k\mathrm{St}} \frac{\mathrm{d}\hat{S}_0}{\mathrm{d}\tau} \hat{S}_0(\tau) + \frac{c_{l0}(\tau, \hat{S}_0(\tau))}{\hat{m}_l} \right), \tag{4.55b}$$

$$\hat{T}_{l0} = -\frac{c_{l0}(\tau, \hat{S}_0(\tau))}{\hat{m}_l}, \tag{4.55c}$$

and the value of c_{l0} is yet to be determined. The problem for c_{l0} is given by

$$\frac{\partial c_{l0}}{\partial \tau} = \frac{\partial^2 c_{l0}}{\partial Z^2}, \qquad \text{in} \quad 0 < Z < \hat{S}_0(\tau), \tag{4.56a}$$

$$\frac{\partial c_{l0}}{\partial Z} = 0, \qquad \text{at} \quad Z = 0, \tag{4.56b}$$

$$c_{l0} \frac{\partial \hat{S}_0}{\partial \tau} + \frac{\partial c_{l0}}{\partial Z} = 0, \qquad \text{at} \quad Z = \hat{S}_0(\tau), \tag{4.56c}$$

$$c_{l0} \sim c_i e^{2\lambda^2 \left(Z + 2\lambda^2 (\tau - \tau^*) \right)}, \qquad \text{as} \quad \tau \to -\infty, \tag{4.56d}$$

where

$$\hat{S}_0(\tau) = -2\lambda^2 (\tau - \tau^*), \quad \tau^* = \frac{k\mathrm{St}}{\rho} \frac{1}{8\lambda^4} \frac{c_i}{\hat{m}_l}. \tag{4.57}$$

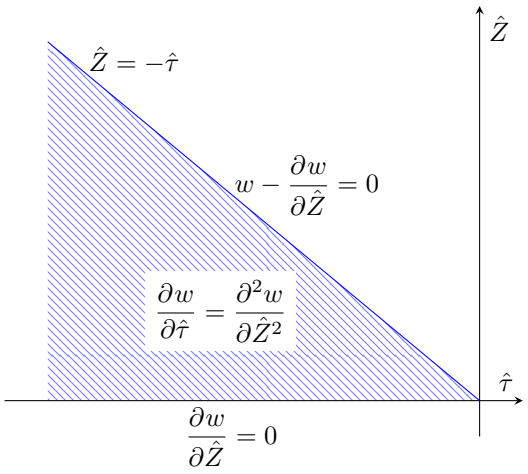


Figure 4.3: Sketch of the problem (4.59). The highlighted area is the domain in which we want to solve the problem (which extends to $\hat{\tau} \to -\infty$). We prescribe the initial condition $w \to e^{\hat{Z}+\hat{\tau}}$ as $\hat{\tau} \to -\infty$.

The condition (4.56d) and the form of the interface (4.57) are determined from the matching conditions derived in Section 4.4.3.

We can eliminate all the parameters in the problem (4.56) by rescaling the variables with

$$\tau = \tau^* + \frac{\hat{\tau}}{(2\lambda^2)^2}, \quad Z = \frac{\hat{Z}}{2\lambda^2}, \quad \text{and} \quad c_{l0} = c_i w, \tag{4.58}$$

so that (4.56) reduces (as shown in Figure 4.3) to

$$\frac{\partial w}{\partial \hat{\tau}} = \frac{\partial^2 w}{\partial \hat{Z}^2}, \qquad \text{in} \quad 0 < \hat{Z} < -\hat{\tau}, \tag{4.59a}$$

$$\frac{\partial w}{\partial \hat{Z}} = 0, \qquad \text{at} \quad \hat{Z} = 0, \tag{4.59b}$$

$$w - \frac{\partial w}{\partial \hat{Z}} = 0, \qquad \text{at} \quad \hat{Z} = -\hat{\tau}, \tag{4.59c}$$

$$w \sim e^{\hat{Z}+\hat{\tau}}, \qquad \text{as} \quad \hat{\tau} \to -\infty. \tag{4.59d}$$

Notice that

$$w(\hat{\tau}, \hat{Z}) = e^{\hat{Z}+\hat{\tau}}, \tag{4.60}$$

almost satisfies (4.59), except for the boundary condition (4.59c). Then, in order to solve (4.59), we superpose infinitely many exponential profiles in a similar manner to the method of images. We find that the solution is given by

$$w(\hat{\tau}, \hat{Z}) = \sum_{n=1}^{\infty} n \left(e^{n(\hat{Z}+n\hat{\tau})} + e^{n(-\hat{Z}+n\hat{\tau})} \right). \tag{4.61}$$

It is immediate to check that (4.61) solves (4.59a) and (4.59b) as each of the terms of the sum satisfies the equations. Truncating (4.61) at N terms, the error at condition (4.59c) is $N(N+1)e^{N(N+1)\hat{\tau}}$ and given that $\hat{\tau} < 0$, it tends to zero as $N \to +\infty$. The exception is in the limit $\hat{\tau} \to 0^-$ however, this latter limit is considered separately in regime iii, hence the solution (4.61) is valid for our purposes. Finally, we need to check that (4.61) satisfies the initial condition (4.59d). Notice that

$$\lim_{\hat{\tau}\to-\infty} e^{\hat{Z}+\hat{\tau}} = \begin{cases} 0, & \text{if } \hat{Z} < -\hat{\tau}, \\ 1, & \text{if } \hat{Z} = -\hat{\tau}. \end{cases} \tag{4.62}$$

Then, it is immediate to check that when $0 \leq \hat{Z} < -\hat{\tau}$ we have

$$\lim_{\hat{\tau}\to-\infty} w(\hat{\tau}, \hat{Z}) = 0, \tag{4.63}$$

while in the case $\hat{Z} = -\hat{\tau}$ the limit is

$$\begin{aligned} \lim_{\hat{\tau}\to-\infty} w(\hat{\tau}, -\hat{\tau}) &= \lim_{\hat{\tau}\to-\infty} \sum_{n=1}^{\infty} n \left(e^{n(n-1)\hat{\tau}} + e^{(n+1)n\hat{\tau}} \right) \\ &= \lim_{\hat{\tau}\to-\infty} 1 + e^{2\hat{\tau}} + \sum_{n=2}^{\infty} n \left(e^{n(n-1)\hat{\tau}} + e^{(n+1)n\hat{\tau}} \right) \\ &= 1. \end{aligned} \tag{4.64}$$

Hence, we conclude that

$$\lim_{\hat{\tau}\to-\infty} w(\hat{\tau}, \hat{Z}) = \begin{cases} 0, & \text{if } \hat{Z} < -\hat{\tau}, \\ 1, & \text{if } \hat{Z} = -\hat{\tau}, \end{cases} \tag{4.65}$$

and therefore $w(\hat{\tau}, \hat{Z})$ in (4.61) is the solution of (4.59).

4.4.3 Matching of the solutions

We start by matching c_s between the outer layer in time B and the inner layer in time E. Taking two terms in both the inner and outer solutions, we find that the solution is constant, so $c_s = \epsilon\hat{\alpha}c_i$. In order to determine the initial conditions for c_l, we need to match it with layer B. Taking one term in each solution, we find

$$(1\text{to})(1\text{ti}) = \lim_{\tau\to-\infty} c_{l0}(\tau, Z), \tag{4.66a}$$

$$(1\text{ti})(1\text{to}) = c_i \exp\left(2\lambda^2 \left(Z + 2\lambda^2 \left(\tau - \frac{k\text{St}}{\rho} \frac{1}{8\lambda^4} \frac{c_i}{\hat{m}_l} \right) \right) \right), \tag{4.66b}$$

so we have that

$$c_{l0} \sim c_i \exp\left(2\lambda^2\left(Z + 2\lambda^2\left(\tau - \frac{k\mathrm{St}}{\rho}\frac{1}{8\lambda^4}\frac{c_i}{\hat{m}_l}\right)\right)\right), \tag{4.67}$$

as $\tau \to -\infty$.

Finally, we need to match T_s with layer D in order to determine the interface position $\hat{S}_0(\tau)$. Taking one term of the outer solution and two terms of the inner solution, we find

$$(2\mathrm{ti})(1\mathrm{to}) = -\epsilon\frac{\rho}{k\mathrm{St}}2\lambda^2 Z, \tag{4.68a}$$

$$(1\mathrm{to})(2\mathrm{ti}) = \epsilon\frac{\rho}{k\mathrm{St}}\frac{\mathrm{d}\hat{S}_0}{\mathrm{d}\tau}Z; \tag{4.68b}$$

therefore, we obtain $\hat{S}_0(\tau) = -2\lambda^2\tau + C_3$, and we need to determine C_3 from matching with regime i. Taking two terms in both the inner and outer solutions, we find

$$(2\mathrm{ti})(2\mathrm{to}) = \epsilon\left(-2\lambda^2\tau + \frac{k\mathrm{St}}{\rho}\frac{1}{4\lambda^2}\frac{c_i}{\hat{m}_l}\right), \tag{4.69a}$$

$$(2\mathrm{to})(2\mathrm{ti}) = \epsilon\left(-2\lambda^2\tau + C_3\right), \tag{4.69b}$$

hence

$$C_3 = \frac{k\mathrm{St}}{\rho}\frac{1}{4\lambda^2}\frac{c_i}{\hat{m}_l}. \tag{4.70}$$

Thus, we have determined the position of the interface, and this completes problem (4.56).

We have now fully determined the leading order solutions in regime ii, which are mainly driven by the build-up of impurities in the liquid phase due to the fact that the two solidification fronts are very close to each other and therefore impurities cannot diffuse away. Because the concentration of impurities is small, compared to the amount required to cause significant supercooling, the limiting behaviour when $\tau \to \tau^*$ results into an infinite amount of impurity concentration in an infinitely small region of liquid. This motivates the study of regime iii, in which we expect the build-up of impurities to continue, but now with an impact over the thermal problem, that in turn slows down the interface.

4.5 Asymptotic solutions in regime iii

We now focus on the regime iii, which has three layers: the outer layer F, the intermediate layer G, and the inner layer H. The motivation for this regime is to capture the quick transition from regime ii, where the interface moves at a high velocity, to

regime iv, where the interface moves very slowly. In this regime, we observe a layer in the solid where heat diffusion occurs, and also a build-up of impurities in the liquid phase that causes enough supercooling to slow down the interface.

4.5.1 Layer F

We consider first the outer layer F, with the rescalings

$$t = t^* + \epsilon\tau^* + \epsilon^{\frac{4}{3}}\theta, \qquad S = \epsilon^{\frac{4}{3}}\hat{S}, \qquad \text{and} \qquad c_s = \epsilon\hat{c}_s. \tag{4.71}$$

The problem is given by

$$\frac{\partial \hat{c}_s}{\partial \theta} = \epsilon^{\frac{10}{3}}\hat{D}\frac{\partial^2 \hat{c}_s}{\partial z^2}, \qquad \frac{\partial T_s}{\partial \theta} = \epsilon^{\frac{4}{3}}\kappa\frac{\partial^2 T_s}{\partial z^2}, \qquad \text{in} \quad 0 < z < 1, \tag{4.72a}$$

$$\frac{\partial \hat{c}_s}{\partial z} = 0, \qquad T_s = -1, \qquad \text{at} \quad z = 1, \tag{4.72b}$$

and the appropriate matching conditions with layers D and G. At leading order, we find that the solutions are independent of time, so the matching conditions with layer D derived in Section 4.4.3 give

$$\hat{c}_{s0} = \frac{2\lambda^2\hat{\alpha}}{2\lambda^2\hat{\alpha}+1}\hat{c}_0 \quad \text{and} \quad T_{s0} = -1 + \frac{\operatorname{erf}\left(\frac{\lambda}{\sqrt{\kappa}}(1-z)\right)}{\operatorname{erf}\left(\frac{\lambda}{\sqrt{\kappa}}\right)}, \tag{4.73}$$

which are the same solutions as (4.51) in layer D.

4.5.2 Layer G

The next layer to study is the intermediate layer G, which is the layer where significant heat diffusion takes place. The scalings in this layer are

$$t = t^* + \epsilon\tau^* + \epsilon^{\frac{4}{3}}\theta, \quad z = \epsilon^{\frac{2}{3}}\xi, \quad S = \epsilon^{\frac{4}{3}}\hat{S}, \quad c_s = \epsilon\hat{c}_s, \quad \text{and} \quad T_s = \epsilon^{\frac{2}{3}}\hat{T}_s. \tag{4.74}$$

In this layer, defined by $\xi > 0$, we have

$$\frac{\partial \hat{c}_s}{\partial \theta} = \epsilon^2\hat{D}\frac{\partial^2 \hat{c}_s}{\partial \xi^2}, \tag{4.75a}$$

$$\frac{\partial \hat{T}_s}{\partial \theta} = \kappa\frac{\partial^2 \hat{T}_s}{\partial \xi^2}, \tag{4.75b}$$

with matching conditions with layers D, F, and H. At $\mathcal{O}(1)$, the problem is

$$\frac{\partial \hat{c}_{s0}}{\partial \theta} = 0, \tag{4.75c}$$

$$\frac{\partial \hat{T}_{s0}}{\partial \theta} = \kappa\frac{\partial^2 \hat{T}_{s0}}{\partial \xi^2}, \tag{4.75d}$$

and, using the matching conditions derived in Section 4.5.4, we immediately determine that $c_s = \epsilon\hat{\alpha}c_i$, where $c_i = \frac{2\lambda^2\hat{c}_0}{2\lambda^2\hat{\alpha}+1}$ is the concentration at the interface as determined in regime i.

In order to determine $\hat{T}_{s0}$, we need to find the boundary conditions of the problem from matching. Using the conditions derived in Section 4.5.4, we can write the problem for $\hat{T}_{s0}$ and $\hat{S}_0$ as

$$\frac{\partial \hat{T}_{s0}}{\partial \theta} = \kappa \frac{\partial^2 \hat{T}_{s0}}{\partial \xi^2}, \qquad \text{in} \quad \xi > 0, \tag{4.76a}$$

$$\hat{T}_{s0} = -\frac{c_{tot}}{\hat{m}_l}\frac{1}{\hat{S}_0(\theta)}, \qquad \text{at} \quad \xi = 0, \tag{4.76b}$$

$$\frac{\partial \hat{T}_{s0}}{\partial \xi} = \frac{\rho}{k\mathrm{St}}\hat{S}_0'(\theta), \qquad \text{at} \quad \xi = 0, \tag{4.76c}$$

$$\hat{T}_{s0} \sim -2\lambda^2\frac{\rho}{k\mathrm{St}}\xi, \qquad \text{as} \quad \xi \to +\infty, \tag{4.76d}$$

$$\hat{T}_{s0} \sim -2\lambda^2\frac{\rho}{k\mathrm{St}}\xi, \qquad \text{as} \quad \theta \to -\infty, \tag{4.76e}$$

$$\frac{\mathrm{d}\hat{S}_0}{\mathrm{d}\tau} \to -2\lambda^2, \qquad \text{as} \quad \theta \to -\infty. \tag{4.76f}$$

where c_{tot} is the total concentration in the liquid phase, as defined in Section 4.5.4.

By introducing the scaled variables

$$\begin{aligned} \hat{T}_{s0} &= \left(2\frac{\kappa\lambda^2\rho^2 c_{tot}}{k^2\hat{m}_l\mathrm{St}^2}\right)^{\frac{1}{3}}(u-x), \qquad & \hat{S}_0 &= \left(\frac{k^2\mathrm{St}^2c_{tot}^2}{2\kappa\lambda^2\hat{m}_l^2\rho^2}\right)^{\frac{1}{3}}S, \\ \theta &= \left(\frac{k^2\mathrm{St}^2c_{tot}^2}{16\kappa\lambda^8\hat{m}_l^2\rho^2}\right)^{\frac{1}{3}}t, & \xi &= \left(\frac{\kappa k\mathrm{St}c_{tot}}{4\lambda^4\hat{m}_l\rho}\right)^{\frac{1}{3}}x, \end{aligned} \tag{4.77}$$

we reduce the problem (4.76) to

$$\frac{\partial u}{\partial t} = \frac{\partial^2 u}{\partial x^2}, \qquad \text{in} \quad x > 0, \tag{4.78a}$$

$$u = -\frac{1}{S(t)}, \qquad \text{at} \quad x = 0, \tag{4.78b}$$

$$\frac{\partial u}{\partial x} = \frac{\mathrm{d}S}{\mathrm{d}t} + 1, \qquad \text{at} \quad x = 0, \tag{4.78c}$$

$$\frac{\partial u}{\partial x} \to 0, \qquad \text{as} \quad x \to +\infty, \tag{4.78d}$$

$$u \to 0, \qquad \text{as} \quad t \to -\infty, \tag{4.78e}$$

$$\frac{\mathrm{d}S}{\mathrm{d}t} \to -1, \qquad \text{as} \quad t \to -\infty. \tag{4.78f}$$

We can use (4.78a), (4.78b), (4.78d), and (4.78e) to determine $u(t,x)$ using Laplace transforms. Notice that our problem starts at $t \to -\infty$, therefore, when taking the

transform, we need to start at $t = -t_0$ and then take $t_0 \to \infty$. We find that the Laplace transform of $u(t,x)$, defined as $\overline{u}(p,x) = \mathcal{L}\{u\}(p)$ where p is the frequency variable, is

$$\overline{u}(p,x) = p\mathcal{L}\left\{-\frac{1}{S(t)}\right\}(p)\frac{e^{-x\sqrt{p}}}{p}. \tag{4.79}$$

We can now take the inverse Laplace transform to obtain $u(t,x)$, which is given by

$$u(t,x) = \left(\frac{\mathrm{d}}{\mathrm{d}t}\left(-\frac{1}{S(t)}\right)\right) * \operatorname{erfc}\left(\frac{x}{2\sqrt{t}}\right), \tag{4.80}$$

where $*$ denotes the convolution defined as

$$F(t) * G(t) = \int_{-\infty}^{t} F(\tau)G(t-\tau)\mathrm{d}\tau. \tag{4.81}$$

Therefore, $u(t,x)$ is given by

$$u(t,x) = \int_{-\infty}^{t} \frac{\mathrm{d}}{\mathrm{d}t}\left(-\frac{1}{S(\tau)}\right)\operatorname{erfc}\left(\frac{x}{2\sqrt{t-\tau}}\right)\mathrm{d}\tau. \tag{4.82}$$

From here, we shall obtain the equation governing $S(t)$. We start taking the derivative of (4.79) with respect to x, to find

$$\frac{\partial \overline{u}}{\partial x} = -p\mathcal{L}\left\{-\frac{1}{S(t)}\right\}(p)\frac{e^{-x\sqrt{p}}}{\sqrt{p}}, \tag{4.83}$$

so taking the inverse Laplace transform we obtain

$$\frac{\partial u}{\partial x} = -\left(\frac{\mathrm{d}}{\mathrm{d}t}\left(-\frac{1}{S(t)}\right)\right) * \left(\frac{e^{-\frac{x^2}{4t}}}{\sqrt{\pi t}}\right). \tag{4.84}$$

Evaluating (4.84) at $x = 0$, we have

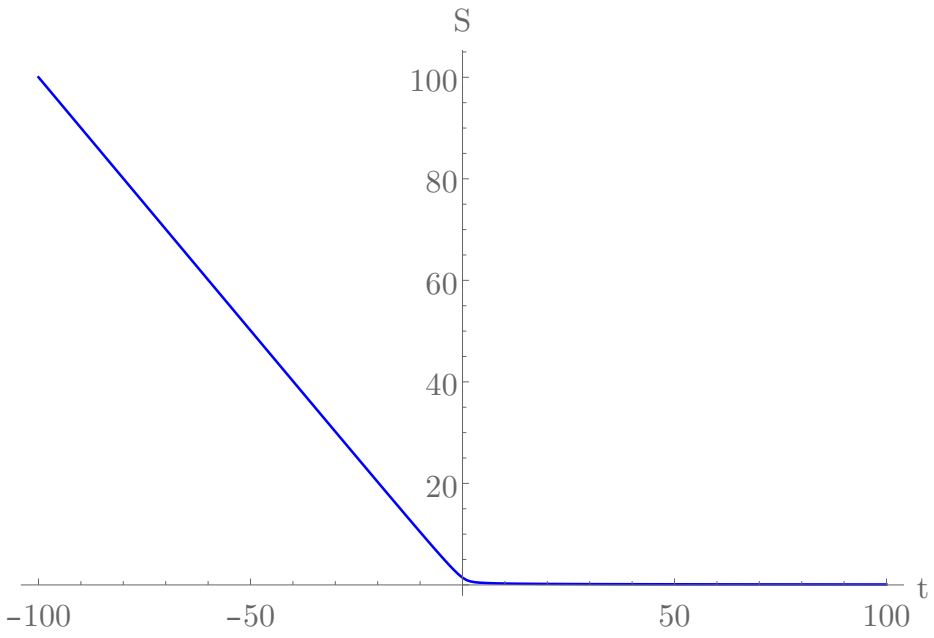
$$\left.\frac{\partial u}{\partial x}\right|_{x=0} = -\frac{1}{\sqrt{\pi}}\int_{-\infty}^{t} \frac{S'(\tau)}{S(\tau)^2}\frac{\mathrm{d}\tau}{\sqrt{t-\tau}}, \tag{4.85}$$

and using the boundary condition (4.78c) we obtain the integro-differential equation

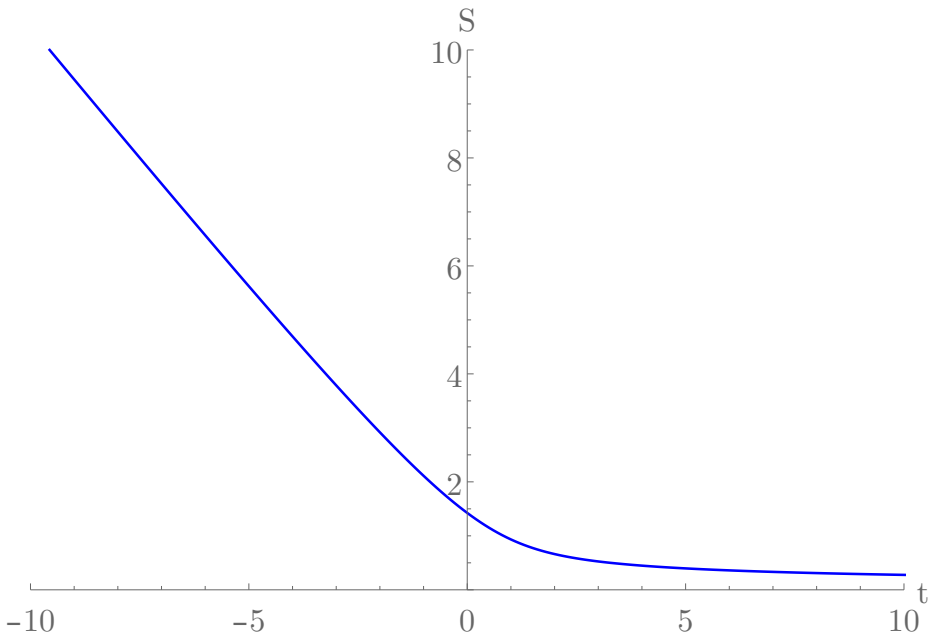
$$\frac{\mathrm{d}S}{\mathrm{d}t} + 1 = -\frac{1}{\sqrt{\pi}}\int_{-\infty}^{t} \frac{S'(\tau)}{S(\tau)^2}\frac{\mathrm{d}\tau}{\sqrt{t-\tau}}, \tag{4.86}$$

which determines $S(t)$.

We cannot find an analytic solution for $S(t)$, but, given that the problem (4.78) has no parameters, we can solve it numerically and then rescale the results for our original problem (4.76). In order to solve (4.78) we use a finite volume scheme. We start the simulation at $t = -100$ with $S = 100$ and $u = 0$, so they are consistent



(a)



(b)

Figure 4.4: Numerical solutions to (4.78) for (a) the range $t \in [-100, 100]$ and (b) the range $t \in [-10, 10]$.

with the initial conditions. The simulation domain is taken to be $x \in [0, 1000]$ which simulations show to be large enough so the boundary at $x = 1000$ does not interfere significantly with the diffusion process. Figure 4.4 shows the numerical solution.

Even though we cannot find analytical solutions, we can calculate the large time behaviour of the solution. Notice that, in the limit $t \to -\infty$, the behaviour is given by the initial condition $\dfrac{\mathrm{d}S}{\mathrm{d}t} \to -1$, hence we have that $S \sim -(t - C_4)$, where C_4 is an integration constant. Because the problem (4.78) is invariant under time shifts, C_4 remains undetermined unless further matching conditions are derived.

The behaviour in the limit $t \to +\infty$ can be found from (4.86), using the assumption that $\dfrac{\mathrm{d}S}{\mathrm{d}t} \to 0$ when $t \to +\infty$, which we have from the numerical solution. Then, (4.86) gives

$$1 = -\frac{1}{\sqrt{\pi}} \int_{-\infty}^{t} \frac{S'(\tau)}{S(\tau)^2} \frac{\mathrm{d}\tau}{\sqrt{t-\tau}} = -\frac{1}{\sqrt{\pi}} \left(\frac{S'(t)}{S(t)^2} \right) * \left(\frac{1}{\sqrt{t}} \right). \tag{4.87}$$

Taking the Laplace transform we find

$$\frac{1}{p} = -\mathcal{L}\left\{ \frac{S'(t)}{S(t)^2} \right\}(p) \frac{1}{\sqrt{p}}, \tag{4.88}$$

therefore

$$\frac{1}{\sqrt{p}} = -\mathcal{L}\left\{ \frac{S'(t)}{S(t)^2} \right\}(p), \tag{4.89}$$

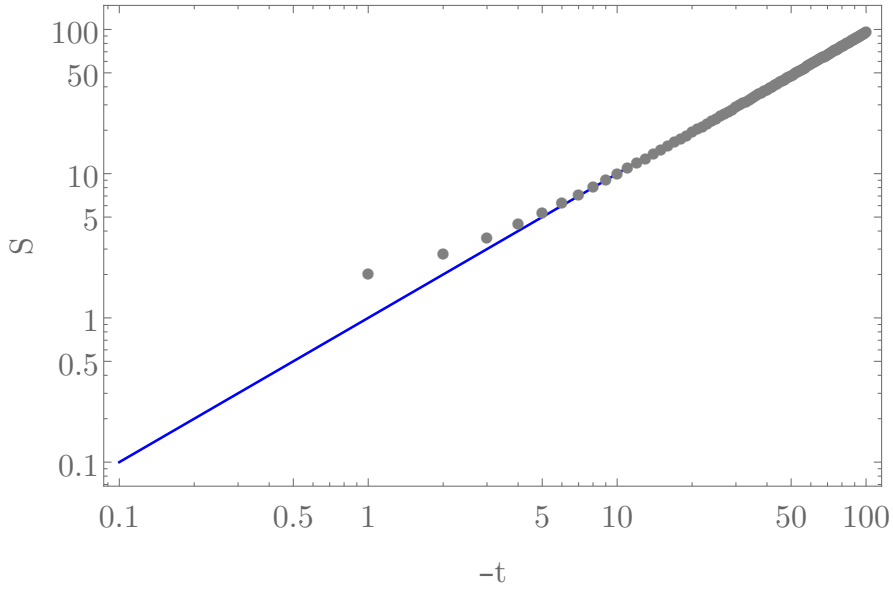
and taking the inverse Laplace transform we have

$$-\frac{S'(t)}{S(t)^2} = \frac{1}{\sqrt{\pi t}}. \tag{4.90}$$

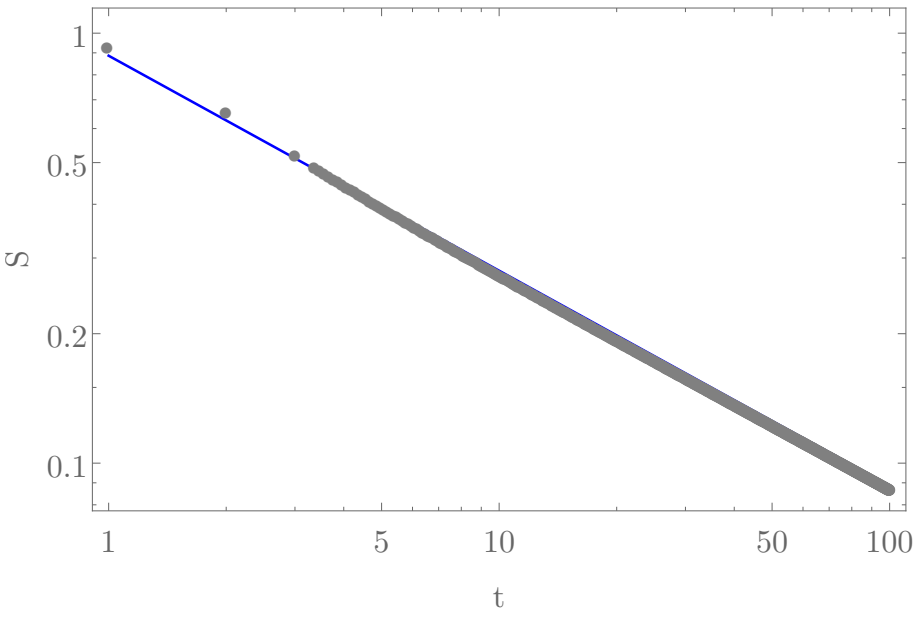
Integrating, we conclude that

$$S(t) = \frac{\sqrt{\pi}}{2\sqrt{t} + C_5}, \tag{4.91}$$

where C_5 is an integrating constant. However, notice that when $t \to +\infty$, $S \sim \frac{\sqrt{\pi}}{2\sqrt{t}}$, therefore the value of this constant does not affect the asymptotic behaviour of $S(t)$. Notice that this result satisfies the assumption $\dfrac{\mathrm{d}S}{\mathrm{d}t} \to 0$ when $t \to +\infty$ that we took at the beginning of the analysis. In Figure 4.5 we compare the behaviour of the numerical simulations in both limits $t \to \pm\infty$ against the predictions on a loglog plot, finding that the numerical solutions agree with the expected asymptotic behaviour.



(a)



(b)

asymptotic behaviour numerics

Figure 4.5: Comparison of the numerical solutions and the asymptotic behaviour in the limits (a) $t \to -\infty$ where the expected behaviour is $S \sim t$ given that for the initial conditions used in the simulations we have $C_4 = 0$ (notice that S is plotted against $-t$), and (b) $t \to +\infty$ where the expected behaviour is $S \sim \frac{\sqrt{\pi}}{2\sqrt{t}}$.

4.5.3 Layer H

Finally, we study the inner layer H where the interface conditions hold. The scalings in this layer are

$$\begin{aligned} t = t^* + \epsilon\tau^* + \epsilon^{\frac{4}{3}}\theta, \quad z = \epsilon^{\frac{4}{3}} Z, \quad S = \epsilon^{\frac{4}{3}}\hat{S}, \\ c_s = \epsilon^{\frac{2}{3}}\hat{c}_s, \quad c_l = \epsilon^{-\frac{1}{3}}\hat{c}_l, \quad T_s = \epsilon^{\frac{2}{3}}\hat{T}_s, \quad T_l = \epsilon^{\frac{2}{3}}\hat{T}_l. \end{aligned} \tag{4.92}$$

The problem in the solid phase $Z > \hat{S}(\theta)$, is

$$\frac{\partial \hat{c}_s}{\partial \theta} = \epsilon^{\frac{2}{3}}\hat{D}\frac{\partial^2 \hat{c}_s}{\partial Z^2}, \tag{4.93a}$$

$$\epsilon^{\frac{4}{3}}\frac{\partial \hat{T}_s}{\partial \theta} = \kappa\frac{\partial^2 \hat{T}_s}{\partial Z^2}, \tag{4.93b}$$

in the liquid phase $0 < Z < \hat{S}(\theta)$, it is

$$\epsilon^{\frac{1}{3}}\frac{\partial \hat{c}_l}{\partial \theta} = \frac{\partial^2 \hat{c}_l}{\partial Z^2}, \tag{4.93c}$$

$$\epsilon^{\frac{4}{3}}\frac{\partial \hat{T}_l}{\partial \theta} = \frac{\partial^2 \hat{T}_l}{\partial Z^2}, \tag{4.93d}$$

and at the interface $Z = \hat{S}(\theta)$, the conditions are

$$\hat{T}_s = \hat{T}_l, \tag{4.93e}$$

$$\hat{c}_s = \hat{\alpha}\hat{c}_l, \tag{4.93f}$$

$$\hat{c}_l = -\hat{m}_l\hat{T}_l, \tag{4.93g}$$

$$\epsilon^{\frac{2}{3}}\frac{\rho}{\mathrm{St}}\frac{\mathrm{d}\hat{S}}{\mathrm{d}\theta} = k\frac{\partial \hat{T}_s}{\partial Z} - \frac{\partial \hat{T}_l}{\partial Z}, \tag{4.93h}$$

$$\epsilon^{\frac{1}{3}}(1 - \epsilon\hat{\alpha})\hat{c}_l\frac{\mathrm{d}\hat{S}}{\mathrm{d}\theta} = \epsilon^2\hat{D}\frac{\partial \hat{c}_s}{\partial Z} - \frac{\partial \hat{c}_l}{\partial Z}. \tag{4.93i}$$

The boundary conditions are

$$\frac{\partial \hat{c}_l}{\partial Z} = 0 \quad \text{and} \quad \frac{\partial \hat{T}_l}{\partial Z} = 0 \quad \text{at} \quad Z = 0. \tag{4.93j}$$

We need to impose appropriate matching conditions in space with layer G and in time with layer E.

The problem at $\mathcal{O}(1)$ is

$$\frac{\partial \hat{c}_{s0}}{\partial \theta} = 0, \tag{4.94a}$$

$$\frac{\partial^2 \hat{T}_{s0}}{\partial Z^2} = 0, \tag{4.94b}$$

in the solid,

$$\frac{\partial^2 \hat{c}_{l0}}{\partial Z^2} = 0, \tag{4.94c}$$

$$\frac{\partial^2 \hat{T}_{l0}}{\partial Z^2} = 0, \tag{4.94d}$$

in the liquid,

$$\hat{T}_{s0} = \hat{T}_{l0}, \tag{4.94e}$$

$$\hat{c}_{s0} = \hat{\alpha}\hat{c}_{l0}, \tag{4.94f}$$

$$\hat{c}_{l0} = -\hat{m}_l \hat{T}_{l0}, \tag{4.94g}$$

$$k\frac{\partial \hat{T}_{s0}}{\partial Z} = \frac{\partial \hat{T}_{l0}}{\partial Z}, \tag{4.94h}$$

$$\frac{\partial \hat{c}_{l0}}{\partial Z} = 0, \tag{4.94i}$$

at the interface. Boundary conditions are

$$\frac{\partial \hat{c}_{l0}}{\partial Z} = 0 \quad \text{and} \quad \frac{\partial \hat{T}_{l0}}{\partial Z} = 0 \quad \text{at} \quad Z = 0. \tag{4.94j}$$

We find the solutions

$$\hat{c}_{s0} = \hat{\alpha} c_{i0}(\hat{S}_0^{-1}(Z)), \tag{4.95}$$

$$\hat{c}_{l0} = c_{i0}(\theta), \tag{4.96}$$

$$\hat{T}_{s0} = -\frac{c_{i0}(\theta)}{\hat{m}_l}, \tag{4.97}$$

$$\hat{T}_{s0} = -\frac{c_{i0}(\theta)}{\hat{m}_l}, \tag{4.98}$$

where $c_{i0}(\theta)$ is a function yet to be determined, which is found from the next order solution.

At $\mathcal{O}\left(\epsilon^{\frac{1}{3}}\right)$, the problem is

$$\frac{\partial \hat{c}_{s\frac{1}{3}}}{\partial \theta} = 0, \tag{4.99a}$$

$$\frac{\partial^2 \hat{T}_{s\frac{1}{3}}}{\partial Z^2} = 0, \tag{4.99b}$$

in the solid,

$$\frac{\partial^2 \hat{c}_{l\frac{1}{3}}}{\partial Z^2} = c'_{i0}(\theta), \tag{4.99c}$$

$$\frac{\partial^2 \hat{T}_{l\frac{1}{3}}}{\partial Z^2} = 0, \tag{4.99d}$$

in the liquid,

$$\hat{T}_{s\frac{1}{3}} = \hat{T}_{l\frac{1}{3}}, \tag{4.99e}$$

$$\hat{c}_{s\frac{1}{3}} = \hat{\alpha}\left(\hat{c}_{l\frac{1}{3}} - \frac{\hat{S}_{\frac{1}{3}}(\theta)}{\hat{S}_0'(\theta)}c_{i0}'(\theta)\right), \tag{4.99f}$$

$$\hat{c}_{l\frac{1}{3}} = -\hat{m}_l\hat{T}_{l\frac{1}{3}}, \tag{4.99g}$$

$$k\frac{\partial\hat{T}_{s\frac{1}{3}}}{\partial Z} = \frac{\partial\hat{T}_{l\frac{1}{3}}}{\partial Z}, \tag{4.99h}$$

$$\frac{\partial\hat{c}_{l\frac{1}{3}}}{\partial Z} + c_{i0}(\theta)\frac{\mathrm{d}\hat{S}_0}{\mathrm{d}\theta} = 0, \tag{4.99i}$$

at the interface, and the boundary conditions are

$$\frac{\partial\hat{c}_{l\frac{1}{3}}}{\partial Z} = 0 \quad \text{and} \quad \frac{\partial\hat{T}_{l\frac{1}{3}}}{\partial Z} = 0 \quad \text{at} \quad Z = 0. \tag{4.99j}$$

We obtain the solutions

$$\hat{c}_{l\frac{1}{3}} = \frac{1}{2}c_{i0}'(\theta)Z^2 + c_{i\frac{1}{3}}(\theta) - \frac{1}{2}c_{i0}'(\theta)\hat{S}_0(\theta)^2, \tag{4.100a}$$

$$\hat{T}_{s\frac{1}{3}} = -\frac{c_{i\frac{1}{3}}(\theta)}{\hat{m}_l}, \tag{4.100b}$$

$$\hat{T}_{l\frac{1}{3}} = -\frac{c_{i\frac{1}{3}}(\theta)}{\hat{m}_l}, \tag{4.100c}$$

and we do not calculate $c_{s\frac{1}{3}}$, since we do not need it for our analysis. From (4.99i), we find

$$\frac{\partial c_{i0}}{\partial\theta}\hat{S}_0 + c_{i0}\frac{\partial\hat{S}_0}{\partial\theta} = 0, \tag{4.101}$$

therefore we conclude that $c_{i0}\hat{S}_0 = c_{tot}$ is constant. Note that this condition is equivalent to conservation of mass in the liquid at leading order, therefore the constant c_{tot} is the total mass of impurities in this regime. Furthermore, we can show that in regime ii the quantity of impurities in the liquid at leading order is conserved, even though the profiles are not constant in time. Therefore, the value of c_{tot} is constant throughout regimes ii and iii, so we can calculate it at the final state of regime i for convenience, that is using solution (4.18b). We find

$$c_{tot} = \int_{-\infty}^{0} c_i e^{2\lambda^2 Z}\mathrm{d}Z = \frac{\hat{c}_0}{2\lambda^2\hat{\alpha}+1}, \tag{4.102}$$

where we have used the definition of c_i given in (4.35).

Finally, we study the problem at $\mathcal{O}\left(\epsilon^{\frac{2}{3}}\right)$, however we consider only the temperature profiles, as they are the ones we need for matching. We have

$$\frac{\partial^2 \hat{T}_{s\frac{2}{3}}}{\partial Z^2} = 0, \qquad \text{in} \quad Z > \hat{S}_0(\theta), \tag{4.103a}$$

$$\frac{\partial^2 \hat{T}_{l\frac{2}{3}}}{\partial Z^2} = 0, \qquad \text{in} \quad 0 < Z < \hat{S}_0(\theta), \tag{4.103b}$$

$$\hat{T}_{s\frac{2}{3}} = \hat{T}_{l\frac{2}{3}} = A_4(\tau), \qquad \text{at} \quad Z = \hat{S}_0(\theta), \tag{4.103c}$$

$$\frac{\rho}{\mathrm{St}} \frac{\mathrm{d}\hat{S}_0}{\mathrm{d}\theta} = k \frac{\partial \hat{T}_{s\frac{2}{3}}}{\partial Z} - \frac{\partial \hat{T}_{l\frac{2}{3}}}{\partial Z}, \qquad \text{at} \quad Z = \hat{S}_0(\theta), \tag{4.103d}$$

$$\frac{\partial \hat{T}_{l\frac{2}{3}}}{\partial Z} = 0, \qquad \text{at} \quad Z = 0, \tag{4.103e}$$

and we find the solutions

$$\hat{T}_{s\frac{2}{3}} = \frac{\rho}{k\mathrm{St}} \frac{\mathrm{d}\hat{S}_0}{\mathrm{d}\theta} Z + A_4(\theta) \quad \text{and} \quad \hat{T}_{l\frac{2}{3}} = A_4(\theta), \tag{4.104}$$

where $A_4(\theta)$ is related to the value of $c_{l\frac{2}{3}}$, which we have not calculated.

4.5.4 Matching of the solutions

We now match the solutions of the different layers to determine the boundary conditions for the temperature problem in layer G. We start matching layers F and G, therefore G now acts as the inner layer because F is the outer layer. Because in this regime we have the expansions of the solutions in powers of $\epsilon^{\frac{1}{3}}$, when we say we take two terms it means up to $\mathcal{O}\left(\epsilon^{\frac{1}{3}}\right)$, three terms means up to $\mathcal{O}\left(\epsilon^{\frac{2}{3}}\right)$, and so on and so forth. Taking three terms in the inner solution (up to $\mathcal{O}\left(\epsilon^{\frac{2}{3}}\right)$) and one term in the outer solution, we find

$$(3\text{ti})(1\text{to}) = \epsilon^{\frac{2}{3}} \left(-2\lambda^2 \frac{\rho}{k\mathrm{St}} \xi\right), \tag{4.105}$$

$$(1\text{to})(3\text{ti}) = \lim_{\xi \to +\infty} \epsilon^{\frac{2}{3}} \hat{T}_{s0}(\theta, \xi), \tag{4.106}$$

and therefore we find the condition

$$\hat{T}_{s0} \sim -2\lambda^2 \frac{\rho}{k\mathrm{St}} \xi, \tag{4.107}$$

as $\xi \to +\infty$.

Similarly, we determine the initial condition by matching the solution in layer G with the solution in layer D. As the solution in layer D does not depend on time, we have the same linearisation as in (4.107), therefore we find

$$\hat{T}_{s0} \sim -2\lambda^2 \frac{\rho}{k\mathrm{St}} \xi, \tag{4.108}$$

as $\theta \to -\infty$.

To complete the problem, we need to calculate the matching between layer G and layer H, where now layer G acts as the outer layer. We take five terms (up to $\mathcal{O}\left(\epsilon^{\frac{4}{3}}\right)$) in both layers finding

$$(5\text{ti})(5\text{to}) = \epsilon^{\frac{2}{3}}\hat{T}_{s0}(\theta,0) + \epsilon\hat{T}_{s\frac{1}{3}}(\theta,0) + \epsilon^{\frac{4}{3}}\left(\left.\frac{\partial\hat{T}_{s0}}{\partial Z}\right|_{\xi=0} Z + \hat{T}_{s\frac{2}{3}}(\theta,0)\right), \tag{4.109a}$$

$$(5\text{to})(5\text{ti}) = -\epsilon^{\frac{2}{3}}\frac{c_{i0}(\theta)}{\hat{m}_l} - \epsilon\frac{c_{i1}(\theta)}{\hat{m}_l} + \epsilon^{\frac{4}{3}}\left(\frac{\rho}{k\mathrm{St}}\hat{S}_0'(\theta)Z + A_4(\theta)\right). \tag{4.109b}$$

As we are only interested in determining $\hat{T}_{s0}$, we take only the conditions

$$\hat{T}_{s0}(\theta,0) = -\frac{c_{i0}(\theta)}{\hat{m}_l} = -\frac{c_{tot}}{\hat{m}_l}\frac{1}{\hat{S}_0(\theta)}, \tag{4.110a}$$

$$\left.\frac{\partial\hat{T}_{s0}}{\partial Z}\right|_{\xi=0} = \frac{\rho}{k\mathrm{St}}\hat{S}_0'(\theta). \tag{4.110b}$$

This finishes the analysis of regime iii, in which we observed that the build-up of impurities in the liquid phase causes enough supercooling to slow the interface down. At the final stages of this regime, that is when $\theta \to +\infty$, we observe that at leading order the position of the interface tends to zero, and thus the interfacial concentration and temperature blow up. Therefore, we need to introduce regime iv to capture the behaviour in that limit.

4.6 Asymptotic solutions in regime iv

Finally, we focus our attention on the late time part of the problem: regime iv. Again, we distinguish two layers: the outer layer I, and the inner layer J. In the previous layers, we took D to be of order ϵ as this assumption was sufficient to decouple the diffusion of impurities in the solid from the remainder of the analysis. With this scaling, in regime iv we would need to consider an extra layer in the solid phase (between layers I and J) where we observe diffusion of impurities. For simplicity, and because this layer would only provide new information for c_s, which is of small relevance to our analysis, we take $D = \mathcal{O}(\epsilon^p)$ for some $p > 3$, which prevents diffusion of impurities from occurring in layer J. This assumption keeps the concentration profile stationary in both layers I and J and, despite the rescaling, does not affect the matching with previous layers.

4.6.1 Layer I

We consider first the outer layer I, using the rescalings

$$S = \epsilon^2 \hat{S}, \qquad \text{and} \qquad c_s = \epsilon \hat{c}_s. \tag{4.111}$$

The problem is defined in $0 < z < 1$ by

$$\frac{\partial \hat{c}_s}{\partial t} = \epsilon^{p+1} \hat{D} \frac{\partial^2 \hat{c}_s}{\partial z^2}, \qquad \frac{\partial T_s}{\partial t} = \kappa \frac{\partial^2 T_s}{\partial z^2}, \qquad \text{in} \quad 0 < z < 1, \tag{4.112a}$$

$$\frac{\partial \hat{c}_s}{\partial z} = 0, \qquad T_s = -1, \qquad \text{at} \quad z = 1, \tag{4.112b}$$

and appropriate matching conditions with layers J and F. At $\mathcal{O}(1)$, the problem is

$$\frac{\partial \hat{c}_{s0}}{\partial t} = 0, \qquad \frac{\partial T_{s0}}{\partial t} = \kappa \frac{\partial^2 T_{s0}}{\partial z^2}, \qquad \text{in} \quad 0 < z < 1, \tag{4.113a}$$

$$\frac{\partial \hat{c}_{s0}}{\partial z} = 0, \qquad T_{s0} = -1, \qquad \text{at} \quad z = 1. \tag{4.113b}$$

In a similar way to what we did before, we find that $\hat{c}_{s0} = \hat{\alpha} c_i$. In Section 4.6.3, we derive the matching conditions that complete the problem for T_{s0}, so we have

$$\frac{\partial T_{s0}}{\partial t} = \kappa \frac{\partial^2 T_{s0}}{\partial z^2}, \qquad \text{in} \quad 0 < z < 1, \tag{4.114a}$$

$$\frac{\partial T_{s0}}{\partial z} = 0, \qquad \text{at} \quad z = 0, \tag{4.114b}$$

$$T_{s0} = -1, \qquad \text{at} \quad z = 1, \tag{4.114c}$$

$$T_{s0} = -1 + \frac{\operatorname{erf}\left(\frac{\lambda}{\sqrt{\kappa}}(1-z)\right)}{\operatorname{erf}\left(\frac{\lambda}{\sqrt{\kappa}}\right)}, \qquad \text{at} \quad t = t^* + \epsilon \tau^*. \tag{4.114d}$$

Using separation of variables (as the problem is defined in the fixed domain $0 < z < 1$), we find

$$T_{s0} = -1 + \sum_{n=0}^{\infty} a_n e^{-\left(\frac{2n+1}{2}\pi\right)^2 \kappa (t - t^* - \epsilon\tau^*)} \cos\left(\frac{2n+1}{2}\pi z\right), \tag{4.115}$$

where the coefficients a_n are defined by

$$a_n = 2 \int_0^1 \frac{\operatorname{erf}\left(\frac{\lambda}{\sqrt{\kappa}}(1-z)\right)}{\operatorname{erf}\left(\frac{\lambda}{\sqrt{\kappa}}\right)} \cos\left(\frac{2n+1}{2}\pi z\right) \mathrm{d}z. \tag{4.116}$$

4.6.2 Layer J

For the inner layer, J, we take the scalings

$$z = \epsilon^2 Z, \qquad S = \epsilon^2 \hat{S}, \qquad \text{and} \qquad c_l = \epsilon^{-1} \hat{c}_l. \tag{4.117}$$

and then rewrite the problem as follows. In the solid phase, $Z > \hat{S}(t)$, we have

$$\frac{\partial c_s}{\partial t} = \epsilon^{p-3}\hat{D}\frac{\partial^2 c_s}{\partial Z^2}, \tag{4.118a}$$

$$\epsilon^4\frac{\partial T_s}{\partial t} = \kappa\frac{\partial^2 T_s}{\partial Z^2}, \tag{4.118b}$$

in the liquid phase, $0 < Z < \hat{S}(t)$, we have

$$\epsilon^3\frac{\partial \hat{c}_l}{\partial t} = \frac{\partial^2 \hat{c}_l}{\partial Z^2}, \tag{4.118c}$$

$$\epsilon^4\frac{\partial T_l}{\partial t} = \frac{\partial^2 T_l}{\partial Z^2}, \tag{4.118d}$$

and at the interface, $Z = \hat{S}(t)$, we have

$$T_s = T_l, \tag{4.118e}$$

$$c_s = \hat{\alpha}\hat{c}_l, \tag{4.118f}$$

$$\hat{c}_l = -\hat{m}_l T_l, \tag{4.118g}$$

$$\epsilon^4\frac{\rho}{\mathrm{St}}\frac{\mathrm{d}\hat{S}}{\mathrm{d}t} = k\frac{\partial T_s}{\partial Z} - \frac{\partial T_l}{\partial Z}, \tag{4.118h}$$

$$\epsilon^3(1-\epsilon\hat{\alpha})\hat{c}_l\frac{\mathrm{d}\hat{S}}{\mathrm{d}\tau} = \epsilon^{p+1}\hat{D}\frac{\partial c_s}{\partial Z} - \frac{\partial \hat{c}_l}{\partial Z}. \tag{4.118i}$$

The boundary conditions are

$$\frac{\partial \hat{c}_l}{\partial Z} = 0 \quad \text{and} \quad \frac{\partial T_l}{\partial Z} = 0 \quad \text{at} \quad Z = 0. \tag{4.118j}$$

At $\mathcal{O}(1)$, the problem is as follows. In the solid phase ($Z > \hat{S}_0(t)$), we have

$$\frac{\partial c_{s0}}{\partial t} = 0, \tag{4.119a}$$

$$\frac{\partial^2 T_{s0}}{\partial Z^2} = 0, \tag{4.119b}$$

in the liquid phase ($0 < Z < \hat{S}_0(t)$), we have

$$\frac{\partial^2 \hat{c}_{l0}}{\partial Z^2} = 0, \tag{4.119c}$$

$$\frac{\partial^2 T_{l0}}{\partial Z^2} = 0, \tag{4.119d}$$

at the interface ($Z = \hat{S}_0(t)$), we have

$$T_{s0} = T_{l0}, \tag{4.119e}$$

$$c_{s0} = \hat{\alpha}\hat{c}_{l0}, \tag{4.119f}$$

$$\hat{c}_{l0} = -\hat{m}_l T_{l0}, \tag{4.119g}$$

$$\frac{\partial T_{s0}}{\partial Z} = \frac{\partial T_{l0}}{\partial Z}, \tag{4.119h}$$

$$\frac{\partial \hat{c}_{l0}}{\partial Z} = 0, \tag{4.119i}$$

with boundary conditions

$$\frac{\partial \hat{c}_{l0}}{\partial Z} = 0 \quad \text{and} \quad \frac{\partial T_{l0}}{\partial Z} = 0 \quad \text{at} \quad Z = 0. \tag{4.119j}$$

The solution is then

$$c_{s0} = \hat{\alpha} c_{i0}(\hat{S}_0^{-1}(Z)), \tag{4.120a}$$

$$\hat{c}_{l0} = c_{i0}(t), \tag{4.120b}$$

$$T_{s0} = -\frac{c_{i0}(t)}{\hat{m}_l}, \tag{4.120c}$$

$$T_{l0} = -\frac{c_{i0}(t)}{\hat{m}_l}, \tag{4.120d}$$

so we will need to determine both $c_{i0}(t)$ and $\hat{S}_0(t)$. The first can be determined from the matching with (4.115), but we need to determine T_s up to $\mathcal{O}(\epsilon^2)$ first. The resulting problems are the same as for $\mathcal{O}(1)$, therefore we find

$$T_s = -\frac{c_{i0}(t)}{\hat{m}_l} - \epsilon\frac{c_{i1}(t)}{\hat{m}_l} - \epsilon^2\frac{c_{i2}(t)}{\hat{m}_l}. \tag{4.121}$$

In order to determine the position of the interface, we need to determine $c_{l3}(t, Z)$, which gives $c_{l3} = \frac{1}{2}c'_{i0}(t)Z^2 + A_5(t)$, where $A_5(t)$ is a function of time that we do not need to determine for the purposes of our analysis. Then, the interface condition (4.118i) at $\mathcal{O}(\epsilon^3)$ gives, as in regime iii, that $c_{i0}(t)\hat{S}_0(t) = c_{tot}$, where the total concentration c_{tot} is the same as in regime iii.

4.6.3 Matching of the solutions

In this regime, we only need to match T_s in layer I both with layers J and F, in order to determine the boundary and initial conditions, respectively. We start by matching

the inner layer J with the outer layer I. Taking one term in the outer solution and three terms in the inner solution, we find

$$(3\text{ti})(1\text{to}) = T_{s0}(t,0) + \epsilon^2 Z \left.\frac{\partial T_{s0}}{\partial z}\right|_{z=0}, \tag{4.122a}$$

$$(1\text{to})(3\text{ti}) = -\frac{c_{i0}(t)}{\hat{m}_l}, \tag{4.122b}$$

and thus we conclude

$$\left.\frac{\partial T_{s0}}{\partial z}\right|_{z=0} = 0, \tag{4.123a}$$

$$c_{i0}(t) = -\hat{m}_l T_{s0}(t,0). \tag{4.123b}$$

The first condition is the boundary condition at $z = 0$ which we need to solve the problem in layer I, while the second condition determines $c_{i0}(t)$.

Finally, we match the outer layer in time I with the inner layer F. As the inner solution does not depend on time, the matching is trivial, and we find

$$T_{s0}(t^* + \epsilon\tau^*, z) = -1 + \frac{\operatorname{erf}\left(\frac{\lambda}{\sqrt{\kappa}}(1-z)\right)}{\operatorname{erf}\left(\frac{\lambda}{\sqrt{\kappa}}\right)}, \tag{4.124}$$

which is the initial condition for the problem in layer I. Therefore, we have completed the problem for T_{s0} in layer I.

This concludes the analysis of the last regime of the problem, as the solutions found here hold up to the limit $t \to +\infty$. Therefore, bringing together the solutions found in each of the four time regimes, we can describe, at leading order, the behaviour of the system (4.2) for $t \in [0, +\infty)$.

4.7 Summary of the asymptotic solutions

To summarize, our analysis has revealed four different time regimes within which we distinguish significantly different behaviours of the solutions. In all four regimes, we found that the impurities in the solid diffuse so slowly that the diffusion process in the solid can be neglected. In this section we provide the leading order solutions in each layer, rewritten in terms of the original dimensionless parameters (i.e. before rescaling) presented in Table 2.2 (see page 39). Remember, that we defined the small parameter $\epsilon = \mathrm{Le}^{-1}$.

In regime i, which is at the beginning of the process, the time scale is $\mathcal{O}(1)$. This regime has two outer layers, one in the liquid and one in the solid, and a transition

layer around the solidification front. In the outer layer in the solid ($z > S(t)$, layer A), we have

$$\begin{aligned} c_s &\approx \alpha c_i, \\ T_s &\approx -1 + \frac{\operatorname{erf}\left(\frac{1-z}{2\sqrt{\kappa t}}\right)}{\operatorname{erf}\left(\frac{\lambda}{\sqrt{\kappa}}\right)}, \end{aligned} \tag{4.125a}$$

in the transition layer ($z = S(t)$, layer B), we have

$$\begin{aligned} c_s &\approx \alpha c_i, \\ T_s &\approx -\frac{\rho}{k\mathrm{St}}\frac{\lambda}{\sqrt{t}}(z - S(t)) - \frac{c_i}{m_l}, \\ c_l &\approx c_i \exp\left(\frac{\lambda}{\sqrt{t}}\mathrm{Le}\,(z - S(t))\right), \\ T_l &\approx -\frac{c_i}{m_l}, \end{aligned} \tag{4.125b}$$

and in the outer layer in the liquid ($z < S(t)$, layer C), we have

$$\begin{aligned} c_l &\approx c_0, \\ T_l &\approx \left(T_0 + \frac{c_i}{m_l}\right)\frac{4}{\pi}\sum_{n=0}^{\infty}\frac{(-1)^n}{2n+1}e^{-\left(\frac{2n+1}{2}\pi\right)^2 t}\cos\left(\frac{2n+1}{2}\pi\frac{z}{S(t)}\right) - \frac{c_i}{m_l}, \end{aligned} \tag{4.125c}$$

where

$$\begin{aligned} S(t) &\approx 1 - 2\lambda\sqrt{t}, \\ c_i &\approx \frac{2\lambda^2 c_0}{2\lambda^2\alpha + \mathrm{Le}^{-1}}, \end{aligned} \tag{4.125d}$$

and the constant λ is found from (4.43). Remember that for T_l in layer C, apart from the asymptotic expansion in the limit of large Lewis number, we have used an asymptotic expansion in the limit of small λ (which is equivalent to small Stefan number), so the solution provided is the leading order term in λ. In this regime, the system is driven by the thermal problem which has the self-similar behaviour of a one-phase Stefan problem, with the classic $\sqrt{t}$ motion of the interface [10]. This is because, in the beginning, due to the small supercooling the two solidification fronts do not interact significantly. For the impurity transport, there is a "snow plough" effect due to the rejection of impurities from the solid into the liquid, resulting in a build-up of impurities in a thin layer of size $\mathcal{O}(\epsilon)$ in the liquid phase adjacent to the interface.

Once the two fronts are within a distance $\mathcal{O}(\epsilon)$ from one another, they begin to notice each other, since the impurities can no longer diffuse away. This corresponds to regime ii, where the time scale is $\mathcal{O}(\epsilon)$ around the critical time $t = t^*$. We distinguish

two layers: the outer layer D, and the inner layer E. In the outer layer D in the solid ($z > 0$), the solutions are

$$\begin{aligned} c_s &\approx \alpha c_i, \\ T_s &\approx -1 + \frac{\operatorname{erf}\left(\frac{\lambda}{\sqrt{\kappa}}(1-z)\right)}{\operatorname{erf}\left(\frac{\lambda}{\sqrt{\kappa}}\right)}, \end{aligned} \tag{4.126a}$$

while in the inner layer E around the origin, with the solid phase in $z > S(t)$ and the liquid in $z < S(t)$, we have

$$\begin{aligned} c_s &\approx \alpha c_i \sum_{n=1}^{\infty} n \left[\exp\left(-2\lambda^2 \mathrm{Le}\, n(n-1)z\right) + \exp\left(-2\lambda^2 \mathrm{Le}\, n(n+1)z\right)\right], \\ T_s &\approx -2\lambda^2 \frac{\rho}{k\mathrm{St}} \left(z - S(t)\right) \\ &\quad - \frac{c_i}{m_l} \sum_{n=1}^{\infty} n \left[\exp\left(-2\lambda^2 \mathrm{Le}\, n(n-1)S(t)\right) + \exp\left(-2\lambda^2 \mathrm{Le}\, n(n+1)S(t)\right)\right], \\ c_l &\approx c_i \sum_{n=1}^{\infty} n \left[\exp\left(2\lambda^2 \mathrm{Le}\, n\left(z - nS(t)\right)\right) + \exp\left(2\lambda^2 \mathrm{Le}\, n\left(-z - nS(t)\right)\right)\right], \\ T_l &\approx -\frac{c_i}{m_l} \sum_{n=1}^{\infty} n \left[\exp\left(-2\lambda^2 \mathrm{Le}\, n(n-1)S(t)\right) + \exp\left(-2\lambda^2 \mathrm{Le}\, n(n+1)S(t)\right)\right], \end{aligned} \tag{4.126b}$$

where

$$\begin{aligned} S(t) &\approx -2\lambda^2 \left(t - t^* - \tau^*\right), \\ t^* &= \frac{1}{4\lambda^2}, \\ \tau^* &= \frac{k\mathrm{St}}{\rho} \frac{1}{8\lambda^4} \frac{c_i}{m_l}, \end{aligned} \tag{4.126c}$$

where the value of τ^* is the leading order term in the small λ expansion. The solutions show a build-up of concentration of impurities in the liquid, due to the interaction between the fronts. At this small time scale, the temperature in the solid remains constant (at leading order), and we find that the motion of the interface is linear. The temperature in the liquid is homogeneous and equal to the supercooling temperature at the interface. This behaviour is explained by the fact that the build-up of impurities is not large enough to cause significant supercooling, and therefore does not affect the temperature in the solid nor the motion of the interface.

In regime iii, the two fronts are within a distance $\mathcal{O}\left(\epsilon^{\frac{4}{3}}\right)$ from one another, and the time scale is $\mathcal{O}\left(\epsilon^{\frac{4}{3}}\right)$ around the critical time $t = t^* + \tau^*$. We distinguish three

layers: an outer layer F in the solid, an inner layer G of size $\mathcal{O}\left(\epsilon^{\frac{2}{3}}\right)$, and an inner layer H of size $\mathcal{O}\left(\epsilon^{\frac{4}{3}}\right)$, both around the origin. In the outer layer F ($z > 0$), we have

$$\begin{aligned} c_s &\approx \alpha c_i, \\ T_s &\approx -1 + \frac{\operatorname{erf}\left(\frac{\lambda}{\sqrt{\kappa}}(1-z)\right)}{\operatorname{erf}\left(\frac{\lambda}{\sqrt{\kappa}}\right)}, \end{aligned} \tag{4.127a}$$

in the inner layer G, we have

$$\begin{aligned} c_s &\approx \alpha c_i, \\ T_s &\approx -2\lambda^2 \frac{\rho}{k\mathrm{St}} z \\ &\quad + \frac{c_{tot}}{m_l} \int_{-\infty}^{t-t^*-\tau^*} \frac{S'(s)}{S(s)^2} \operatorname{erfc}\left(\frac{z}{2\sqrt{\kappa}\sqrt{t-t^*-\tau^*-s}}\right) \mathrm{d}s, \end{aligned} \tag{4.127b}$$

and in the inner layer H ($z > S(t)$ for the solid, and $z < S(t)$ for the liquid), we have

$$\begin{aligned} c_s &\approx \frac{\alpha c_{tot}}{z}, \\ T_s &\approx -\frac{1}{m_l}\frac{c_{tot}}{S(t)}, \\ c_l &\approx \frac{c_{tot}}{S(t)}, \\ T_l &\approx -\frac{1}{m_l}\frac{c_{tot}}{S(t)}, \end{aligned} \tag{4.127c}$$

where

$$c_{tot} = \frac{c_0}{2\lambda^2 \alpha \mathrm{Le} + 1}, \tag{4.127d}$$

and $S(t)$ is the solution to the integro-differential equation (4.86). Given that we can eliminate all the parameters from the problem, we can use the numerical solution of the parameter-free problem (4.78) shown in Figure 4.4 and then rescale it to obtain the solution to the problem (4.76). Both temperature and concentration fields in the liquid are homogeneous at leading order, since the length scale is much smaller than the diffusive length scale. The concentration evolves so that mass is conserved in the shrinking liquid domain, and temperature evolves to preserve thermodynamic equilibrium. The concentration of impurities in the liquid is now large enough to cause significant supercooling, and the temperature gradient in the solid near the interface decreases as a result, causing the inward motion of the solidification fronts to slow down.

In regime iv, the final temporal regime, the time scale is $\mathcal{O}(1)$ and the fronts are within a distance of $\mathcal{O}(\epsilon^2)$ from one another. We distinguish an outer layer I and an inner layer J of $\mathcal{O}(\epsilon^2)$. In the outer layer, we have

$$\begin{aligned} c_s &\approx \alpha c_i, \\ T_s &\approx -1 + \sum_{n=0}^{\infty} a_n e^{-\left(\frac{2n+1}{2}\pi\right)^2 \kappa (t - t^* - \tau^*)}, \end{aligned} \tag{4.128a}$$

while in the inner layer ($z > S(t)$ for the solid and $z < S(t)$ for the liquid), we have

$$\begin{aligned} c_s &\approx \frac{\alpha c_{tot}}{z}, \\ T_s &\approx -1 + \sum_{n=0}^{\infty} a_n e^{-\left(\frac{2n+1}{2}\pi\right)^2 \kappa (t - t^* - \tau^*)}, \\ c_l &\approx m_l \left(1 - \sum_{n=0}^{\infty} a_n e^{-\left(\frac{2n+1}{2}\pi\right)^2 \kappa (t - t^* - \tau^*)}\right), \\ T_l &\approx -1 + \sum_{n=0}^{\infty} a_n e^{-\left(\frac{2n+1}{2}\pi\right)^2 \kappa (t - t^* - \tau^*)}, \end{aligned} \tag{4.128b}$$

where

$$S(t) \approx \frac{c_{tot}}{m_l} \left(1 - \sum_{n=0}^{\infty} a_n e^{-\left(\frac{2n+1}{2}\pi\right)^2 \kappa (t - t^* - \tau^*)}\right)^{-1}, \tag{4.128c}$$

and the coefficients a_n are as given in (4.116). As in regime iii, we observe that the temperature and concentration profiles in the liquid are homogeneous and evolve preserving thermodynamic equilibrium jointly with the temperature in the solid, which now decays to the temperature at the boundary. The interface position evolves so that the total concentration of impurities in the liquid is conserved.

4.8 Comparison with numerical simulations and experimental data

In order to validate the asymptotic solutions, we compare them to numerical simulations of the full problem (2.33) obtained via a finite volume scheme [59]. We also compare our solutions to experimental data.

4.8.1 Numerical scheme

In order to solve the problem (2.33) numerically, we choose a fixed boundary scheme, similar to those described in [27, 99]. The idea is to rescale the solid and liquid

domains so that they have fixed boundaries. Because the Péclet number of the advection-diffusion equations ranges from large in the beginning to small at the end, extra care must be taken in order to avoid numerical instabilities.

We introduce the variables $x = \frac{z-S(t)}{1-S(t)}$ for the solid phase and $y = \frac{z}{S(t)}$ for the liquid phase, both of which range from 0 to 1. We define the following quantities

$$\phi_1(t,x) = (1-S(t))c_s(t,x), \tag{4.129a}$$
$$\phi_2(t,x) = (1-S(t))T_s(t,x), \tag{4.129b}$$
$$\phi_3(t,y) = S(t)c_l(t,y), \tag{4.129c}$$
$$\phi_4(t,y) = S(t)T_l(t,y), \tag{4.129d}$$

so we can rewrite the system (2.33) in conservation form. In the solid phase $x \in (0,1)$, we have

$$\frac{\partial \phi_1}{\partial t} + \frac{\partial}{\partial x}\left(-\frac{S'(t)}{1-S(t)}(1-x)\phi_1 - \frac{D}{\mathrm{Le}(1-S(t))^2}\frac{\partial \phi_1}{\partial x}\right) = 0, \tag{4.130a}$$
$$\frac{\partial \phi_2}{\partial t} + \frac{\partial}{\partial x}\left(-\frac{S'(t)}{1-S(t)}(1-x)\phi_2 - \frac{\kappa}{(1-S(t))^2}\frac{\partial \phi_2}{\partial x}\right) = 0; \tag{4.130b}$$

in the liquid phase $y \in (0,1)$, we have

$$\frac{\partial \phi_3}{\partial t} + \frac{\partial}{\partial y}\left(-\frac{S'(t)}{S(t)}y\phi_3 - \frac{1}{\mathrm{Le}S(t)^2}\frac{\partial \phi_3}{\partial y}\right) = 0, \tag{4.130c}$$
$$\frac{\partial \phi_4}{\partial t} + \frac{\partial}{\partial y}\left(-\frac{S'(t)}{S(t)}y\phi_4 - \frac{1}{S(t)^2}\frac{\partial \phi_4}{\partial y}\right) = 0; \tag{4.130d}$$

at the interface (given by $x = 0$ and $y = 1$), we have

$$S(t)\phi_2 = (1-S(t))\phi_4, \tag{4.130e}$$
$$S(t)\phi_1 = \alpha(1-S(t))\phi_3, \tag{4.130f}$$
$$\phi_3 = -m_l\phi_4, \tag{4.130g}$$
$$\frac{\rho}{\mathrm{St}}\frac{\mathrm{d}S}{\mathrm{d}t} = \frac{k}{(1-S(t))^2}\frac{\partial \phi_2}{\partial x} - \frac{1}{S(t)^2}\frac{\partial \phi_4}{\partial y}, \tag{4.130h}$$
$$-\frac{S'(t)}{1-S(t)}\phi_1 - \frac{D}{\mathrm{Le}(1-S(t))^2}\frac{\partial \phi_1}{\partial x} = -\frac{S'(t)}{S(t)}\phi_3 - \frac{1}{\mathrm{Le}S(t)^2}\frac{\partial \phi_3}{\partial y}; \tag{4.130i}$$

the boundary conditions are

$$\frac{\partial \phi_1}{\partial x} = 0, \qquad \phi_2 = -(1-S(t)), \qquad \text{at} \quad x = 1, \tag{4.130ja}$$
$$\frac{\partial \phi_3}{\partial y} = 0, \qquad \frac{\partial \phi_4}{\partial y} = 0, \qquad \text{at} \quad y = 0, \tag{4.130jb}$$

and we prescribe appropriate initial conditions for ϕ_1, ϕ_2, ϕ_3, ϕ_4, and S.

Since α is very small, we take $\alpha = 0$, and therefore we neglect the impurities in the solid, considering only impurities in the liquid when performing our simulations. This reduces the condition (4.130i) to a no-flux condition and removes the equations (4.130a) and (4.130f) from the system. We use a finite volume scheme with a TVD discretisation for the advection term. We implement the scheme in MATLAB using the finite volume toolbox FVToolbox [22].

At each time step, we iterate using a relaxation scheme until convergence. At the $(k+1)$-th iteration, knowing the values of the k-th iteration ϕ_2^k, ϕ_3^k, ϕ_4^k, S^k and V^k, and the values at the previous time step ϕ_2^*, ϕ_3^*, ϕ_4^* and S^*, we proceed in the following order:

1. Calculate ϕ_2^{k+1}, ϕ_3^{k+1}, and ϕ_4^{k+1} from (4.130b)-(4.130d) and the boundary conditions (4.130e), (4.130g), and (4.130i). We use the values of ϕ_3^k, S^k, and V^k at the previous iteration for the calculations.

2. Use equation (4.130h) to calculate the variation in velocity between iterations k and $k+1$, using the new values of ϕ_2^{k+1} and ϕ_4^{k+1} and the old value of S^k:

$$\Delta V^{k+1} = \frac{\mathrm{St}}{\rho}\left(\frac{k}{(1-S^k)^2}\frac{\partial \phi_2^{k+1}}{\partial x} - \frac{1}{(S^k)^2}\frac{\partial \phi_4^{k+1}}{\partial y}\right) - V^k. \tag{4.11}$$

3. Calculate the new velocity using a relaxation coefficient, ω, as

$$V^{k+1} = V^k + \omega \Delta V^{k+1}. \tag{4.12}$$

4. Update the position of the interface with the new velocity and the position of the interface at the previous time step. That is,

$$S^{k+1} = S^* + \Delta t V^{k+1}. \tag{4.13}$$

We keep iterating until $\left|\frac{\Delta V^{k+1}}{V^{k+1}}\right| < \delta$, where δ is a prescribed tolerance. Then we can move to the next time step, and start iterating again.

4.8.2 Comparison with numerical results

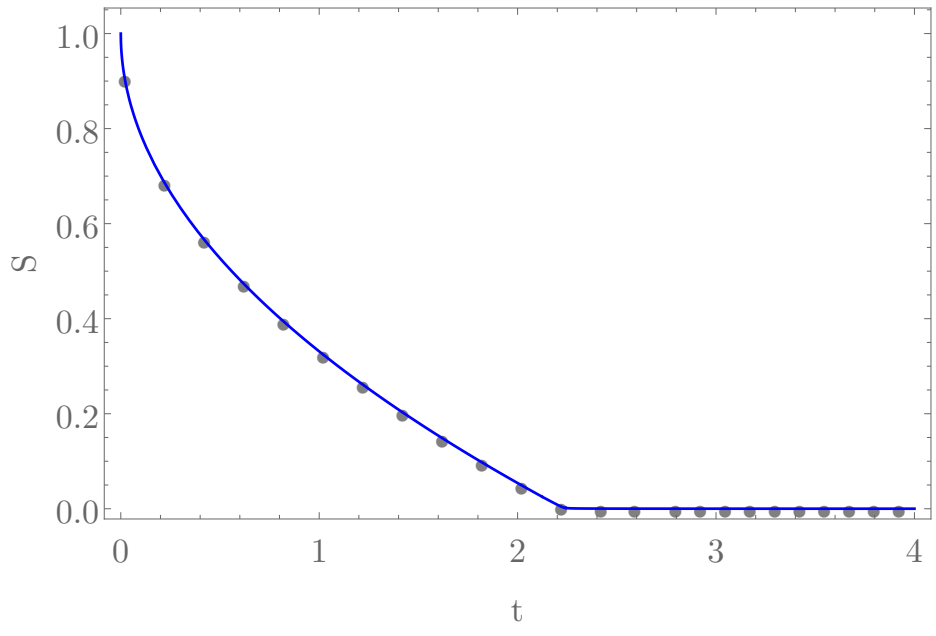
When performing our simulations, we set $\mathrm{St} = 0.77$, $\mathrm{Le} = 100$, $\rho = 1$, $c_p = 1$, $k = 0.36$, $m_l = 100$, $c_0 = 0.01$, and $T_0 = 0$, which are parameter values close to metallurgical grade silicon (see Table 2.2 in page 39). The reason to use these parameters instead of those in Table 2.2 was because with the values used here the algorithm runs faster and

thus we can capture a larger time span in the plots. However, numerical simulations with the actual values show the same behaviour. We take $N_s = 5 \cdot 10^3$ grid points in the solid phase, $N_l = 10^4$ grid points in the liquid phase, and an initial time step of $\Delta t = 10^{-4}$. For the relaxation iterations, we take a relaxation parameter $\omega = 0.1$ and a tolerance of $\delta = 0.01$. To aid convergence of the algorithm, if one time step takes more than 100 iterations before converging and the time step is larger than 10^{-5}, we halve the time step. This algorithm is capable of solving the full problem with a total mass variation smaller than 0.01%.

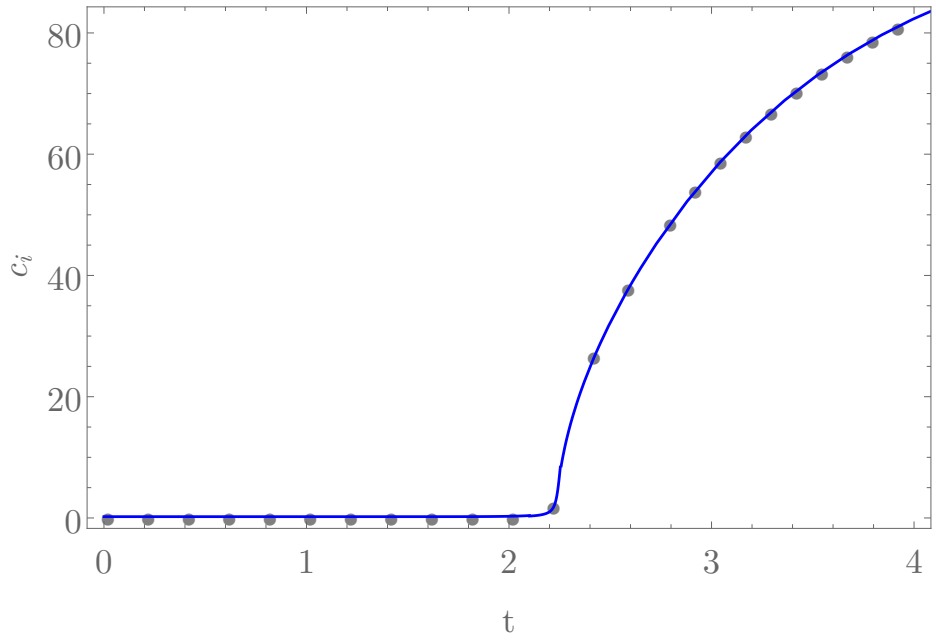
The comparison between our asymptotic solutions and numerical simulations is shown in Figure 4.6. Based on the good agreement with the asymptotic solutions, we believe that the asymptotics accurately describe the true dynamics of the system, even as the fronts approach closely. In Figure 4.6(a), we plot the position of the interface, observing self-similar-like behaviour for $t < t^* = 2.2294$, while for $t > t^*$ we observe exponential decay toward the final position of the interface, determined by $c_{tot} m_l^{-1} = 9.57 \cdot 10^{-5}$. In Figure 4.6(b), we plot the concentration in the liquid side of the interface. In regime i, the concentration is constant until near t^* (regime ii), when the build-up of impurities becomes noticeable. For $t > t^*$, the build-up of impurities continues, with the concentration tending exponentially to a concentration $m_l = 100$. Other asymptotic solutions, such as those for T_s and c_l, show good agreement with the numerical simulations, as well.

4.8.3 Comparison with experimental results

As mentioned in Section 4.1, an application which motivates our work is the casting of metallurgical grade silicon, and we now compare our results with experimental data from the casting of 99% purity silicon over a water cooled copper plate. This experimental data was provided by Elkem. In order to obtain the data, after the cast has cooled down, it is sliced into parts and treated in order to take the measurements on the internal faces of each slice. Grain size, pore size, and impurity concentration are then recorded. These magnitudes are averaged over a certain width at every cross section, so that the output data is recorded against the thickness direction variable. An image of the measured sample is shown in Figure 4.7(a). We are interested in measurements of the (cross-section averaged) concentration of impurities in the solid against the thickness of the cast. This data can be immediately compared to c_s, which we have found will not depend on time (to leading order). As the cast thickness is much smaller than its width, and the impurity concentration is averaged



(a)



(b)

asymptotics numerics

Figure 4.6: Comparison of the analytical and numerical solutions over time for the (a) interface position and (b) concentration of impurities on the liquid side of the interface.

over a few centimetres of cross section, our planar model is a reasonable match to the experimental geometry configuration.

In Figure 4.7(b), we plot the asymptotic solution and the experimental data. Due to scale, in the experimental data we only resolve regimes i and ii. The corresponding composite asymptotic solution for both regimes (at leading order) is

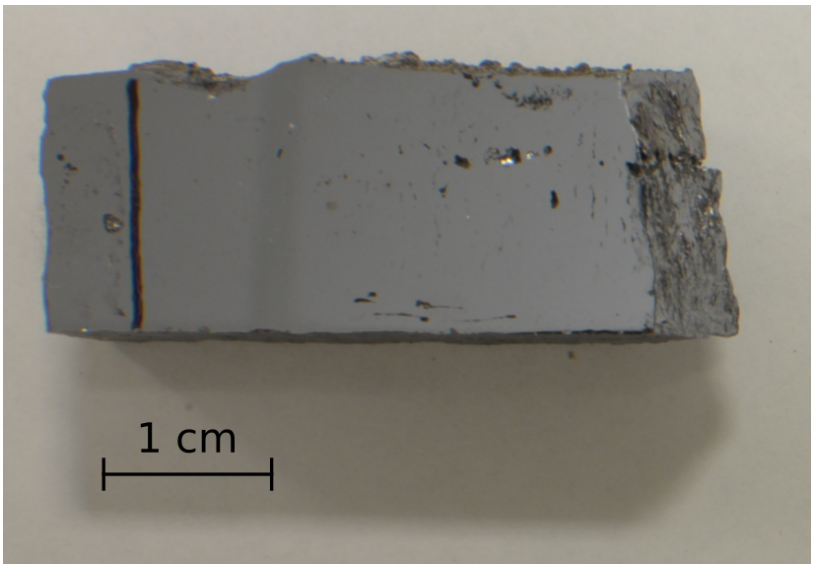
$$c_s(z) \approx \frac{\alpha\mu}{\alpha\mu+1} c_0 \sum_{n=1}^{\infty} n \left(e^{-\mu(n+1)nz} + e^{-\mu n(n-1)z} \right), \tag{4.14}$$

where $\mu = 2\lambda^2 \mathrm{Le}$. Thus, the concentration profile depends only on three dimensionless parameters, μ, α, and c_0.

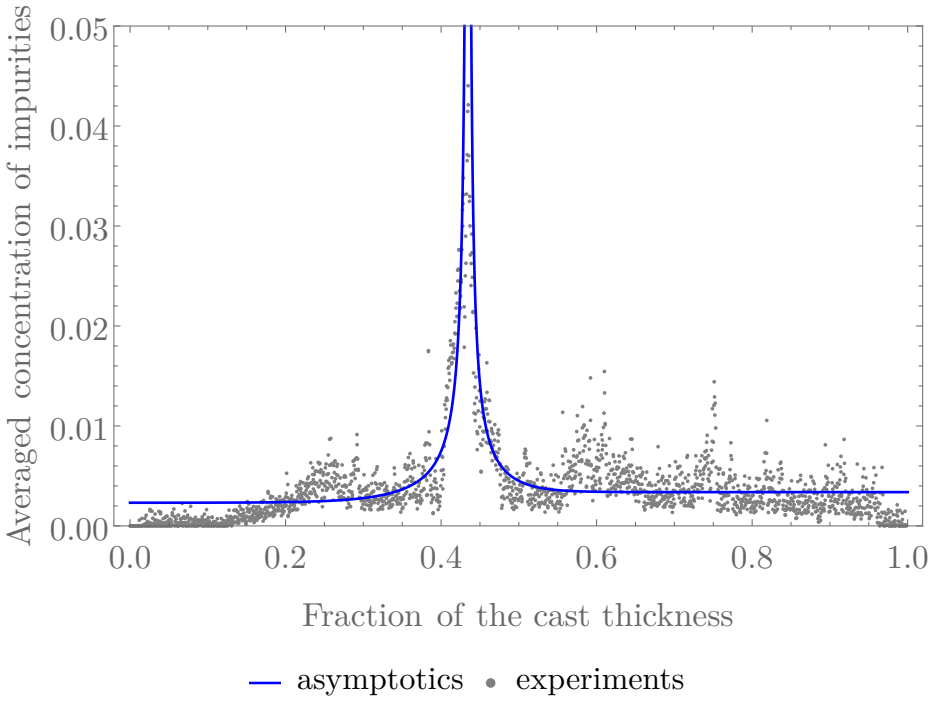
From the experimental data, we observe the concentration profiles produced by two solidification fronts are not symmetric and eventually meet at a point z_0 of the cast. To match this data with asymptotic solutions where symmetry was assumed, we assume each side of the plot can be modelled, using (4.14), by $c_s(z - z_0)$ and $c_s(z_0 - z)$, both with the same parameters α and c_0 (as these are given by the material properties). On the other hand, the parameter μ depends on the cooling rate, which has different values for each solidification front due to the different heat transfer mechanisms at the top and bottom of the cast. However, we know that both fronts meet at the same time at $z = z_0$, therefore we have the relation

$$\mu_l = \left(\frac{z_0}{1 - z_0} \right)^2 \mu_r, \tag{4.15}$$

where subscripts r and l denote the right and left side of the central cross section $z = z_0$. We use reasonable parameter values for our problem to compare the asymptotic solution (4.14) with the experimental data. Using the parameter values $c_0 = 0.01$, $\mu_r = 17$, $\mu_l = 10$, $\alpha = 0.03$, and $z_0 = 0.43$, we obtain the asymptotic solution shown in Figure 4.7(b). Notice that these values of μ_l, μ_r and α are significantly different than the ones given in (or calculated from) Table 2.2. Given the simplicity of our model, we treat these parameters as effective coefficients that can be determined experimentally for a given physical set-up. The asymptotic solution captures the rapid growth of the concentration near the region where the solidification fronts meet, and the constant concentration outside of this region. The noise in the data is caused by bubbles and pores within the cast, as impurities tend to aggregate around them. In spite of these complexities, the asymptotic solutions show good qualitative agreement with the experimental data.



(a)



(b)

Figure 4.7: (a) Sample of the cast used for the experimental data. The experiment corresponds to a 14mm silicon cast over a water cooled copper plate. The data is taken at a given central section of the cast, which has been polished and chemically treated in order to take the measurements. (b) Comparison of the asymptotic solution and experimental data for the concentration in the solid phase. Both the picture and the experimental data have been provided by Elkem. For the asymptotic solution, we used parameter values $c_0 = 0.01$, $\mu_r = 17$, $\mu_l = 10$, $\alpha = 0.03$, and $z_0 = 0.43$.

4.9 Discussion

We have performed an asymptotic analysis for the extended Stefan problem modeling the solidification of a binary alloy in a finite slab. We have distinguished four different time regimes, each featuring multiple spatial layers. The early-time dynamics are akin to those of the classical one-phase Stefan problem (for which there exist self-similar solutions). The impurities are rejected from the solid into the liquid and then diffuse away within a thin layer near the solidification front. The value of the concentration at the interface remains constant. When the two fronts move close to each other, the interaction between the fronts causes the concentration in the liquid to increase, since the rejected impurities can no longer diffuse away. As time increases, the concentration of impurities in the liquid phase becomes large enough to influence the temperature field, resulting in a slowing of the solidification front motion (so that the fronts do not collide). In the late stages of the process, the system is driven by cooling of the solid towards the uniform state given by the thermal boundary value. These asymptotic solutions are shown to agree with numerical simulations and experimental data.

We conclude that supercooling plays a crucial role in the time evolution of the system as the fronts approach one another and the impurities build-up. It is also noteworthy that the transition between the two main regimes occurs in two stages. In the first stage, there is a quick build-up of impurities in the liquid, yet the interface continues to move as it has for earlier times. In the second stage, a significant change in the motion of the solidification front occurs, as it slows down due to the fact that the impurity build-up has modified the thermal properties of the system. We also find that the cooling rate, λ, has a large impact for the late-time dynamics, particularly in the concentration fields, as it determines the value of c_{tot}.

Our comparison between the analytical solutions and experimental data showed good agreement, but we noticed that in experiments we seem to only observe the first two regimes. This is reasonable, as from regime iii onwards the concentration of impurities in the liquid is so large that some aspects of the modelling, such as the dilute alloy or the linear phase diagram, are no longer valid. In addition, we expect physical phenomena that have not been considered (nucleation, for example) to play a more dominant role in these situations. The inlcusion of these effects should help to improve the model.

One potential industrial application of our analysis would be an improved understanding of the casting process for materials such as silicon. We have shown that the

distribution of impurities in the final solidified slab is determined by the cooling rate, λ, the initial impurity concentration, c_0, the segregation coefficient, α, and the Lewis number, Le. The latter two are physical parameters which depend on the material and the impurities, and hence cannot be controlled. The parameter c_0 is also normally restricted by the specific application, so the only possible control parameter is λ. The parameter $\mu = 2\lambda^2 \mathrm{Le}$ defines the thickness of the impurity build-up layer, therefore λ influences both the concentration far from the central layer and the thickness of the layer of impurities. As λ depends on the heat exchange of each boundary, the cooling conditions applied to the cast could, in principle, be used to control the profile of the concentration of impurities in the solid slab. Moreover, the experimental data suggests that the thickness of this layer correlates with the thickness of the equiaxed grain layer, therefore the results presented here could be used to obtain a semi-empirical estimation of the thickness of the equiaxed layer.

Possible extensions of this work would be to consider two-dimensional radially symmetric (cylindrical) and three-dimensional (spherical) geometries, thereby extending the work presented in [27, 63, 84] to an extended Stefan problem for binary alloys in these geometries. Another extension would be to consider arbitrary two- and three-dimensional geometries to generalize the results presented in [61, 62]. One might also consider the role of non-uniform boundaries, such as configurations where the molten material is placed on a bed of fines, resulting in initially uneven penetration of the solidification front at small times, as discussed in [7]. In these configurations, the differences in the heat exchange mechanisms due to the layer of fines could also be considered. Finally, the stability of the solutions for each regime could be studied, which may potentially lead to a better understanding of the columnar to equiaxed transition. Identifying particular instabilities possible on each time scale might provide a better understanding of the grain formation process.

In the next chapter, we study one of the areas of further research suggested here. We consider the solidification problem in the three-dimensional spherically symmetric geometry, performing an asymptotic analysis that generalises the results previously introduced in [63, 84] to binary alloys.

Chapter 5

Asymptotic analysis of the inward solidification of a sphere

5.1 Introduction

Having determined asymptotic solutions to the solidification problem for a binary alloy in a planar finite slab, we focus our attention on the corresponding solidification problem in a spherical geometry. Even though this model is relevant for some casting techniques, its main interest is to generalise the results presented in Chapter 4 to a three-dimensional geometry to understand how this change in spatial structure affects the solidification process. It is well-known in the literature [63, 84] that inward solidification in spherical domains does not admit exact solutions, even for the pure material problem, so asymptotic solutions have been studied for years. The main goal of this chapter is to extend the results of these analyses to consider a binary alloy with constitutional supercooling.

The asymptotic analysis of the solidification of spheres was first approached by Pedroso and Domoto [71], who considered asymptotic solutions of the one-phase Stefan problem in a sphere in the small Stefan number limit (latent heat dominated), finding good agreement with numerical simulations of the problem. This analysis was subsequently extended and refined by Riley et al. [77], Stewartson and Waechter [88], and Soward [84], requiring the consideration of several layers in the problem. Some of these papers also considered the cylindrically symmetric geometry, as its analysis is conceptually similar to the sphere one. More generally, McCue et al. [62] provided an asymptotic analysis for the one-phase Stefan problem in an arbitrary three-dimensional geometry near the end of the solidification process. The two-phase Stefan problem has received less attention. Jiji and Weinbaum [44] considered the two-phase Stefan problem in a cylindrical shell, while Kucera and Hill [50] studied

the two-phase Stefan problem for a cylinder and a sphere. Finally, more than twenty years later, McCue et al. [63] provided a comprehensive analysis of the two-phase Stefan problem in a sphere, in which they brought together the previous work on the problem and extended it by introducing one last exponentially small time scale in the problem.

The two-phase Stefan problem with constitutional supercooling in a sphere has been studied by Feltham and Garside [27]. The authors provide an asymptotic analysis in the small time regime, but they do not consider the dynamics at later times, which we shall later show to be crucial. Because they assume that constitutional supercooling is sufficiently small, the solutal problem fully decouples from the thermal problem and can be calculated numerically, once the thermal field and the position of the interface are known. The analysis is found to have good agreement with the numerical simulations calculated using a fixed boundary method. Finally, the late time behaviour of the problem is discussed qualitatively, but no formal analysis is provided.

5.1.1 Outline of the chapter

In this chapter, we perform an asymptotic analysis to study the extended Stefan problem with constitutional supercooling in a spherical domain, in the limits of large Lewis number and small Stefan number. As we did for the analysis in Chapter 4, we assume as well that the diffusivity of impurities in the solid, the segregation coefficient and the initial concentration and temperatures are small; and that the supercooling coefficient is large, meaning that a large concentration of impurities is required to cause a significant change in the solidification temperature. The results here generalise the results in [27, 63, 84] considering all time regimes for the Stefan problem with impurities and constitutional supercooling. Due to their definition of the Stefan number, their analysis corresponds to the limit of large Stefan number (i.e. the case when the problem is dominated by latent heat).

The outline of the present chapter is as follows. In Section 5.2, we present the model for the solidification of a sphere, reducing the model derived in Section 2.4 to a quasi-one-dimensional model in the radial coordinate, and we introduce the scalings for the asymptotic analysis. Our asymptotic analysis in the large Lewis number limit reveals eight different layers which are studied in Sections 5.3 to 5.6 and then matched together. In Section 5.4, we study the layers that arise from the problem in Section 5.3 when the small Stefan number limit is taken. All of these asymptotic results are summarised and discussed in Section 5.7. We then compare the asymptotic solutions

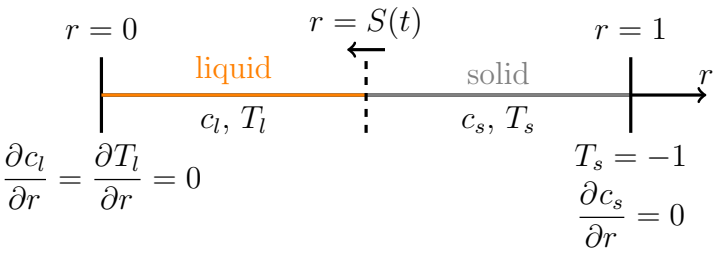


Figure 5.1: Sketch of the sphere solidification problem. As the problem is symmetric, we can just consider a one-dimensional problem with a symmetry condition at $r = 0$.

with numerical simulations in Section 5.8, using a finite volume scheme in a fixed boundary method for the numerical simulations, similar to the algorithm discussed in Chapter 4. We conclude this chapter with a discussion of the results, in Section 5.9.

5.2 Model for the solidification of a sphere

In this chapter we study the solidification of a binary alloy in a three-dimensional spherically symmetric geometry. Therefore, we use the model presented in Section 2.4, taking $n = 3$, as we are interested in the three-dimensional problem. Recall that as we have assumed spherical symmetry, the problem can be reduced to a one-dimensional model in the radial coordinate with the geometry shown in Figure 5.1.

As we did in Chapter 4, we are interested in the limit of very large Lewis number. However, as could be expected from the results in the literature [63, 84, 88], in order to find analytic solutions we need to take the limit of small Stefan number as well. In our analysis, we first take the large Lewis number; for convenience, as we did in the planar geometry case, we write $\epsilon = \mathrm{Le}^{-1}$ and consider the limit $\epsilon \to 0$, and next we take the limit $\mathrm{St} \to 0$. This procedure is valid provided $\epsilon^{\frac{2}{3}} \ll \mathrm{St}$, which is true in our problem. The validity of this distinguished limit between the two small parameters is discussed in Section 5.4.

The rest of the parameters are scaled as in the asymptotic analysis of the planar slab, following (4.1). Then we can write the rescaled dimensionless model in the following way. The solid phase is defined by $S(t) < r < 1$, and the equations are

$$\frac{\partial c_s}{\partial t} = \epsilon^2 \hat{D} \left(\frac{\partial^2 c_s}{\partial r^2} + \frac{2}{r} \frac{\partial c_s}{\partial r} \right), \tag{5.1a}$$

$$\frac{\partial T_s}{\partial t} = \kappa \left(\frac{\partial^2 T_s}{\partial r^2} + \frac{2}{r} \frac{\partial T_s}{\partial r} \right). \tag{5.1b}$$

The liquid phase is defined by $0 < r < S(t)$, and the equations are

$$\frac{\partial c_l}{\partial t} = \epsilon \left(\frac{\partial^2 c_l}{\partial r^2} + \frac{2}{r} \frac{\partial c_l}{\partial r} \right), \tag{5.1c}$$

$$\frac{\partial T_l}{\partial t} = \frac{\partial^2 T_l}{\partial r^2} + \frac{2}{r} \frac{\partial T_l}{\partial r}. \tag{5.1d}$$

At the interface $r = S(t)$, the equations are

$$T_s = T_l, \tag{5.1e}$$

$$c_s = \epsilon \hat{\alpha} c_l, \tag{5.1f}$$

$$\epsilon c_l = -\hat{m}_l T_l, \tag{5.1g}$$

$$\frac{\rho}{\mathrm{St}} \frac{\mathrm{d}S}{\mathrm{d}t} = k \frac{\partial T_s}{\partial r} - \frac{\partial T_l}{\partial r}, \tag{5.1h}$$

$$(1 - \epsilon \hat{\alpha}) c_l \frac{\mathrm{d}S}{\mathrm{d}t} = \epsilon^2 \hat{D} \frac{\partial c_s}{\partial r} - \epsilon \frac{\partial c_l}{\partial r}. \tag{5.1i}$$

The boundary conditions are given by

$$\frac{\partial c_l}{\partial r} = 0 \quad \text{and} \quad \frac{\partial T_l}{\partial r} = 0, \quad \text{at } r = 0, \tag{5.1j}$$

$$\frac{\partial c_s}{\partial r} = 0 \quad \text{and} \quad T_s = -1, \quad \text{at } r = 1, \tag{5.1k}$$

and the initial conditions

$$c_l = \epsilon \hat{c}_0, \quad T_l = \epsilon \hat{T}_0, \quad \text{and} \quad S = 1, \quad \text{at} \quad t = 0. \tag{5.1l}$$

In order to solve the problem we need shall employ the method at matched asymptotics. When we take the large Lewis number limit, we identify three different time regimes in the problem, and within each regime there are different spatial layers. Overall we identify the eight layers shown in Figure 5.2, which have the scalings described in Table 5.1. When we then take the small Stefan number limit, we need to consider five extra layers within regime i, which are studied in Section 5.4. Once solutions are obtained in each layer, we will then match these solutions in order to obtain the asymptotic solution for the whole problem. Notice that we use hats for the position of the interface and the temperature and concentration profiles whenever they are rescaled with powers of ϵ. On the other hand, we use tildes when a variable is rescaled with powers of St, regardless of whether it has been previously rescaled with powers of ϵ or not. To minimise confusion, we give a reminder of the rescalings at the beginning of the analysis of each layer.

Similarly to the analysis in Chapter 4, the scalings in Table 5.1 are primarily picked by the physics. At the start of the process, which is regime i, we expect to

see diffusion of both heat and impurities, but, given the difference on the size of the diffusion coefficients, we need to introduce an inner layer of size $\mathcal{O}(\epsilon)$ around the interface (named layer B) to capture the rejection and transport of impurities, while heat diffusion is observed in the outer layers (A and C). As opposed to what we observed in the planar problem, now the interfacial concentration does not remain constant at leading order, therefore the solutions in regime i no longer hold when the interfacial concentration $c_i = \mathcal{O}(\epsilon^{-1})$, which implies that $S = \mathcal{O}\left(\epsilon^{\frac{1}{3}}\right)$. This motivates the introduction of regime ii, in which we need to distinguish three layers: an outer layer in the solid phase D where temperature and concentration remain constant, an intermediate layer E of size $\mathcal{O}\left(\epsilon^{\frac{1}{3}}\right)$ near the origin in which we observe the motion of the solidification front (and which, using the Stefan condition, provides the time scale of this regime), and an inner layer F around the moving boundary where we observe rejection and transport of impurities, similarly to what we previously observed in layer B. At the end of this regime, we have that the position of the interface becomes zero at leading order, and, therefore, the liquid part of layer E vanishes so the inner layer F notices the symmetry condition at $r = 0$. Hence, we need to introduce regime iii, in which the scalings are motivated by the diffusion of impurities in the liquid phase. These scalings reveal two layers: an outer layer G in the solid phase where temperature and concentration remain constant, and an inner layer H near the origin where we observe diffusion of impurities in the liquid phase and the motion of the solidification front.

Again, we observe that in regimes ii and iii the interfacial concentration $c_i = \mathcal{O}(\epsilon^{-1})$, which is not physical. We notice as well that the model predicts that the solidification process never finishes, contradicting the experimental observations. Therefore, similarly to what happened for the planar problem in Chapter 4, we find that in regimes ii and iii the model looses its physical sense as some of the modelling assumptions no longer hold, but it still has interest from the mathematical point of view as it provides a full picture of (5.1).

In the following sections, we determine asymptotic solutions in each layer, and then match them to construct solutions valid over the whole problem domain.

5.3 Asymptotic solutions in regime i

We start by considering the behaviour at the beginning of the process, described in regime i. In this regime, the interface is far from the centre and we distinguish three space layers: the outer layer, A, in the solid, the inner layer, B, around the moving

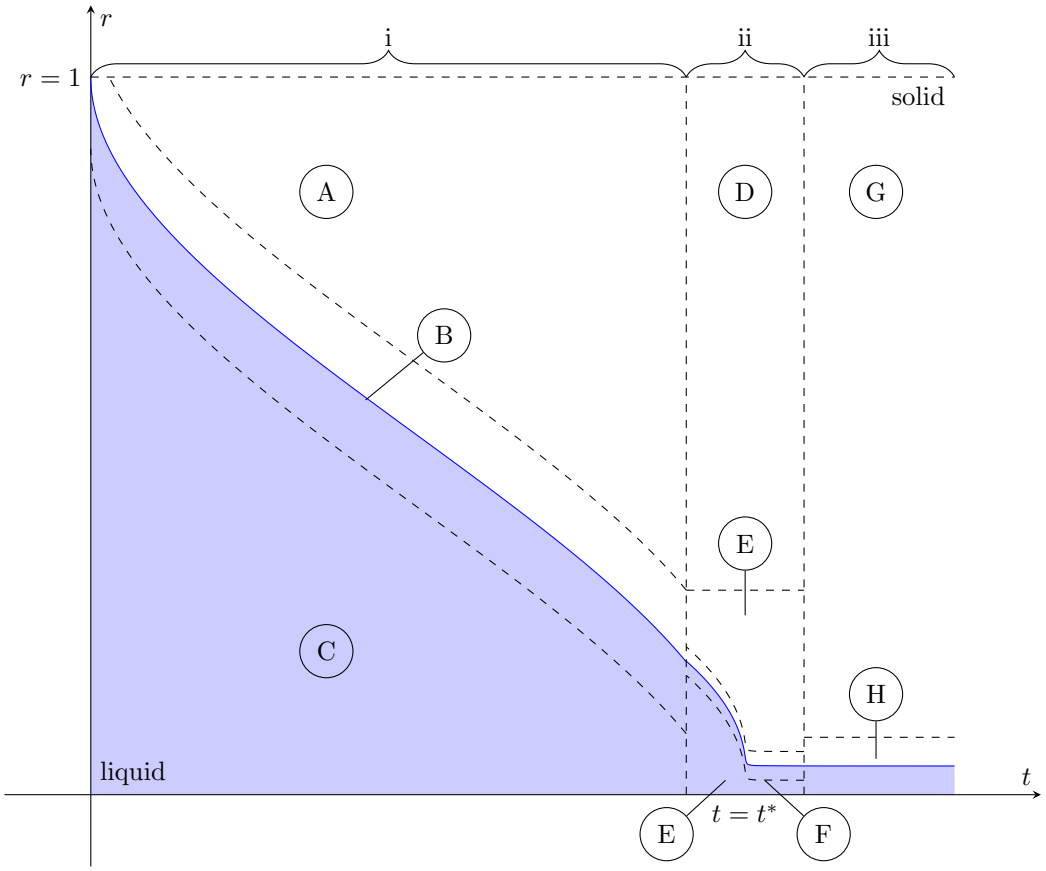


Figure 5.2: Sketch of the regimes and layers in the process. The sketch shows the evolution of the interface $S(t)$ in time, so the area above (in white) is the solid and the area below (in blue) is the liquid. The three regimes, identified with lower case Roman numerals, are the behaviours at different times. In each regime we consider various layers which are labelled with letters. The scalings in each layer are shown in Table 5.1.

		t	r	S	c_s	c_l	T_s	T_l
Regime i	A	t	r	S	$\epsilon\hat{c}_s$	-	T_s	-
	B	t	$S(t)+\epsilon R$	S	$\epsilon\hat{c}_s$	c_l	$\epsilon\hat{T}_s$	$\epsilon\hat{T}_l$
	C	t	r	S	-	$\epsilon\hat{c}_l$	-	$\epsilon\hat{T}_l$
Regime ii	D	$t^*+\epsilon^{\frac{2}{3}}\tau$	r	$\epsilon^{\frac{1}{3}}\hat{S}$	$\epsilon\hat{c}_s$	-	T_s	-
	E	$t^*+\epsilon^{\frac{2}{3}}\tau$	$\epsilon^{\frac{1}{3}}\xi$	$\epsilon^{\frac{1}{3}}\hat{S}$	c_s	$\epsilon\hat{c}_l$	T_s	T_l
	F	$t^*+\epsilon^{\frac{2}{3}}\tau$	$\epsilon^{\frac{1}{3}}\left(\hat{S}(\tau)+\epsilon R\right)$	$\epsilon^{\frac{1}{3}}\hat{S}$	c_s	$\epsilon^{-1}\hat{c}_l$	T_s	T_l
Regime iii	G	$t^*+\epsilon^{\frac{1}{3}}\theta$	r	$\epsilon^{\frac{2}{3}}\hat{S}$	$\epsilon\hat{c}_s$	-	T_s	-
	H	$t^*+\epsilon^{\frac{1}{3}}\theta$	$\epsilon^{\frac{2}{3}}R$	$\epsilon^{\frac{2}{3}}\hat{S}$	c_s	$\epsilon^{-1}\hat{c}_l$	T_s	T_l

Table 5.1: Scalings for the variables in each layer of the problem. The variables τ and θ represent time at different scalings and the variables ξ and R are the space variables in the intermediate and inner layers of each regime, respectively. For temperature and concentration, we use hats whenever they are rescaled.

interface which comprises both phases, and the outer layer, C, in the liquid. We solve the equations for each layer and then proceed to match the layers between them in order to fully determine the solutions.

5.3.1 Layer A

The first layer in this regime is the outer layer in the solid phase: layer A. Rescaling the problem using the scalings in Table 5.1, which for this layer it is only $c_s = \epsilon\hat{c}_s$, we find that the problem is defined in $S(t) < r < 1$ by

$$\frac{\partial \hat{c}_s}{\partial t} = \epsilon^2 \hat{D}\left(\frac{\partial^2 \hat{c}_s}{\partial r^2} + \frac{2}{r}\frac{\partial \hat{c}_s}{\partial r}\right), \tag{5.2a}$$

$$\frac{\partial T_s}{\partial t} = \kappa\left(\frac{\partial^2 T_s}{\partial r^2} + \frac{2}{r}\frac{\partial T_s}{\partial r}\right), \tag{5.2b}$$

with boundary conditions

$$\frac{\partial \hat{c}_s}{\partial r} = 0 \quad \text{and} \quad T_s = -1, \quad \text{at } r = 1, \tag{5.2c}$$

and, as initially all the material is liquid, we have no additional initial conditions. The problem is completed with the corresponding matching conditions which are discussed in Section 5.3.4. Expanding $\hat{c}_s$ and T_s as

$$\hat{c}_s = \hat{c}_{s0} + \epsilon\hat{c}_{s1} + \mathcal{O}\left(\epsilon^2\right), \tag{5.3a}$$

$$T_s = T_{s0} + \epsilon T_{s1} + \mathcal{O}\left(\epsilon^2\right), \tag{5.3b}$$

we can linearise the problem.

At $\mathcal{O}(1)$, the problem is

$$\frac{\partial \hat{c}_{s0}}{\partial t} = 0, \tag{5.4a}$$

$$\frac{\partial T_{s0}}{\partial t} = \kappa \left(\frac{\partial^2 T_{s0}}{\partial r^2} + \frac{2}{r} \frac{\partial T_{s0}}{\partial r} \right), \tag{5.4b}$$

with boundary conditions

$$\hat{c}_{s0} = \hat{\alpha} c_i(t) \quad \text{and} \quad T_{s0} = 0, \quad \text{at } r = S_0(t), \tag{5.4c}$$

$$\frac{\partial \hat{c}_{s0}}{\partial r} = 0 \quad \text{and} \quad T_{s0} = -1, \quad \text{at } r = 1, \tag{5.4d}$$

where the matching conditions with layer B are derived later in Section 5.3.4. We find that

$$\hat{c}_{s0} = \hat{\alpha} c_i \left(S_0^{-1}(r) \right) = \hat{\alpha} \frac{\hat{c}_0}{3} \frac{k\mathrm{St}}{\rho} \frac{1 - r^3}{(1 - r) r^3}, \tag{5.5}$$

and T_{s0} is the solution to the problem

$$\frac{\partial T_{s0}}{\partial t} = \kappa \left(\frac{\partial^2 T_{s0}}{\partial r^2} + \frac{2}{r} \frac{\partial T_{s0}}{\partial r} \right), \tag{5.6a}$$

with boundary conditions

$$T_{s0} = 0 \quad \text{at } r = S_0(t), \quad \text{and} \quad T_{s0} = -1 \quad \text{at } r = 1, \tag{5.6b}$$

and the equation for the moving boundary, derived later in Section 5.3.4,

$$\frac{\rho}{\mathrm{St}} \frac{\mathrm{d}S_0}{\mathrm{d}t} = k \left. \frac{\partial T_{s0}}{\partial r} \right|_{r = S_0(t)}. \tag{5.6c}$$

Notice that this problem corresponds to the one phase Stefan problem, so, within this regime, we need to distinguish different time scales, as discussed in [63, 84]. We give the analysis of these different time scales in Section 5.4.

5.3.2 Layer B

Layer B is the inner layer of size ϵ around the moving interface. Therefore, defining the inner variable

$$R = \frac{r - S(t)}{\epsilon}, \tag{5.7}$$

and using the scalings

$$c_s = \epsilon \hat{c}_s, \qquad T_s = \epsilon \hat{T}_s, \qquad \text{and} \qquad T_l = \epsilon \hat{T}_l, \tag{5.8}$$

we find that the problem is defined as follows. The solid phase is defined by $R > 0$, and the equations are

$$\epsilon \frac{\partial \hat{c}_s}{\partial t} = S'(t) \frac{\partial \hat{c}_s}{\partial R} + \epsilon \hat{D} \left(\frac{\partial^2 \hat{c}_s}{\partial R^2} + \epsilon \frac{2}{S(t) + \epsilon R} \frac{\partial \hat{c}_s}{\partial R} \right), \tag{5.9a}$$

$$\epsilon^2 \frac{\partial \hat{T}_s}{\partial t} = \epsilon S'(t) \frac{\partial \hat{T}_s}{\partial R} + \kappa \left(\frac{\partial^2 \hat{T}_s}{\partial R^2} + \epsilon \frac{2}{S(t) + \epsilon R} \frac{\partial \hat{T}_s}{\partial R} \right). \tag{5.9b}$$

The liquid phase is defined by $R < 0$, and the equations are

$$\epsilon \frac{\partial c_l}{\partial t} = S'(t) \frac{\partial c_l}{\partial R} + \frac{\partial^2 c_l}{\partial R^2} + \epsilon \frac{2}{S(t) + \epsilon R} \frac{\partial c_l}{\partial R}, \tag{5.9c}$$

$$\epsilon^2 \frac{\partial \hat{T}_l}{\partial t} = \epsilon S'(t) \frac{\partial \hat{T}_l}{\partial R} + \frac{\partial^2 \hat{T}_l}{\partial Z^2} + \epsilon \frac{2}{S(t) + \epsilon R} \frac{\partial \hat{T}_l}{\partial R}. \tag{5.9d}$$

At the interface $R = 0$, the equations are

$$\hat{T}_s = \hat{T}_l, \tag{5.9e}$$

$$\hat{c}_s = \hat{\alpha} c_l, \tag{5.9f}$$

$$c_l = -\hat{m}_l \hat{T}_l, \tag{5.9g}$$

$$\frac{\rho}{\mathrm{St}} \frac{\mathrm{d}S}{\mathrm{d}t} = k \frac{\partial \hat{T}_s}{\partial R} - \frac{\partial \hat{T}_l}{\partial R}, \tag{5.9h}$$

$$(1 - \epsilon \hat{\alpha}) c_l \frac{\mathrm{d}S}{\mathrm{d}t} = \epsilon^2 \hat{D} \frac{\partial \hat{c}_s}{\partial R} - \frac{\partial c_l}{\partial R}. \tag{5.9i}$$

The remaining conditions are given by the matching conditions with layers A and C.

At $\mathcal{O}(1)$, in the solid phase, $R > 0$, we have

$$S_0'(t) \frac{\partial \hat{c}_{s0}}{\partial R} = 0, \tag{5.10a}$$

$$\frac{\partial^2 \hat{T}_{s0}}{\partial R^2} = 0, \tag{5.10b}$$

in the liquid phase, $R < 0$, we have

$$S_0'(t) \frac{\partial c_{l0}}{\partial R} + \frac{\partial^2 c_{l0}}{\partial R^2} = 0, \tag{5.10c}$$

$$\frac{\partial^2 \hat{T}_{l0}}{\partial R^2} = 0, \tag{5.10d}$$

at the interface, $R = 0$, we have

$$\hat{T}_{s0} = \hat{T}_{l0}, \tag{5.10e}$$

$$\hat{c}_{s0} = \hat{\alpha} c_{l0}, \tag{5.10f}$$

$$c_{l0} = -\hat{m}_l \hat{T}_{l0}, \tag{5.10g}$$

$$\frac{\rho}{\mathrm{St}} \frac{\mathrm{d}S_0}{\mathrm{d}t} = k \frac{\partial \hat{T}_{s0}}{\partial R} - \frac{\partial \hat{T}_{l0}}{\partial R}, \tag{5.10h}$$

$$c_{l0} \frac{\mathrm{d}S_0}{\mathrm{d}t} + \frac{\partial c_{l0}}{\partial R} = 0. \tag{5.10i}$$

At $\mathcal{O}(\epsilon)$, in the solid phase, $R > 0$, we have

$$S_0'(t) \frac{\partial \hat{c}_{s1}}{\partial R} = \frac{\partial \hat{c}_{s0}}{\partial t} - S_1'(t) \frac{\partial \hat{c}_{s0}}{\partial R} - \hat{D} \frac{\partial^2 \hat{c}_{s0}}{\partial R^2}, \tag{5.11a}$$

$$\kappa \frac{\partial^2 \hat{T}_{s1}}{\partial R^2} = -\left(S_0'(t) + \kappa \frac{2}{S_0(t)} \right) \frac{\partial \hat{T}_{s0}}{\partial R}, \tag{5.11b}$$

in the liquid phase, $R < 0$, we have

$$S_0'(t) \frac{\partial c_{l1}}{\partial R} + \frac{\partial^2 c_{l1}}{\partial R^2} = \frac{\partial c_{l0}}{\partial t} - \left(S_1'(t) + \frac{2}{S_0(t)} \right) \frac{\partial c_{l0}}{\partial R}, \tag{5.11c}$$

$$\frac{\partial^2 \hat{T}_{l1}}{\partial R^2} = -\left(S_0'(t) + \frac{2}{S_0(t)} \right) \frac{\partial \hat{T}_{l0}}{\partial R}, \tag{5.11d}$$

at the interface, $R = 0$, we have

$$\hat{T}_{s1} = \hat{T}_{l1}, \tag{5.11e}$$

$$\hat{c}_{s1} = \hat{\alpha} c_{l1}, \tag{5.11f}$$

$$c_{l1} = -\hat{m}_l \hat{T}_{l1}, \tag{5.11g}$$

$$\frac{\rho}{\mathrm{St}} \frac{\mathrm{d}S_1}{\mathrm{d}t} = k \frac{\partial \hat{T}_{s1}}{\partial R} - \frac{\partial \hat{T}_{l1}}{\partial R}, \tag{5.11h}$$

$$c_{l1} \frac{\mathrm{d}S_0}{\mathrm{d}t} + \frac{\partial c_{l1}}{\partial R} = -c_{l0} \frac{\mathrm{d}S_1}{\mathrm{d}t} + \alpha c_{l0} \frac{\mathrm{d}S_0}{\mathrm{d}t}. \tag{5.11i}$$

Then, we can write the solutions, up to $\mathcal{O}(\epsilon)$, as

$$c_s = \epsilon \hat{\alpha} c_i(t), \tag{5.12a}$$

$$c_l = c_i(t) e^{-S_0'(t) R} + \epsilon \left(\mathcal{A}_1(t) + \mathcal{A}_2(t, R) e^{-S_0'(t) R} \right), \tag{5.12b}$$

$$T_s = \epsilon \left(A_1(t) R - \frac{c_i(t)}{\hat{m}_l} \right), \tag{5.12c}$$

$$T_l = \epsilon \left(\left(k A_1(t) - \frac{\rho}{\mathrm{St}} S_0'(t) \right) R - \frac{c_i(t)}{\hat{m}_l} \right), \tag{5.12d}$$

with

$$\mathcal{A}_1(t) = \frac{c_i'(t)}{S_0'(t)^2} + c_i(t)\left(\hat{\alpha} + \frac{2}{S_0(t)S_0'(t)} - \frac{S_0''(t)}{S_0'(t)^3}\right), \tag{5.13a}$$

$$\begin{aligned}\mathcal{A}_2(t,R) = &-\frac{c_i'(t)}{S_0'(t)^2}\left(1 + S_0'(t)R\right) + A_2(t) \\ &+ c_i(t)\left[\frac{S_0''(t)}{S_0'(t)^3}\left(1 + S_0'(t)R + \frac{1}{2}S_0'(t)^2R^2\right) - \frac{\left(1 + S_0'(t)R\right)\left(2 + S_0(t)S_1'(t)\right)}{S_0'(t)S_0(t)}\right],\end{aligned} \tag{5.13b}$$

where $c_i(t)$, $A_1(t)$, and $A_2(t)$ are functions to be determined from the matching.

Matching c_l, we obtain the equation

$$c_i'(t) + c_i(t)\left(\hat{\alpha}S_0'(t)^2 + 2\frac{S_0'(t)}{S_0(t)} - \frac{S_0''(t)}{S_0'(t)}\right) = \hat{c}_0 S_0'(t)^2, \tag{5.14}$$

which allows us to determine $c_i(t)$ once we know $S_0(t)$. We give the calculations for $c_i(t)$ in Section 5.4.

5.3.3 Layer C

The last layer in regime i is layer C, the outer layer in the liquid. Rescaling the problem with

$$c_l = \epsilon\hat{c}_l \qquad \text{and} \qquad T_l = \epsilon\hat{T}_l, \tag{5.15}$$

we find that the problem is defined in $0 < r < S(t)$ by

$$\frac{\partial\hat{c}_l}{\partial t} = \epsilon\left(\frac{\partial^2\hat{c}_l}{\partial r^2} + \frac{2}{r}\frac{\partial\hat{c}_l}{\partial r}\right), \tag{5.16a}$$

$$\frac{\partial\hat{T}_l}{\partial t} = \frac{\partial^2\hat{T}_l}{\partial r^2} + \frac{2}{r}\frac{\partial\hat{T}_l}{\partial r}, \tag{5.16b}$$

with the boundary conditions

$$\frac{\partial\hat{c}_l}{\partial r} = 0 \quad \text{and} \quad \frac{\partial\hat{T}_l}{\partial r} = 0, \quad \text{at } r = 0, \tag{5.16c}$$

and the initial conditions

$$\hat{c}_l = \hat{c}_0 \quad \text{and} \quad \hat{T}_l = \hat{T}_0, \quad \text{at } t = 0. \tag{5.16d}$$

The problem is completed by the matching conditions with layer B.

At $\mathcal{O}(1)$, the problem is

$$\frac{\partial \hat{c}_{l0}}{\partial t} = 0, \tag{5.17a}$$

$$\frac{\partial \hat{T}_{l0}}{\partial t} = \frac{\partial^2 \hat{T}_{l0}}{\partial r^2} + \frac{2}{r}\frac{\partial \hat{T}_l}{\partial r}, \tag{5.17b}$$

with the boundary conditions

$$\frac{\partial \hat{c}_{l0}}{\partial r} = 0 \quad \text{and} \quad \frac{\partial \hat{T}_{l0}}{\partial r} = 0, \quad \text{at } r = 0, \tag{5.17c}$$

and the initial conditions

$$\hat{c}_{l0} = \hat{c}_0 \quad \text{and} \quad \hat{T}_{l0} = \hat{T}_0, \quad \text{at } t = 0. \tag{5.17d}$$

Therefore, the leading order solutions are

$$c_l = \epsilon \hat{c}_0, \tag{5.18a}$$

$$T_l = \epsilon \hat{T}_{l0}(t, r), \tag{5.18b}$$

where $\hat{T}_{l0}$ is the solution to the problem below, where we have included the matching conditions derived in Section 5.3.4. The problem for $\hat{T}_{l0}$ is

$$\frac{\partial \hat{T}_{l0}}{\partial t} = \frac{\partial^2 \hat{T}_{l0}}{\partial r^2} + \frac{2}{r}\frac{\partial \hat{T}_{l0}}{\partial r}, \tag{5.19a}$$

with boundary conditions

$$\frac{\partial \hat{T}_{l0}}{\partial r} = 0 \quad \text{at } r = 0, \quad \text{and} \quad \hat{T}_{l0} = -\frac{c_i(t)}{\hat{m}_l} \quad \text{at } r = S_0(t), \tag{5.19b}$$

and the initial condition

$$\hat{T}_{l0} = \hat{T}_0 \quad \text{at } t = 0, \tag{5.19c}$$

where conditions (5.19b) and (5.19c) are derived later in Section 5.3.4.

5.3.4 Matching of the solutions

We now can match the solutions between the different layers using Van Dyke's rule (see [94] for details).

We start matching c_l between the outer layer C and the inner layer B. We take two terms in the inner solution and two terms in the outer solution, and write them both in terms of the inner variable, so

$$(2\text{ti})(2\text{to}) = \epsilon \hat{c}_0, \tag{5.20a}$$

$$(2\text{to})(2\text{ti}) = \epsilon \mathcal{A}_1(t), \tag{5.20b}$$

therefore we have

$$\frac{c_i'(t)}{S_0'(t)^2} + c_i(t)\left(\hat{\alpha} + \frac{2}{S_0(t)S_0'(t)} - \frac{S_0''(t)}{S_0'(t)^3}\right) = \hat{c}_0, \tag{5.21}$$

which is the equation (5.14) we have used to determine $c_i(t)$ at leading order.

We then match c_s between the outer layer A and the inner layer B. We take two terms in the inner solution and two terms in the outer solution, and write them both in terms of the inner variable, so

$$(2\text{ti})(2\text{to}) = \epsilon\hat{c}_{s0}(S_0(t)), \tag{5.22a}$$

$$(2\text{to})(2\text{ti}) = \epsilon\hat{\alpha}c_i(t), \tag{5.22b}$$

and equating both expressions we determine

$$\hat{c}_{s0}(S_0(t)) = \hat{\alpha}c_i(t) \tag{5.23}$$

so we can conclude that $\hat{c}_{s0}(r)$ is

$$\hat{c}_{s0}(r) = \hat{\alpha}c_i\left(S_0^{-1}(r)\right). \tag{5.24}$$

We now match the temperature in the solid phase, T_s, between layers A and B. Taking two terms in the inner solution and two terms in the outer solution, and writing them in terms of the inner variable, we find

$$(2\text{ti})(2\text{to}) = T_{s0}(t, S_0(t)) + \epsilon\left(T_{s1}(t, S_0(t)) + (R + S_1(t))\left.\frac{\partial T_{s0}}{\partial r}\right|_{r=S_0(t)}\right), \tag{5.25a}$$

$$(2\text{to})(2\text{ti}) = \epsilon\left(A_1(t)R - \frac{c_i(t)}{\hat{m}_l}\right), \tag{5.25b}$$

so we conclude that

$$A_1(t) = \left.\frac{\partial T_{s0}}{\partial r}\right|_{r=S_0(t)}, \tag{5.26a}$$

$$T_{s0}(t, S_0(t)) = 0, \tag{5.26b}$$

and we can use the latter as a boundary condition to complete (5.6).

Finally, we match the temperature in the liquid phase between layers B and C. Taking two terms in both the inner and outer solution, and writing them in terms of the inner variable, we find

$$(2\text{ti})(2\text{to}) = \epsilon\hat{T}_{l0}(t, S_0(t)), \tag{5.27a}$$

$$(2\text{to})(2\text{ti}) = \epsilon\left(\left(kA_1(t) - \frac{\rho}{\text{St}}S_0'(t)\right)R - \frac{c_i(t)}{\hat{m}_l}\right), \tag{5.27b}$$

which give the boundary condition we need for (5.19)

$$\hat{T}_{l0}(t, S_0(t)) = -\frac{c_i(t)}{\hat{m}_l}, \tag{5.28}$$

and the condition for the moving boundary,

$$\frac{\rho}{\mathrm{St}} S_0'(t) = k \left.\frac{\partial T_{s0}}{\partial r}\right|_{r=S_0(t)}. \tag{5.29}$$

This completes the problem in this regime. In the next section we perform an asymptotic analysis in the limit $\mathrm{St} \to 0$ in order to find approximate solutions for regime i.

5.4 Small St analysis of regime i

In this section, we perform the small Stefan number analysis of the thermal problem found in the previous section. Taking the limit $\mathrm{St} \to 0$, we can determine approximate analytical solutions to the problem in regime i. Because the concentration problem has almost decoupled from the thermal problem when taking the limit $\epsilon \to 0$, the problem we have to solve is very similar to the one studied in [63].

There are three main differences between the problem in [63] and the problem studied here. The first difference is the scalings we took for the non-dimensionalisation and thus where the dimensionless parameters appear in the solutions. The second difference is that we consider constitutional supercooling, therefore the temperature at the interface depends on the concentration of impurities at the interface which is found from an ODE that depends on the position of the interface, but not on the temperature. The last difference is that in our problem we have assumed that the initial temperature of the melt is small, and hence is the amount of supercooling. Therefore, we find that the temperature gradient in the liquid will have no influence on the position of the interface at leading order, reducing the free boundary problem to a one-phase Stefan problem.

This last assumption is crucial to decouple the thermal problem into the following subproblems. The first subproblem is a one-phase Stefan problem, involving temperature in the solid phase and the moving boundary and, from (5.6), we know it is given

by

$$\frac{\partial T_{s0}}{\partial t} = \kappa \left(\frac{\partial^2 T_{s0}}{\partial r^2} + \frac{2}{r} \frac{\partial T_{s0}}{\partial r} \right), \qquad \text{in} \quad S_0(t) < r < 1, \tag{5.30a}$$

$$T_{s0} = 0, \qquad \text{at} \quad r = S_0(t), \tag{5.30b}$$

$$T_{s0} = -1, \qquad \text{at} \quad r = 1, \tag{5.30c}$$

$$\frac{\rho}{\mathrm{St}} \frac{\mathrm{d}S_0}{\mathrm{d}t} = k \frac{\partial T_{s0}}{\partial r}, \qquad \text{at} \quad r = S_0(t), \tag{5.30d}$$

$$S_0 = 1, \qquad \text{at} \quad t = 0. \tag{5.30e}$$

Once we have solved problem (5.30), we can use $S_0(t)$ to calculate the concentration at the interface from (5.14), which is

$$c_i'(t) + c_i(t) \left(\hat{\alpha} S_0'(t)^2 + 2 \frac{S_0'(t)}{S_0(t)} - \frac{S_0''(t)}{S_0'(t)} \right) = \hat{c}_0 S_0'(t)^2. \tag{5.31}$$

Finally, knowing the concentration at the interface, we can solve the problem for the temperature in the liquid given in (5.19), which is

$$\frac{\partial \hat{T}_{l0}}{\partial t} = \frac{\partial^2 \hat{T}_{l0}}{\partial r^2} + \frac{2}{r} \frac{\partial \hat{T}_{l0}}{\partial r}, \qquad \text{in} \quad 0 < r < S_0(t), \tag{5.32a}$$

$$\frac{\partial \hat{T}_{l0}}{\partial r} = 0, \qquad \text{at} \quad r = 0, \tag{5.32b}$$

$$\hat{T}_{l0} = -\frac{c_i(t)}{\hat{m}_l}, \qquad \text{at} \quad r = S_0(t), \tag{5.32c}$$

$$\hat{T}_{l0} = \hat{T}_0, \qquad \text{at} \quad t = 0. \tag{5.32d}$$

To solve these problems, we follow the same method as in [63], finding asymptotic solutions in the limit $\mathrm{St} \to 0$. Therefore, within regime i, we need to distinguish five different sublayers which now scale with St. This new five sublayers are showed in red in Figure 5.3, and their scalings are described in Table 5.2. Notice that to avoid confusion with rescalings with ϵ, we use tilde to denote the rescalings with St.

5.4.1 Subregime i(1)

The first subregime we have to study is subregime i(1) which corresponds to early time. The time in this layer is $t = \mathcal{O}(1)$, which is small compared to the critical time $t^* = \mathcal{O}\left(\mathrm{St}^{-1}\right)$. This critical time corresponds to the solidification time of the equivalent pure melt problem. In this layer, the interface has not moved much, so it is near $r = 1$ and we can write it as $S_0 = 1 + \sqrt{\mathrm{St}}\tilde{S}_0$. Therefore, we need to consider an outer layer in the liquid phase and an inner layer comprising both phases defined as $r = 1 + \sqrt{\mathrm{St}}R$, where R is the inner variable.

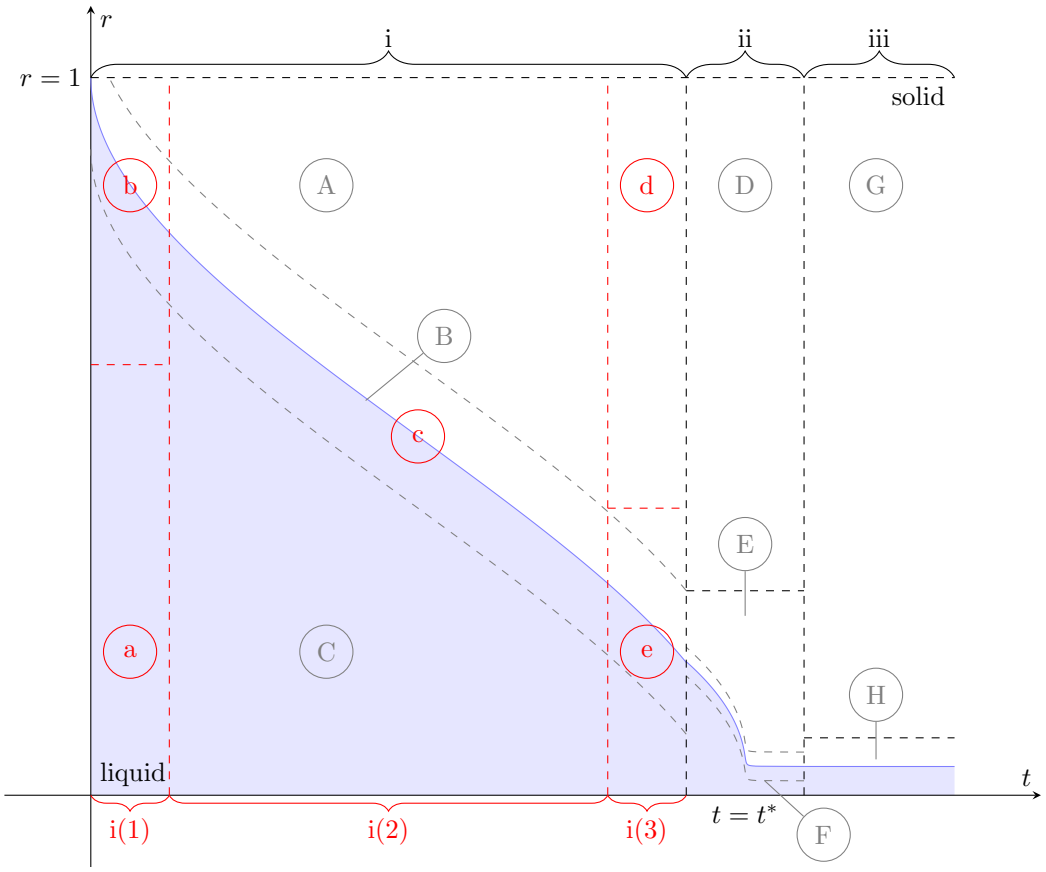


Figure 5.3: Sketch of the layers in St in regime i. The new layers are shown on top of the layers in ϵ discussed in Figure 5.2, and they are identified with lower case letters. The subregimes within regime i are identified as subregimes i(1), i(2) and i(3). The scalings of these new layers are shown in Table 5.2.

		t	r	S_0	T_{s0}	$\hat{T}_{l0}$	c_i
Subregime i(a)	a	t	r	$1+\sqrt{\mathrm{St}}\tilde{S}_0$	-	$\hat{T}_{l0}$	$\mathrm{St}\tilde{c}_i$
	b	t	$1+\sqrt{\mathrm{St}}R$	$1+\sqrt{\mathrm{St}}\tilde{S}_0$	T_{s0}	$\sqrt{\mathrm{St}}\tilde{T}_{l0}$	$\mathrm{St}\tilde{c}_i$
Subregime i(2)	c	$\mathrm{St}^{-1}\tilde{t}$	r	S_0	T_{s0}	$\hat{T}_{l0}$	$\mathrm{St}\tilde{c}_i$
Subregime i(3)	d	$t^*+\tilde{t}$	r	$\sqrt{\mathrm{St}}\tilde{S}_0$	T_{s0}	-	$\mathrm{St}^{-\frac{1}{2}}\tilde{c}_i$
	e	$t^*+\tilde{t}$	$\sqrt{\mathrm{St}}R$	$\sqrt{\mathrm{St}}\tilde{S}_0$	T_{s0}	$\mathrm{St}^{-\frac{1}{2}}\tilde{T}_{l0}$	$\mathrm{St}^{-\frac{1}{2}}\tilde{c}_i$

Table 5.2: Scalings for the variables in each sublayer of regime i. The variable R is the space variable in the inner layers. For temperature, concentration, and time, we use hats whenever they are rescaled.

5.4.1.1 Layer a

We first focus on the outer solution in the liquid phase. The thermal problem in the liquid is

$$\frac{\partial \hat{T}_{l0}}{\partial t} = \frac{\partial^2 \hat{T}_{l0}}{\partial r^2} + \frac{2}{r}\frac{\partial \hat{T}_{l0}}{\partial r}, \qquad \text{in} \quad 0 < r < 1, \tag{5.33a}$$

$$\frac{\partial \hat{T}_{l0}}{\partial r} = 0, \qquad \text{at} \quad r = 0, \tag{5.33b}$$

$$\hat{T}_{l0} = 0, \qquad \text{at} \quad r = 1, \tag{5.33c}$$

$$\hat{T}_{l0} = \hat{T}_0, \qquad \text{at} \quad t = 0, \tag{5.33d}$$

where (5.33c) comes from the matching conditions with layer b. Using separation of variables, we find that the solution at leading order is

$$\hat{T}_{l0} = \frac{2\hat{T}_0}{\pi r}\sum_{n=1}^{\infty}\frac{(-1)^{n+1}}{n}e^{-n^2\pi^2 t}\sin(n\pi r) + \mathcal{O}\left(\sqrt{\mathrm{St}}\right), \tag{5.34}$$

as shown in [63].

5.4.1.2 Layer b

We now solve the system in the inner layer b. This layer accounts for both the solid and liquid phases, therefore we need to solve for both thermal fields and the concentration at the interface. We start by solving the one-phase Stefan problem that determines the temperature in the solid and the position of the interface. With the rescalings

$$r = 1+\sqrt{\mathrm{St}}R, \qquad S_0 = 1+\sqrt{\mathrm{St}}\tilde{S}_0, \qquad \hat{T}_{l0} = \sqrt{\mathrm{St}}\tilde{T}_{l0} \qquad \text{and} \qquad c_i = \epsilon\tilde{c}_i, \tag{5.35}$$

the problem (5.30) becomes

$$\mathrm{St}\frac{\partial T_{s0}}{\partial t} = \kappa\left(\frac{\partial^2 T_{s0}}{\partial R^2} + \frac{2\sqrt{\mathrm{St}}}{1+\sqrt{\mathrm{St}}R}\frac{\partial T_{s0}}{\partial R}\right), \qquad \text{in} \quad \tilde{S}_0(t) < R < 0, \tag{5.36a}$$

$$T_{s0} = 0, \qquad \text{at} \quad R = \tilde{S}_0(t), \tag{5.36b}$$

$$T_{s0} = -1, \qquad \text{at} \quad R = 0, \tag{5.36c}$$

$$\rho\frac{\mathrm{d}\tilde{S}_0}{\mathrm{d}t} = k\frac{\partial T_{s0}}{\partial R}, \qquad \text{at} \quad R = \tilde{S}_0(t), \tag{5.36d}$$

$$\tilde{S}_0 = 0, \qquad \text{at} \quad t = 0. \tag{5.36e}$$

Then, expanding T_{s0} and $\tilde{S}_0$ in powers of $\sqrt{\mathrm{St}}$ as

$$T_{s0} = T_{s0,0} + \sqrt{\mathrm{St}}T_{s0,\frac{1}{2}} + \mathcal{O}\left(\mathrm{St}\right), \tag{5.37a}$$

$$\tilde{S}_0 = \tilde{S}_{0,0} + \sqrt{\mathrm{St}}\tilde{S}_{0,\frac{1}{2}} + \mathcal{O}\left(\mathrm{St}\right), \tag{5.37b}$$

we can linearise the problem and determine the solutions. We find

$$T_{s0} = -1 + \frac{R}{\tilde{S}_{0,0}(t)} + \sqrt{\mathrm{St}}\left(-\frac{R^2}{\tilde{S}_{0,0}(t)} + \left(1 - \frac{\tilde{S}_{0,1}(t)}{\tilde{S}_{0,0}(t)^2}\right)R\right) + \mathcal{O}\left(\mathrm{St}\right), \tag{5.38a}$$

$$\tilde{S}_0 = -\sqrt{\frac{2k}{\rho}t} - \sqrt{\mathrm{St}}\frac{2k}{3\rho}t + \mathcal{O}\left(\mathrm{St}\right). \tag{5.38b}$$

We now need to determine $\tilde{c}_i$ using the calculated values of $\tilde{S}_0$. With the rescaled concentration, (5.31), becomes

$$\tilde{c}_i'(t) + \tilde{c}_i(t)\left(\mathrm{St}\hat{\alpha}\tilde{S}_0'(t)^2 + 2\sqrt{\mathrm{St}}\frac{\tilde{S}_0'(t)}{1+\sqrt{\mathrm{St}}\tilde{S}_0(t)} - \frac{\tilde{S}_0''(t)}{\tilde{S}_0'(t)}\right) = \hat{c}_0\tilde{S}_0'(t)^2, \tag{5.39}$$

and expanding $\tilde{c}_i(t)$ in powers of $\sqrt{\mathrm{St}}$ as

$$\tilde{c}_i(t) = \tilde{c}_{i,0}(t) + \sqrt{\mathrm{St}}\tilde{c}_{i,\frac{1}{2}} + \mathcal{O}\left(\mathrm{St}\right), \tag{5.40}$$

we find

$$\tilde{c}_i = \frac{\hat{c}_0 k}{\rho} + \sqrt{\mathrm{St}}\hat{c}_0\sqrt{\left(\frac{2k}{\rho}\right)^3 t} + \mathcal{O}\left(\mathrm{St}\right), \tag{5.41}$$

where we have used the fact that we require $\tilde{c}_i$ to remain bounded as $t \to 0$ as our initial condition.

Finally, we can use the values of $\tilde{c}_i$ and $\tilde{S}_0$ to determine the temperature in the liquid. Rescaling (5.32), we have

$$\mathrm{St}\frac{\partial \tilde{T}_{l0}}{\partial t} = \frac{\partial^2 \tilde{T}_{l0}}{\partial R^2} + \frac{2\sqrt{\mathrm{St}}}{1+\sqrt{\mathrm{St}}R}\frac{\partial \tilde{T}_{l0}}{\partial R}, \qquad \text{in} \quad R < \tilde{S}_0(t), \tag{5.42a}$$

$$\tilde{T}_{l0} = -\frac{\tilde{c}_i(t)}{\hat{m}_l}, \qquad \text{at} \quad R = \tilde{S}_0(t), \tag{5.42b}$$

and the remaining condition is given by the matching with the outer layer. Then, in the inner layer, the temperature is given by

$$\tilde{T}_{l0} = -2\hat{T}_0 R \sum_{n=1}^{\infty} e^{-n^2\pi^2 t} \left(R - \hat{S}_{0,0}(t)\right) \sqrt{\mathrm{St}} + \mathcal{O}\left(\mathrm{St}\right). \tag{5.43}$$

Notice that the supercooling effects are of $\mathcal{O}\left(\mathrm{St}\right)$, therefore they are only seen at higher order.

Then, the solution to the problem in this subregime is given, at leading order, by

$$T_{s0} \approx -1 + \sqrt{\frac{\rho}{2k\mathrm{St}}} \frac{1-r}{\sqrt{t}}, \tag{5.44a}$$

$$\hat{T}_{l0} \approx \frac{2\hat{T}_0}{\pi r} \sum_{n=1}^{\infty} \frac{(-1)^{n+1}}{n} e^{-n^2\pi^2 t} \sin\left(n\pi r\right), \tag{5.44b}$$

$$S_0 \approx 1 - \sqrt{\frac{2k\mathrm{St}}{\rho}} t, \tag{5.44c}$$

$$c_i \approx \hat{c}_0 \frac{k\mathrm{St}}{\rho}. \tag{5.44d}$$

5.4.2 Subregime i(2) (layer c)

Now we need to consider the central subregime i(2), in which $t = \mathcal{O}\left(\mathrm{St}^{-1}\right)$. For this problem, we only need to consider one layer. We start solving the one-phase Stefan problem (5.30) which, with the new time scaling $t = \mathrm{St}^{-1}\tilde{t}$, becomes

$$\mathrm{St}\frac{\partial T_{s0}}{\partial \tilde{t}} = \kappa \left(\frac{\partial^2 T_{s0}}{\partial r^2} + \frac{2}{r}\frac{\partial T_{s0}}{\partial r}\right), \qquad \text{in} \quad S_0(\tilde{t}) < r < 1, \tag{5.45a}$$

$$T_{s0} = 0, \qquad \text{at} \quad r = S_0(\tilde{t}), \tag{5.45b}$$

$$T_{s0} = -1, \qquad \text{at} \quad r = 1, \tag{5.45c}$$

$$\rho\frac{\mathrm{d}S_0}{\mathrm{d}\tilde{t}} = k\frac{\partial T_{s0}}{\partial r}, \qquad \text{at} \quad r = S_0(\tilde{t}), \tag{5.45d}$$

and the initial conditions come from matching with subregime i(1). For convenience, as done in [63], we take r and S_0 to be the independent variables, so then the dependent variables are $T_{s0}(S_0, r)$ and $\tilde{t}(S_0)$. Then, we expand T_{s0} and $\tilde{t}$ as

$$T_{s0} = T_{s0,0} + \mathrm{St}T_{s0,1} + \mathcal{O}\left(\mathrm{St}^2\right), \tag{5.46a}$$

$$\tilde{t} = \tilde{t}_{,0} + \mathrm{St}\tilde{t}_{,1} + \mathcal{O}\left(\mathrm{St}^2\right), \tag{5.46b}$$

and we find that the solutions are

$$T_{s0,0} = \frac{1}{1-S_0}\left(\frac{S_0}{r} - 1\right), \tag{5.47a}$$

$$\tilde{t}_{,0} = \frac{\rho}{k}\left(\frac{1}{2}(1-S_0)^2 - \frac{1}{3}(1-S_0)^3\right), \tag{5.47b}$$

$$T_{s0,1} = \frac{k}{\kappa\rho}\frac{1-r}{6rS_0(1-S_0)}\left(1 - \left(\frac{1-r}{1-S_0}\right)^2\right), \tag{5.47c}$$

$$\tilde{t}_{,1} = \frac{1}{6\kappa}(1-S_0)^2. \tag{5.47d}$$

Notice that when $S_0^2 = \mathcal{O}(\mathrm{St})$, the solution breaks down, so this motivates the study of subregime i(3). Now we need to determine the concentration at the interface from (5.31), which, rescaling time and the concentration itself as $c_i = \mathrm{St}\tilde{c}_i$, becomes

$$\tilde{c}_i'(\tilde{t}) = \hat{c}_0 S_0'(\tilde{t})^2 - \tilde{c}_i(\tilde{t})\left(\mathrm{St}\hat{\alpha}S_0'(\tilde{t})^2 + 2\frac{S_0'(\tilde{t})}{S_0(\tilde{t})} - \frac{S_0''(\tilde{t})}{S_0'(\tilde{t})}\right). \tag{5.48}$$

As we did before, we take S_0 to be the time-like independent variable and $\hat{t}$ the dependent variable. Then, we rewrite (5.48) as

$$\tilde{c}_i'(S_0)\tilde{t}'(S_0) = \hat{c}_0 - \tilde{c}_i(S_0)\left(\mathrm{St}\hat{\alpha} + \frac{2}{S_0}\tilde{t}'(S_0) + \tilde{t}''(S_0)\right). \tag{5.49}$$

Expanding $\tilde{c}_i(\tilde{t})$ and $\tilde{t}$ in powers of St, we find that at leading order

$$\tilde{c}_{i,0}'(S_0)\tilde{t}_{,0}'(S_0) = \hat{c}_0 - \tilde{c}_{i,0}(S_0)\left(\frac{2}{S_0}\tilde{t}_{,0}'(S_0) + \tilde{t}_{,0}''(S_0)\right), \tag{5.50}$$

therefore, using the definition of $\tilde{t}_{,0}(S_0)$ from (5.47b), we find

$$\tilde{c}_{i,0}(S_0) = \frac{3C_1\rho - \hat{c}_0 k S_0^3}{3\rho(1-S_0)S_0^3}, \tag{5.51}$$

where C_1 is a constant to be determined. Matching with the solution in subregime i(1), we find

$$C_1 = \frac{\hat{c}_0 k}{3\rho}, \tag{5.52}$$

therefore we conclude that

$$\tilde{c}_{i,0} = \frac{\hat{c}_0}{3}\frac{k}{\rho}\frac{1-S_0^3}{(1-S_0)S_0^3}. \tag{5.53}$$

Notice that we could determine the value of C_1 by imposing that we want $\tilde{c}_i$ to be bounded as $S_0 \to 1$, finding the same result.

Finally, we need to determine the temperature in the liquid from the rescaled version of (5.32), which is

$$\mathrm{St}\frac{\partial \hat{T}_{l0}}{\partial \hat{t}} = \frac{\partial^2 \hat{T}_{l0}}{\partial r^2} + \frac{2}{r}\frac{\partial \hat{T}_{l0}}{\partial r}, \qquad \text{in} \quad 0 < r < S_0(\tilde{t}), \tag{5.54a}$$

$$\frac{\partial \hat{T}_{l0}}{\partial r} = 0, \qquad \text{at} \quad r = 0, \tag{5.54b}$$

$$\hat{T}_{l0} = -\mathrm{St}\frac{\tilde{c}_i(\hat{t})}{\hat{m}_l}, \qquad \text{at} \quad r = S_0(\tilde{t}), \tag{5.54c}$$

and the initial conditions from the matching with regime i(1).

In order to solve this problem, we proceed as in [63], however we need to introduce introduce extra terms in powers of St to account for the non-homogeneous boundary condition. Taking an expansion of the form

$$\hat{T}_{l0} = \exp\left(-\frac{g(\tilde{t})}{\mathrm{St}}\right)\left[u_0(\tilde{t}, r) + \mathcal{O}\left(\mathrm{St}\right)\right] + \mathrm{St}\left[v_0(\tilde{t}, r) + \mathcal{O}\left(\mathrm{St}\right)\right], \tag{5.55}$$

we find that the leading order solution is given by

$$\hat{T}_{l0} = \frac{2\hat{T}_0 S_0(\tilde{t})}{\pi r}\sum_{n=1}^{\infty}\frac{(-1)^{n+1}}{n}\exp\left(-\frac{n^2\pi^2}{\mathrm{St}}\int_0^{\tilde{t}}\frac{\mathrm{d}\tilde{s}}{S_0(\tilde{s})^2}\right)\sin\left(\frac{n\pi r}{S_0(\tilde{t})}\right) - \mathrm{St}\frac{\tilde{c}_{i0}(\tilde{t})}{\hat{m}_l} + \text{h.o.t.} \tag{5.56}$$

Notice that, as discussed in [63], the inclusion of the exponentially small terms allows us to match the initial conditions and thus it is not necessary to consider subregime i(1).

Then, the solution to the problem in this subregime at leading order is given by

$$T_{s0} \approx \frac{1}{1 - S_0(t)}\left(\frac{S_0(t)}{r} - 1\right), \tag{5.57a}$$

$$\hat{T}_{l0} \approx -\frac{c_i(t)}{\hat{m}_l} + \frac{2\hat{T}_0 S_0(t)}{\pi r}\sum_{n=1}^{\infty}\frac{(-1)^{n+1}}{n}\exp\left(-n^2\pi^2\int_0^{t}\frac{\mathrm{d}s}{S_0(s)^2}\right)\sin\left(\frac{n\pi r}{S_0(t)}\right), \tag{5.57b}$$

$$t \approx \frac{\rho}{k\mathrm{St}}\left(\frac{1}{2}(1 - S_0)^2 - \frac{1}{3}(1 - S_0)^3\right), \tag{5.57c}$$

$$c_i \approx \frac{\hat{c}_0}{3}\frac{k\mathrm{St}}{\rho}\frac{1 - S_0(t)^3}{(1 - S_0(t))S_0(t)^3}. \tag{5.57d}$$

The explicit form of $S_0(t)$ can be found inverting (5.57c), but for simplicity we do not reproduce the result here.

5.4.3 Subregime i(3)

We finally consider the last subregime, which corresponds to the late time behaviour. This late time is $t^* - t = \mathcal{O}(1)$, where $t^* = \mathcal{O}\left(\mathrm{St}^{-1}\right)$ is the critical time in which the pure material would finish solidifying. Then, we define the time variable as $t = t^* + \tilde{t}$, where $\tilde{t} < 0$ is the new time variable. In this subregime, the interface position is of $\mathcal{O}\left(\sqrt{\mathrm{St}}\right)$, so we rescale $S_0 = \sqrt{\mathrm{St}}\tilde{S}_0$ and $c_i = \mathrm{St}^{-\frac{1}{2}}\tilde{c}_i$. Therefore, we need to consider an outer layer in the solid phase and an inner layer comprising both phases.

5.4.3.1 Layer d

We start by considering the outer layer in the solid phase. With the rescalings

$$t = t^* + \tilde{t}, \qquad S_0 = \sqrt{\mathrm{St}}\tilde{S}_0, \qquad \text{and} \qquad c_i = \mathrm{St}^{-\frac{1}{2}}\tilde{c}_i, \tag{5.58}$$

the system (5.30) becomes

$$\frac{\partial T_{s0}}{\partial \tilde{t}} = \kappa\left(\frac{\partial^2 T_{s0}}{\partial r^2} + \frac{2}{r}\frac{\partial T_{s0}}{\partial r}\right), \qquad \text{in} \quad 0 < r < 1, \tag{5.59a}$$

$$T_{s0} = -1, \qquad \text{at} \quad r = 1, \tag{5.59b}$$

with the corresponding matching conditions with the inner layer and the previous subregime. The latter matching gives that, at leading order, $T_{s0,0} = -1 + \mathcal{O}\left(\sqrt{\mathrm{St}}\right)$, thus we conclude that

$$T_{s0} \approx -1. \tag{5.60}$$

5.4.3.2 Layer e

The last layer we need to study is the inner layer near the origin. The scalings in this layer are

$$t = t^* + \tilde{t}, \quad r = \sqrt{\mathrm{St}}R, \quad S_0 = \sqrt{\mathrm{St}}\tilde{S}_0, \quad \hat{T}_{l0} = \mathrm{St}^{-\frac{1}{2}}\tilde{T}_{l0}, \quad \text{and} \quad c_i = \mathrm{St}^{-\frac{1}{2}}\tilde{c}_i, \tag{5.61}$$

We consider the one-phase Stefan problem (5.30), which once rescaled becomes

$$\mathrm{St}\frac{\partial T_{s0}}{\partial \tilde{t}} = \kappa\left(\frac{\partial^2 T_{s0}}{\partial R^2} + \frac{2}{R}\frac{\partial T_{s0}}{\partial R}\right), \qquad \text{in} \quad R > \tilde{S}_0(\tilde{t}), \tag{5.62a}$$

$$T_{s0} = 0, \qquad \text{at} \quad R = \tilde{S}_0(\tilde{t}), \tag{5.62b}$$

$$\rho\frac{\mathrm{d}\tilde{S}_0}{\mathrm{d}\tilde{t}} = k\frac{\partial T_{s0}}{\partial R}, \qquad \text{at} \quad R = \tilde{S}_0(\tilde{t}), \tag{5.62c}$$

with matching conditions with the outer layer and the previous subregime. We find

$$T_{s0} = -1 + \frac{\tilde{S}_{0,0}(\tilde{t})}{R} + \mathcal{O}\left(\sqrt{\mathrm{St}}\right), \tag{5.63a}$$

$$\tilde{S}_0 = \sqrt{-\frac{2k}{\rho}\tilde{t}} + \mathcal{O}\left(\sqrt{\mathrm{St}}\right). \tag{5.63b}$$

We use the value of $\tilde{S}_0$ to calculate the concentration at the interface, which is given by

$$\tilde{c}_i'(\tilde{t}) + \tilde{c}_i(\tilde{t})\left(\mathrm{St}\hat{\alpha}\tilde{S}_0'(\tilde{t})^2 + 2\frac{\tilde{S}_0'(\tilde{t})}{\tilde{S}_0(\tilde{t})} - \frac{\tilde{S}_0''(\tilde{t})}{\tilde{S}_0'(\tilde{t})}\right) = \mathrm{St}^{\frac{3}{2}}\hat{c}_0\tilde{S}_0'(\tilde{t})^2. \tag{5.64}$$

Expanding $\tilde{c}_i$ in powers of $\sqrt{\mathrm{St}}$, we find that

$$\tilde{c}_{i,0} = \frac{\hat{c}_0}{3}\frac{k}{\rho}\frac{1}{\tilde{S}_{0,0}(\tilde{t})^3}. \tag{5.65}$$

Finally, we determine the temperature in the liquid phase. Rescaling (5.32), we find

$$\mathrm{St}\frac{\partial \tilde{T}_{l0}}{\partial \tilde{t}} = \frac{\partial^2 \tilde{T}_{l0}}{\partial R^2} + \frac{2}{R}\frac{\partial \tilde{T}_{l0}}{\partial R}, \qquad \text{in} \quad 0 < R < \tilde{S}_0(\tilde{t}), \tag{5.66a}$$

$$\frac{\partial \tilde{T}_{l0}}{\partial R} = 0, \qquad \text{at} \quad R = 0, \tag{5.66b}$$

$$\tilde{T}_{l0} = -\frac{\tilde{c}_i(\tilde{t})}{\hat{m}_l}, \qquad \text{at} \quad R = \tilde{S}_0(\tilde{t}), \tag{5.66c}$$

and the matching conditions with subregime i(2) as initial conditions. Expanding the temperature in powers of $\sqrt{\mathrm{St}}$, we determine the leading order solution as

$$\tilde{T}_{l0} = -\frac{\tilde{c}_{i,0}(\tilde{t})}{\hat{m}_l} + \mathcal{O}\left(\sqrt{\mathrm{St}}\right). \tag{5.67}$$

Then, the solution to the problem in this subregime at leading order is given by

$$T_{s0} \approx -1 + \frac{S_0(t)}{r}, \tag{5.68a}$$

$$\hat{T}_{l0} \approx -\frac{c_i(t)}{\hat{m}_l}, \tag{5.68b}$$

$$S_0 \approx \sqrt{-\frac{2k\mathrm{St}}{\rho}(t^* - t)}, \tag{5.68c}$$

$$c_i \approx \frac{\hat{c}_0}{3}\frac{k\mathrm{St}}{\rho}\frac{1}{S_0(t)^3}, \tag{5.68d}$$

$$t^* \approx \frac{\rho}{6k\mathrm{St}}. \tag{5.68e}$$

5.4.4 Discussion of the solutions

In this section, we have considered the three subregimes that arise from taking the small Stefan number limit to solve the problems found in regime i, after first taking the large Lewis number limit. As we have mentioned, our analysis is very similar to that of McCue et al. [63]. However, we remark that, with their definition of the Stefan number, this corresponds to their large Stefan number limit.

After calculating the solutions, which are given in (5.44), (5.57), and (5.68), we notice that at leading order, the solutions in subregimes i(1) and i(3) are linearisations of the solution in subregime i(2). Therefore, to find the leading order behaviour when we expand in St, it is enough to consider the solution in subregime i(2).

Finally, we need to discuss the validity of the analysis, given that we have taken first the limit $\epsilon \to 0$ and second the limit $\mathrm{St} \to 0$. The physical meaning of the limit $\epsilon \to 0$ is that mass diffusion happens at a much slower time scale than heat diffusion does. The limit $\mathrm{St} \to 0$ means that the time scale of the motion of the interface is much smaller than the thermal diffusive time scale. We expect that the concentration profile to be driven by the motion of the interface, which corresponds to the limit $\epsilon \ll \mathrm{St} \ll 1$, which in terms of time scales means that the solute diffusion time scale is much smaller than the interface motion time scale, which in turn is much smaller than the heat diffusion time scale. Mathematically, this condition ensures that we can first take the small epsilon limit, and second the small Stefan number limit.

However, we shall use the more restrictive condition of $\epsilon^{\frac{2}{3}} \ll \mathrm{St}$, which arises from considering that subregime i(3) happens before regime ii. We have that, when $S = \mathcal{O}\left(\epsilon^{\frac{1}{3}}\right)$, the concentration at the interface $c_i = \mathcal{O}\left(\epsilon^{-1}\right)$ and thus we need to consider another regime. Knowing that in subregime i(3) the interface position is $S = \mathcal{O}\left(\sqrt{\mathrm{St}}\right)$, in order for subregime i(3) to happen before regime ii, we require $\sqrt{\mathrm{St}} \gg \epsilon^{\frac{1}{3}}$. Notice that in [63] the authors consider a fourth time scale, which is exponentially small. However, regime ii happens before this new subregime, as long as $\epsilon \gg \exp\left(-3\sqrt{\frac{2\pi}{\mathrm{St}}}\right)$ which is satisfied, as well.

5.5 Asymptotic solutions in regime ii

We now consider the transition regime ii. In this regime, the interface is still far away from the centre, so we need to distinguish three layers. The outer layer D in the solid, the thermal inner layer E near the centre of the cast, and the concentration inner layer F around the moving interface.

5.5.1 Layer D

We consider first the outer layer in the solid. Taking the scalings

$$t = t^* + \epsilon^{\frac{2}{3}}\tau, \qquad S = \epsilon^{\frac{1}{3}}\hat{S}, \qquad \text{and} \qquad c_s = \epsilon\hat{c}_s, \tag{5.69}$$

we find that the governing equations, which are defined in $0 < r < 1$, are

$$\frac{\partial \hat{c}_s}{\partial t} = \epsilon^{\frac{8}{3}}\hat{D}\left(\frac{\partial^2 \hat{c}_s}{\partial r^2} + \frac{2}{r}\frac{\partial \hat{c}_s}{\partial r}\right), \tag{5.70a}$$

$$\frac{\partial T_s}{\partial t} = \epsilon^{\frac{2}{3}}\kappa\left(\frac{\partial^2 T_s}{\partial r^2} + \frac{2}{r}\frac{\partial T_s}{\partial r}\right), \tag{5.70b}$$

with boundary conditions

$$\frac{\partial \hat{c}_s}{\partial r} = 0 \quad \text{and} \quad T_s = -1, \quad \text{at } r = 1, \tag{5.70c}$$

and with boundary conditions at $r = 0$ given by the matching with layer E. Initial conditions are given by the matching with layer A.

At leading order, we find that the solutions are constant in time and using the matching conditions, which are detailed in Section 5.5.4, we conclude that

$$c_s = \epsilon\hat{\alpha}\frac{\hat{c}_0}{3}\frac{k\mathrm{St}}{\rho}\frac{1-r^3}{(1-r)r^3}, \tag{5.71a}$$

$$T_s = -1. \tag{5.71b}$$

5.5.2 Layer E

Now we consider the inner layer of size $\mathcal{O}\left(\epsilon^{\frac{1}{3}}\right)$ around the centre of the sphere. This layer comprises both phases and it is in this layer where we see thermal diffusion. We use the rescalings

$$t = t^* + \epsilon^{\frac{2}{3}}\tau, \qquad r = \epsilon^{\frac{1}{3}}\xi, \qquad S = \epsilon^{\frac{1}{3}}\hat{S}, \qquad \text{and} \qquad c_l = \epsilon\hat{c}_l, \tag{5.72}$$

so that we can write down the problem at this layer.

The solid phase is defined by $\xi > \hat{S}(\tau)$, and the equations are

$$\frac{\partial c_s}{\partial \tau} = \epsilon^2\hat{D}\left(\frac{\partial^2 c_s}{\partial \xi^2} + \frac{2}{\xi}\frac{\partial c_s}{\partial \xi}\right), \tag{5.73a}$$

$$\frac{\partial T_s}{\partial \tau} = \kappa\left(\frac{\partial^2 T_s}{\partial \xi^2} + \frac{2}{\xi}\frac{\partial T_s}{\partial \xi}\right). \tag{5.73b}$$

The liquid phase is defined by $0 < \xi < \hat{S}(\tau)$, and the equations are

$$\frac{\partial \hat{c}_l}{\partial \tau} = \epsilon \left(\frac{\partial^2 \hat{c}_l}{\partial \xi^2} + \frac{2}{\xi} \frac{\partial \hat{c}_l}{\partial \xi} \right), \tag{5.73c}$$

$$\frac{\partial T_l}{\partial \tau} = \frac{\partial^2 T_l}{\partial \xi^2} + \frac{2}{\xi} \frac{\partial T_l}{\partial \xi}. \tag{5.73d}$$

The boundary conditions are given by

$$\frac{\partial \hat{c}_l}{\partial \xi} = 0 \quad \text{and} \quad \frac{\partial T_l}{\partial \xi} = 0, \quad \text{at } \xi = 0. \tag{5.73e}$$

In this layer we have no interface conditions, as they are imposed through the matching with layer F in each phase. The remaining conditions are found by matching the solutions with layer D.

At $\mathcal{O}(1)$, the problem in the solid phase, $\xi > \hat{S}_0(\tau)$, is

$$\frac{\partial c_{s0}}{\partial \tau} = 0, \tag{5.74a}$$

$$\frac{\partial T_{s0}}{\partial \tau} = \kappa \left(\frac{\partial^2 T_{s0}}{\partial \xi^2} + \frac{2}{\xi} \frac{\partial T_{s0}}{\partial \xi} \right), \tag{5.74b}$$

while the problem in the liquid phase, $0 < \xi < \hat{S}_0(\tau)$, is

$$\frac{\partial \hat{c}_{l0}}{\partial \tau} = 0, \tag{5.74c}$$

$$\frac{\partial T_{l0}}{\partial \tau} = \frac{\partial^2 T_{l0}}{\partial \xi^2} + \frac{2}{\xi} \frac{\partial T_{l0}}{\partial \xi}, \tag{5.74d}$$

with boundary conditions

$$\frac{\partial \hat{c}_{l0}}{\partial \xi} = 0 \quad \text{and} \quad \frac{\partial T_{l0}}{\partial \xi} = 0, \quad \text{at } \xi = 0. \tag{5.74e}$$

We can immediately determine the concentrations

$$c_s = \hat{\alpha} c_i \left(\hat{S}_0^{-1}(\xi) \right), \tag{5.75a}$$

$$c_l = \epsilon \hat{c}_0, \tag{5.75b}$$

where for c_s we have used the matching condition with layer F and for c_l we have used the matching condition with layer C.

For the temperature fields, we need the extra conditions given by the matching with layers D and F. The details of the matching are shown in Section 5.5.4, but they give the following thermal problem at leading order. In the solid phase, $\xi > \hat{S}_0(\tau)$, the equation is

$$\frac{\partial T_{s0}}{\partial \tau} = \kappa \left(\frac{\partial^2 T_{s0}}{\partial \xi^2} + \frac{2}{\xi} \frac{\partial T_{s0}}{\partial \xi} \right), \tag{5.76a}$$

while in the liquid phase, $0 < \xi < \hat{S}_0(\tau)$, the equation is

$$\frac{\partial T_{l0}}{\partial \tau} = \frac{\partial^2 T_{l0}}{\partial \xi^2} + \frac{2}{\xi}\frac{\partial T_{l0}}{\partial \xi}, \tag{5.76b}$$

with the interface conditions at $\xi = \hat{S}_0(\tau)$ given by

$$T_{s0} = T_{l0} = -\frac{c_{i0}(\tau)}{\hat{m}_l}, \tag{5.76c}$$

$$\frac{\rho}{\mathrm{St}}\frac{\mathrm{d}\hat{S}_0}{\mathrm{d}\tau} = k\frac{\partial T_{s0}}{\partial \xi} - \frac{\partial T_{l0}}{\partial \xi}, \tag{5.76d}$$

and the boundary conditions

$$\frac{\partial T_{l0}}{\partial \xi} = 0, \quad \text{at} \quad \xi = 0, \quad \text{and} \quad T_{s0} \to -1, \quad \text{as} \quad \xi \to +\infty. \tag{5.76e}$$

Here $c_{i0}(\tau)$ is the solution of

$$c'_{i0}(\tau) + c_{i0}(\tau)\left(\hat{\alpha}\hat{S}'_0(\tau)^2 + 2\frac{\hat{S}'_0(\tau)}{\hat{S}_0(\tau)} - \frac{\hat{S}''_0(\tau)}{\hat{S}'_0(\tau)}\right) = 0. \tag{5.76f}$$

The initial conditions are provided by the matching with regime i.

We cannot give exact solutions to this problem, but we can find asymptotic approximations in the limit $\mathrm{St} \to 0$. In order to solve the problem we introduce the following scalings

$$\tau = \mathrm{St}^{-\frac{1}{3}}\tilde{\tau}, \qquad \xi = \mathrm{St}^{\frac{1}{3}}\tilde{\xi}, \qquad \text{and} \qquad \hat{S}_0 = \mathrm{St}^{\frac{1}{3}}\tilde{S}_0. \tag{5.77}$$

With these scalings, the problem given in (5.76) becomes the following. In the solid phase, $\tilde{\xi} > \tilde{S}_0(\tilde{\tau})$

$$\mathrm{St}\frac{\partial T_{s0}}{\partial \tilde{\tau}} = \kappa\left(\frac{\partial^2 T_{s0}}{\partial \tilde{\xi}^2} + \frac{2}{\tilde{\xi}}\frac{\partial T_{s0}}{\partial \tilde{\xi}}\right), \tag{5.78a}$$

while in the liquid phase, $0 < \tilde{\xi} < \tilde{S}_0(\tilde{\tau})$

$$\mathrm{St}\frac{\partial T_{l0}}{\partial \tilde{\tau}} = \frac{\partial^2 T_{l0}}{\partial \tilde{\xi}^2} + \frac{2}{\tilde{\xi}}\frac{\partial T_{l0}}{\partial \tilde{\xi}}, \tag{5.78b}$$

with the interface conditions at $\tilde{\xi} = \tilde{S}_0(\tilde{\tau})$ given by

$$T_{s0} = T_{l0} = -\frac{c_{i0}(\tilde{\tau})}{\hat{m}_l}, \tag{5.78c}$$

$$\rho\frac{\mathrm{d}\tilde{S}_0}{\mathrm{d}\tilde{\tau}} = k\frac{\partial T_{s0}}{\partial \tilde{\xi}} - \frac{\partial T_{l0}}{\partial \tilde{\xi}}, \tag{5.78d}$$

and the boundary conditions

$$\frac{\partial T_{l0}}{\partial \tilde{\xi}} = 0, \quad \text{at } \tilde{\xi} = 0, \quad \text{and} \quad T_{s0} \to -1, \quad \text{as } \tilde{\xi} \to +\infty. \tag{5.78e}$$

The condition when $\tilde{\xi} \to +\infty$ comes from considering the outer layer (within which we have not rescaled ξ), which gives that at leading order the temperature is constant in time. Matching shows that temperature is homogeneous in space and equal to -1. Because the analysis of this outer layer is trivial, we do not give the details here.

Under the scalings in (5.77), equation (5.76f) becomes

$$c'_{i0}(\tilde{\tau}) + c_{i0}(\tilde{\tau}) \left(\mathrm{St}\hat{\alpha}\tilde{S}'_0(\tilde{\tau})^2 + 2\frac{\tilde{S}'_0(\tilde{\tau})}{\tilde{S}_0(\tilde{\tau})} - \frac{\tilde{S}''_0(\tilde{\tau})}{\tilde{S}'_0(\tilde{\tau})} \right) = 0. \tag{5.78f}$$

We take $\tilde{\xi}$ and $\tilde{S}_0$ as the independent variables, with T_{s0}, T_{l0}, c_{i0}, and $\tilde{\tau}$ as the dependent variables, and we expand them in powers of St using the following notation

$$T_{s0} = T_{s0,0} + \mathrm{St}T_{s0,1} + \mathcal{O}\left(\mathrm{St}^2\right), \tag{5.79a}$$

$$T_{l0} = T_{l0,0} + \mathrm{St}T_{l0,1} + \mathcal{O}\left(\mathrm{St}^2\right), \tag{5.79b}$$

$$c_{i0} = c_{i0,0} + \mathrm{St}c_{i0,1} + \mathcal{O}\left(\mathrm{St}^2\right), \tag{5.79c}$$

$$\tilde{\tau} = \tilde{\tau}_{,0} + \mathrm{St}\tilde{\tau}_{,1} + \mathcal{O}\left(\mathrm{St}^2\right). \tag{5.79d}$$

Substituting (5.79) into (5.78) and linearising, we find that at $\mathcal{O}(1)$ the problem is the following. In the solid phase, $\tilde{\xi} > \tilde{S}_0$, we have

$$\frac{\partial^2 T_{s0,0}}{\partial \tilde{\xi}^2} + \frac{2}{\tilde{\xi}}\frac{\partial T_{s0,0}}{\partial \tilde{\xi}} = 0, \tag{5.80a}$$

while in the liquid phase, $0 < \tilde{\xi} < \tilde{S}_0$, we have

$$\frac{\partial^2 T_{l0,0}}{\partial \tilde{\xi}^2} + \frac{2}{\tilde{\xi}}\frac{\partial T_{l0,0}}{\partial \tilde{\xi}} = 0. \tag{5.80b}$$

The interface conditions at $\tilde{\xi} = \tilde{S}_0$ are given by

$$T_{s0,0} = T_{l0,0} = -\frac{c_{i0,0}(\tilde{S}_0)}{\hat{m}_l}, \tag{5.80c}$$

$$\rho = \frac{\mathrm{d}\tilde{\tau}_{,0}}{\mathrm{d}\tilde{S}_0}\left(k\frac{\partial T_{s0,0}}{\partial \tilde{\xi}} - \frac{\partial T_{l0,0}}{\partial \tilde{\xi}} \right), \tag{5.80d}$$

while the boundary conditions read

$$\frac{\partial T_{l0,0}}{\partial \tilde{\xi}} = 0, \quad \text{at} \quad \tilde{\xi} = 0, \quad \text{and} \quad T_{s0,0} \to -1, \quad \text{as} \quad \tilde{\xi} \to +\infty. \tag{5.80e}$$

Finally, $c_{i0,0}(\tilde{S}_0)$ is the solution of

$$c'_{i0,0}(\tilde{S}_0)\tilde{\tau}'_{,0}(\tilde{S}_0) + c_{i0,0}(\tilde{S}_0)\left(\frac{2}{\tilde{S}_0}\tilde{\tau}'_{,0}(\tilde{S}_0) + \tilde{\tau}''_{,0}(\tilde{S}_0)\right) = 0. \tag{5.80f}$$

We can directly integrate (5.80a) and (5.80b) with the boundary conditions (5.80c) and (5.80e), finding

$$T_{s0,0} = -1 + \left(-\frac{c_{i0,0}(\tilde{S}_0)}{\hat{m}_l} + 1\right)\frac{\tilde{S}_0}{\tilde{\xi}}, \tag{5.81a}$$

$$T_{l0,0} = -\frac{c_{i0,0}(\tilde{S}_0)}{\hat{m}_l}, \tag{5.81b}$$

while solving (5.80f) gives us

$$c_{i0,0} = \frac{C_2}{\tilde{S}_0^2\tilde{\tau}'_{,0}(\tilde{S}_0)}, \tag{5.82}$$

where C_2 is a constant yet to be determined.

We substitute these expressions into (5.80d), to find

$$\tilde{\tau}_{,0} = -\frac{C_2}{\hat{m}_l}\frac{1}{\tilde{S}_0} - \frac{\rho}{2k}\tilde{S}_0^2 + C_3, \tag{5.83}$$

where C_3 is a constant yet to be determined. Plugging (5.83) back into (5.82), we find

$$c_{i0,0} = \frac{C_2 k\hat{m}_l}{C_2 k - \hat{m}_l\rho\tilde{S}_0^3}. \tag{5.84}$$

We can determine C_2 by matching concentration at the interface with regime i(3). As shown later in Section 5.5.4, we find that

$$C_2 = -\frac{\hat{c}_0}{3}. \tag{5.85}$$

Substituting this expression back into (5.83) and (5.84) we have

$$\tilde{\tau}_{,0} = \frac{\hat{c}_0}{3\hat{m}_l}\frac{1}{\tilde{S}_0} - \frac{\rho}{2k}\tilde{S}_0^2 + C_3, \tag{5.86a}$$

$$c_{i0,0} = \frac{\hat{c}_0 k\hat{m}_l}{\hat{c}_0 k + 3\hat{m}_l\rho\tilde{S}_0^3}, \tag{5.86b}$$

where C_3 is a time shift that requires higher order matching and thus is not determined here. Rescaling using (5.77) to original variables, we have

$$\tau \approx \frac{\hat{c}_0}{3\hat{m}_l}\frac{1}{\hat{S}_0} - \frac{\rho}{2\mathrm{St}k}\hat{S}_0^2 + \tau^*, \tag{5.87a}$$

$$c_{i0} \approx \frac{\hat{c}_0 k\mathrm{St}\hat{m}_l}{\hat{c}_0 k\mathrm{St} + 3\hat{m}_l\rho\hat{S}_0^3}, \tag{5.87b}$$

where $\tau^* = \mathrm{St}^{-\frac{1}{3}}C_3$ is the time-shift previously discussed.

5.5.3 Layer F

We finally study the layer F. This layer is of thickness $\mathcal{O}\left(\epsilon^{\frac{4}{3}}\right)$ around the moving boundary, and it is in this layer where we observe the diffusion and advection of impurities in the liquid phase. The rescaling for this layer is

$$t = t^* + \epsilon^{\frac{2}{3}}\tau, \qquad r = \epsilon^{\frac{1}{3}}\left(\hat{S}(\tau) + \epsilon R\right), \qquad S = \epsilon^{\frac{1}{3}}\hat{S}, \qquad \text{and} \qquad c_l = \epsilon^{-1}\hat{c}_l. \tag{5.88}$$

The solid phase is defined by $R > 0$, and the equations are

$$\epsilon\frac{\partial c_s}{\partial \tau} = \hat{S}'(\tau)\frac{\partial c_s}{\partial R} + \epsilon\hat{D}\left(\frac{\partial^2 c_s}{\partial R^2} + \epsilon\frac{2}{\hat{S}(\tau)+\epsilon R}\frac{\partial c_s}{\partial R}\right), \tag{5.89a}$$

$$\epsilon^2\frac{\partial T_s}{\partial \tau} = \epsilon\hat{S}'(\tau)\frac{\partial T_s}{\partial R} + \kappa\left(\frac{\partial^2 T_s}{\partial R^2} + \epsilon\frac{2}{\hat{S}(\tau)+\epsilon R}\frac{\partial T_s}{\partial R}\right). \tag{5.89b}$$

The liquid phase is defined by $R < 0$, and the equations are

$$\epsilon\frac{\partial \hat{c}_l}{\partial \tau} = \hat{S}'(\tau)\frac{\partial \hat{c}_l}{\partial R} + \frac{\partial^2 \hat{c}_l}{\partial R^2} + \epsilon\frac{2}{\hat{S}(\tau)+\epsilon R}\frac{\partial \hat{c}_l}{\partial R}, \tag{5.89c}$$

$$\epsilon^2\frac{\partial T_l}{\partial \tau} = \epsilon\hat{S}'(\tau)\frac{\partial T_l}{\partial R} + \frac{\partial^2 T_l}{\partial R^2} + \epsilon\frac{2}{\hat{S}(\tau)+\epsilon R}\frac{\partial T_l}{\partial R}. \tag{5.89d}$$

At the interface $R = 0$, the equations are

$$T_s = T_l, \tag{5.89e}$$

$$c_s = \hat{\alpha}\hat{c}_l, \tag{5.89f}$$

$$\hat{c}_l = -\hat{m}_l T_l, \tag{5.89g}$$

$$\epsilon\frac{\rho}{\mathrm{St}}\frac{\mathrm{d}\hat{S}}{\mathrm{d}\tau} = k\frac{\partial T_s}{\partial R} - \frac{\partial T_l}{\partial R}, \tag{5.89h}$$

$$(1-\epsilon\hat{\alpha})\hat{c}_l\frac{\mathrm{d}\hat{S}}{\mathrm{d}\tau} = \epsilon^2\hat{D}\frac{\partial c_s}{\partial R} - \frac{\partial \hat{c}_l}{\partial R}. \tag{5.89i}$$

Notice that this is almost the same problem as in layer B, therefore we do not detail the procedure here. We expand in powers of $\epsilon^{\frac{1}{3}}$, due to the matching with layer E, and find that the solutions are

$$c_s = \hat{\alpha}c_{i0}(\tau) + \epsilon^{\frac{1}{3}}\hat{\alpha}c_{i\frac{1}{3}}(\tau) + \epsilon^{\frac{2}{3}}\hat{\alpha}c_{i\frac{2}{3}}(\tau) + \epsilon\left(\frac{\hat{\alpha}c_{i0}(\tau)}{\hat{S}_0'(\tau)}R + \hat{\alpha}c_{i1}(\tau)\right), \tag{5.90a}$$

$$\begin{aligned} c_l = {} & \epsilon^{-1}c_{i0}(\tau)e^{-\hat{S}_0'(\tau)R} + \epsilon^{-\frac{2}{3}}\left(c_{i\frac{1}{3}}(\tau) - Rc_{i0}(\tau)\hat{S}_{\frac{1}{3}}'(\tau)\right)e^{-\hat{S}_0'(\tau)R} \\ & + \epsilon^{-\frac{1}{3}}\left(c_{i\frac{2}{3}}(\tau) - R\left(c_{i\frac{1}{3}}(\tau)\hat{S}_{\frac{1}{3}}'(\tau) + c_{i0}(\tau)\hat{S}_{\frac{2}{3}}'(\tau)\right) + \frac{R^2}{2}c_{i0}(\tau)\hat{S}_{\frac{1}{3}}'(\tau)\right)e^{-\hat{S}_0'(\tau)R} \\ & + \left(\mathcal{A}_1(\tau) + \left(c_{i1}(\tau) - \mathcal{A}_1(\tau) + R\mathcal{A}_2(\tau,R)\right)e^{-\hat{S}_0'(\tau)R}\right), \end{aligned} \tag{5.90b}$$

$$T_s = -\frac{c_{i0}(\tau)}{\hat{m}_l} - \epsilon^{\frac{1}{3}}\frac{c_{i\frac{1}{3}}(\tau)}{\hat{m}_l} - \epsilon^{\frac{2}{3}}\frac{c_{i\frac{2}{3}}(\tau)}{\hat{m}_l} + \epsilon\left(A_4(\tau)R - \frac{c_{i1}(\tau)}{\hat{m}_l}\right), \tag{5.90c}$$

$$T_l = -\frac{c_{i0}(\tau)}{\hat{m}_l} - \epsilon^{\frac{1}{3}}\frac{c_{i\frac{1}{3}}(\tau)}{\hat{m}_l} - \epsilon^{\frac{2}{3}}\frac{c_{i\frac{2}{3}}(\tau)}{\hat{m}_l} + \epsilon\left(\left(kA_4(\tau) - \frac{\rho}{\mathrm{St}}\hat{S}_0'(\tau)\right)R - \frac{c_{i1}(\tau)}{\hat{m}_l}\right), \tag{5.90d}$$

with

$$\mathcal{A}_1(\tau) = \frac{c_{i0}'(\tau)}{\hat{S}_0'(\tau)^2} + c_{i0}(\tau)\left(\hat{\alpha} + \frac{2}{\hat{S}_0(\tau)\hat{S}_0'(\tau)} - \frac{\hat{S}_0''(\tau)}{\hat{S}_0'(\tau)^3}\right), \tag{5.91a}$$

$$\begin{aligned}\mathcal{A}_2(\tau, R) = &-\frac{c_{i0}'(\tau)}{\hat{S}_0'(\tau)} - c_{i\frac{2}{3}}\hat{S}_1'(\tau) + \frac{1}{2}c_{i\frac{1}{3}}(\tau)\left(R\hat{S}_{\frac{1}{3}}'(\tau)^2 - 2\hat{S}_2'3(\tau)\right)\\ &+ c_{i0}(\tau)\left(-\frac{2}{\hat{S}_0(\tau)} - \frac{R^2}{6}\hat{S}_{\frac{1}{3}}'(\tau)^3 + R\hat{S}_{\frac{1}{3}}'\hat{S}_{\frac{2}{3}}' - \hat{S}_1'(\tau) + \left(1 + \frac{R}{2}\hat{S}_0'(\tau)\right)\frac{\hat{S}_0''(\tau)}{\hat{S}_0'(\tau)^2}\right),\end{aligned} \tag{5.91b}$$

where $c_{i0}(\tau)$ and $A_4(\tau)$ are determined from matching. The values of $c_{i\frac{1}{3}}$, $c_{i\frac{2}{3}}$, and c_{i1} require matching of higher order solutions not presented here.

5.5.4 Matching of the solutions

In this section, we detail the matching between the solutions of the different layers that we have used in the previous sections to fully determine the problem.

We start matching layer D with layer A to obtain the initial conditions that determine the leading order solutions in layer D. The matching for c_s is trivial, as the solution is independent of time in both layers. For T_s, we take one term in the inner solution and one term in the outer solution, finding

$$(1\mathrm{ti})(1\mathrm{to}) = -1 = \lim_{\tau\to-\infty} T_{s0} = (1\mathrm{to})(1\mathrm{ti}), \tag{5.92}$$

so we can fully determine the leading order solutions in layer D. Similarly, we can match c_l and T_l between layers C and E.

We now have to match the space layer D with layer E, which provides the boundary condition needed for T_s (it is not necessary to match for c_s, as at leading order the condition is not required). Then, taking one term in both the inner and outer solutions, we find

$$(1\mathrm{ti})(1\mathrm{to}) = -1 = \lim_{\xi\to+\infty} T_{s0} = (1\mathrm{to})(1\mathrm{ti}). \tag{5.93}$$

The next layers we have to match are layers E and F. We start by matching the temperature fields, both in the solid and the liquid, taking two terms in the inner and the outer solutions. For the solid, we find

$$(2\text{ti})(2\text{to}) = T_{s0}(\tau, \hat{S}_0(\tau)) + \epsilon^{\frac{1}{3}}(\cdots) + \epsilon^{\frac{2}{3}}(\cdots) + \epsilon\left((\cdots) + \left(R + \hat{S}_1(\tau)\right)\left.\frac{\partial T_{s0}}{\partial \xi}\right|_{\xi=\hat{S}_0}\right), \quad (5.94a)$$

$$(2\text{to})(2\text{ti}) = -\frac{c_{i0}(\tau)}{\hat{m}_l} - \epsilon^{\frac{1}{3}}\frac{c_{i\frac{1}{3}}(\tau)}{\hat{m}_l} - \epsilon^{\frac{2}{3}}\frac{c_{i\frac{2}{3}}(\tau)}{\hat{m}_l} + \epsilon\left(RA_4(\tau) - \frac{c_{i1}(\tau)}{\hat{m}_l}\right). \quad (5.94b)$$

The $(\cdots)$ here represent terms that are known, as shown in (5.90), but not necessary for the matching, given the purpose of our analysis. Therefore, to simplify the notation, we do not reproduce these terms here. We conclude

$$T_{s0}(\tau, \hat{S}_0(\tau)) = -\frac{c_{i0}(\tau)}{\hat{m}_l}, \quad (5.95a)$$

$$A_4(\tau) = \left.\frac{\partial T_{s0}}{\partial \xi}\right|_{\xi=\hat{S}_0}. \quad (5.95b)$$

In the liquid, we find

$$(2\text{ti})(2\text{to}) = T_{l0}(\tau, \hat{S}_0(\tau)) + \epsilon^{\frac{1}{3}}(\cdots) + \epsilon^{\frac{2}{3}}(\cdots) + \epsilon\left((\cdots) + \left(R + \hat{S}_1(\tau)\right)\left.\frac{\partial T_{l0}}{\partial \xi}\right|_{\xi=\hat{S}_0}\right), \quad (5.96a)$$

$$(2\text{to})(2\text{ti}) = -\frac{c_{i0}(\tau)}{\hat{m}_l} - \epsilon^{\frac{1}{3}}\frac{c_{i\frac{1}{3}}(\tau)}{\hat{m}_l} - \epsilon^{\frac{2}{3}}\frac{c_{i\frac{2}{3}}(\tau)}{\hat{m}_l} + \epsilon\left(\left(kA_4(\tau) - \frac{\rho}{\mathrm{St}}\frac{\mathrm{d}\hat{S}_0}{\mathrm{d}\tau}\right)R - \frac{c_{i1}(\tau)}{\hat{m}_l}\right), \quad (5.96b)$$

which gives

$$T_{l0}(\tau, \hat{S}_0(\tau)) = -\frac{c_{i0}(\tau)}{\hat{m}_l}, \quad (5.97a)$$

$$kA_4(\tau) - \frac{\rho}{\mathrm{St}}\frac{\mathrm{d}\hat{S}_0}{\mathrm{d}\tau} = \left.\frac{\partial T_{l0}}{\partial \xi}\right|_{\xi=\hat{S}_0}. \quad (5.97b)$$

We have the boundary conditions for both T_{s0} and T_{l0} in layer E, as well as the Stefan condition

$$\frac{\rho}{\mathrm{St}}\frac{\mathrm{d}\hat{S}_0}{\mathrm{d}\tau} = k\left.\frac{\partial T_{s0}}{\partial \xi}\right|_{\xi=\hat{S}_0} - \left.\frac{\partial T_{l0}}{\partial \xi}\right|_{\xi=\hat{S}_0}, \quad (5.98)$$

so we have fully determined the problem (5.76).

Now we match c_s between layers E and F, so taking one term in both the inner and outer solution, we find

$$(1\text{ti})(1\text{to}) = c_{s0}(\hat{S}_0(\tau)) = \hat{\alpha} c_i(\tau) = (1\text{to})(1\text{ti}). \tag{5.99}$$

In order to match c_l between layers E and F, we proceed in the same way as we did to match between layers B and C. We take one term in the inner and outer solutions, finding

$$(1\text{ti})(1\text{to}) = \mathcal{A}_1(\tau), \tag{5.100a}$$

$$(1\text{to})(1\text{ti}) = 0, \tag{5.100b}$$

which gives

$$\frac{c'_{i0}(\tau)}{\hat{S}'_0(\tau)^2} + c_{i0}(\tau)\left(\hat{\alpha} + \frac{2}{\hat{S}_0(\tau)\hat{S}'_0(\tau)} - \frac{\hat{S}''_0(\tau)}{\hat{S}'_0(\tau)^3}\right) = 0. \tag{5.101}$$

Finally, we need to match c_i between regimes i and ii, where regime i acts as the outer layer and ii as the inner layer. This matching determines $\hat{S}_0(\tau)$ up to a time shift, which requires higher order matching and is not studied here. For simplicity of our analysis, we take c_i as a function of $\hat{S}_0$. We can rescale (5.84), using $\hat{S}_0 = \mathrm{St}^{\frac{1}{3}}\tilde{S}_0$, to put it into the form

$$c_{i0}(\hat{S}_0) = \frac{C_2 \mathrm{St} k \hat{m}_l}{C_2 \mathrm{St} k - \hat{m}_l \rho \hat{S}_0^3}. \tag{5.102}$$

Now, using that $S_0 = \epsilon^{\frac{1}{3}}\hat{S}_0$, we can take the inner solution up to $\mathcal{O}(\epsilon^{-1})$ and the outer solution up to $\mathcal{O}(1)$, finding

$$(1\text{ti})(1\text{to}) = \frac{\hat{c}_0}{3}\frac{k\mathrm{St}}{\rho}\frac{1}{\hat{S}_0^3}\epsilon^{-1}, \tag{5.103a}$$

$$(1\text{to})(1\text{ti}) = -C_2\frac{k\mathrm{St}}{\rho}\frac{1}{\hat{S}_0^3}\epsilon^{-1}, \tag{5.103b}$$

therefore we find

$$C_2 = -\frac{\hat{c}_0}{3}. \tag{5.104}$$

This concludes the analysis of regime ii. In this regime, we have observed how the solidification process is driven by a build-up of the interfacial concentration due to rejection from the solid phase. This build-up causes a decrease in the interfacial temperature due to constitutional supercooling and, therefore, a decrease in the thermal gradients at the interface that slows down the motion of the solidification front. At the end of this regime, when $\tau \to +\infty$, we find that the position of the interface at leading order goes to zero. That means that the liquid part of layer E vanishes and therefore we need to consider another regime in which the impurity diffusion inner layer now notices the symmetry boundary condition at $r = 0$.

5.6 Asymptotic solutions in regime iii

We finally consider regime iii. In this regime, the interface is at a distance $\mathcal{O}\left(\epsilon^{\frac{2}{3}}\right)$ from the origin and we need to distinguish two different layers, namely the outer layer in the solid, G, and the inner layer, H, that comprises both phases.

5.6.1 Layer G

We first consider the outer layer in the solid. Taking the scalings

$$t = t^* + \epsilon^{\frac{1}{3}}\theta, \qquad S = \epsilon^{\frac{2}{3}}\hat{S}, \qquad \text{and} \qquad c_s = \epsilon\hat{c}_s, \tag{5.105}$$

we find the equations in this layer, defined in $0 < r < 1$, which are

$$\frac{\partial \hat{c}_s}{\partial \theta} = \epsilon^{\frac{7}{3}}\hat{D}\left(\frac{\partial^2 \hat{c}_s}{\partial r^2} + \frac{2}{r}\frac{\partial \hat{c}_s}{\partial r}\right), \tag{5.106a}$$

$$\frac{\partial T_s}{\partial \theta} = \epsilon^{\frac{1}{3}}\kappa\left(\frac{\partial^2 T_s}{\partial r^2} + \frac{2}{r}\frac{\partial T_s}{\partial r}\right), \tag{5.106b}$$

with boundary conditions

$$\frac{\partial \hat{c}_s}{\partial r} = 0 \quad \text{and} \quad T_s = -1, \quad \text{at } r = 1, \tag{5.106c}$$

and with the remaining conditions given by the matching with layers D and H.

At leading order, we find that the solutions are constant in time and from the matching given in Section 5.6.3, we conclude

$$c_s = \epsilon\hat{\alpha}c_i\left(S_0^{-1}(r)\right), \tag{5.107a}$$

$$T_s = -1. \tag{5.107b}$$

5.6.2 Layer H

Finally, we consider the inner layer H of thickness $\mathcal{O}\left(\epsilon^{\frac{2}{3}}\right)$ around the origin. In this layer the scalings are

$$t = t^* + \epsilon^{\frac{1}{3}}\theta, \qquad r = \epsilon^{\frac{2}{3}}R, \qquad S = \epsilon^{\frac{2}{3}}\hat{S}, \qquad \text{and} \qquad c_l = \epsilon^{-1}\hat{c}_l. \tag{5.108}$$

The solid phase is defined in $R > \hat{S}(\theta)$ by

$$\frac{\partial c_s}{\partial \theta} = \epsilon\hat{D}\left(\frac{\partial^2 c_s}{\partial R^2} + \frac{2}{R}\frac{\partial c_s}{\partial R}\right), \tag{5.109a}$$

$$\epsilon\frac{\partial T_s}{\partial \theta} = \kappa\left(\frac{\partial^2 T_s}{\partial R^2} + \frac{2}{R}\frac{\partial T_s}{\partial R}\right). \tag{5.109b}$$

The liquid phase is defined in $R < \hat{S}(\theta)$ by

$$\frac{\partial \hat{c}_l}{\partial \theta} = \frac{\partial^2 \hat{c}_l}{\partial R^2} + \frac{2}{R}\frac{\partial \hat{c}_l}{\partial R}, \tag{5.109c}$$

$$\epsilon \frac{\partial T_l}{\partial \theta} = \frac{\partial^2 T_l}{\partial R^2} + \frac{2}{R}\frac{\partial T_l}{\partial R}. \tag{5.109d}$$

At the interface, $R = \hat{S}(\theta)$, the conditions are

$$T_s = T_l, \tag{5.109e}$$

$$c_s = \hat{\alpha}\hat{c}_l, \tag{5.109f}$$

$$\hat{c}_l = -\hat{m}_l T_l, \tag{5.109g}$$

$$\epsilon \frac{\rho}{\mathrm{St}} \frac{\mathrm{d}\hat{S}}{\mathrm{d}\theta} = k\frac{\partial T_s}{\partial R} - \frac{\partial T_l}{\partial R}, \tag{5.109h}$$

$$(1 - \epsilon\hat{\alpha})\, \hat{c}_l \frac{\mathrm{d}\hat{S}}{\mathrm{d}\theta} = \epsilon^2 \hat{D}\frac{\partial c_s}{\partial R} - \frac{\partial \hat{c}_l}{\partial R}. \tag{5.109i}$$

The boundary conditions at $R = 0$ are

$$\frac{\partial \hat{c}_l}{\partial R} = 0 \quad \text{and} \quad \frac{\partial T_l}{\partial R} = 0, \quad \text{at } R = 0. \tag{5.109j}$$

The remaining conditions come from matching with other layers, and are detailen in Section 5.6.3.

At $\mathcal{O}(1)$, the problem is the following. In the solid phase, $R > \hat{S}_0(\theta)$, we have

$$\frac{\partial c_{s0}}{\partial \theta} = 0, \tag{5.110a}$$

$$\frac{\partial^2 T_{s0}}{\partial R^2} + \frac{2}{R}\frac{\partial T_{s0}}{\partial R} = 0. \tag{5.110b}$$

In the liquid phase, $R < \hat{S}_0(\theta)$, we have

$$\frac{\partial \hat{c}_{l0}}{\partial \theta} = \frac{\partial^2 \hat{c}_{l0}}{\partial R^2} + \frac{2}{R}\frac{\partial \hat{c}_{l0}}{\partial R}, \tag{5.110c}$$

$$\frac{\partial^2 T_{l0}}{\partial R^2} + \frac{2}{R}\frac{\partial T_{l0}}{\partial R} = 0. \tag{5.110d}$$

At the interface, $R = \hat{S}_0(\theta)$, the conditions are

$$T_{s0} = T_{l0}, \tag{5.110e}$$

$$c_{s0} = \hat{\alpha}\hat{c}_{l0}, \tag{5.110f}$$

$$\hat{c}_{l0} = -\hat{m}_l T_{l0}, \tag{5.110g}$$

$$k\frac{\partial T_{s0}}{\partial R} = \frac{\partial T_{l0}}{\partial R}, \tag{5.110h}$$

$$\hat{c}_{l0}\frac{\mathrm{d}\hat{S}_0}{\mathrm{d}\theta} + \frac{\partial \hat{c}_{l0}}{\partial R} = 0. \tag{5.110i}$$

The boundary conditions at $R = 0$ are

$$\frac{\partial \hat{c}_{l0}}{\partial R} = 0 \quad \text{and} \quad \frac{\partial T_{l0}}{\partial R} = 0, \quad \text{at } R = 0. \tag{5.110j}$$

Notice that we can solve the thermal problem which, with the matching with the T_s in layer G derived later in Section 5.6.3, gives

$$T_s = T_l = -1. \tag{5.111}$$

From here, we conclude that $\hat{c}_{l0} = \hat{m}_l$ at the interface. We also determine that

$$c_s = \hat{\alpha}\hat{m}_l. \tag{5.112}$$

Finally, we need to determine $\hat{c}_{l0}$ and $\hat{S}_0$, which come from the problem

$$\frac{\partial \hat{c}_{l0}}{\partial \theta} = \frac{\partial^2 \hat{c}_{l0}}{\partial R^2} + \frac{2}{R}\frac{\partial \hat{c}_{l0}}{\partial R}, \qquad \text{in} \quad 0 < R < \hat{S}_0(\theta), \tag{5.113a}$$

$$\frac{\partial \hat{c}_{l0}}{\partial R} = 0, \qquad \text{at} \quad R = 0, \tag{5.113b}$$

$$\hat{c}_{l0} = \hat{m}_l, \qquad \text{at} \quad R = \hat{S}_0(\theta), \tag{5.113c}$$

$$\hat{c}_{l0}\frac{\mathrm{d}\hat{S}_0}{\mathrm{d}\theta} + \frac{\partial \hat{c}_{l0}}{\partial R} = 0, \qquad \text{at} \quad R = \hat{S}_0(\theta), \tag{5.113d}$$

$$\hat{c}_{l0} \sim \hat{m}_l \exp\left(-\frac{\mathrm{d}\hat{S}_0}{\mathrm{d}\theta}\left(R - \hat{S}_0(\theta)\right)\right), \qquad \text{when} \quad \theta \to 0, \tag{5.113e}$$

$$\hat{S}_0 \sim \frac{\hat{c}_0}{3\hat{m}_l}\frac{1}{\theta}, \qquad \text{when} \quad \theta \to 0. \tag{5.113f}$$

Rescaling the variables as

$$\hat{c}_{l0} = \hat{m}_l c, \quad \hat{S}_0 = \left(\frac{\hat{c}_0}{3\hat{m}_l}\right)^{\frac{1}{3}} S, \quad R = \left(\frac{\hat{c}_0}{3\hat{m}_l}\right)^{\frac{1}{3}} r, \quad \theta = \left(\frac{\hat{c}_0}{3\hat{m}_l}\right)^{\frac{2}{3}} t, \tag{5.114}$$

we can eliminate all the parameters of the problem. Then, for $t > 0$, the problem to solve is

$$\frac{\partial c}{\partial t} = \frac{\partial^2 c}{\partial r^2} + \frac{2}{r}\frac{\partial c}{\partial r}, \qquad \text{in} \quad 0 < r < S(t), \tag{5.115a}$$

$$\frac{\partial c}{\partial r} = 0, \qquad \text{at} \quad r = 0, \tag{5.115b}$$

$$c = 1, \qquad \text{at} \quad r = S(t), \tag{5.115c}$$

$$c\frac{\mathrm{d}S}{\mathrm{d}t} + \frac{\partial c}{\partial r} = 0, \qquad \text{at} \quad r = S(t), \tag{5.115d}$$

$$c \sim \exp\left(-\frac{\mathrm{d}S}{\mathrm{d}t}\left(r - S(t)\right)\right), \qquad \text{when} \quad t \to 0, \tag{5.115e}$$

$$S \sim \frac{1}{t}, \qquad \text{when} \quad t \to 0, \tag{5.115f}$$

which is a one-phase Stefan problem describing the impurity diffusion in a shrinking core.

We are unable to determine analytic solutions to this problem. However, as we have eliminated all parameters of the problem, we can calculate the solution numerically. We use a finite volume scheme similar to the one we shall describe in Section 5.8, but in this case it is simpler as we only need to solve the problem for the concentration and the position of the interface. Because of the singularity in the initial condition as $t \to 0$, we have to impose the initial conditions of the numerical scheme at some initial time $t = t_0$ close to zero. As the problem (5.115) with an initial condition at $t = t_0$, with t_0 arbitrarily small, is a classical one-phase Stefan problem with sufficiently smooth data, from Theorem III.2 in [23] we know that the solution on $t \in [t_0, \infty)$ is unique. The different numerical simulations for different values of t_0 seem to converge as $t_0 \to 0$, even though we do not have an analytical proof that in this limit the solution to the problem is unique. Notice as well that the problem is a supercooled Stefan problem, and therefore it could go unstable. These problems have been studied in the literature [24, 25, 26, 35], but it remains an open question whether this particular problem is stable. The numerical simulations, however, do not show instability. The plots for the position of the interface and the concentration profiles are shown in Figure 5.4.

Even though we cannot find analytic solutions to the problem (5.115), we can calculate the steady state. One can check that the total amount of impurities in problem (5.115) is conserved. Then, since we know that the steady state concentration profile is homogeneous in space, we have that the total concentration at the steady state is

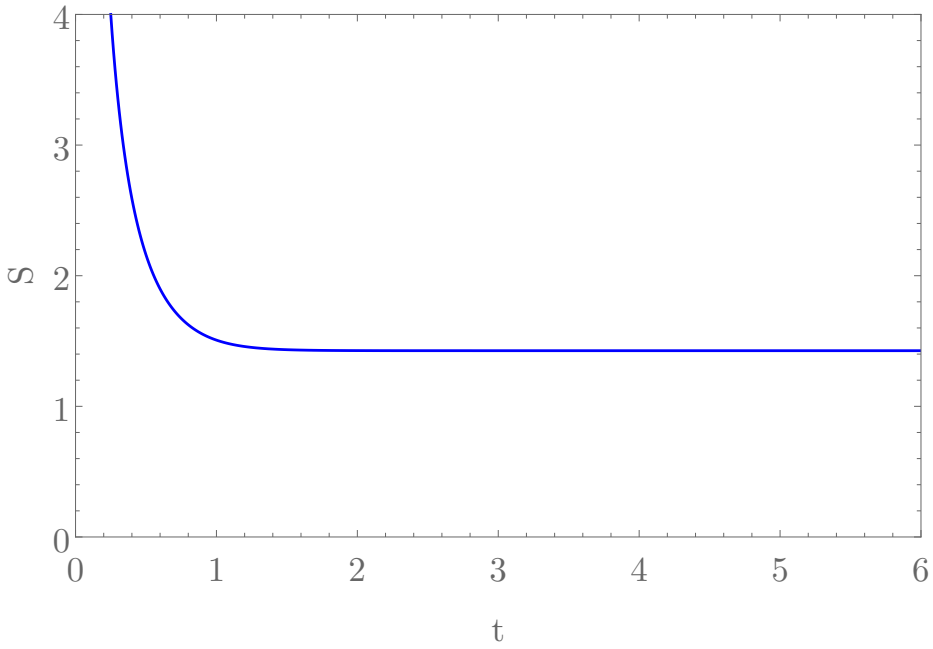
$$c_{tot} = \frac{4}{3}\pi S_{end}^3 c_{end}, \tag{5.116}$$

where S_{end} and c_{end} are the interface position and the concentration at the steady state, respectively. Because the total concentration is conserved, c_{tot} must be equal to the initial amount, which is given by

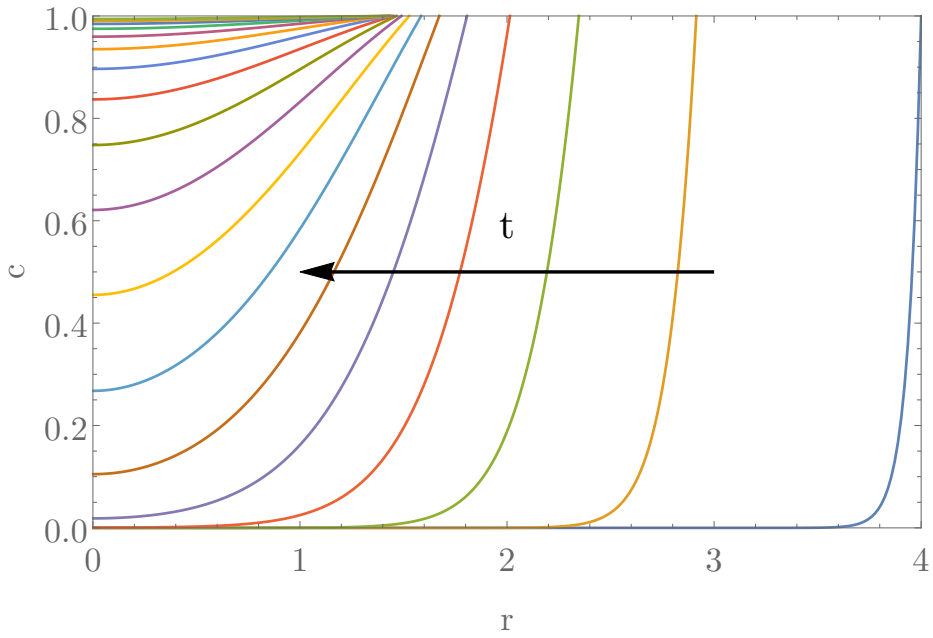
$$\begin{aligned} c_{tot} &= \lim_{t\to 0} 4\pi \int_0^{S(t)} r^2 \exp\left(-\frac{\mathrm{d}S}{\mathrm{d}t}(r - S(t))\right) \mathrm{d}r \\ &= \lim_{t\to 0} 4\pi \left(1 - 2t^3 + 2t^6\left(1 - e^{-\frac{1}{t^3}}\right)\right) \\ &= 4\pi. \end{aligned} \tag{5.117}$$

We know that the steady state concentration is $c_{end} = 1$, as given by the boundary condition (5.115c), so hence conclude

$$S_{end} = \sqrt[3]{3} \approx 1.4423, \tag{5.118}$$



(a) Position of the interface



(b) Concentration profiles

Figure 5.4: Numerical solutions of problem (5.115), calculated using a fixed boundary method and a finite volume scheme. In (a) we show the position of interface against time. The interface quickly decays to the steady state value. In (b) we show the concentration profiles. For late time, we notice the flattening of the profile until it reaches the steady state.

which agrees with the numerical result shown in Figure 5.4(a).

5.6.3 Matching of the solutions

In this section, we match the solutions of the different layers. We start by matching the temperature and concentration in layer G with the solutions in layer D.

$$(1\text{ti})(1\text{to}) = \lim_{\theta\to 0} T_{s0} = -1 = (1\text{to})(1\text{ti}), \tag{5.119}$$

For $\hat{c}_{s0}$, because the solutions in both layers do not depend on time, the matching is trivial.

The next condition we need to derive is the matching of T_s between layers G and H. Taking one term both in the inner and outer solutions, we find

$$(1\text{ti})(1\text{to}) = -1 = \lim_{R\to+\infty} T_{s0} = (1\text{to})(1\text{ti}), \tag{5.120}$$

which is used to determine T_{s0}.

Finally, we need to determine the initial conditions used in (5.113). We start with $\hat{c}_{l0}$ which we have to match with the solution found in layer F. Taking the solutions up to $\mathcal{O}\left(\epsilon^{-1}\right)$, we determine the matching condition

$$(1\text{ti})(1\text{to}) = \lim_{\theta\to 0} \epsilon^{-1}\hat{c}_{l0}, \tag{5.121a}$$

$$(1\text{to})(1\text{ti}) = \lim_{\tau\to+\infty} \epsilon^{-1} c_i(\tau) \exp\left(\frac{\mathrm{d}\hat{S}_0}{\mathrm{d}\tau}\left(R - \hat{S}_0(\tau)\right)\right), \tag{5.121b}$$

and we know from the solution in regime ii that $c_i \to \hat{m}_l$ and $\hat{S}_0 \to \frac{\hat{c}_0}{3\hat{m}_l \mathrm{St}}\frac{1}{\tau}$ as $\tau \to +\infty$.

The last condition is the one for $\hat{S}_0(\theta)$. We match the solution in regime iii with the solution in regime ii. Taking the solutions at leading order in each regime (so $\mathcal{O}\left(\epsilon^{\frac{1}{3}}\right)$ in regime ii and $\mathcal{O}\left(\epsilon^{\frac{2}{3}}\right)$ in regime iii), we find

$$(1\text{ti})(1\text{to}) = \lim_{\theta\to 0} \epsilon^{\frac{2}{3}} S_0 = \epsilon^{\frac{2}{3}} \frac{\hat{c}_0}{3\hat{m}_l}\frac{1}{\theta} = (1\text{to})(1\text{ti}). \tag{5.122}$$

We have now finished the analysis of regime iii and notice that the solutions given here hold up to $\theta \to +\infty$, therefore this is the last regime to consider. With the solutions found in each regime, we can now describe the behaviour of the system (5.1) at leading order for $t \in [0, +\infty)$.

5.7 Summary of the asymptotic solutions

After performing the asymptotic analysis to the extended Stefan problem in the spherically symmetric three-dimensional geometry, we have distinguished three different time regimes with significantly different behaviours of the solution. Similar to what we observed in the finite planar geometry, the concentration of impurities in the solid remains constant over time, while the concentration at each point is only determined by the time when it solidified. In this section, we provide the leading order solutions in each layer. The solutions are written in terms of the original dimensionless parameters (i.e. before rescaling) presented in Table 2.2 (see page 39). Remember, that we defined the small parameter $\epsilon = \mathrm{Le}^{-1}$.

Regime i corresponds to the beginning of the process and has three different layers: two outer layers, one in the solid phase and one in the liquid phase, and an inner layer around the interface. Recall that, in order to determine the solutions for this layer, we required a further expansion in the small Stefan number, as discussed in Section 5.4. In the outer layer in the solid ($r > S(t)$, layer A), we have

$$\begin{aligned} c_s &\approx \alpha \frac{c_0}{3} \frac{k\mathrm{St}}{\rho} \mathrm{Le} \frac{1-r^3}{(1-r)r^3}, \\ T_s &\approx \frac{1}{1-S(t)} \left(\frac{S(t)}{r} - 1 \right), \end{aligned} \tag{5.123a}$$

in the transition layer ($r = S(t)$, layer B), we have

$$\begin{aligned} c_s &\approx \alpha c_i(t), \\ T_s &\approx -\frac{r - S(t)}{(1-S(t))S(t)} - \frac{c_i(t)}{m_l}, \\ c_l &\approx c_i(t) \exp\left(-\frac{\mathrm{d}S}{\mathrm{d}t} \mathrm{Le}\,(r - S(t)) \right), \\ T_l &\approx -\frac{c_i(t)}{m_l}, \end{aligned} \tag{5.123b}$$

and in the outer layer in the liquid ($r < S(t)$, layer C), we have

$$\begin{aligned} c_l &\approx c_0, \\ T_l &\approx -\frac{c_i(t)}{m_l} + \frac{2T_0 S(t)}{\pi r} \sum_{n=1}^{\infty} \frac{(-1)^{n+1}}{n} \exp\left(-n^2\pi^2 \int_0^t \frac{\mathrm{d}s}{S(s)^2} \right) \sin\left(\frac{n\pi r}{S(t)} \right), \end{aligned} \tag{5.123c}$$

where

$$\begin{aligned} t &\approx \frac{\rho}{k\mathrm{St}} \left(\frac{1}{2}(1-S(t))^2 - \frac{1}{3}(1-S(t))^3 \right) + \frac{1}{6\kappa}(1-S(t))^2, \\ c_i(t) &\approx \frac{c_0}{3} \frac{k\mathrm{St}}{\rho} \mathrm{Le} \frac{1-S(t)^3}{(1-S(t))S(t)^3}. \end{aligned} \tag{5.123d}$$

In this regime, the system is driven by the thermal problem since the supercooling is small, and therefore we observe similar behaviour to that described in [63]. The impurity build-up happens only in a small layer around the solidification front. However, in this geometry, because the volume shrinks as the cube of the position of the interface (as opposed to the linear relation we observed in the finite planar problem), the rejection of impurities is stronger and we observe that the concentration of impurities at the interface is no longer constant but grows in time. This is the reason why the next regime to consider is driven by supercooling while the solidification front is still far away from the centre of the sphere.

Then, in this new regime, the front is still at a distance $\mathcal{O}\left(\epsilon^{\frac{1}{3}}\right)$ from the centre, but the impurity build-up causes a significant change in the melting temperature that affects the dynamics of the solidification front. This corresponds to a time of $\mathcal{O}\left(\epsilon^{\frac{2}{3}}\right)$ around the critical time $t = t^*$. We distinguish three layers: an outer layer in the solid, an intermediate layer $\mathcal{O}\left(\epsilon^{\frac{1}{3}}\right)$ around the centre of the sphere, and an inner layer $\mathcal{O}(\epsilon)$ around the solidification front. To obtain analytical solutions we need to take the small Stefan number limit, as well. In the outer layer D ($r > 0$), we have

$$\begin{aligned} c_s &\approx \alpha \frac{c_0}{3} \frac{k\mathrm{St}}{\rho} \mathrm{Le} \frac{1 - r^3}{(1 - r) r^3}, \\ T_s &\approx -1, \end{aligned} \tag{5.124a}$$

in the intermediate layer E ($r > 0$), we have

$$\begin{aligned} c_s &\approx \alpha m_l \left(1 + \frac{3 m_l}{c_0} \frac{\rho}{k\mathrm{St}} \frac{r^3}{\mathrm{Le}}\right)^{-1}, \\ T_s &\approx -1 + \left(-\frac{c_i(t)}{m_l} + 1\right) \frac{S(t)}{r}, \\ c_l &\approx c_0, \\ T_l &\approx -\frac{c_i(t)}{m_l}, \end{aligned} \tag{5.124b}$$

and in the inner layer F around $r = S(t)$, the solutions are

$$\begin{aligned} c_s &\approx \alpha c_i(t), \\ T_s &\approx -\frac{c_i(t)}{m_l}, \\ c_l &\approx c_i(t) \exp\left(-\frac{\mathrm{d}S}{\mathrm{d}t} \mathrm{Le}\left(r - S(t)\right)\right), \\ T_l &\approx -\frac{c_i(t)}{m_l}, \end{aligned} \tag{5.124c}$$

where

$$
\begin{aligned}
t &\approx \frac{c_0}{3m_l}\mathrm{Le}\frac{1}{S(t)} + \frac{\rho}{2k\mathrm{St}}S(t)^2 + t^* + \epsilon^{\frac{2}{3}}\tau^*, \\
c_i &\approx m_l\left(1 + \frac{3m_l}{c_0}\frac{\rho}{k\mathrm{St}}\frac{S(t)^3}{\mathrm{Le}}\right)^{-1}, \\
t^* &\approx \frac{\rho}{6k\mathrm{St}} + \frac{1}{6\kappa}.
\end{aligned}
\tag{5.124d}
$$

We observe that the dynamics in this regime are driven by the build-up of impurities at the interface, which causes enough supercooling to decrease the temperature in the whole domain down to the temperature of the boundary. This change in the interface temperature results in a decrease in the thermal gradients, and thus the interface slows down. Because the liquid region is still large, the impurities can diffuse away, so we still observe an exponential profile in the impurity concentration.

Finally, we consider regime iii, at a late time $\mathcal{O}\left(\epsilon^{\frac{1}{3}}\right)$ after the critical time $t = t^*$, where the interface is within a distance $\mathcal{O}\left(\epsilon^{\frac{2}{3}}\right)$ of the centre of the sphere. We distinguish two layers: an outer layer in the solid, and an inner layer of $\mathcal{O}\left(\epsilon^{\frac{2}{3}}\right)$ around the centre. In the outer layer ($r > 0$, layer G), the solutions are

$$
\begin{aligned}
c_s &\approx \alpha\frac{c_0}{3}\frac{k\mathrm{St}}{\rho}\mathrm{Le}\frac{1-r^3}{(1-r)r^3}, \\
T_s &\approx -1,
\end{aligned}
\tag{5.125a}
$$

while in the inner layer around $r = 0$, we have

$$
\begin{aligned}
c_s &\approx \alpha m_l, \\
T_s &\approx -1, \\
T_l &\approx -1,
\end{aligned}
\tag{5.125b}
$$

while c_l and S have to be determined numerically. In this layer, the temperature in both phases is identical to the boundary temperature, therefore the thermal problem is in its steady state. This means that the concentration at the interface remains constant. The concentration in the liquid and the position of the interface evolve following a classical one-phase Stefan problem, which ensures that total mass is conserved.

5.8 Numerical simulations

As we did for the problem in a planar geometry, we use numerical simulations of the full system (5.1) to validate the matched asymptotic solutions.

5.8.1 Numerical scheme

In order to solve the full problem numerically, we choose a fixed boundary scheme as we did in the planar analysis. The key idea is the same: rescale each domain so they have fixed boundaries, at the expense of introducing an advection term in the diffusion equation. However, because the difference in the topology of each phase (the liquid is a sphere and the solid is a spherical shell) the conservation form of the system is significantly different to the one presented in (4.130). Again, we need to be careful with the discretisation, to make sure that the algorithm conserves the total amount of impurities.

We introduce the variable x for the solid phase and y for the liquid phase

$$x = \frac{r - S(t)}{1 - S(t)}, \tag{5.126a}$$

$$y = \frac{r}{S(t)}, \tag{5.126b}$$

which are both defined in the domain $[0, 1]$. In order to write the system in conservation form, we define the following quantities

$$\phi_1(t, x) = \left(x + \frac{S(t)}{1 - S(t)}\right)^2 (1 - S(t))^3 c_s(t, x), \tag{5.127a}$$

$$\phi_2(t, x) = \left(x + \frac{S(t)}{1 - S(t)}\right)^2 (1 - S(t))^3 T_s(t, x), \tag{5.127b}$$

$$\phi_3(t, y) = S(t)^3 c_l(t, y), \tag{5.127c}$$

$$\phi_4(t, y) = S(t)^3 T_l(t, y), \tag{5.127d}$$

so that we can rewrite the system (5.1) in the following way. In the solid phase $x \in (0, 1)$, we have

$$\frac{\partial \phi_1}{\partial t} = \frac{\partial}{\partial x}\left(\left(\frac{S'(t)}{1 - S(t)}(1 - x) - \frac{2D\mathrm{Le}^{-1}}{\left(x + \frac{S(t)}{1-S(t)}\right)(1 - S(t))^2}\right)\phi_1 + \frac{D\mathrm{Le}^{-1}}{(1 - S(t))^2}\frac{\partial \phi_1}{\partial x}\right), \tag{5.128a}$$

$$\frac{\partial \phi_2}{\partial t} = \frac{\partial}{\partial x}\left(\left(\frac{S'(t)}{1 - S(t)}(1 - x) - \frac{2\kappa}{\left(x + \frac{S(t)}{1-S(t)}\right)(1 - S(t))^2}\right)\phi_2 + \frac{\kappa}{1 - S(t)^2}\frac{\partial \phi_2}{\partial x}\right). \tag{5.128b}$$

In the liquid phase $y \in (0, 1)$, we have

$$\frac{\partial \phi_3}{\partial t} + \frac{1}{y^2}\frac{\partial}{\partial y}\left[y^2\left(-\frac{S'(t)}{S(t)}y\phi_3 - \frac{1}{\mathrm{Le}S(t)^2}\frac{\partial \phi_3}{\partial y}\right)\right] = 0, \tag{5.128c}$$

$$\frac{\partial \phi_4}{\partial t} + \frac{1}{y^2}\frac{\partial}{\partial y}\left[y^2\left(-\frac{S'(t)}{S(t)}y\phi_4 - \frac{1}{S(t)^2}\frac{\partial \phi_4}{\partial y}\right)\right] = 0. \tag{5.128d}$$

At the interface, given by $x = 0$ and $y = 1$, we have

$$S(t)\phi_2 = (1 - S(t))\phi_4, \tag{5.128e}$$

$$S(t)\phi_1 = \alpha(1 - S(t))\phi_3, \tag{5.128f}$$

$$\phi_3 = -m_l\phi_4, \tag{5.128g}$$

$$\frac{\rho}{\mathrm{St}}\frac{\mathrm{d}S}{\mathrm{d}t} = \frac{k}{(1 - S(t))^2 S(t)^2}\frac{\partial\phi_2}{\partial x} - \frac{2k}{(1 - S(t))S(t)^3}\phi_2 - \frac{1}{S(t)^4}\frac{\partial\phi_4}{\partial y}, \tag{5.128h}$$

$$\left(-\frac{S'(t)}{(1 - S(t))S(t)^2} + \frac{2D}{\mathrm{Le}(1 - S(t))S(t)^3}\right)\phi_1 - \frac{D}{\mathrm{Le}(1 - S(t))^2 S(t)^2}\frac{\partial\phi_1}{\partial x} = -\frac{S'(t)}{S(t)}\phi_3 - \frac{1}{\mathrm{Le}S(t)^2}\frac{\partial\phi_3}{\partial y}. \tag{5.128i}$$

The boundary conditions are

$$\frac{\partial\phi_3}{\partial y} = 0 \quad \text{and} \quad \frac{\partial\phi_4}{\partial y} = 0, \quad \text{at } y = 0, \tag{5.128j}$$

$$\frac{\partial\phi_1}{\partial x} = 2(1 - S(t))\phi_1 \quad \text{and} \quad \phi_2 = -(1 - S(t)), \quad \text{at } x = 1. \tag{5.128k}$$

To avoid numerical instabilities, we use a TVD discretisation for the advection term, and we implement the finite volume scheme in Matlab using FVToolbox [22]. We take $\alpha = 0$, as we did in the planar geometry, so we consider only impurities in the liquid. This reduces the condition (5.128i) to a no-flux condition and removes equations (5.128a) and (5.128f) from the system. The outline of the scheme is the same as that described in Section 4.8.1.

5.8.2 Results

When performing our simulations, we set $\mathrm{St} = 0.1$, $\mathrm{Le} = 1000$, $\rho = 1$, $c_p = 1$, $k = 0.36$, $m_l = 1000$, $c_0 = 0.01$, and $T_0 = 0$, which are parameter values close to metallurgical grade silicon (see Table 2.2 in page 39), but that make the algorithm run faster. The reason to take $\mathrm{Le} = 1000$ and $\mathrm{St} = 0.1$ is to make sure that the condition $\epsilon^{\frac{2}{3}} \ll \mathrm{St} \ll 1$ is satisfied and thus the asymptotic solutions are valid. We take $N_s = 2 \cdot 10^3$ grid points in the solid phase, $N_l = 2 \cdot 10^4$ grid points in the liquid phase, and an initial time step of $\Delta t = 10^{-3}$. For the relaxation iterations, we take a relaxation parameter $\omega = 0.1$ and a tolerance of $\delta = 0.01$. To help convergence, if one time step takes more than 100 iterations before converging, and the time step is larger than 10^{-5}, we halve the time step. This algorithm is capable of solving the full problem with a total mass variation smaller than 0.01%.

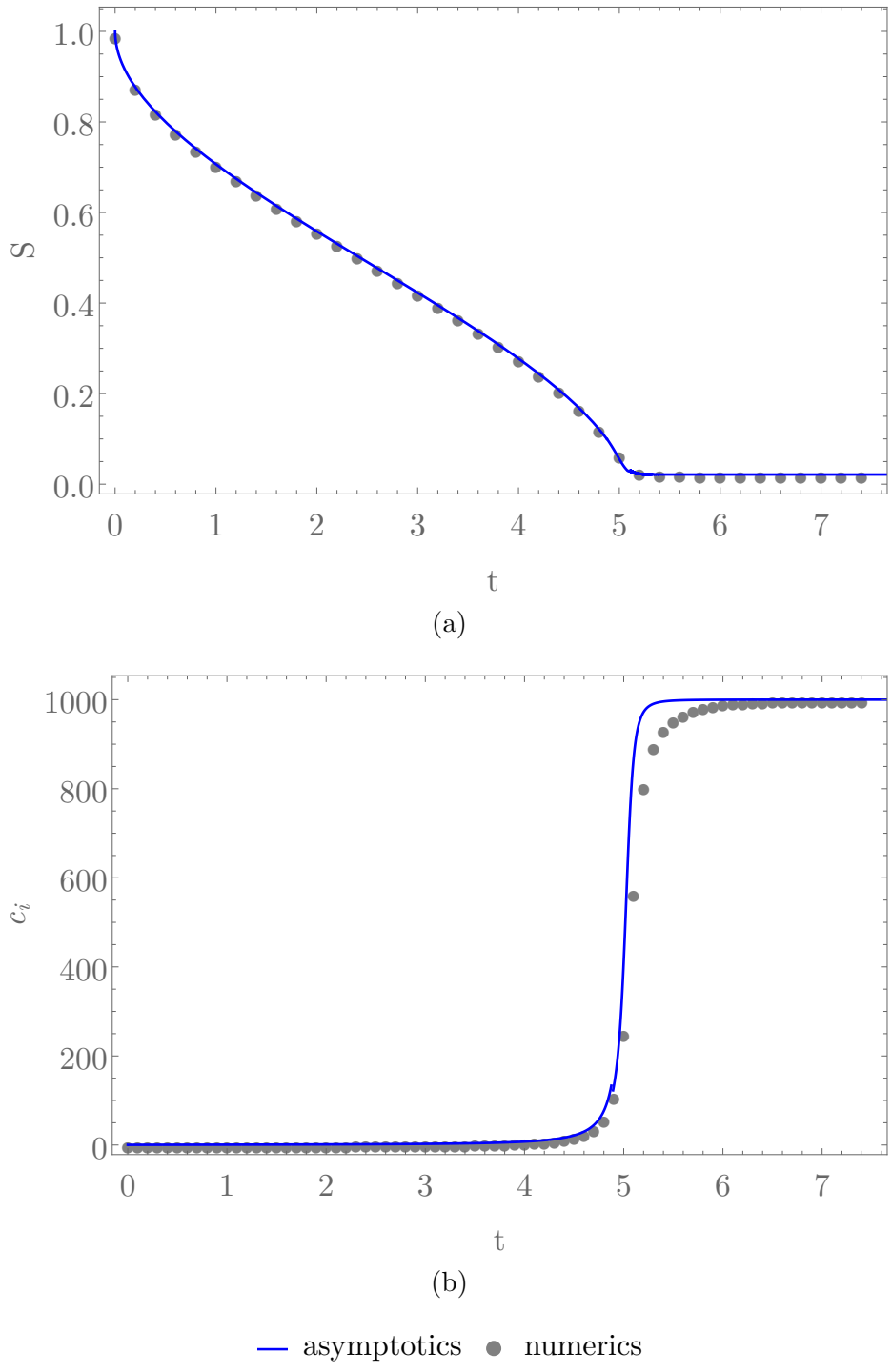


Figure 5.5: Comparison of the analytical and numerical solution of (a) the interface position and (b) the concentration of impurities on the liquid side of the interface, plotted against time.

The comparison between our asymptotic solutions and numerical simulations is shown in Figure 5.5. Even though the agreement is not as good as for the planar geometry, we still find quite good qualitative agreement, and thus we believe that the asymptotic solutions describe the dynamics of the solidification process for the entire time domain. This agreement could possibly be improved by calculating higher order terms for the solution in regime ii, given that for the solution plotted here we only took the leading order terms in both St and ϵ expansion. Figure 5.5(a) shows the position of the interface as a function of time, and we can clearly observe the behaviour for $t < t^*$, which is similar to the pure material problem [63, 84]. Near the critical time we observe a rapid transition that slows down the interface, and at late times ($t > t^*$) we see a decay to the steady state at a very small length scale. Figure 5.5(b) shows the concentration of impurities at the interface as a function of time. At the beginning of the process, we notice that concentration of impurities increases, but remaining of $\mathcal{O}(1)$, while around the critical time there is a very quick build-up until they reach the maximum concentration $c_l = m_l$. Finally, at late time, the concentration remains equal to this maximum value.

5.9 Discussion

In this chapter we have considered the solidification problem of a binary alloy in a spherical domain. Because analytical solutions cannot be found, we have performed an asymptotic expansion in large Lewis number limit and then in small Stefan number (assuming $\mathrm{Le}^{-\frac{2}{3}} \ll \mathrm{St}$). We also take the following assumptions: small diffusivity of impurities in the solid, segregation coefficient, initial concentration and initial temperature; and large supercooling coefficient. We distinguish eight different layers over three time regimes. The dynamics of the early stage of the problem are similar to the problem for the pure material described in [63], as the supercooling effects are small. The impurities are rejected into the liquid phase, and diffuse away over a very short length scale and in this geometry the concentration at the interface does not remain constant but grows in time. It is this growth which leads to the second regime, around the critical time $t^* \approx \frac{\rho}{6k\mathrm{St}} + \frac{1}{6\kappa}$. In this regime, the concentration of impurities has become large enough to cause a significant change in the melting temperature, resulting in a change in the thermal problem and a deceleration of the moving boundary. At late times, the temperature of the whole system has reached the minimum temperature and thus the thermal problem remains in steady state, implying that the interfacial concentration stays constant. Then, we need to solve

the one-phase Stefan problem for the diffusion of impurities in a shrinking core, in order to find the concentration in the liquid and the position of the interface, which has to be solved numerically. The asymptotic solutions show good agreement with the numerical simulations.

The analysis highlights the crucial role of constitutional supercooling in the behaviour of the system, even though its contribution was assumed to be small in the model. It is constitutional supercooling which triggers regime ii, and thus we observe a different behaviour to that described in previous works on the solidification of pure materials [63, 84, 88], or in [27], where supercooling was taken to be much smaller so that it fully decoupled from the thermal problem. Compared to the planar problem, we also observe a change of the order of the regimes. For the sphere, we first see the supercooling effects bring the temperature of the system down to the minimal temperature and slowing the interface down, and later the diffusion of impurities in the liquid region to the homogeneous steady state.

These results may be of interest to our industrial partner, Elkem, as they provide insight into the behaviour of the solidification problem in three-dimensional geometries. In a direct way, our results could provide a more accurate model to describe the water granulation process, in which liquid silicon is solidified into small spherical particles by splashing the hot liquid over a water bath. We do not have experimental data for these particles, but we expect that this analysis could be useful for better understanding the distribution of impurities. In a more general sense, we know from [62] that for an arbitrary three-dimensional geometry, near the end of the process the liquid region tends to an ellipsoid. Therefore, one could expect that the dynamics of the spherically symmetric problem studied here are similar to the ones of a more generic three-dimensional ellipsoidal geometry, and thus can provide insight for certain three-dimensional casting processes.

One could extend this work considering other aspects of the symmetric problem. A possible extension is to determine higher order asymptotic solutions, in order to increase the accuracy of our approximations; however, we suspect that this will require one to consider other layers and the problem complexity will increase, similarly to what happened with [63, 84, 88]. Other extensions would be to consider a more general geometry and extend the analysis of [62] to binary alloys. One could perform a similar asymptotic analysis for other special geometries, such as a cylinder, which should be conceptually similar to the sphere. Finally, one might also consider a stability analysis for the spherical problem, or other three-dimensional geometries,

akin to what we did for infinite and semi-infinite planar domain problems, in Chapter 3.

The asymptotic analysis of the solidification problem in a sphere presented in this chapter concludes the mathematical content of this thesis. In the next chapter, we summarise the results and discuss the conclusions of the thesis.

Chapter 6

Discussion

6.1 Summary and discussion of the thesis

In this thesis, we have studied different aspects of the extended Stefan problem for binary alloys accounting for constitutional supercooling, in order to better understand the casting process of metallurgical grade silicon.

In Chapter 2 we derived the general extended Stefan problem for the solidification of a binary alloy in an arbitrary n-dimensional domain. The model was derived from basic principles and then non-dimensionalised. The dimensionless model for an arbitrary n-dimensional geometry has been then reduced to the one-dimensional planar geometry and the n-dimensional spherically symmetric geometry. For the first geometry, we proposed a semi-infinite and an infinite geometry for which we could find self-similar solutions. We then studied the stability of these self-similar solutions in Chapter 3. Meanwhile, the finite geometry problem does not admit exact solutions so we studied that problem via matched asymptotics in Chapter 4. The spherical geometry in the three-dimensional case is later studied in Chapter 5, also using matched asymptotic techniques. We concluded Chapter 2 with a discussion of the parameter values for the particular case of metallurgical grade silicon, which gave insight into the relative sizes of the parameters and how these can be exploited in the asymptotic analyses.

In Chapter 3 we considered the stability of the exact self-similar solutions both for infinite and semi-infinite planar geometries. We performed a linear stability analysis, introducing self-similar perturbations to the system, the behaviour of which determined the stability of the problem: we considered the system unstable if a perturbation grows unboudedly in time away from the exact solution. The analyses revealed that, for both geometries, perturbations exist that grow unboudedly in time regardless of the parameter choice. The main difference between the two geometries

is that the semi-infinite domain allows only for one type of perturbation, which is unstable, while the infinite domain allows for two types of perturbation, which can be separated into a stable perturbation and an unstable perturbation. We then compared the unstable perturbations in each domain, noticing that they have very similar forms which suggests that they are caused by the same mechanism, the motion of the interface, as this is the only perturbation which may grow unboudedly in time. This is a reasonable result as it is well known that the solutions of the diffusion equation are stable, and thus one can expect them to remain stable in the free boundary problem as well, provided that the motion of the interface is stable. From this stability analysis, we concluded that the planar self-similar solidification front is unstable, and therefore it will break down into other spatial configurations which are not captured by the one-dimensional analysis presented here.

For finite planar domains, the extended Stefan problem does not have exact solutions and thus, in Chapter 4, we performed an asymptotic analysis to obtain approximate analytic solutions for the solidification problem of a planar slab in the limit of large Lewis number. This means that the diffusive time scale of the impurities is much smaller than the thermal diffusion time scale, and therefore the solutal and thermal problems decouple at lowest order. In addition, we assumed small diffusivity of impurities in the solid, small constitutional supercooling, almost complete rejection of impurities from the solid phase, small concentration of impurities, and small initial superheating. All of these assumptions are reasonable for the cast of metallurgical grade silicon. The geometry considered was a symmetric planar slab, initially composed of liquid, and cooled at a fixed temperature from the boundaries. The solidification fronts start at each boundary and move in opposite directions toward the centre. The asymptotic analysis revealed ten different layers in the problem distributed over four distinct time regimes, which had to be solved separately and then matched together using the method of matched asymptotics.

In the first regime, the fronts are far away from each other, and we noticed that they do not interact as the behaviour is the same as in the classical one-phase Stefan problem in the semi-infinite domain. Impurities rejected into the liquid phase diffuse only over a very short length scale, and thus we observed a "snow plough" effect, driven by the moving boundary. This behaviour continues until the two fronts are close to each other. Then the impurity field in the liquid notices the other solidification front approaching, and we observe rapid diffusion of impurities until the distribution is homogeneous in the liquid phase. Because the supercooling is small, the thermal problem is not affected by the build-up of impurities, and thus the temperature fields

and the moving boundary still have a self-similar behaviour. In the next regime, there is a very rapid transition in which the build-up of impurities is so large that it has an effect over the thermal problem, causing enough supercooling to decrease the thermal gradients near the interface and slow down the solidification front. Finally, the whole system cools down to the minimal temperature and the concentration of impurities in the liquid and the position of the interface evolve accordingly to ensure thermodynamic equilibrium and conservation of mass. Throughout, the whole problem impurities in the solid phase are constant in time and therefore fully determined at each point by the concentration of the interface at the moment that point solidified.

We validated the asymptotic solutions with numerical simulations of the full problem, as well as with experimental data for silicon. For the numerical simulations, we used a fixed boundary method in a finite volume scheme, with a relaxation scheme to couple the thermal and solutal problems. We found very good agreement between the numerical results and the asymptotic solutions, which validates our asymptotic analysis. We also found good agreement with the experimental data provided by Elkem, showing that the model is a valuable tool to understand the distribution of impurities in the cast. The comparison with experimental data showed that the most relevant regimes for the physical application we considered are those corresponding to the first two time regimes. It is likely that after the second regime some of the modelling assumptions are no longer reasonable, and the model should be extended by the inclusion of additional physics.

To conclude the thesis, in Chapter 5 we considered the asymptotic analysis of the solidification of a binary alloy in a spherical geometry which can be seen as an extension of the planar analysis presented in Chapter 4 to one specific three-dimensional geometry. We assumed that the problem was spherically symmetric so that the three-dimensional problem could be reduced to a quasi-one-dimensional model, with the radius acting as the single space variable. The aim of the chapter was to extend the existing literature on inward solidification of spheres to include the case of binary alloys. Due to the more complex geometry, in order to determine asymptotic solutions we took the large Lewis number limit (with the assumptions described for the planar case), and also the small Stefan number limit. We assumed that the relation $\mathrm{Le}^{-\frac{2}{3}} \ll \mathrm{St}$ holds so the large Lewis number limit can be taken first and then the small Stefan number limit taken after that. The asymptotic analysis revealed eight different layers in the large Lewis number limit, distributed over three distinct time regimes, in addition to five sublayers in the small Stefan number limit. However,

these small Stefan number sublayers were shown to not be relevant to determine the leading order solutions, manifesting only in higher order terms.

In the first regime, at early time, the interface is still far away from the centre and therefore the thermal problem fully decouples from the solutal problem. In this case, we find that the temperature profiles and the interface follow the behaviour of the classical Stefan problem for a spherical domain. The impurities in the liquid build-up in a very small layer ahead of the interface, but for this geometry the concentration at the interface grows in time instead of remaining constant. This growth of the interfacial concentration leads to the next regime, in which the concentration builds up over a short time scale, and due to constitutional supercooling this build-up has an impact over the thermal problem. The temperature at the interface then decreases, and so do the thermal gradients near the interface, causing the solidification front to slow down. Eventually, the temperature fields reach the minimal temperature of the system and thus remain steady, causing the concentration at the interface to reach its maximum given by thermodynamic equilibrium. Finally, we reach the last regime in which the temperature fields remain steady, and the problem is driven by the concentration in the liquid, which follows a diffusion in a shrinking core process, described by a classical one-phase Stefan problem. Again, the impurity profile in the solid phase remains constant in time due to the small diffusivity.

For this problem we did not have experimental data, but we could validate the asymptotic solutions with numerical simulations, using a similar scheme to the one described for the planar geometry in Chapter 4. We found good agreement between asymptotics and numerics, even though it could be useful to determine higher order terms in the asymptotics to obtain better approximations, especially in the second regime.

6.2 Guidelines for the industrial partner

One motivation for this project came from an industrial problem proposed by Elkem, which was to obtain a better understanding of the dynamics of the solidification process and the distribution of impurities in the cast of metallurgical grade silicon. The models and analyses presented in this thesis allow us to provide some advice to the industrial partner.

In Chapter 2, we derived the extended Stefan problem for the solidification of a binary alloy. The general model from which we derived all the subsequent models could be used as a basis to implement numerical algorithms to study the problem,

as the model is derived from basic physical principles. In addition, the model can be used as starting point to derive other models that include more physical phenomena.

The stability analysis presented in Chapter 3 proves from a mathematical point of view that stable planar solidification fronts are not possible unless the cooling of the system is controlled and the velocity of the solidification front kept below a certain threshold, like in directional solidification or the Czochralski process. Even though this was known from experimental evidence, the mathematical analysis provides theoretical background and highlights the role of the moving boundary as the trigger of the instability, which can potentially lead to the development of new casting techniques.

The asymptotic solutions derived in Chapter 4 provide insight into the solidification of thin layers of silicon which, due to their aspect ratio, can be modelled as one-dimensional processes. The solutions show the leading phenomena at each stage of the process and the impact of each parameter over the dynamics. This is important, as the high temperatures prevent Elkem from obtaining this information experimentally. The model allows us to understand which parameters play a role in the impurity distribution over the solid silicon, namely, the concentration of impurities in the initial melt, the segregation coefficient, and a parameter μ related to the cooling rate. The initial concentration acts only as a scaling of the concentration profile and, as it can be easily measured, we suggest to fix its value using the experimental measurements of the liquid used in the cast. The other two parameters should be fit to experimental data. We observe that both parameters play a role on the scaling of the concentration profile, but μ has an impact on the thickness of the layer where the impurities build up as well. Therefore, our model suggests that varying the cooling rate can be used as a way to control the thickness of those layers. Because these layers appear to be correlated to the equiaxed layers, where the grains are smaller, one could use our model for an empirical approximation to the columnar to equiaxed transition.

We have obtained asymptotic solutions to the solidification of a binary alloy in a sphere in Chapter 5. As an immediate application, one could use this model to better understand water granulation and atomisation processes. It would be useful to verify our model with experimental data obtained from this casting method. In a more generic sense, because this is a three-dimensional model, it should help us understand the qualitative behaviour of casting processes in which three-dimensional effects have an important role, and thus our spherical geometry results might be viewed as a step toward a better understanding of the effects of the geometry on the cast.

6.3 Future work

Although interest in understanding the solidification of binary alloys is not new, and much research has been conducted, the problem is very complex and there are still aspects of the problem to consider.

The stability analysis presented in Chapter 3 determined that the self-similar solutions are always unstable, therefore a flat solidification front moving without being controlled is not stable. However, the analysis does not provide any information on what the possible higher-dimension stable configurations are. Knowing such configurations may lead to some insight on the grain size. Therefore, one of the lines of research that could be followed is the extension of the stability analysis to the two-dimensional problem. Because of the second space variable introduced into the problem, it is not obvious how to extend the current analysis to higher dimensions, therefore other techniques might be required. One of the options is to perform the stability analysis numerically, to obtain some insight on the size and shape of the stable perturbations. However, we need numerical schemes able to cope with complex higher-dimension models, such as the level set method [92] or the phase field method [46]. By considering higher-dimension models, one could also include geometric effects such as the Gibbs-Thomson effect or faceted growth of the crystals.

The first direction to extend the asymptotic analyses presented in Chapters 4 and 5 would be to study the solidification of a cylinder, thereby extending the work in [27, 84]. Due to its geometry, one might expect the cylinder behaviour to be between the planar slab and the sphere, and thus it would help to complete the picture of the effect of geometry on the solidification process. We expect the problem to be conceptually similar to the analysis of the sphere, but with the added technical complexity of logarithmic terms arising in the asymptotic analysis. The results could be validated using a similar numerical scheme to that described in Section 5.8. Another direction would be to consider the late time behaviour in arbitrary two-dimensional and three-dimensional geometries, to see if the behaviour described by McCue et al. [61, 62] for pure materials holds as well for binary alloys. These results could be helpful to our industrial partners as they would provide insight into the late stages of the solidification process for more general geometries which are closer to the actual casting set-up. For the spherical geometry in particular, we have considered a certain distinguished limit between the Lewis and the Stefan numbers ($\mathrm{Le}^{-\frac{2}{3}} \ll \mathrm{St}$). This distinguished limit is relevant for the solidification of silicon (and actually for many

binary alloys), but it would be a very interesting challenge to generalise the analysis to arbitrary Lewis and Stefan numbers.

Another area of possible further work is to study the stability of the asymptotic solutions for the finite slab and sphere geometries. Understanding the possible instabilities of the problem may potentially lead to a better understanding of the microstructure formation at the different times of the process, and thus of the columnar to equiaxed transition. The model could be generalised by considering non-uniform boundaries and other heat exchange conditions at the boundary, in order to obtain a better understanding of the casting methods where molten silicon is poured over a bed of fines, as discussed in [7].

Finally, one could consider extensions of the Stefan problem for binary alloys presented and studied in this thesis. For example, one could include more realistic phase diagrams and several types of impurities to better capture how each element is distributed within the cast. This could lead to the study of reaction-diffusion processes for the different components in the intermetallic phase. Another physical effect that could be included is nucleation, as it is expected to have an important role toward the end of the process. In particular, the assumption that there is a single sharp interface would be removed. We note that the commonly used enthalpy method, for numerically solving Stefan problems, considers mushy regions to occur when constitutional supercooling is accounted for, and this model might be analysed asymptotically in a manner similar to that presented here. And, naturally, one could aim to extend and study the models in higher spatial dimensions, so that phenomena such as the Gibbs-Thomson effect can be considered.

Bibliography

[1] M. Abramowitz and I. A. Stegun, editors. *Handbook of Mathematical Functions With Formulas, Graphs, and Mathematical Tables*. U.S. Department of Commerce, NIST, 10th edition, 1964.

[2] D. V. Alexandrov. The effect of concentrational supercooling on the morphological stability of self-similar solidification with a planar front. *Doklady Physics*, 46(7):453–458, 2001.

[3] D. V. Alexandrov. Self-similar solidification: morphological stability of the regime. *International Journal of Heat and Mass Transfer*, 47(6):1383–1389, 2004.

[4] D. N. de G. Allen and R. T. Severn. The application of relaxation methods to the solution of non-elliptic partial differential equations: II. The solidification of liquids. *The Quarterly Journal of Mechanics and Applied Mathematics*, 5(4):447–454, 1952.

[5] A. Autruffe. *Silicon directional solidification: Impurity segregation and defects*. PhD thesis, NTNU Norges Teknisk-Naturvitenskapelige Universitet, 2014.

[6] G. P. Benham, K. Hildal, C. P. Please, and R. A. Van Gorder. Solidification of silicon. Technical report, University of Oxford, 2015.

[7] G. P. Benham, K. Hildal, C. P. Please, and R. A. Van Gorder. Penetration of molten silicon into a bed of fines. *International Communications in Heat and Mass Transfer*, 75:323–327, 2016.

[8] G. P. Benham, K. Hildal, C. P. Please, and R. A. Van Gorder. Solidification of silicon in a one-dimensional slab and a two-dimensional wedge. *International Journal of Heat and Mass Transfer*, 98:530–540, 2016.

[9] F. Brosa Planella, C. P. Please, and R. A. Van Gorder. Extended Stefan problem for binary alloys for inward solidification in planar finite domains. *Submitted for publication*, 2018.

[10] F. Brosa Planella, C. P. Please, and R. A. Van Gorder. Instability in the self-similar motion of a planar solidification front. *IMA Journal of Applied Mathematics*, 83(1):106–130, 2018.

[11] W. D. Callister and D. G. Rethwisch. *Materials Science and Engineering*, volume 5. John Wiley & Sons NY, 2011.

[12] C. J. Cawthorn, L. Briant, J. Brimlow, S. Cook, M. Davies Wykes, I. Hewitt, N. Letchford, J. R. Ockendon, A. Peace, C. P. Please, A. H. Ramos, and M. Zagorowska. Thin casting of silicon. Study group report, 91st European Study Group with Industry, 2013.

[13] J. Chadam, S. D. Howison, and P. Ortoleva. Existence and stability for spherical crystals growing in a supersaturated solution. *IMA Journal of Applied Mathematics*, 39(1):1–15, 1987.

[14] S. Chen, B. Merriman, S. Osher, and P. Smereka. A simple level set method for solving Stefan problems. *Journal of Computational Physics*, 135(1):8–29, 1997.

[15] S. R. Coriell, G. B. McFadden, and R. F. Sekerka. Selection mechanisms for multiple similarity solutions for solidification and melting. *Journal of Crystal Growth*, 200(1):276–286, 1999.

[16] S. R. Coriell, G. B. McFadden, R. F. Sekerka, and W. J. Boettinger. Multiple similarity solutions for solidification and melting. *Journal of Crystal Growth*, 191(3):573–585, 1998.

[17] J. Crank and R. S. Gupta. Isotherm migration method in two dimensions. *International Journal of Heat and Mass Transfer*, 18(9):1101–1107, 1975.

[18] A. B. Crowley. Numerical solution of Stefan problems. *International Journal of Heat and Mass Transfer*, 21(2):215–219, 1978.

[19] A. B. Crowley and J. R. Ockendon. On the numerical solution of an alloy solidification problem. *International Journal of Heat and Mass Transfer*, 22(6):941–947, 1979.

[20] G. B. Davis and J. M. Hill. A moving boundary problem for the sphere. *IMA Journal of Applied Mathematics*, 29(1):99–111, 1982.

[21] S. H. Davis. *Theory of Solidification*. Cambridge University Press, 2001.

[22] A. A. Eftekhari and K. Schüller. FVTool: A finite volume toolbox for Matlab. https://github.com/simulkade/FVTool, April 2018.

[23] C. M. Elliott and J. R. Ockendon. *Weak and Variational Methods for Moving Boundary Problems*, volume 59. Pitman Publishing, 1982.

[24] A. Fasano, M. Primicerio, S. D. Howison, and J. R. Ockendon. *On the singularities of one-dimensional Stefan problems with supercooling*, pages 215–226. Springer, 1989.

[25] A. Fasano, M. Primicerio, S. D. Howison, and J. R. Ockendon. Some remarks on the regularization of supercooled one-phase Stefan problems in one dimension. *Quarterly of Applied Mathematics*, 48(1):153–168, 1990.

[26] A. Fasano, M. Primicerio, and A. A. Lacey. New results on some classical parabolic free-boundary problems. *Quarterly of Applied Mathematics*, 38(4):439–460, 1981.

[27] D. L. Feltham and J. Garside. Analytical and numerical solutions describing the inward solidification of a binary melt. *Chemical Engineering Science*, 56(7):2357–2370, 2001.

[28] Ch.-A. Gandin. Modeling of solidification: Grain structures and segregations in metallic alloys. *Comptes Rendus Physique*, 11(3):216–225, 2010.

[29] Ch.-A. Gandin, J.-L. Desbiolles, M. Rappaz, and Ph. Thevoz. A three-dimensional cellular automation-finite element model for the prediction of solidification grain structures. *Metallurgical and Materials Transactions A*, 30(12):3153–3165, 1999.

[30] Ch.-A. Gandin and M. Rappaz. A 3D cellular automaton algorithm for the prediction of dendritic grain growth. *Acta Materialia*, 45(5):2187–2195, 1997.

[31] M. Gunzburger, E. Ozugurlu, J. Turner, and H. Zhang. Controlling transport phenomena in the Czochralski crystal growth process. *Journal of Crystal Growth*, 234(1):47–62, 2002.

[32] S. C. Gupta. Numerical and analytical solutions of one-dimensional freezing of dilute binary alloys with coupled heat and mass transfer. *International Journal of Heat and Mass Transfer*, 33(4):593–602, 1990.

[33] F. S. Ham. Shape-preserving solutions of the time-dependent diffusion equation. *Quarterly of Applied Mathematics*, 17(2):137–145, 1959.

[34] T. Hannesson. The Si process – drawings. Elkem Iceland, 2016.

[35] M. A. Herrero and J. J. L. Velázquez. Singularity formation in the one-dimensional supercooled Stefan problem. *European Journal of Applied Mathematics*, 7(2):119–150, 1996.

[36] J. M. Hill and A. Kucera. Freezing a saturated liquid inside a sphere. *International Journal of Heat and Mass Transfer*, 26(11):1631–1637, 1983.

[37] J. M. Hill and A. Kucera. The time to complete reaction or solidification of a sphere. *Chemical Engineering Science*, 38(8):1360–1362, 1983.

[38] R. N. Hills, D. E. Loper, and P. H. Roberts. A thermodynamically consistent model of a mushy zone. *The Quarterly Journal of Mechanics and Applied Mathematics*, 36(4):505–540, 1983.

[39] S. D. Howison. Similarity solutions to the Stefan problem and the binary alloy problem. *IMA Journal of Applied Mathematics*, 40(3):147–161, 1988.

[40] S. D. Howison. *Practical Applied Mathematics: Modelling, Analysis, Approximation*. Number 38. Cambridge University Press, 2005.

[41] H. E. Huppert. The fluid mechanics of solidification. *Journal of Fluid Mechanics*, 212:209–240, 1990.

[42] H. E. Huppert and M. G. Worster. Dynamic solidification of a binary melt. *Nature*, 314(6013):703–707, 1985.

[43] M. A. Jaafar, D. R. Rousse, S. Gibout, and J.-P. Bédécarrats. A review of dendritic growth during solidification: mathematical modeling and numerical simulations. *Renewable and Sustainable Energy Reviews*, 74:1064–1079, 2017.

[44] L. M. Jiji and S. Weinbaum. Perturbation solutions for melting or freezing in annular regions initially not at the fusion temperature. *International Journal of Heat and Mass Transfer*, 21(5):581–592, 1978.

[45] A. Karma and W.-J. Rappel. Phase-field method for computationally efficient modeling of solidification with arbitrary interface kinetics. *Physical Review E*, 53(4):R3017, 1996.

[46] S. G. Kim, W. T. Kim, J. S. Lee, M. Ode, and T. Suzuki. Large scale simulation of dendritic growth in pure undercooled melt by phase-field model. *ISIJ International*, 39(4):335–340, 1999.

[47] J. R. King, D. S. Riley, and A. M. Wallman. Two–dimensional solidification in a corner. *Proceedings of the Royal Society of London A: Mathematical, Physical and Engineering Sciences*, 455(1989):3449–3470, 1999.

[48] S. Krukowski and L. A. Turski. Time-dependent solution for a spherically symmetric freezing precipitate. *Journal of Crystal Growth*, 58(3):631–635, 1982.

[49] O. Kubaschewski. *Iron-Binary Phase Diagrams*. Springer-Verlag, 1982.

[50] A. Kucera and J. M. Hill. On inward solidifying cylinders and spheres initially not at their fusion temperature. *International Journal of Non-linear Mechanics*, 21(1):73–82, 1986.

[51] W. Kurz and D. J. Fisher. *Fundamentals of Solidification*. Trans Tech Publications, 4th revised edition, 1998.

[52] J. Kyselica. Evolution of the solidification front of a binary mixture. *Applied Mathematical Modelling*, 37(6):3761–3776, 2013.

[53] A. A. Lacey and A. B. Tayler. A mushy region in a Stefan problem. *IMA Journal of Applied Mathematics*, 30(3):303–313, 1983.

[54] R. A. Lambert and R. H. Rangel. Linear stability analysis of the solidification of a supercooled liquid in a half-space. *International Journal of Heat and Mass Transfer*, 45(23):4577–4587, 2002.

[55] G. Lamé and B. P. E. Clapeyron. Mémoire sur la solidification par refroidissement d'un globe liquide. *Annales Chimie Physique*, 47:250–256, 1831.

[56] J. S. Langer. Instabilities and pattern formation in crystal growth. *Reviews of Modern Physics*, 52(1):1–30, 1980.

[57] A. Lazaridis. A numerical solution of the multidimensional solidification (or melting) problem. *International Journal of Heat and Mass Transfer*, 13(9):1459–1477, 1970.

[58] L. G. Leal. *Advanced Transport Phenomena: Fluid Mechanics and Convective Transport Processes*. Cambridge University Press, 2007.

[59] R. J. LeVeque. *Finite volume methods for hyperbolic problems*, volume 31. Cambridge University Press, 2002.

[60] F. Liu and D. L. S. McElwain. A computationally efficient solution technique for moving-boundary problems in finite media. *IMA Journal of Applied Mathematics*, 59(1):71–84, 1997.

[61] S. W. McCue, J. R. King, and D. S. Riley. Extinction behaviour for two–dimensional inward-solidification problems. *Proceedings of the Royal Society of London A: Mathematical, Physical and Engineering Sciences*, 459(2032):977–999, 2003.

[62] S. W. McCue, J. R. King, and D. S. Riley. The extinction problem for three-dimensional inward solidification. *Journal of Engineering Mathematics*, 52(4):389–409, 2005.

[63] S. W. McCue, B. Wu, and J. M. Hill. Classical two-phase Stefan problem for spheres. *Proceedings of the Royal Society of London A: Mathematical, Physical and Engineering Sciences*, 464(2096):2055–2076, 2008.

[64] G. J. Merchant and S. H. Davis. Morphological instability in rapid directional solidification. *Acta Metallurgica et Materialia*, 38(12):2683–2693, 1990.

[65] M. F. Møll. *Solidification of Silicon: Macro- and Microstructure as Functions of Thermal History and Composition*. PhD thesis, NTNU Norges Teknisk-Naturvitenskapelige Universitet, 2014.

[66] W. W. Mullins and R. F. Sekerka. Stability of a planar interface during solidification of a dilute binary alloy. *Journal of Applied Physics*, 35(2):444 – 451, 1964.

[67] J. Ni and C. Beckermann. A volume-averaged two-phase model for transport phenomena during solidification. *Metallurgical Transactions B*, 22(3):349–361, 1991.

[68] J. R. Ockendon, S. D. Howison, A. A. Lacey, and A. B. Movchan. *Applied Partial Differential Equations*. Oxford University Press, 1999.

[69] J. R. Ockendon and A. B. Tayler. *Free Boundary Problems: Applications and Theory*, chapter 2, pages 157–165. Number 120 in Research Notes in Mathematics. Pitman Advanced Publishing Program, 1985.

[70] S. Osher and J. A. Sethian. Fronts propagating with curvature-dependent speed: algorithms based on Hamilton-Jacobi formulations. *Journal of Computational Physics*, 79(1):12–49, 1988.

[71] R. I. Pedroso and G. A. Domoto. Perturbation solutions for spherical solidification of saturated liquids. *Journal of Heat Transfer*, 95(1):42–46, 1973.

[72] A. D. Polyanin. *Handbook of Linear Partial Differential Equations for Engineers and Scientists*. CRC Press, 2001.

[73] N. Provatas and K. Elder. *Phase-field Methods in Materials Science and Engineering*. John Wiley & Sons, 2011.

[74] M. Rappaz. Modelling of microstructure formation in solidification processes. *International Materials Reviews*, 34(3):93–123, 1989.

[75] M. Rappaz. Modeling and characterization of grain structures and defects in solidification. *Current Opinion in Solid State and Materials Science*, 20(1):37–45, 2016.

[76] M. Rappaz and Ch.-A. Gandin. Probabilistic modelling of microstructure formation in solidification processes. *Acta Metallurgica et Materialia*, 41(2):345–360, 1993.

[77] D. S. Riley, F. T. Smith, and G. Poots. The inward solidification of spheres and circular cylinders. *International Journal of Heat and Mass Transfer*, 17(12):1507–1516, 1974.

[78] M. E. Rose. A method for calculating solutions of parabolic equations with a free boundary. *Mathematics of Computation*, 14(71):249–256, 1960.

[79] L. I. Rubinstein. *The Stefan Problem*, volume 27 of *Translations of Mathematical Monographs*. American Mathematical Society, 1971.

[80] A. Schei, J. K. Tuset, and H. Tveit. *Production of High Silicon Alloys*. Tapir, 1998.

[81] M. S. Selim and R. C. Seagrave. Solution of moving-boundary transport problems in finite media by integral transforms. II. Problems with a cylindrical or spherical moving boundary. *Industrial & Engineering Chemistry Fundamentals*, 12(1):9–13, 1973.

[82] W. Shyy, H.S. Udaykumar, and S.-J. Liang. An interface tracking method applied to morphological evolution during phase change. *International Journal of Heat and Mass Transfer*, 36(7):1833–1844, 1993.

[83] G. I. Sivashinsky. On cellular instability in the solidification of a dilute binary alloy. *Physica D: Nonlinear Phenomena*, 8(1-2):243–248, 1983.

[84] A. M. Soward. A unified approach to Stefan's problem for spheres and cylinders. *Proceedings of the Royal Society of London A: Mathematical, Physical and Engineering Sciences*, 373(1752):131–147, 1980.

[85] J. Stam and R. Schmidt. On the velocity of an implicit surface. *ACM Transactions on Graphics (TOG)*, 30(3):21, 2011.

[86] J. Stefan. Über die Theorie der Eisbildung. *Monatshefte für Mathematik*, 1(1):1–6, 1890.

[87] D. M. Stefanescu. Methodologies for modeling of solidification microstructure and their capabilities. *ISIJ International*, 35(6):637–650, 1995.

[88] K. Stewartson and R. T. Waechter. On Stefan's problem for spheres. *Proceedings of the Royal Society of London. Series A, Mathematical and Physical Sciences*, 348(1655):415–426, 1976.

[89] J. M. Sullivan Jr, D. R. Lynch, and K. O'Neill. Finite element simulation of planar instabilities during solidification of an undercooled melt. *Journal of Computational Physics*, 69(1):81–111, 1987.

[90] K. Tang, E. J. Øvrelid, G. Tranell, and M. Tangstad. Critical assessment of the impurity diffusivities in solid and liquid silicon. *JOM*, 61(11):49–55, 2009.

[91] L. C. Tao. Generalized numerical solutions of freezing a saturated liquid in cylinders and spheres. *AIChE Journal*, 13(1):165–169, 1967.

[92] M. Theillard, F. Gibou, and T. Pollock. A sharp computational method for the simulation of the solidification of binary alloys. *Journal of Scientific Computing*, 63(2):330–354, 2015.

[93] B. D. Turland and R. S. Peckover. The stability of planar melting fronts in two-phase thermal Stefan problems. *IMA Journal of Applied Mathematics*, 25(1):1–15, 1980.

[94] M. Van Dyke. *Perturbation Methods in Fluid Mechanics*. Parabolic Press, 1975.

[95] V. Voller and M. Cross. Accurate solutions of moving boundary problems using the enthalpy method. *International Journal of Heat and Mass Transfer*, 24(3):545–556, 1981.

[96] A. M. Wallman, J. R. King, and D. S. Riley. Asymptotic and numerical solutions for the two-dimensional solidification of a liquid half-space. *Proceedings of the Royal Society of London A: Mathematical, Physical and Engineering Sciences*, 453(1962):1397–1410, 1997.

[97] C. Y. Wang and C. Beckermann. Equiaxed dendritic solidification with convection: Part I. Multiscale/multiphase modeling. *Metallurgical and Materials Transactions A*, 27(9):2754–2764, 1996.

[98] C. Y. Wang and C. Beckermann. Equiaxed dendritic solidification with convection: Part II. Numerical Simulations for an Al-4 Wt Pct Cu Alloy. *Metallurgical and Materials Transactions A*, 27(9):2765–2783, 1996.

[99] G.-X. Wang, V. Prasad, and E. F. Matthys. An interface-tracking numerical method for rapid planar solidification of binary alloys with application to microsegregation. *Materials Science and Engineering: A*, 225(1-2):47–58, 1997.

[100] S.-L. Wang, R. F. Sekerka, A. A. Wheeler, B. T. Murray, S. R. Coriell, R. J. Braun, and G. B. McFadden. Thermodynamically-consistent phase-field models for solidification. *Physica D: Nonlinear Phenomena*, 69(1-2):189–200, 1993.

[101] A. A. Wheeler, W. J. Boettinger, and G. B. McFadden. Phase-field model for isothermal phase transitions in binary alloys. *Physical Review A*, 45(10):7424, 1992.

[102] A. A. Wheeler, W. J. Boettinger, and G. B. McFadden. Phase-field model of solute trapping during solidification. *Physical Review E*, 47(3):1893, 1993.

[103] A. A. Wheeler, B. T. Murray, and R. J. Schaefer. Computation of dendrites using a phase field model. *Physica D: Nonlinear Phenomena*, 66(1-2):243–262, 1993.

[104] D. J. Wollkind and L. A. Segel. A nonlinear stability analysis of the freezing of a dilute binary alloy. *Philosophical Transactions of the Royal Society of London A: Mathematical, Physical and Engineering Sciences*, 268(1191):351 – 380, 1970.

[105] M. G. Worster. Solidification of an alloy from a cooled boundary. *Journal of Fluid Mechanics*, 167:481–501, 1986.

[106] M. G. Worster. *Perspectives in Fluid Dynamics*, chapter 8. Cambridge University Press, 2002.

[107] J. Yang, C.-Y. Zhao, and D. Hutchins. Modelling the effect of binary phase composition on inward solidification of a particle. *International Journal of Heat and Mass Transfer*, 55(23):6766–6774, 2012.

[108] M. Založnik and H. Combeau. An operator splitting scheme for coupling macroscopic transport and grain growth in a two-phase multiscale solidification model: Part I – model and solution scheme. *Computational Materials Science*, 48(1):1–10, 2010.

[109] M. Založnik, A. Kumar, and H. Combeau. An operator splitting scheme for coupling macroscopic transport and grain growth in a two-phase multiscale solidification model: Part II – application of the model. *Computational Materials Science*, 48(1):11–21, 2010.